Digging into Biologically-Driven Injury Mechanisms in the Intervertebral Disc

-

An Evidence-Based Network Modelling Approach to Estimate Cell Dynamics within Complex Multicellular Systems

Laura Baumgartner

DOCTORAL THESIS UPF / 2021

Directors of the thesis

Dr. Jérôme Noailly

Prof. Miguel Ángel González Ballester

DEPARTMENT OF INFORMATION AND COMMUNICATION TECHNOLOGIES

Universitat Pompeu Fabra Barcelona

This research was carried out in the research laboratory "Biomechanics and Mechanobiology" of BCN MedTech, Department of Information and Communication Technologies, Universitat Pompeu Fabra (UPF), Barcelona, Spain. This work was funded by an UPF postgraduate scholarship from the Department of Information and Communication Technologies (DTIC-UPF).

Supervision:

Dr. Jérôme Noailly	Ramon y Cajal Researcher, Tenure-Track Faculty Principal Investigator Biomechanics and Mechanobiology Universitat Pompeu Fabra
Prof. Miguel Ángel González Ballester	ICREA Research Professor Head of BCN MedTech ICREA / Universitat Pompeu Fabra

Review Committee (Main):

Prof. Ioannis Xenarios	Professor of computational Biology and bioinformatics and Chief Data Analyst University of Lausanne, Health2030 Genome Center, Switzerland
Prof. Liesbet Geris	Professor at the University of Liège and KU Leuven, Belgium
Prof. Bart Bijnens	ICREA Research Professor at Institut d'investigacions Biomèdiques August Pi I Sunyer (IDIBAPS), Spain

Review Committee (Reserve):

Prof. Oscar Camara	Professor at Universitat Pompeu Fabra, Spain
Dr. Carlos Ruiz Wills	Postdoctoral researcher at Universitat Pompeu Fabra, Spain

Acknowledgements

To everyone who supported me during my PhD. To everyone who encouraged me to follow my inspiration to develop this set of methods. To everyone who was cheering me up in difficult moments.

My family.

My friends.

My colleagues.

My supervisors.

"Probleme kann man niemals mit derselben Denkweise lösen, mit der sie entstanden sind"

"You can never solve problems with the same mindset that created them"

A. E.

Abstract / Resumen / Kurzbeschreibung

Abstract. It is well known that injuries affect the tissue integrity. It might be less known that injury mechanisms could be initiated through a compromised cell response, which subsequently affects the tissue integrity. Such injuries are subsequently referred to as biologically-driven injuries. They usually develop over long time periods, and disease progression remains largely silent. Biologically-driven injury mechanisms are still poorly understood, which is partly related to limited methodologies to estimate complex, dynamic cell responses over long periods of time.

To this end, this work presents a novel network modelling approach to tackle complex multicellular systems. Thereby, the cell is considered as a "black box" and cell activities, such as mRNA expressions, were directly linked to the surrounding stimulus environment, based on experimental knowledge. To achieve that, a set of integrative methodologies was developed to translate experimental findings into parameters suitable for systems biology models, and to numerically approximate cell activities within complex multicellular environments. This set of methodologies is presented as "PN_t-Methodology". The acronym "PN_t" refers to the conceptualization of cell activities, as numerous potentially time-dependent (subscript t) networks that are simultaneously acting, i.e. parallel networks (PN).

The PN_t-Methodology was developed to investigate the intervertebral disc (IVD) Nucleus Pulposus, the degradation of which is assumed to be highly biologically-driven. The objective was to better understand the initiation of IVD degeneration. The effects of key relevant biochemical (glucose, lactate) and mechanical stimuli (load magnitude and frequency) on non-degenerated Nucleus Pulposus cells were investigated. The multicellular system was simulated within a 3D agent-based model and contained both non-inflamed and inflamed cells, whereby the proinflammatory mediators IL1β and TNF-α were considered. This led to four different cell states; non-inflamed, inflamed with IL1β, TNF-α or both, IL1β&TNF-α. For each cell state, the mRNA expressions of the main tissue proteins Aggrecan and Collagen Types I & II and of the crucial proteases MMP3 and ADAMTS4 were estimated. The qualitative results of the model could successfully be validated with findings from the literature through the different steps of development. Eventually, CA of different CS were approximated for different body postures and physical activities, including long-term predictions.

To the best of our knowledge, this is the first *in silico* approach that tackles the cellular level in IVD research. Furthermore, thanks to its generic and scalable design, the PN_t-Methodology is adaptable to more complex cell environments and is expected to be applicable to multicellular systems of other tissue. Hence, this contribution complements existing *in silico* methods by providing a new top-down high-level network modelling approach based on biological measurements to approximate the dynamics of biologically-driven injury mechanisms.

Resumen. Está conocido que las lesiones afectan la integridad de un tejido. Lo que quizás está menos conocido es que los mecanismos que causan estas lesiones podrían ser iniciados por una respuesta celular comprometida, la cual afecta la integridad de un tejido. A continuación, se refiere a este tipo de lesiones como lesiones con origen biológico. Estas lesiones suelen desarrollarse muy lentamente con una progresión mayormente silenciosa. Todavía no se entienden bien los mecanismos de este tipo de lesiones, lo cual en parte está relacionado con limitaciones metodológicas que permiten estimar respuestas complejas y dinámicas de células durante largos periodos de tiempo.

Este trabajo presenta una metodología nueva de modelado de redes para aproximar sistemas complejos en un entorno multicelular. Se considera la célula como una caja negra y las actividades celulares, como expresiones de ARNm, se vinculan directamente con los estímulos que reciben las células, según datos experimentales. Para conseguir esto, se desarrolló un conjunto de métodos integrativos que permiten el traslado de resultados experimentales en parámetros adecuados para modelos de biología de sistemas, y para aproximar numéricamente actividades celulares en entornos complejos multicelulares. Este conjunto de métodos esta presentado como "Métodología-RP_t" (PN_t-Methodology). El acrónimo "RP_t" se refiere a la conceptualización de actividades celulares como numerosas redes, potencialmente dependiendo del tiempo (indexado t) que están actuando simultáneamente, es decir, como redes paralelas (RP).

La Metodología-RP_t se desarrolló para investigar el Nucleus Pulposus del disco intervertebral, la degradación del cual podría ser mayoritariamente causada por lesiones de origen biológicos. El objetivo fue entender mejor el inicio de la degeneración del disco intervertebral. Los efectos de estímulos claves bioquímicos (glucosa, lactato) y mecánicos (magnitud y frecuencia de una carga) fueron investigados en

células no degeneradas del Nucleus Pulposus. El sistema multicelular es simuló en un modelo 3D basado en agentes que incluyó células tanto no inflamadas como inflamadas, considerando los mediadores proinflamatorios IL1β y TNF-α. En consecuencia, se definieron cuatro estados celulares: células no inflamadas, inflamadas con IL1β, inflamadas con TNF-α o inflamadas con ambos, IL1β&TNF-α. Para cada estado celular, se estimó la expresión de ARNm de las proteínas estructurales principales del tejido, Agrecano y Colágeno tipo I & II y de las proteasas claves MMP3 y ADAMTS4. Los resultados cualitativos del modelo se pudieron validar exitosamente con resultados experimentales de la literatura a lo largo del desarrollo. Finalmente, se pudieron aproximar las actividades celulares para diferentes posturas corporales y actividades físicas, incluyendo predicciones durante largos periodos tiempo.
A nuestro entender, este es el primer método *in silico* que trata el nivel celular en la investigación del disco intervertebral. Además, gracias a su diseño genérico y escalable, la Metodología-RP_t se puede adaptar a entornos más complejos, y se puede vislumbrar su aplicación a sistemas multicelulares de otros tejidos.
Por lo tanto, esta contribución complementa los métodos *in silico* existentes al ofrecer una nueva estrategia top-down de modelado de redes de alto nivel (high-level), basado en resultados experimentales para aproximar las dinámicas de los mecanismos causantes de lesiones con origen biológico.

Kurzbeschreibung. Es ist bekannt, dass Verletzungen die Integrität eines Gewebes stören. Es ist möglicherweise jedoch weniger bekannt, dass ein beeinträchtigtes Zellverhalten ursächlich für solche Verletzungen sein kann. Diese werden im Folgenden als biologisch-basierte Verletzungen bezeichnet. Biologisch-basierte Verletzungen entwickeln sich normalerweise langsam und dessen Fortschreiten bleibt oft unbemerkt. Das Verständnis solcher Verletzungsmechanismen ist limitiert, da die Möglichkeiten, komplexes, dynamisches Zellverhalten über längere Zeitspannen anzunähern, eingeschränkt sind.
Demzufolge präsentiert diese Arbeit einen systembiologischen Ansatz mit dem Ziel, komplexe multizelluläre Systeme zu simulieren. Dafür wurde die Zelle als «black box» interpretiert und ihre Aktivitäten, zum Beispiel die Expression von mRNA, mittels experimenteller Erkenntnisse in Verbindung zum zellulären Stimulus Umfeld gesetzt. Eine Reihe von integrativen Methoden ermöglichte es, Informationen aus Experimentalstudien in Parameter zu überführen, welche für systembiologische Modelle genutzt werden können und es erlauben, ein

komplexes multizelluläres Umfeld rechnerisch anzunähern. Diese integrativen Methoden werden unter dem Überbegriff «PN_t-Methodik» zusammengefasst. Das Akronym «PN_t» beschreibt die Betrachtungsweise von Zellaktivitäten als zahlreiche, zeitabhängige (Index t) nebeneinander laufende Netzwerke, parallele Netzwerke (PN) genannt.

Die PN_t-Methodik wurde entwickelt, um Zellen des Nucleus Pulposus einer Bandscheibe zu approximieren, da diese ein Gewebe darstellt, dessen Degeneration auf biologisch-basierte Verletzungsmechanismen zurückgeführt werden. Ziel war es, Gründe, die zu Bandscheibendegenerationen führen zu eruieren. Dafür wurde der Einfluss von entscheidenden biochemischen (Glucose, Laktat) und mechanischen Stimuli (axiale Belastung (Magnitude) und Frequenz) auf nicht-degenerierte Nucleus Pulposus Zellen simuliert. Das multizelluläre System wurde in einem 3D Agentenbasierten Modell simuliert und besteht aus nicht-entzündeten und entzündeten Nucleus Pulposus Zellen, wobei der Effekt der Entzündungsparameter IL1β und TNF-α berücksichtigt wurde. Dies führte zu vier verschiedenen Zellstatus: nicht entzündet, oder unter dem Einfluss von IL1β, TNF-α oder IL1β&TNF-α stehend. Für jeden Zellstatus wurden die mRNA Expressionen für die zentralen Gewebeproteine Aggrecan und Kollagen Typen I & II und die Proteasen MMP3 und ADAMTS4 approximiert. Die qualitativen Resultate waren in jeder Entwicklungsphase in guter Übereinstimmung mit Erkenntnissen aus der Literatur. Letztlich konnten Zellaktivitäten bei unterschiedlichen Bewegungsverhalten, inklusive Prognosen über längere Zeiträume, approximiert werden.

Gemäss unserem Wissen ist dies die erste *in silico* Studie in der Bandscheibenforschung, die Ergebnisse auf der zellulären Ebene liefert. Dank ihrem generischen und skalierbaren Design ist die PN_t-Methodik grundsätzlich auch auf multizelluläre Systeme von anderen Geweben anwendbar und erlaubt eine Extension des existierenden Netzwerks. Somit ergänzt die hier präsentierte Arbeit existierende *in silico* Methoden durch einen neuen Netzwerk-basierten Top-down-Ansatz, basierend auf experimentellen Erkenntnissen, der es erlaubt, die Dynamiken von biologisch-basierten Verletzungsmechanismen anzunähern.

Preface

The objective of this PhD project was to contribute to a better understanding of biologically-driven injury mechanisms, hence, injuries that emerge from adverse cell behavior. Therefore, a set of *in silico* methods was developed to allow an approximation of individual cell responses to heterogenous, multifactorial (micro-) environments, including dose- and time-dependent cell responses.

This work consists of four self-contained papers that are reflected as Chapters 2 – 5.

- Chapter 2: Baumgartner L., Wuertz-Kozak K., Le Maitre C. L., Wignall F., Richardson S. M., Hoyland J., et al. (2021): Multiscale regulation of the intervertebral disc: Achievements in experimental, *in silico*, and regenerative research. Int. J. Mol. Sci. 22, 703. doi:10.3390/ijms22020703.
- Chapter 3: Baumgartner L., Reagh J. J., González Ballester M. A., and Noailly J. (2020): Simulating intervertebral disc cell behaviour within 3D multifactorial environments. Bioinformatics, 1–8. doi: 10.1093/bioinformatics/btaa939
- Chapter 4: Baumgartner L., Sadowska A., Tío L., González Ballester M. A., Wuertz-Kozak K. and Noailly J.: *Evidence-based Network Modelling to Simulate Nucleus Pulposus Multicellular Activity in different Nutritional and pro-Inflammatory Environments* Submitted to Front. Bioeng. Biotechnol. (accepted for publication, doi: 10.3389/fbioe.2021.734258).
- Chapter 5: Baumgartner L., González Ballester M. A. and Noailly J.: *The PN_t-Methodology: a Top-Down Network Modelling Approach to Estimate Dose- and Time-Dependent Cell Responses to Complex Multifactorial Environments* (Manuscript ready)

Table of contents

Acronyms

AB	Agent-based
AF	Annulus Fibrosus
ADAMTS	A disitegrin and metalloproteinase with thrombospindin motifs
Agg	Aggrecan
BC	Boundary condition
CA	Cell activity
CEP	Cartilage Endplate
Col-I	Collagen Type I
Col-II	Collagen Type II
CS	Cell state
ECM	Extracellular matrix
ERK	Extracellular signal-regulated kinase
FA	Focal adhesion
FCS	Fetal calf serum
FE	Finite Element
FEM	Finite Element modelling
GAG	Glycosaminoglycan
GF	Growth factor
glc	Glucose
HIF	Hypoxia inducible factor
IL	Interleukin
IVD	Intervertebral disc
lac	Lactate
MAPK	Mitogen-activated protein kinases
MMP	Matrix metalloproteinase
mTOR	Mammalian target of rapamycin
NF-κB	Nuclear factor kappa B
NP	Nucleus Pulposus
ODE	Ordinary differential equation
PG	Proteoglycan
PKN	Prior-knowledge-network
PN	Parallel network
TNF	Tumor necrosis factor
TonEBP	Tonicity-responsive enhancer binding protein
TonEBP/NFAT5	Tonicity-responsive enhancer binding protein/nuclear factor of activated T-cells 5
TRP	Transient receptor potential

1 Introduction

1.1 Motivation and objective

Mechanical loads play a crucial role in the development and maintenance of biological structures. Thereby, aspects such as loading type, intensity, duration and direction largely determine their effect on a body structure. If loading conditions exceed a tissue-specific threshold, injury might occur (Schmitt et al., 2019). The research field that investigates the severity of a loading condition on a body structure is the field of trauma biomechanics (biomechanics of injury). Thereby, tolerance levels of load are estimated throughout spatial scales from cellular to whole body levels.
Although injury biomechanics usually focusses on the impact of load on tissue integrity, recently more attention has been brought to biological aspects (Meaney et al., 2014; Gennarelli, 2019). This includes the biological response to an injured tissue, but also the effect of loads on cell responses. Cells are responsible for the tissue maintenance, and they build and degrade the extracellular matrix (ECM) according to the (micro-) environmental stimuli they perceive. A hypothesized injury mechanism suggests that an adverse cell activity (CA) progressively decreases the ability of a tissue to resist to external loads. As a result, already physiological loading conditions are able to cause injuries within tissue structures, leading to (local) accumulations of small injuries (microtrauma). Such an injury mechanism is subsequently referred to as biologically-driven injury mechanism.

Hence, there is an unmet need for advanced research on the understanding of biological aspects of injury emergence.

Biologically-driven injuries usually reflect a slowly advancing disruption of a tissue, such as observed within the intervertebral disc (IVD).
The IVD is a conjunction of cartilaginous tissues that separates the vertebras of the spine and provides the back with flexibility. It consists of a load-bearing, gel-like center, the Nucleus Pulposus (NP), which is surrounded by the Annulus Fibrosus (AF), a juxtaposition of fibrotic lamellae. A thin layer of cartilage, the Cartilage Endplate (CEP) separates the NP and the inner part of the AF from the bony endplate (Urban and Roberts, 2003)(Figure 1.1).

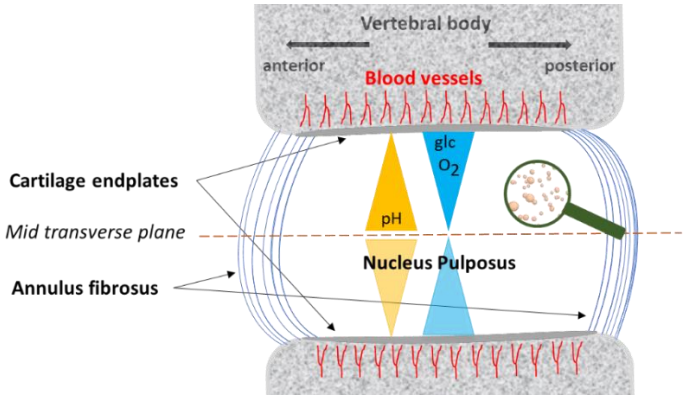

Figure 1.1: schematic, sagittal cut through an IVD, indicating a glucose (glc), oxygen (O_2) and pH gradient between the cartilage endplates and the mid-transverse plane.

The IVD is the biggest avascular tissue of the human body (mentioned by Soukane et al., 2007). Nutrient transport to cells is diffusion dependent, with a main nutrition supply of the NP by the capillaries within the bony endplates, passing through the CEP (Urban et al., 2004). Consequently, important concentration gradients of glucose (glc) and oxygen molecules between the CEP and the mid-transversal plane of the IVD exist (Figure 1.1). Due to the low oxygen availability within the tissue, cell metabolism is highly anerobic, with only around 1.5 % of glc being converted to carbon dioxide (Holm et al., 1981). This leads to high concentrations of lactic acids, forming an opposite gradient between the NP mid transverse plane towards the CEP (Figure 1.1). Hence, in addition to the constant exposure of the IVD to complex loading conditions, the nutritional environment within the tissue, especially within the NP, is harsh.

Nevertheless, under non-degenerated conditions, the IVD is highly loading-resistant and clinical pictures from high impact accidents, such as falls from high heights, reveal IVD failure mostly in the context of extended soft tissue injuries and vertebral fractures, whilst isolated IVD failures are unlikely to occur (Veres et al., 2008; Schmitt et al., 2019).

However, the tissue appears to be prone to progressive, adverse changes, as IVD degeneration is a common clinical condition. It is diagnosed as the reason for around 40% of low back pain cases, which up to 85% of people suffer at some point during their lifetime (Smith et al., 2011; Baumgartner et al., 2021). Thus, accelerated degeneration of IVD, instead of "normal" aging, reflects an important socioeconomic burden, since low back pain causes more disability worldwide than any other condition (Hoy et al., 2014).

However, reasons why IVD degenerate, rather than age, are still not entirely understood.

Cell responses in terms of mRNA expression or protein synthesis are the result of complex intracellular dynamics regulated by a vast amount of mainly biochemical and mechanical stimuli within the cellular (micro-) environment. Impressive experimental research allowed for a better understanding of cell responses to altered stimulus environments and intracellular signal transduction pathways (cf. Chapter 2). However, within the IVD research area, *in silico* advances focus on Finite Element (FE) simulations at the organ/tissue level (e.g. Magnier et al., 2009; Malandrino et al., 2015b; Ruiz Wills et al., 2018) rather than on cellular and subcellular levels.

To the best of our knowledge, no in silico approach is available so far that allows to approximate individual cell activity within the IVD

This might be due to general, technical limitations to investigate biologically-driven injury mechanisms, which require

i. an estimation of manifold cell responses to complex, multifactorial microenvironments
ii. approximations of changes in cell responses due chronic (adverse) stimulus environments
iii. a mathematical solution that allows to simulate cell responses over long periods of time (months to years) under a reasonable computational cost

Current *in silico* methodologies usually focus on complex simulations of vast intracellular pathways using logic modeling approaches such as fuzzy-logic, Boolean and ordinary differential equation (ODE) formalisms (cf. Chapter 2). To simulate dynamics (usually at a cellular or tissue level) modelling techniques such as FE or Agent-based (AB) models are widely used. However, such techniques are usually coupled to time consuming calculations accompanied by elevated computational costs. Network models, in contrast, allow large scalability in terms of nodes and interactions but can easily loose directionality, which makes difficult the proper integration of experimental evidence and the calculations of unequivocal results. Moreover, an integration of dose- and time-dependent network responses and a consideration of heterogenous stimulus environments is challenging.

Hence, there is a need for straightforward approximations of complex multifactorial cell environments, which allow for predictions of dynamic cell responses over long time periods.

Therefore, the objective of this PhD thesis is:

The development of in silico methods that allow to approximate dynamic cell responses to complex (heterogenous) multifactorial environments present in the IVD to tackle biologically-driven injury mechanisms.

These methods have to be scalable in terms of the variety of environments and cell responses that can be represented and they should be able to simulate long-term cell stimulation effects.

1.2 Contributions

Accordingly, this thesis presents a novel numerical approach to tackle complex cellular dynamics, which is presented as the PN_t-Methodology. The acronym "PN_t" reflects the view of different cell responses, e.g. in terms of mRNA expression or protein synthesis, as numerous potentially time-dependent (subscript t) simultaneously acting networks, hence, parallel networks (PN). The PN_t-Methodology is a high-level, top-down network modelling approach. Thereby, the cell is considered as a "black box" that shows a certain response to a given multifactorial stimulus environment. Hence, the stimulus environment is directly linked to key relevant CA without considering subcellular network regulations. This approach is spatially located at a multicellular level, i.e. between the subcellular and the tissue level (Figure 1.2).
It is based on the hypothesis that alterations in homeostasis (e.g. catabolic shifts in cell responses) is not a spontaneous event, but is initiated by alterations of external stimuli. External stimuli refer to stimuli that are not locally synthesized but reach a cell from external sources. Such external stimuli regulate adaptations in cellular homeostasis, e.g. tissue proteins or protease production or the secretion of local stimuli, such as proinflammatory parameters or growth factors. That been stated, this methodological approach requires a careful preselection of key relevant stimuli and CA. For its determination, knowledge from experimental research is used.

The PN_t-Methodology was developed throughout this thesis and encloses

- *methods to:*
  - *estimate the effect of a stimulus concentration on a CA*
  - *estimate the effect of a stimulus type on a CA*
  - *approximate time sensitivities (depending on the stimulus dose) of a CA exposed to chronic stimulus environments.*
- *a mathematical framework that allows to integrate the aforementioned methods and estimate complex multicellular environments over extended periods of time.*

The complex multicellular environment within the NP was simulated by tackling key relevant external stimuli that appear to be nutrition-related and mechanical factors (e.g. Urban et al., 2004; Chan et al., 2011). Furthermore, locally expressed inflammatory parameters play a crucial role in IVD degeneration (Wuertz and Haglund, 2013), since their presence might alter cell responses (e.g. Le Maitre et al., 2005). The proinflammatory cytokines Interleukin 1 beta (IL1β) and the tumor necrosis factor alpha (TNF-α) seem to be particularly relevant in degenerative processes (Johnson et al., 2015b). Cells immunopositive for IL1β and TNF-α were generally present in the NP, i.e. also within the non-degenerated tissue (Le Maitre et al., 2007b). Hence, the multicellular environment opted for this work consisted of cells of different proinflammatory cell states (CS), being either non-inflamed, IL1β inflamed, TNF-α inflamed and inflamed for both IL1β & TNF-α (Figure 1.2).
The cell responses to those microenvironmental cues, i.e. the tackled CA, were the mRNA expressions of tissue proteins and proteases relevant in IVD degeneration. This included Aggrecan (Agg), Collagen Types I & II (Col-I, Col-II) and proteases from the metalloproteinase (MMP) and "a disintegrin and metalloproteinase with thrombospondin motifs" (ADAMTS) families (Figure 1.2). mRNA expressions were simulated for each CS within the multicellular system.
The multicellular environment was simulated within a 3D AB model, where NP cells were reflected as agents. The user defines initial doses of external stimuli (glc, lac, mag, freq) and the duration, over which the given stimulus combination acts on the cells. Based on the user-defined input, the model estimates and visualizes different CS. The PN_t-Methodology is embedded within the AB model and predicts the CA of each CS under given environmental conditions.

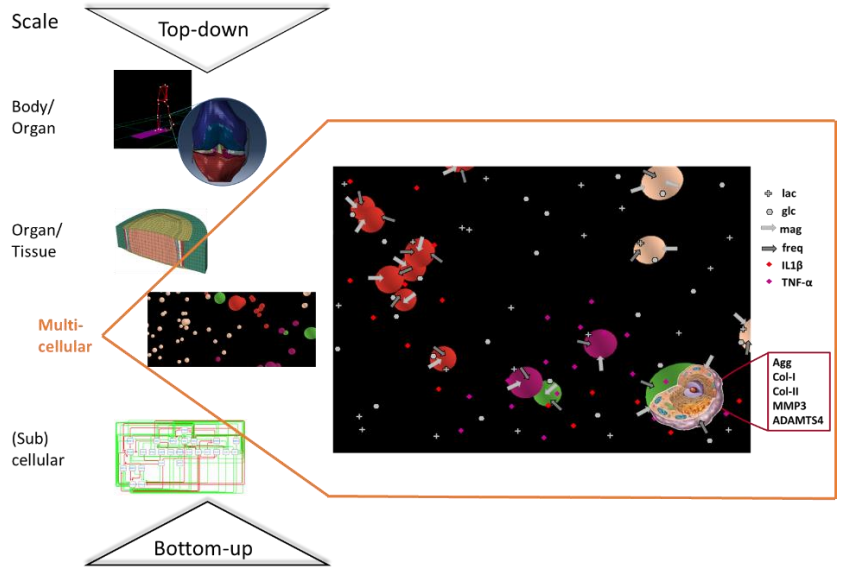

Figure 1.2: The PN_t-Methodology tackles the multicellular level, where multifactorial and multicellular environments are approximated. Thereby, the effect of nutrient-related and mechanical external stimuli were considered. This included glucose (glc), lactate (lac), magnitude (mag), frequency (freq). Heterogenous multicellular environments emerge from the locally expressed proinflammatory mediators interleukin 1 beta (IL1β) and tumor necrosis factor alpha (TNF-α). Thus, the multicellular environment consists of four different cell states: non-inflamed cells (beige) and cells immunopositive for IL1β (red), TNF-α (violet) or both, IL1β&TNF-α (green). Cell activities in terms of tissue protein (Aggrecan (Agg), Collagen Type I & II (Col-I, Col-II)) and protease (MMP3 and ADAMTS4) mRNA expressions of each cell state were obtained. Pictures were kindly provided by the Biomechanics and Mechanobiology laboratory: Simone Tassani (Body/Organ level), Carlos Ruiz Wills (Organ/Tissue level) and Maria Segarra ((Sub) cellular level). The cell anatomy was obtained from: https://www.thinglink.com/user/611122 694879969280, accessed the 18.04.2018.

1.3 Structure of the thesis

The thesis consists of six chapters. Chapters 2-5 are self-contained and reflect published papers or papers under internal / external review. Chapter VI wraps this work up in a conclusion, research summary and future work.

Chapter 2 provides the state of the art of research on multiscale regulation of the IVD. It encloses sections 1-3 and 5 of the review paper

published in the International Journal of Molecular Sciences (Baumgartner et al., 2021).

Chapter 3 reflects the work presented in Bioinformatics (Baumgartner et al., 2020). It provides a detailed description of the AB model and the methodology to estimate the effect of the sensitivity of a CA to a stimulus concentration (in chapters 4 and 5 referred to as x_S^{CA}). Furthermore, approaches are presented to estimate the effect of the proinflammatory cytokine IL1β and cell viability. Thereby, the effect of indirect mechanotransduction is tackled. Hence, the impact of nutrition-related external stimuli (glc and lac) on cell viability and CA of non-inflamed and IL1β inflamed cells is investigated. CA are the principal tissue proteins Aggrecan (Agg) and Collagens Type I & II (Col-I, Col-II), the protease MMP3 and a general estimation for the ADAMTS protease family.

Chapter 4 corresponds to a journal paper currently under review. It reflects interdisciplinary work consisting of experimental, numerical and modelling parts. Specific *in vitro* experiments were carried out to improve current model predictions (e.g. to allow to punctually target ADAMTS4 mRNA expression out of the ADAMTS-family) and to extend the simulation of indirect mechanotransduction by integrating the impact of the proinflammatory cytokine TNF-α. Accordingly, *in silico* developments focus on the simulation of a multicellular environment of four CS: non-inflamed, IL1β inflamed, TNF-α inflamed and inflamed for both IL1β&TNF-α. The PN_t-Methodology was further developed by presenting an approach to approximate the effect of a stimulus type on a CA.

Chapter 5 presents work on the development of the core element of the PN_t-Methodology; a mathematical framework that allows to calculate time-sensitive parallel networks by an integration of the previously defined parameters to estimate the impact of a stimulus concentration (Chapter 3) and the stimulus type (Chapter 4) on a CA. Furthermore, an approach is presented to integrate direct mechanotransduction, i.e. the mechanical loading parameters magnitude and frequency. The integration of direct mechanotransduction includes a method to estimate time-sensitive cell responses in function of a current stimulus dose.

Chapter 6 contains an overall conclusion of the presented work and summarizes the workflow of its development over time, including the most relevant findings at each research stage. Eventually, most relevant future reserach directions were pointed out.

2 *State of the Art*

This chapter is adapted from the chapters 1-3 and 5 of the review paper: Baumgartner L., Wuertz-Kozak K., Le Maitre C. L., Wignall F., Richardson S. M., Hoyland J., et al. (2021): *Multiscale regulation of the intervertebral disc: Achievements in experimental, in silico, and regenerative research.* Int. J. Mol. Sci. 22, 703. doi:10.3390/ijms22020703.

2.1 Introduction

The intervertebral disc (IVD) is a major mechanical load-bearing organ and is responsible for the functional articulation of the spine. It is composed of three tissues: the nucleus pulposus (NP), the annulus fibrosus (AF), and the cartilage endplate (CEP) that strongly interact among each other. These interactions depend on the composition and ultrastructure of each tissue that are largely regulated by the response of the disc cells to microenvironmental biological, chemical, and physical cues, transmitted to the cells through the extracellular matrix (ECM). A balance between anabolic and catabolic processes on a cellular level, i.e., tissue homeostasis, is essential for a healthy turnover of the ECM components and optimal aging (Urban and Roberts, 2003; Le Maitre et al., 2004, 2007c; Shapiro and Risbud, 2016). In contrast, the perturbation of this equilibrium might cause IVD degeneration, with elevated catabolic activity leading to disease progression (Sztrolovics et al., 1997; Roberts et al., 2000; Weiler et al., 2002; Shapiro and Risbud, 2016).

The first morphological signs of IVD degeneration might appear already during adolescence and largely progress toward moderate to advanced degeneration within the three next decades of life (Antoniou et al., 1996). Such progression is manifest in MRI images (Benneker et al., 2005b), visible though a general reduction of the disc height; a shift of image signal in the NP toward inhomogeneous, gray or black shaded nuances that reflect dehydration and cracks; a loss of distinction between the NP and AF regions; and possible endplate defects and disc bulging or herniation (Pfirrmann et al., 2001; Benneker et al., 2005b; Galbusera et al., 2014). It is commonly believed that these changes start with a drop of pressure within the NP because of dehydration.

On the one hand, the drop of intradiscal pressure makes the axial deformation of the disc increase under the action of external mechanical loads, which eventually favors the collapse of the AF structure. The AF lamellae become unorganized, fissured, and used to bulge within the NP and/or outward (Adams and Roughley, 2006). On the other hand, water loss is commonly interpreted as a consequence of proteoglycan (PG) depletion (Urban and Roberts, 2003). Interestingly, theoretical simulations associated the loss of PG and tissue swelling with the propagation of radial crack formation (Wognum et al., 2006), leading to radiating annular tears (Osti et al., 1992), which might end up in IVD herniation.

Though appealing, such a systematic explanation of IVD degeneration progression explains only a subset of herniated IVD phenotypes (Lama

et al., 2013), i.e. the AF-driven phenotype of IVD degeneration. Even though, the spatiotemporal emergence of several subsets of phenotypes related to different types of AF tears (Osti et al., 1992; Sharma et al., 2009) remains difficult to explain. Furthermore, endplate-driven IVD degeneration is also recognized as a source of important disc disease phenotypes (Adams and Dolan, 2012). Signs of inflammation around the endplate, called Modic changes, are often visible (Teichtahl et al., 2016) and have been associated with IVD degeneration (Kerttula et al., 2012), with endplate defects and with severe low back pain (Määttä et al., 2018; Munir et al., 2018a). Yet, the associated pathophysiology remains largely unexplained. Interestingly, the understanding of IVD-related diseases differs between authors, which led to an attempt to standardize the nomenclature about normal and pathological lumbar disc by the "Combined Task Forces of the North American Spine Society" (Fardon et al., 2014). In any case, degenerative disc changes at the tissue level alter the mechanics of the entire IVD (Adams and Roughley, 2006) and account for at least 40% of all low back pain cases (MacGregor et al., 2004; Livshits et al., 2011).

The IVD architecture provides the non-degenerated IVD with adequate resistance to traumatic loading, as seen in sport or traffic accidents, such that isolated, traumatic IVD ruptures are hardly seen (Schmitt et al., 2019). Disc rupture is, therefore, widely accepted to be a slow process, consisting of an accumulation of micro injuries under rather physiological loads, promoted by intricate biochemical and mechanobiological processes that end up in debilitated tissues. Considerable progress has been made over the past 20 years identifying risk factors for IVD degeneration, and the condition, long thought to be secondary to occupational loading, has also been shown to be highly heritable (Sambrook et al., 1999; Battié et al., 2009). Yet, heredity was confirmed to be significant (55%) for a reduced number of phenotypes such as endplate defects (Munir et al., 2018a) and explains less than 50% of the progression of IVD degeneration in the lower lumbar spine (Battié et al., 2009) where mechanical loads are the highest. More recently, greater understanding of the interplay between genes, cellular behavior, and mechanobiology has been achieved (Hughes et al., 2012), and a causal link has been proposed between IVD pathology and the expression of cytokines and of structural protein proteases from resident cells (Le Maitre et al., 2005; Séguin et al., 2008; Wang et al., 2011; Risbud and Shapiro, 2014; Dudli et al., 2018).

The understanding of the multiple interplays within the IVD is further challenged by the need to consider the delicate nutritional balance to

ensure cell survival and activity (Huang et al., 2014) in what is the largest avascular organ of the human body. Controlling inflammation, nutrition, mechanical deformations, and the interactions thereof appears cornerstone, therefore, to understand where to act, to slow down, stop, or reverse IVD degeneration through molecular or cellular therapies or biomaterial-based strategies. Current literature provides a wealth of information about the response of IVD cells to inflammatory, nutritional, and mechanical isolated stimuli. Yet, such knowledge is not sufficient to apprehend and control the complex combination of factors that effectively shape the microenvironment of disc cells *in situ*. The comprehensive understanding of the emergence and net effect of multiple combinations of cell stimulators is difficult to achieve through experimental and/or clinical observations. Fortunately, computational implementations of theoretical mechanical, multiphysics, and biology models are constantly growing, and simulations reveal unsuspected capacity to reasonably predict multifactorial tissue or ECM regulation at different scales (Gu et al., 2014; Baumgartner et al., 2020) or specific degeneration paths (Ruiz Wills et al., 2018).
Accordingly, this review aimed to provide an overview of the latest findings about the IVD function and regulation in health and disease at the tissue, cell, and molecular levels; about progresses in IVD regenerative medicine; and about *in silico* research for knowledge integration and discovery over different time and length scales.

2.2 IVD Extracellular Matrix in Health and Disease

The biochemistry and the ultrastructure of the intervertebral disc ECM regulate the physical interactions among the disc tissues, i.e., the CEP, the AF, and the NP, and provide the IVD with unique mechanical functions (Setton and Chen, 2004; Raj, 2008). The main ECM components of the IVD tissues are water, collagen (types I and II), and PG, and the relative contents and organization of these components are finely tuned in each disc tissue (Raj, 2008; Schroeder et al., 2010) (Figure 2.1).

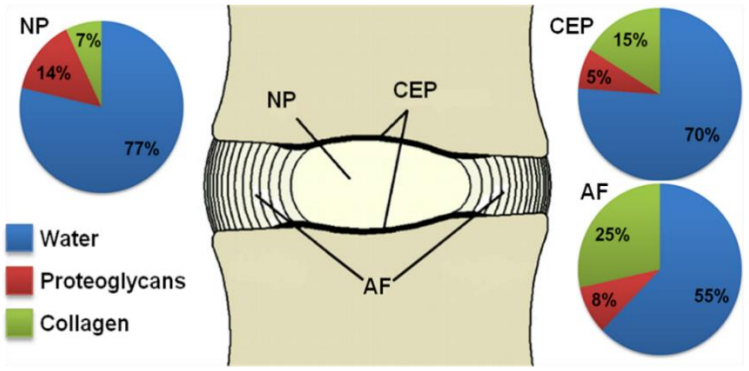

Figure 2.1: Biochemical composition of disc tissues ((Ruiz Wills, 2015), adapted from (Smith et al., 2011)).

The solid matrix of the NP mostly contains PG and non-oriented collagen type II, while the CEP contains PG and highly oriented collagen type II (DeLucca et al., 2016). The AF is made of concentric bundles of collagen types I and II. While collagen type I is predominant, the relative amounts of collagen type II increase from the outer AF to the inner AF, adjacent to the NP (Brickley-Parsons and Glimcher, 1984). PG is present in the interlamellar space, along with small amounts of elastic fibers and other types of fibrils (Tavakoli et al., 2016). It has been demonstrated that the turnover rate of collagen and aggrecan in the IVD is relatively slow due to long half-lives, i.e., around 95 and 12 years, respectively (Sivan et al., 2006, 2008).
Interestingly, collagen turnover rate decreases with age, along with increased synthesis of types I and III collagen (Le Maitre et al., 2007c), whereas the turnover rate of aggrecan increases, the result being a gradual progression of a more fibrotic and less hydrated tissue with increasing age. In the following subsections, the current knowledge about the main ECM components' PG, collagens, and water is summarized.

2.2.1 Proteoglycans

Aggrecan is the principal PG inside the IVD. Glycosaminoglycan (GAG) chains are attached to the main core protein of the PG, and they contain negatively charged sulphated groups (Roberts and Urban, 2011). The size and aggregation of PG molecules impedes these negative charges to move spatially and, because tissue electro-neutrality needs to be respected, small counter-ions, e.g., potassium and sodium, are attracted from the interstitial fluid, generating a gradient of chemical potentials between the regions respectively internal and external to the

disc. Such a gradient can only be reduced through the entrance of water in the IVD, known as Donnan osmosis. The tissues swell and the collagen fibers become tensed, leading to an intradiscal osmotic pressure. Osmotic pressurization and IVD hydration are crucial for the basal hydration of the NP and the functional biomechanics of the IVD. With age or degeneration, the total content of PG decreases in all disc tissues (Singh et al., 2009; Fields et al., 2014), and increased amounts of small non-aggregating PG are found (Roughley et al., 2006; Singh et al., 2009). In the NP, the drop of PG content and non-aggregating PG negatively affect the osmotic potential and the capacity of the tissue to attract water. Whether the loss of PG affects the mechanical stability of the IVD at the macroscopic level remains unclear (van Rijsbergen et al., 2017), but theoretical approaches suggest that it favors the initiation and propagation of radial cracks through the IVD (Wognum et al., 2006), as observed in IVD specimens (Osti et al., 1992). Furthermore, the accumulation of non-aggregating PG might favor the transport of small glycans out of the disc during daily load cycles (DeLucca et al., 2016), and IVD glycoprofiles might be a hallmark of IVD degeneration (Joyce et al., 2018). High-weight hyaluronan-based molecules were pointed out as potential protectors against IVD degeneration (Pandit and Mohd Isa, 2020), whereas hyaluronic acid fragments would increase the expression of key inflammatory cytokines by IVD cells (Quero et al., 2013). Interestingly, during normal aging the IVD shows less than 1% height loss per year, whereas degenerating discs loose approximately 3% height per year (Adams and Dolan, 2012).

In the AF, PG is mostly present in interlamellar spaces. On the one hand, these interlamellar spaces have been identified as the preferred path for the extrusion of nuclear material (Veres et al., 2008). On the other hand, single nucleotide polymorphism associated to the aggrecanase ADAMTS 5 has been significantly associated with AF tears in IVD degeneration (Rajasekaran et al., 2013), suggesting a relevant implication of interlamellar PG in the IVD pathophysiology. In the CEP, the control of the mobility of molecules by PG probably ensures key protection against the loss of structural proteins and water through the bony endplates (Roberts et al., 1996). While PG depletion with age or IVD degeneration might explain the increased permeability of the CEP measured with aging (Rodriguez et al., 2011), *in silico* models suggest that the fine-tuning of PG contents within the CEP is actually important to avoid critical chronic dehydration of the IVD under daily mechanical loads (Ruiz Wills et al., 2018).

2.2.2 Collagen

Collagen types II and I are the major structural component of the IVD. Type I collagen forms highly oriented concentric lamella within the AF, which provides the AF with resistance to multiaxial loads and finely tunes the mechanical strength of the disc. Collagen type II forms a loose network, especially within the NP, and it is more extensible than collagen type I (Silver et al., 2002; Fernandes et al., 2003).

In the NP, the flexibility of collagen type II network allows the swelling of the PG through Donnan osmosis, whereas the elastic response of the stretching fibers generates tissue turgidity, providing the IVD with strength under high pressurization and relative flexibility otherwise. The first oriented collagen bundles appear in the transition zone between the NP and the AF and the proportion of collagen type I to collagen type II increases toward the outer AF (Brickley-Parsons and Glimcher, 1984). The presence of collagen type II would limit the lateral aggregation of collagen type I fibrils and leads to matrices of increased porosity (Vázquez-Portalatín et al., 2016), which fosters proper hydration of the inner IVD and the transport of molecules to disc cells. At the same time, the increasing amount of collagen type I toward the outer AF increases the effective resistance to fluid flow, favoring hydrostatic pressures and proper cell phenotypes in the inner AF (Bruehlmann et al., 2002). The CEP matrix has predominantly collagen type II fibers. While it needs to allow the transport of important solutes between the disc and the bone marrow (Rajasekaran et al., 2004), its hydraulic permeability, of the order of 1.10^{-14} m^4/Ns (Accadbled et al., 2008), is one order of magnitude lower than the radial permeability of the AF (Gu et al., 1999). Interestingly, piezoelectric potentials associated with the disc collagen fibers have been measured and were suggested to be one of the triggers of functional cell alignments, especially in the AF (Poillot et al., 2020). In general, it is clear that the functional distribution of collagen types I and II throughout the IVD supports multiple important functions.

With degeneration or aging, the relative amount of collagen type I increases in the NP (Antoniou et al., 1996), which in addition to PG depletion would also explain the dehydration of the IVD, i.e., reductions of tissue porosities (Ruiz Wills et al., 2016), in general. Decreased tissue porosity due to modified balance between collagen types I and II would explain why water and PG contents only moderately correlate to each other (Iatridis et al., 2007). Collagen cross-links are also important; within the normal NP, high concentrations of pyridonoline cross-links are found, but with degeneration these cross

links are replaced with the pentosidine cross-links (Duance et al., 1998; Pokharna and Phillips, 1998), which increase the susceptibility of the tissue to tears (Pokharna and Phillips, 1998; Gruber and Hanley, 2002). Other collagens such as types III, V, VI, IX, and XI make up around 20% of the total collagen components of the disc and are thought to be involved in the organization of the collagen fibrils (Nerlich et al., 1998) and to play a key role in the functional mechanical behavior of the complex AF interlamellar regions (Tavakoli et al., 2016). Remarkably, type VI collagen is an important pericellular molecule (Hayes et al., 2016) thought to be essential for the mechanosensing of IVD cells (Duncan, 2006; Wilusz et al., 2014; Hodson et al., 2018).

2.2.3 Water

As discussed in subchapters 2.2.1 and 2.2.2, the function of the IVD tissue matrices cannot be dissociated from the very specific interactions of the ECM components with interstitial water. Remarkably, the physics of water in the IVD and the macroscopic effect thereof depend on the balance of PG and collagen contents. While PG controls Donnan osmosis, it might further affect the shear stiffness of cartilage-like tissues (Roos et al., 2013). Multi-physics models and experiments also suggest that the effective turgidity of disc tissues is additionally controlled by the existence of a dual porosity, generated by volumes of exclusion of PG molecules generated by the fibrillar matrix (Huyghe et al., 2003; Schroeder et al., 2007).

2.3 IVD Cell Activity and Molecular Biology in Health and Disease

The cells responsible for disc maintenance represent only 1% of the volume of the organ (Encyclopaedia of Occupational Health and Safety 4th Edition), the disc cell densities (~4×10^3 cells/mm^3 in the NP; ~9×10^3 cells/mm^3 in the AF; ~15×10^3 cells/mm^3 in the CEP) being among the lowest within the body, due to the low nutrient supply (Maroudas et al., 1975). These densities decrease with aging and IVD degeneration (Maroudas et al., 1975; Liebscher et al., 2011; Tomaszewski et al., 2015). The cells of the CEP are chondrocytes (Maroudas et al., 1975), while those in the outer AF are similar to fibroblasts. The NP cells of a mature human disc are spherical and, while similar to chondrocytes (Buckwalter, 1995), they synthesize a greater proportion of PG than chondrocytes, with a PG-to-collagens ratio of about 27:1 (Mwale et al., 2004), and have a number of distinctive

cell markers (Risbud et al., 2015; Thorpe et al., 2016). Mature NP cells are uniquely derived from notochordal cells, which, in humans, are lost during adolescence (Risbud and Shapiro, 2011; McCann et al., 2012; Chan et al., 2014). From one IVD tissue to another, cells display transitional phenotypes, illustrating the likely influence of their microenvironment on their phenotype and activity (Bruehlmann et al., 2002).

2.3.1 Multifactorial Regulation of Cell Activity in Health

The IVD has low nutritional supply with blood vessels located in the vertebral endplates and outer AF (Maroudas et al., 1975). This leads to a hostile environment for cells, characterized by low oxygen tension, low glucose concentrations, high lactate levels, i.e. low pH, and high osmolality, altogether under the action of dynamic loads (Kraemer et al., 1985; Sélard et al., 2003; Soukane et al., 2005; Mokhbi Soukane et al., 2009; Chen et al., 2014a; Thorpe et al., 2018). However, the cells of the IVD are remarkably adapted to such conditions (Bibby et al., 2005). In hypoxia, the increased production of lactate generated during adenosine triphosphate synthesis decreases the pH. Accordingly, IVD cells express a number of control mechanisms that maintain pH homeostasis, such as expression of plasma membrane monocarboxylate transporters (Silagi et al., 2020) and bicarbonate recycling mechanisms (Silagi et al., 2018). NP cells further show robust and constitutive hypoxia inducible factor (HIF) 1 expression, and under hypoxic conditions the inducible subunit of HIF-1, HIF-1α, accumulates due to the inhibition of prolyl hydroxylase enzymes. Then, it translocates to the nucleus, where it binds to the constitutively expressed subunit HIF-1β. Subsequent binding of this dimer to hypoxia response elements on the promoter region of target genes allows the regulation of gene expression (Carroll and Ashcroft, 2005). HIF-1α has been shown to contribute to the survival of NP cells in the harsh, hypoxic environment by increasing gal-3 expression, thereby inhibiting Fas receptor/Fas ligand-mediated apoptosis (Li et al., 2013). It may also be involved in hypoxia-driven suppression of NP cells' autophagy via inactivation of the mTOR (mammalian target of rapamycin) signaling pathway (Chen et al., 2015). Furthermore, HIF-1 seems to play a crucial role in supporting adequate energy metabolism (i.e., anaerobic glycolysis) in NP cells by regulating the expression of the glucose transporters GLUT-1, GLUT-3, and GLUT-9 (Richardson et al., 2008b). The crucial role of HIF-1α in NP homeostasis has been underlined by knockout experiment in mice, whereby HIF-1α deficiency resulted in IVD

degeneration, as evidenced by reduced PG and collagen II contents (Meng et al., 2018). Interestingly, research in other areas points toward cross talk between the nuclear factor kappa B (NF-κB) and HIF-1 signaling pathways (Han et al., 2016), which could constitute a molecular link between hypoxia and inflammation. First data in NP cells support this notion as prolyl hydroxylase domain-containing protein 2, able to degrade HIF-1α (Risbud et al., 2010), was shown to co-activate NF-κB signaling (Li et al., 2015).

ECM osmolarity fluctuates (~430 to 496 mOsm) with normal daily activity in the IVD (Urban, 1994; Roberts et al., 1998) and disc cells are well adapted to respond to these fluctuations (Ishihara et al., 1997; van Dijk et al., 2011) through robust expression of osmosensitive transcription factor TonEBP (tonicity-responsive enhancer binding protein), which maintains cellular function under daily osmotic changes (Tsai et al., 2006; Johnson et al., 2014). TonEBP (or NFAT5, nuclear factor of activated T-cells 5, or OREBP, osmotic response element-binding protein) is a transcription factor modulated by growth factors (GF) (Halterman et al., 2012), cytokines (Halterman et al., 2012; Johnson et al., 2017), and calcium (Hiyama et al., 2009). It is involved also in the survival of NP cells in the hyperosmotic milieu (Sadowska et al., 2018). Together with other osmosensitive pathways and receptors, especially from the mitogen-activated protein kinases (MAPK), transient receptor potential (TRP) channel and Aquaporin family, TonEBP/NFAT5 (tonicity-responsive enhancer binding protein/nuclear factor of activated T-cells 5) plays a crucial role in cell volume regulatory mechanisms (Sadowska et al., 2018). In rat NP cells, extracellular signal-regulated kinase (ERK) phosphorylation following hyperosmotic stress results in TonEBP/NFAT5 activation, thereby promoting cell survival (Tsai et al., 2006, 2007). The tight cross talk between ERK and TonEBP/NFAT5 and the link to cell survival/apoptosis have also been demonstrated through pharmacological ERK inhibition (Tsai et al., 2007; Dong et al., 2014; Li et al., 2017a). In addition to MAPK, TonEBP/NFAT5 interconnects to the NF-kB pathway (López-Rodríguez et al., 2001; Roth et al., 2010) and interacts with members of the TRP family (Sadowska et al., 2018). The TRPV subfamily (especially TRPV4) has been identified as potential osmo- and volume-sensors involved in regulatory volume change mechanisms and cell signaling, following osmotically driven opening of the channel pore and subsequent influx of extracellular Ca^{2+} (Sadowska et al., 2018). Consequently, TonEBP/NFAT5 has a wide variety of target genes, ranging from organic osmolytes (Lee et al.,

2011b) and aquaporins (Gajghate et al., 2009) to ECM molecules (Tsai et al., 2006) and pro-inflammatory cytokines (Johnson et al., 2017). In particular, aquaporins form transmembrane water channels and are able to regulate intra- and extracellular water balance, which is essential to keep cells alive in fluctuating osmotic environments (Richardson et al., 2008a; Gajghate et al., 2009; Johnson et al., 2015a; Snuggs et al., 2019; Wang et al., 2019).

The IVD is constantly subjected to dynamic loads and the cells embedded within the ECM experience compressive, tensile, and shear mechanical stresses and strains (Neidlinger-Wilke et al., 2014). They respond to these loads via a number of mechanotransduction mechanisms, which have been reviewed previously (Iatridis et al., 2006; Neidlinger-Wilke et al., 2014; Tsai et al., 2014). For example, TRP channels, whereby TRPV4 as well as TRPC6, TRPM2, and TRPML1 stand out due to fundamental roles in osmo- and mechano-sensing (Krupkova et al., 2017; Sadowska et al., 2018; Cambria et al., 2020). NP cells are more responsive to hydrostatic pressure, while AF cells respond better to cyclic strain (Neidlinger-Wilke et al., 2005). Mechanical loads considered physiological for non-degenerative IVD cells promote matrix synthesis, while higher loading regimes can promote catabolism and contribute to IVD degeneration (Iatridis et al., 2006; Neidlinger-Wilke et al., 2014; Tsai et al., 2014). IVD cells activate distinctive signaling pathways depending on the load magnitude, frequency, and duration, in a zone-specific manner (Setton and Chen, 2006; Latridis et al., 2011; Chan et al., 2013). Over the past years, the YAP/TAZ signaling has also come into focus in mechanobiology due to its regulation by the mechanical signals elicited by the surrounding ECM (Piccolo et al., 2014; Pocaterra et al., 2020), whereby integrins in focal adhesions (FA) evidently play a crucial role (Boopathy and Hong, 2019). YAP and TAZ are transcriptional coactivators with involvement in development, tissue homeostasis, tissue renewal/regeneration, and cell proliferation and survival to stress (Piccolo et al., 2014). Previous research clearly indicated that cell stretching over the ECM with reformation of the cytoskeleton causes YAP/TAZ activation, whereas restriction of cell adhesion inhibits YAP/TAZ-related transcription (Dupont et al., 2011). Such responses were observed when NP cells were cultured in laminin-functionalized polyethylene glycol (PEG) hydrogels with different stiffnesses (Fearing et al., 2019). In AF cells, the degree of fiber alignment and fiber stress was shown to affect YAP/TAZ activation, with lower nuclear YAP/TAZ in the case of fiber alignment and prestress (highly elongated cell morphology and lower

FA area). In contrast, slack and random fibers promoted larger FA and nuclear YAP/TAZ localization (Bonnevie et al., 2019). YAP inhibition seems to occur by cell-to-cell contact in IVD cells (Zhang et al., 2018b). Remarkably, while the expression of YAP decreases with age (Zhang et al., 2018a), YAP silencing was shown to promote NP cell senescence (Zhang et al., 2018b), which adds to the difficulty to duly apprehend the variation of disc cell regulation, upon multifactorial simulation and aging.

IVD cell activity is finely related with careful balance of multifactorial cell cues. Altered balance might result in a vicious cycle of catabolic cell responses and functions (Vo et al., 2016), which leads to a loss of functional sensitivity to, e.g., mechanical loads at a cellular level, to undue osmolarity, and to ECM depletion over time at a tissue level, which finally results in IVD degeneration (Vergroesen et al., 2015; Lama et al., 2019).

2.3.2 Multifactorial Regulation of Cell Activity in Disease

During IVD degeneration, cellular changes lead to increased production of catabolic cytokines (Le Maitre et al., 2005; Hoyland et al., 2008; Wuertz and Haglund, 2013; Risbud and Shapiro, 2014; Johnson et al., 2015b; Phillips et al., 2015; Khan et al., 2017; Ruiz-Fernández et al., 2019), matrix-degrading enzymes (Crean et al., 1997; Le Maitre et al., 2004; Pockert et al., 2009; Neidlinger-Wilke et al., 2012; Vo et al., 2013; Sivan et al., 2014; Binch et al., 2016; Li et al., 2016), and neurotropic and angiogenic factors (Johnson et al., 2006; Purmessur et al., 2008; García-Cosamalón et al., 2010; Lee et al., 2011a; Jung et al., 2011; Navone et al., 2012; Richardson et al., 2012; Gruber et al., 2012; Hiyama et al., 2013; Kao et al., 2014; Krock et al., 2014, 2016; LA Binch et al., 2014; Binch et al., 2015a; Ohtori et al., 2018), which lead to ECM degradation, catabolism, and nerve and blood vessel ingrowth (Freemont et al., 1997, 2002; Tolofari et al., 2010; Stefanakis et al., 2012; Liang et al., 2013; Binch et al., 2015b; Gruber et al., 2017; Lama et al., 2018; Wu et al., 2019) (Figure 2.2).

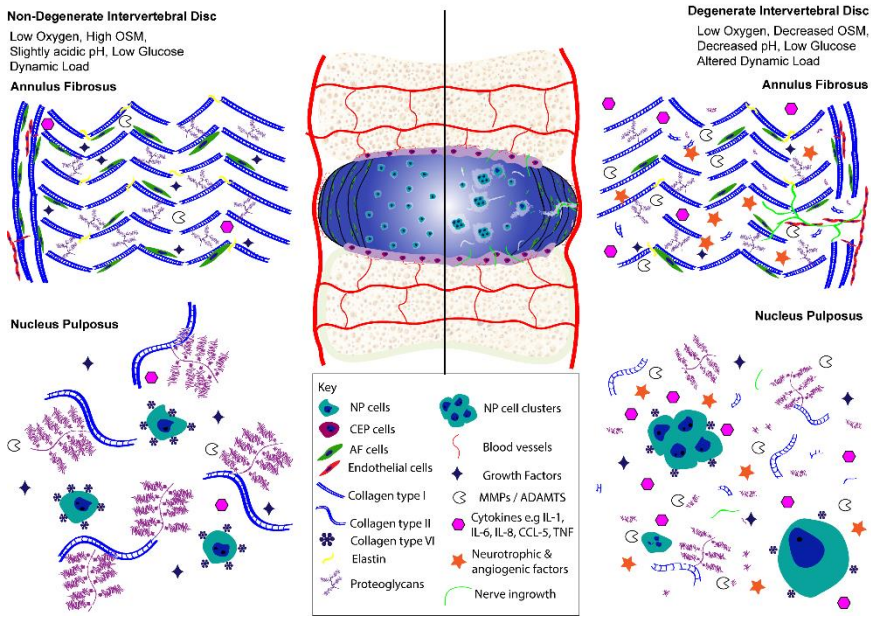

Figure 2.2: Cellular regulation of the intervertebral disc under degenerated and non-degenerated conditions.

Furthermore, the number of functional cells decreases with increases in apoptosis, autophagy (Zhang et al., 2016a), and cellular senescence (Roberts et al., 2006; Gruber et al., 2007; Le Maitre et al., 2007a; Heathfield et al., 2008; Feng et al., 2016; Vo et al., 2016; Patil et al., 2018, 2019; Xu et al., 2019). The initiating trigger of these catabolic events is clearly multifactorial, and different processes are likely to predominate in individual patients, with links to genetics, abnormal loading profiles, infection, and diabetes, among other potential risk factors (Gorth et al., 2015; Yang et al., 2015; Martirosyan et al., 2016).

For example, cells from a degenerative IVD respond differently to mechanical stimuli with mechanotransduction pathways altered during degeneration, which further leads to decreased synthesis and increased degradation of the ECM (Setton and Chen, 2006; Le Maitre et al., 2008; Gilbert et al., 2010, 2013; Hodson et al., 2018). IVD cells respond to altered biomechanics, infection, or metabolic changes with increased production of catabolic cytokines, leading to the generation of a 'cytokine soup' regulated predominantly by the pleiotropic cytokine interleukin (IL)-1 (Phillips et al., 2013, 2015). The IVD environment becomes progressively more hostile for cells with decreased IVD hydration and nutritional supply, leading to increased lactate production, decrease of pH, and decreased osmolarity (Thorpe et al., 2018). Cells become less able to withstand these conditions and lose the

physiological response mechanisms that would maintain homeostasis (Johnson et al., 2017; Sadowska et al., 2018; Guo et al., 2019; Snuggs et al., 2019; Tessier et al., 2020). Low glucose (Horner and Urban, 2001; Bibby and Urban, 2004; Rinkler et al., 2010; Neidlinger-Wilke et al., 2012) and high lactate concentrations (Horner and Urban, 2001; Bibby and Urban, 2004; Neidlinger-Wilke et al., 2012; Gilbert et al., 2016) lead to a higher rate of cell death and a catabolic shift in mRNA expression. However, the role of oxygen remains controversial. While it seems that NP cells survive well with limited oxygen levels (Horner and Urban, 2001; Neidlinger-Wilke et al., 2012), on the one hand, the lack of oxygen has been alternatively linked to either lower (Horner and Urban, 2001) or unmodified (Mwale et al., 2011) GAG synthesis by NP or AF cells. On the other hand, a significant rise in aggrecan mRNA expression at 1%, compared to 6% or 21% oxygen concentrations, was found, while mRNA expression for collagen type II was decreased (Neidlinger-Wilke et al., 2012). Other studies report increases in both collagen type II and aggrecan at 1% oxygen (Mwale et al., 2011).

Cell senescence has been reported to be a contributing factor toward the progression of IVD degeneration, and the causes and molecular mechanisms that are seen to take place were already nicely reviewed (Feng et al., 2016). A correlation between age and increased measures of senescence has been shown as well as associations between senescence and elevated MMP and ADAMTS expression (Le Maitre et al., 2007a; Hiyama et al., 2010). As well as losing replicative ability, senescent cells also release pro-inflammatory cytokines and matrix-degrading enzymes. This cell characteristic is referred to as senescence-associated secretory phenotype (SASP) (Feng et al., 2016). Secretion of pro-inflammatory cytokines by senescent disc cells includes various catabolic factors, including tumor necrosis factor α (TNF-α) and IL-1β (Risbud and Shapiro, 2014).

Apoptosis and autophagy are other important aspects of cell activity in the IVD. The mechanisms of action and roles in matrix homeostasis and degeneration have been reviewed and discussed in detail (Zhao et al., 2006; Ding et al., 2013; Zhang et al., 2016a). It has been observed in human, animal, and *in vitro* studies that excessive NP and AF cell apoptosis and autophagy takes place during IVD degeneration, which may be exacerbated by harsh disc cell microenvironments (Gruber and Hanley, 1998; Zhang et al., 2016a). Autophagy is also important in natural cell and protein turnover within the IVD as low levels have been reported in non-degenerate rat NP and AF cells (Kong et al., 2014). However, its role during IVD degeneration is more complicated, as

both higher (Jiang et al., 2013; Ye et al., 2013) and lower (Jiang et al., 2014) levels of autophagy have been shown. The potentially conflicting roles of autophagy during IVD degeneration is reviewed and discussed elsewhere (Zhang et al., 2016b). In regards to the role of cytokines , IL-1β has been shown to induce both autophagy and apoptosis in rat AF cells, but only in serum-deprived conditions (Zhao et al., 2007; Shen et al., 2011), which may be a more reflective condition of the IVD, where nutrient levels are low due to avascularity.

Cell survival and cell death under multifactorial cell environments are strongly controlled though mTOR and Notch cell signaling pathways. mTOR is downstream of PI3/Akt, whereby mTOR is substrate of Akt (Lopiccolo et al., 2008). Akt can induce direct and indirect activation of mTOR and, similar to PI3/Akt, the protein kinase mTOR has a central role in cell metabolism, growth, proliferation, and survival (Sabatini, 2017). Increasing evidence highlights that mTOR controls the decision between cell survival and cell death in case of endoplasmic reticulum (ER) stress (Hebert and Molinari, 2007; Walter and Ron, 2011). In the IVD, mTOR has mostly been investigated in the context of autophagy (Zhang et al., 2016a), i.e. an intracellular process that allows cells to remove misfolded or aggregated proteins and eliminate damaged organelles occurring due to stressors such as nutrient deprivation (Chen et al., 2015; Yurube et al., 2020), oxidative stress (Ma et al., 2013; Chen et al., 2014b), or overloading (Ma et al., 2013), thus ensuring cell survival and appropriate cell metabolism (Glick et al., 2010). Inhibition of mTORC1 promoted rabbit AF and human NP cell survival and reduced catabolic responses under serum and nutrient deprivation as well as by IL-1β treatment via autophagy induction (Ito et al., 2017; Kakiuchi et al., 2019; Yurube et al., 2020). Furthermore, the beneficial effect of osteogenic protein 1 treatment on rat NP cell survival under hyperosmotic culture conditions was associated with mTOR (and PI3/Akt) activation (Yang et al., 2018). Interestingly, mTOR inhibition has also been found to affect matrix synthesis and degradation in the IVD in mice, with reduced aggrecanolysis (likely via reduction in cell senescence) but simultaneous suppression of PG synthesis, thus not leading to any changes in total PG content (Ngo et al., 2014).

The Notch signaling pathway is a highly conserved pathway with a wide variety of functions in development, tissue homeostasis and diseases, ranging from stimulation of tissue growth to promotion of cell death under different cell microenvironments (Hori et al., 2013). As transmembrane receptors with a direct route from the membrane to the nucleus, Notch 1-4 can only exhibit such diverse functionality by a range

of regulatory mechanisms such as tissue topology, ligand expression patterns, expression of certain enzymes, or the extent of cell–cell contact (Bray, 2016). In IVD cells, the expression of Notch 2 is increased during IVD degeneration (Wang et al., 2013), whereas intradiscal injection of JAG2 (which induces Notch 2) reduced IVD degeneration processes in rats (Long et al., 2019). Notch signaling in the IVD was activated by hypoxia (Hiyama et al., 2011) and pro-inflammatory cytokine exposure (Wang et al., 2013), thereby activating NP and AF cell proliferation (Hiyama et al., 2011; Long et al., 2019), inhibiting NP cell apoptosis promoted by TNF-α (Long et al., 2019) and modulating the expression of anabolic and catabolic genes (Millward-Sadler et al., 2009). Yet, these effects seem to be zone-dependent, with Notch activation causing catabolic and anabolic responses in AF and NP cells, respectively (Millward-Sadler et al., 2009). Importantly, cross talk between the Notch signaling pathway and MAPK, NF-kB, PI3K/Akt ,and Wnt/β-catenin seems to exist (Wang et al., 2013; Long et al., 2019). Despite these fascinating findings, relatively little research has this far been conducted on the Notch pathway in the IVD.

2.4 Systems' Modeling for the Exploration of IVD Degenerative and Regenerative Mechanisms

Successful IVD treatment/regeneration strategies rely on a holistic understanding of the highly multifactorial (patho)physiological dynamics of the disc system, to be understood at different time and length scales. In this sense, theoretical and computer modeling offers unique possibilities (Figure 2.3).

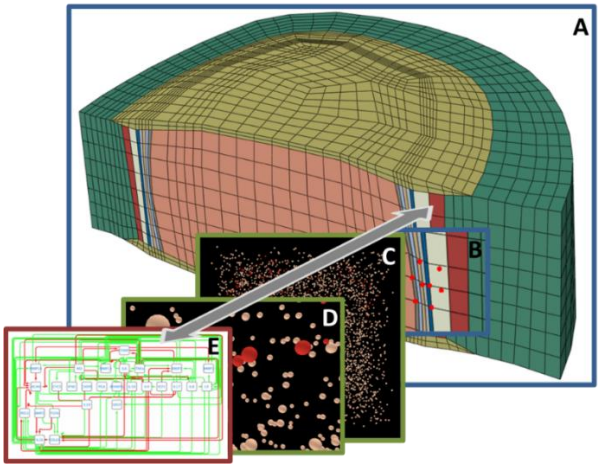

Figure 2.3: *In silico* multiscale/integrative modeling as an objective in IVD research. (A) Organ level: 3D finite element modelling. Deformable nonlinear geometry, heterogeneous assembly of tissues. (B) Tissue level: 3D finite element modelling. Composition-dependent multiphysics and anisotropic behavior of the tissues, transport of solutes through tissue matrices. (C–D) Multicellular levels: agent-based modeling in regions of interest. Prediction of cell responses to multifactorial (micro-) environments. (E) Cell/subcellular levels: network modeling. Single cell stimulation, multiple states.

For musculoskeletal joints commonly affected by highly prevalent disorders such as osteoarthritis, efforts in model developments have spanned over the scales, from the multibody musculoskeletal system to cell regulation networks, passing through detailed knee joint finite element models (Mukherjee et al., 2020). Even if the systematic integration of models of different nature at different scales is still incomplete, developments use to be much more modest as far as the IVD and IVD degeneration are concerned. Indeed, model developments to simulate and virtually explore the pathophysiology of IVD degeneration have long remained largely limited to the tissue and organ scales (Malandrino et al., 2015a). Only very recently, cell-scale models have finally emerged out of novel integrations of knowledge in IVD cell biology and computer methods in systems biology (Baumgartner et al., 2020). Arguably, the holistic modeling of the heterogenous IVD system and the degeneration thereof is a tremendous challenge that will surely contribute to further progress in the development of *in silico* tools and medicine in other fields of rheumatology.

On the one hand, the process of model construction and assessment against evidences provides important clues about the minimum hypotheses and quantitative factors essential to reproduce known phenomena in health and disease. On the other hand, the huge capacity for parametrical studies turns *in silico* models into unique virtual laboratories to design new hypotheses and experiments. Eventually, model predictability, even in terms of relative analyses of simulation results, i.e., semiquantitative predictability, is definitively cornerstone to enable mechanistic explicability and better control of patient stratification and treatment prognosis. Significant progress in IVD modeling has been made during the last years at multiple scales and is summarized below, along with relevant findings about IVD regulation, IVD degeneration, and possible therapies.

2.4.1 Organ- and Tissue-Scale Simulations of the IVD Biophysical Regulation

IVD tissues can be considered as biphasic materials, i.e., a combination of solid and liquid phases, at the millimetric scale. The porous solid phase corresponds to the tissue ECM, i.e., mostly collagen and PG. The liquid phase is mainly composed of water and solutes that flow through the pores of the solid phase. Biphasic mixture theory and Biot poroelastic theory allow to model IVD tissues and discriminate the respective roles of the solid and the fluid (Biot, 1941; Mow et al., 1980), especially in terms of mechanically coupled solute transport to the cells, for further simulations of cell activity (Malandrino et al., 2015a). The effect of mechanically coupled solute transport on cell activity has been referred to as indirect mechanotransduction, which depends on the capacity of the IVD tissues to deform (Iatridis et al., 2006) and control both the diffusion distances and the porosity, i.e., water content, in the disc (Malandrino et al., 2011). Obviously, the whole process depends on tissue composition, i.e., on the effective condition of the IVD.

Composition-based tissue models were developed for the articular cartilage (Wilson et al., 2005) and were later applied to the IVD (Schroeder et al., 2006). Implemented into detailed finite element models of the whole IVD, these models included the osmotic pressure in the disc tissues, controlled by PG, collagen, and water contents as explicit model parameters. Strain energy density calculations in the AF further considered the anisotropy induced by the oriented collagen type I. Composition-dependent tissue modeling has paved the way to map the relative effects of local ECM depletion, in the NP, the AF, and the CEP, on the biphasic behavior of the IVD and on the indirect

mechanotransduction phenomena (Ruiz Wills et al., 2016, 2018). Such tissue models were also coupled to phenomenological direct mechanotransduction theories, initially developed to predict the fate of bone mesenchymal stromal cell in endochondral bone healing, to calculate the likely long-term IVD remodeling after spine surgery (Van Rijsbergen et al., 2018). The effect of PG and fixed-charge density contents on the diffusion of antibiotics from the vasculature to the IVD was also assessed through finite element mechano-transport simulations (Jackson et al., 2018; Zhu et al., 2019).

The hypothesis that impaired diffusion of metabolites across the IVD might accelerate IVD degeneration through cell nutritional stress (Urban and Roberts, 2003; Huang et al., 2014) has motivated experimental measurements of cell viability in function of local pH and glucose concentrations in a diffusion chamber (Horner and Urban, 2001) and the establishment of empirical relationships between the oxygen, glucose, and lactate metabolism by IVD cells (Bibby et al., 2005). These works have been instrumental for the implementation of the aforementioned mechano-transport models, to couple IVD tissue mechanics, IVD morphology, local cell metabolism, and cell death (Malandrino et al., 2015a). Such simulations revealed that water contents in the disc, especially in the NP, largely control the effective diffusion of solutes, as well as the diffusion distances, under physiological mechanical loads (Huang and Gu, 2008; Malandrino et al., 2011).

The diffusion process in the disc ECM is relatively low and disc cell populations can withstand adverse nutritional environments during several hours to a few days before dying (Horner and Urban, 2001). Accordingly, model simulations point out that the effect of molecule mechano-transport on IVD cell activity becomes remarkable under sustained rather than under transient mechanical loads (Malandrino et al., 2011). Furthermore, mechano-transport simulations suggested that indirect mechanotransduction on the long term, i.e., decades, might explain natural aging in the IVD (Gu et al., 2014). Interestingly, a collection of patient-specific IVD models showed that large lumbar discs, i.e., higher than 14 mm, might be prone to spontaneous degeneration in contrast to average seize IVD, i.e., 8–12 mm high, because diffusion distances were too large to allow the nutrients to reach the cells in the center of the NP (Malandrino et al., 2015b).

Remarkably, models and simulations have proven great ability to identify specific risk factors and multifactorial mechanisms. Endplate obstruction because of sclerosis/calcification has been long suspected

to be responsible for nutritional disturbances in the IVD (Urban et al., 2004; Benneker et al., 2005a; van der Werf et al., 2007). However, micro-modeling of vertebral endplate specimens coupled with full IVD finite element simulations suggests that the variability of the calcified endplate structure and porosity with aging and degeneration is unlikely to generate any barrier able induce nutritional stress in the IVD (Malandrino et al., 2014). In contrast, the use of a composition-based IVD model showed that the early depletion of CEP in terms of PG and collagen type II increases the overall permeability of the endplate, with a specially high influence of the loss of PG (Ruiz Wills et al., 2018). Such a permeability increase was also measured with aging (Rodriguez et al., 2011), and simulations indicated that it might provoke a chronic dehydration of the NP, down to water contents characteristic of Pfirrmann grade III degenerated discs, under daily physiological loads. This reduction of water largely reduced the capacity of the nutrients to reach NP cells located in the anterior part of the IVD, close to the AF. Interestingly, these results may provide mechanistic explanations of the severity of endplate-driven IVD degeneration and low back pain, as eventually revealed by Modic changes and vertebral endplate defects, in the general population (Määttä et al., 2014, 2018; Dudli et al., 2016). Yet, such level of modeling cannot explain the pathophysiology of the CEP degeneration, per se, for which it is necessary to go down the scale.

2.4.2 IVD Cell Models and Integration of Experimental Cell Stimulation Data

As reflected in section 2.3, experimental studies at a cellular level increased our understanding of anabolic or catabolic processes by IVD cells, and biochemical, metabolic, and mechanical stimuli that affect cell activity could be revealed. However, critical interactions within the multifactorial environment to which a cell is exposed over long periods of time are difficult to capture experimentally or clinically, pointing out the need for *in silico* approaches down to the cell level.

Recently, a first agent-based modeling approach was proposed to simulate the behavior of NP cells in multicellular systems depending on biochemical microenvironments (Baumgartner et al., 2020). The model uses experimental findings to estimate cell viability and cell activity in terms of relative mRNA expressions of collagen types I and II and aggrecan and of MMP and ADAMTS proteins, based on user-defined nutritional factors and on inflammation. It exploited network modeling approaches from systems biology (Mendoza and Xenarios, 2006), to integrate the respective effect of different micro-environmental cell

cues on effective cell activities. It was then further developed to integrate direct mechanotransduction, i.e., load magnitude and frequency, effects (Baumgartner et al., 2019). On the one hand, such an approach informed about the likely differential behavior of non-inflamed and inflamed NP cells in similar microenvironments. On the other hand, simulations captured the expected relative influence of different mechanical load regimes on the capacity of NP cells to retain a full anabolic activity or provoke ECM depletion.

Complex interactions at a (sub)cellular level can be approached through different modeling formalisms such as Boolean or Bayesian networks, Petri nets, constraint-based, rule-based, or agent-based models, differential equations, process algebra, interacting state machines, or cellular automata (Machado et al., 2011). Still incipient in IVD research, models in systems biology often focus on one type of network, mainly metabolic-, signaling- and gene-regulatory networks, facing limitations in interconnecting these networks toward holistic representations of cell simulations (Machado et al., 2011). Future developments shall couple systems biology approaches and organ/tissue-scale finite element models (Subchapter 2.4.1). As such, the multiscale dynamics that control the IVD fate, and the mechanisms that lead to different phenotypes of IVD failure, will be represented, thereby allowing the mechanistic identification of new therapeutical targets. Furthermore, integrating cell regulation pathways into single and collective cell behavior models could uniquely bridge the gap between IVD tissue phenotypes and the intracellular machinery to explain the apparent links with different genetic variants (Rajasekaran et al., 2013; Munir et al., 2018b).

2.4.3 Cell Signalling Pathway Models and Integration of Multi-Omics Data

As exposed in section 2.3, cell signaling (or signal transduction) is the process that describes how cells communicate with their environment and how they respond to external or internal stimuli (Bradshaw and Dennis, 2003). Signal transduction pathways describe the transformation of a stimulus into a biochemical signal often starting with ligand-receptor binding, followed by an intracellular cascade of protein–protein interactions and resulting in a cellular response/cell fate decision such as expression of a certain gene, apoptosis, proliferation, etc. Signal transduction plays a fundamental role in cellular behavior and the high complexity of cell signaling has led to many mathematical modeling approaches in order to better understand the underlying

dynamics and deduce quantifiable conclusions (Klamt et al., 2006). In general, signaling pathways can be described as node-edge graphs (directed or undirected) with the proteins as the nodes and the edges as the interactions between the proteins. These protein–protein interaction networks are stored in several publicly available databases and aim to represent the existing knowledge of the scientific literature about either the entire interactome or the structure of specific pathways. Some of the popular databases are presented in Table 2.1, which can serve as a starting point for the creation of signal transduction pathways.

Table 2.1: Publicly available databases on signaling pathways and protein–protein interactions.

Title	Content	Size	Address
KEGG	Integrated database resource consisting of 18 databases including systems, genomic, chemical, and health information on the molecular interaction networks in biological systems	KEGG Pathway: 536 pathways	https://www.genome.jp/kegg/ (Kanehisa and Goto, 2000)
Reactome	Pathway database with interactive web visualization tool	2272 pathways, 10833 proteins, 12505 interactions	https://reactome.org/ (Fabregat et al., 2016)
STRING	Protein–protein interaction networks	5000 organisms, 24.6 mio proteins, >2000 mio interactions	https://string-db.org/ (Szklarczyk et al., 2019)
WikiPathways	Pathways of different species stored in wiki format	2785 pathways, 28 species	https://wikipathways.org/ (Slenter et al., 2018)
Pathway Commons	Biological pathway data extracted from various databases with visualization tool	4700 pathways, 2.3 mio interactions	https://pathwaycommons.org/ (Cerami et al., 2011)
Omnipath	Literature-curated mammalian signaling pathways from >50 databases	10934 proteins, 53542 interactions	http://omnipathdb.org/ (Türei et al., 2016)
MatrixDB	Database focused on interactions established by extracellular matrix proteins, PG and polysaccharides	106453 associations from 38921 experiments	http://matrixdb.univ-lyon1.fr/ (Clerc et al., 2019)

After extraction of the pathways of interest, prior-knowledge network (PKN) can be modeled with various mathematical approaches. The most widely used ones are either logic modeling employing Boolean or fuzzy-logic formalisms (Aldridge et al., 2009; Morris et al., 2010; Mitsos et al., 2012) or ordinary differential equation models (Orton et al., 2005; Yue et al., 2006). Whereas the former ignores time-dependent behavior and assumes instantaneous state changes of the system, the latter can describe transient behavior at a cost of a high number of reaction parameters that are difficult to identify experimentally. Interestingly, methodologies as presented by Mendoza and Xenarios (Mendoza and Xenarios, 2006) and Krumsiek et al. (Krumsiek et al., 2010) use a generalized formulation to transfer discrete node-edge graphs into continuous systems, to include dynamics into logic models.

Although considerable effort has been put to create databases on protein interaction and cell signaling pathways, the existing information has and will always have limitations, e.g., biases (well-known proteins are studied more often than under-reported players), assumptions during the data mining algorithms, and ambivalent behavior of individual protein pairs (stimulation and inhibition). The best approach to overcome this intrinsic limitation is to fit the PKN structure to experimental data. On this front, various massive parallel sequencing platforms can be used to provide systematic molecular profiling of human cells, which will be tackled in the next few years by the European Innovative Training Network Disc4All in IVD research (Disc4All – Training Network to advance integrated computational simulations in translational medicine, applied to intervertebral disc degeneration, 2020). The technologies are summarized under the term '*omics*, considering, e.g., genomics, proteomics, metabolomics, lipidomics, and other high-throughput technologies (Zhang et al., 2017).

Attractive techniques allowing protein detection with high sensitivity and specificity as well as relatively simple experimental protocols are multiplexed ELISA immunoassays on magnetic beads (Alexopoulos et al., 2008). This technique allows the simultaneous measurement of phosphoprotein activity and cytokine abundance (several dozens in one sample) after stimulation of biological samples (Clarke et al., 2013). This high-dimensional data serves as a starting point to optimize and fit the developed signaling pathway models. Here, either genetic algorithms (Saez-Rodriguez et al., 2009) or integer linear programming formulations (Mitsos et al., 2009) are viable approaches to systematically fit node-edge graphs to the experimental data. In particular, the CellNOpt (Terfve et al., 2012) and SigNetTrainer that is part of the

CellNetAnalyzer toolbox (von Kamp et al., 2017) offer user-friendly ways to perform such optimization routines. A recently developed alternative is DoRoTHea (Garcia-Alonso et al., 2019) that creates signal transduction graphs based on gene expression measurements taken, for example, from microarray studies. In the end, these pathways models can be used to investigate the overall dynamics of the system, identify the most influential nodes, or focus on the specific parts of the signal transduction network to see the effect of various stimuli and/or knockouts (Klamt et al., 2006).

Many pathways are involved in IVD cell regulation (Zhang et al., 2016a) and their individual analysis has been performed in the past in a vast amount of studies (Choi and Harfe, 2011; Fang et al., 2018; Liang et al., 2018; Shen et al., 2019). Until now a holistic representation of pathways in the IVD is still missing and a possible approach to tackle this obstacle might follow the strategy described above, as proposed in the Disc4All project (Disc4All – Training Network to advance integrated computational simulations in translational medicine, applied to intervertebral disc degeneration, 2020). Especially, the requirement of high-quality experimental data (ideally from relevant *in vitro* models) is one of the major challenges, in order to capture the mechanisms of multifactorial diseases such as IVD degeneration. However, the falling costs of high-throughput technologies will lead to increasing amounts of publicly available molecular information. The rapid developments in computational biology tools might then bridge the gap between information and mechanistic knowledge in IVD degeneration and IVD regenerative therapies.

3 *Simulating Intervertebral Disc Cell Behavior within 3D Multifactorial Environments*

This chapter is adapted from: Baumgartner L., Reagh J. J., González Ballester M. A., and Noailly J. (2020): *Simulating intervertebral disc cell behaviour within 3D multifactorial environments.* Bioinformatics, 1–8. doi: 10.1093/bioinformatics/btaa939

3.1 Abstract

Motivation: Low back pain is responsible for more global disability than any other condition. Its incidence is closely related to intervertebral disc (IVD) failure, which is likely caused by an accumulation of microtrauma within the IVD. Crucial factors in microtrauma development are not entirely known yet, probably because their exploration *in vivo* or *in vitro* remains tremendously challenging. *In silico* modelling is, therefore, definitively appealing, and shall include approaches to integrate influences of multiple cell stimuli at the microscale. Accordingly, this study introduces a hybrid Agent-based (AB) model in IVD research and exploits network modelling solutions in systems biology to mimic the cellular behavior of Nucleus Pulposus cells exposed to a 3D multifactorial biochemical environment, based on mathematical integrations of existing experimental knowledge. Cellular activity reflected by mRNA expression of Aggrecan, Collagen type I, Collagen type II, MMP-3 and ADAMTS were calculated for inflamed and non-inflamed cells. mRNA expression over long periods of time is additionally determined including cell viability estimations. Model predictions were eventually validated with independent experimental data.

Results: As it combines experimental data to simulate cell behavior exposed to a multifactorial environment, the present methodology was able to reproduce cell death within 3 days under glucose deprivation and a 50% decrease in cell viability after 7 days in an acidic environment. Cellular mRNA expression under non-inflamed conditions simulated a quantifiable catabolic shift under an adverse cell environment, and model predictions of mRNA expression of inflamed cells provide new explanation possibilities for unexpected results achieved in experimental research.

3.2 Introduction

Intervertebral discs (IVD) connect the vertebral bodies of the vertebras of the spine. They provide flexibility to the spinal column, act as dampers and transfer the loads from one vertebra to another. Failure of those structures, clinically reflected by degenerative disc disorders or disc herniation, is assumed to be highly related to low back pain, a disorder that causes more global disability than any other (Hoy et al., 2014). The IVD consists of three distinct, specialized tissues, (i) the Nucleus Pulposus (NP), i.e. the gel-like center of the disc, (ii) the Annulus Fibrosus (AF), i.e. a concentrically layered fibrocartilage that

laterally confines the NP and (iii) the Cartilage Endplate (CEP) that cranially and caudally separates the NP and the inner AF from the bony endplates of the vertebra. It is widely accepted that IVD failure is the result of tissue fatigue caused by repetitive (physiological) mechanical loads (e.g. Wade et al., 2016) rather than the result of unique traumatic high impact loads (e.g. Lee and Kwon, 2013). A suggested mechanism leading to IVD failure is the accumulation of microtrauma (micro lesions) in the IVD tissue over time, which depends on both, the external loads and the local capacity of the tissue to resist these loads. Yet, such capacity is strongly related to disc cell activity, as cells dynamically build and/or degrade extracellular matrix (ECM). Cell regulation mechanisms are still not fully understood, but local cellular behavior is known to be guided by micro- environmental mechanical and biochemical stimuli, including nutritional stimulation. The latter is of special interest, since IVD are large avascular organs, and local disc cell nutrition relies on solute diffusion (Urban et al., 1977) from the adjacent vertebra. Therefore, important nutritional gradients exist within the NP between regions adjacent to the CEP and the mid-transversal plane (Huang et al., 2014). Biochemical solute diffusion and cell nutrition in the NP is further strain-dependent: external loads influence disc tissue porosity and therefore local amounts of metabolites (Malandrino et al., 2015a), which has been called indirect mechanotransduction (Iatridis et al., 2006).

The influence of biochemical stimuli on NP cell activity has been explored through numerous *in vitro* studies (e.g. Rinkler et al., 2010; Neidlinger-Wilke et al., 2012; Gilbert et al., 2016). While such studies provide valuable information about the overall cell sensitivity to specific microenvironmental cues, they were not designed to capture the spatiotemporal effects of these cues. A further limitation is the limited capacity, mainly because of cost issues, to explore the combined effects of different cell stimuli. Consequently, the cellular behavior over long time periods within a dynamic, multifactorial biochemical environment remain poorly understood. To our best knowledge, no methodology was reported so far that combines findings from different experiments in order to approach, in an integrative way, the complex environmental regulation of IVD cell behavior. Current *in silico* modelling approaches to explore the IVD are to a great extent limited to Finite Element modelling (FEM). FEM integrate boundary condition (BC) and structural/composition effects in the local description of disc tissue behaviour, which could be extended to the exploration of both, direct (Van Rijsbergen et al., 2018) (i.e. the mechanical loads directly sensed

by cells on their membranes) and indirect mechanotransduction (Malandrino et al., 2015a), even including tissue regulation (Gu et al., 2014). However, the utility of FEM to simulate the dynamic biological processes responsible for IVD tissue maintenance and failure is limited. In contrast, Agent-based (AB) modelling allows approximating such processes, since it can integrate manifold biological processes, in representative tissue volume elements. AB model studies can realistically improve current understandings of biological or disease mechanisms (Holcombe et al., 2012; Olivares et al., 2016) and can be coupled with FEM studies for bottom-up explorations of tissue regulation mechanisms (Ceresa et al., 2018). To the best of our knowledge, no such approach has been developed for the IVD so far. As for other cartilaginous systems, modelling efforts have rather focused on single cell gene regulation (Kerkhofs et al., 2016) or signaling pathways (Melas et al., 2014) instead of collective cell behavior in representative tissue. Consequently, this work focusses on the development and the evaluation of a new methodology to model the behavior of IVD cells in representative volume elements. The methodology was designed to explicitly and robustly integrate heterogeneous experimental results through AB modelling. Simulations targeted the effect of cell multifactorial biochemical micro-environments to address indirect mechanotransduction phenomena in local tissue volumes. Predicted NP cell behavior was assessed against individual mRNA expressions and cell viability.

3.3 Materials and methods

The open source software Netlogo version 6.0.2 was used to create an AB model world, consisting of a cube with a volume of $1mm^3$, represented by 1000 patches. The AB model world was initially seeded with 4000 agents and each agent represented an NP cell, with a diameter of 10 μm (Chen et al., 2009). This modelled concentration of 4000 NP cells/mm^3 represented the mean cell density found in a human non-degenerated lumbar NP (Maroudas et al., 1975). The biochemical environment of the NP cells was represented as homogenized quantities to limit the number of agents. Calculation time step-length was set to one hour. The biochemical, nutrition-related factors lactate (lac) and glucose (glc) were simulated, since they were found to be potentially important stimuli in indirect mechanotransduction (Huang et al., 2014). Additionally, cellular inflammation was deemed to affect the cellular behavior. The AB model represented inflammation by predicting

Interleukin 1β (IL-1β) mRNA expression and a corresponding amount of IL-1β protein, since this proinflammatory cytokine appears to be a key factor in IVD degeneration (Vo et al., 2013). To evaluate cellular activity, the respective mRNA expressions of the NP tissue components Aggrecan (Agg), Collagen type II (Col-II) and Collagen type I (Col-I) were simulated, as well as the expression of ECM-degrading enzymes Metalloproteinase 3 (MMP-3) and ADAMTS. Cell activity was differentiated between inflamed and non-inflamed cells (Figure 3.1).

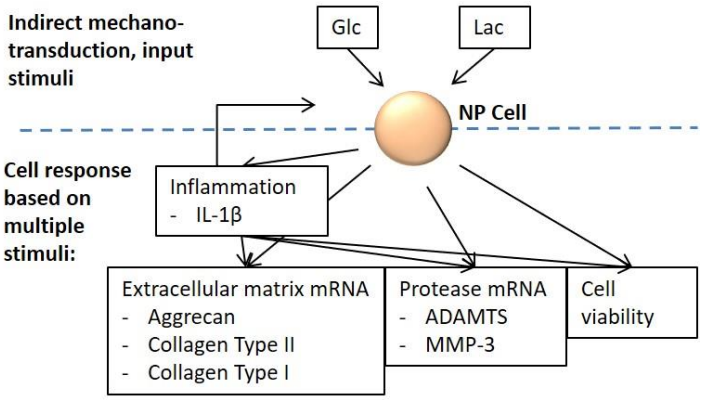

Figure 3.1: Schematic illustration of included factors in AB model simulations. Glc, glucose; Lac, lactate; IL-1β, Interleukin 1β

To estimate the effective mRNA expression over time, current cell viability was also calculated, depending on glc, lac and inflammation levels. The overall simulation workflow is described in Figure 3.2, and the different submodels for inflammation, cell viability and mRNA expression predictions are detailed in the next subsections.

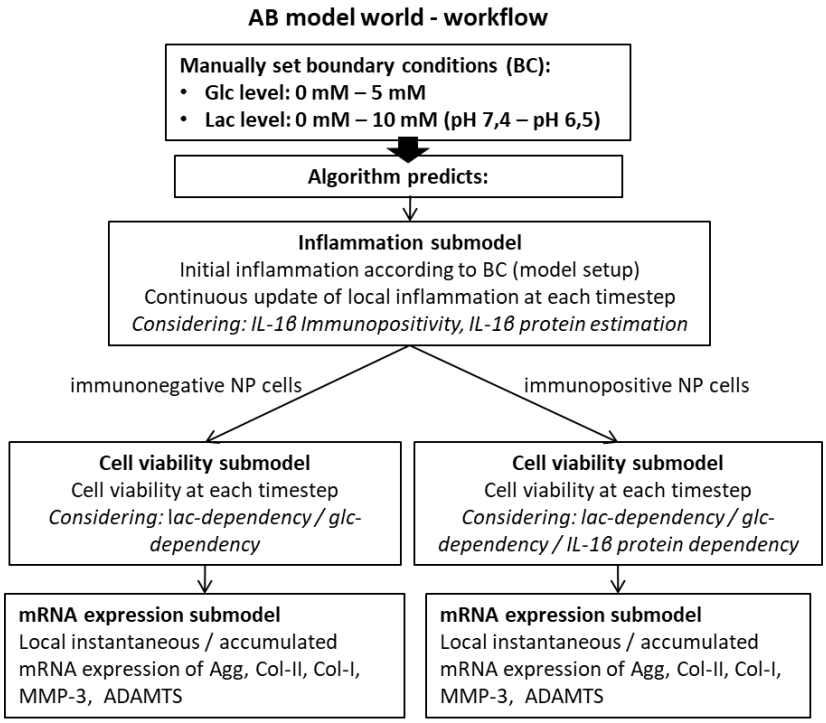

Figure 3.2: Overview of the AB simulation workflow

Model parameters are summarized in Supplementary Material S1 (Appendix 1).

3.3.1 mRNA expression submodel

Prediction of individual mRNA expressions according to varying glc and lac concentrations

To model the influence of a metabolite, i.e. glc or lac (via pH), on cell mRNA expression, continuous mathematical functions were built based on experimental findings, usually reported as discrete semiquantitative measurements (x-fold mRNA expression compared to control). Experimental data were chosen according to cell type (human preferred, followed by bovine), degenerative status of the tissue (not-degenerated preferred over degenerated) and according to the overall consistency of the experimental findings with current knowledge. Measurements associated with both significant findings and tendencies were considered for the development of the mathematical functions. These functions were based on the studies of Moroney et al., 2002; Neidlinger-Wilke et al., 2012; Gilbert et al., 2016; Saggese et al., 2018 (Supplementary Material S2, Appendix 1, for more detailed

information) and covered the whole physiological spectrum of metabolite concentrations. Each metabolite concentration was related to a specific mRNA expression for each protein. mRNA expressions ranged between 0 and 1, to reflect the lowest and the highest relative levels of expression, respectively (Figure 3.3).

Glucose [mM]	Rinkler et al. 2010: fraction estimation	Additional information Finite Element Model	Scaling: $0 \leq \text{value} \leq 1$	Values given by the fitted function
0	0.67	-	0	0.000033
0.5	0.74	-	0.21	0.212662
~1	-	Non-degenerated conditions -> Agg expression close to 1	1	0.999543
5	1	-	1	1

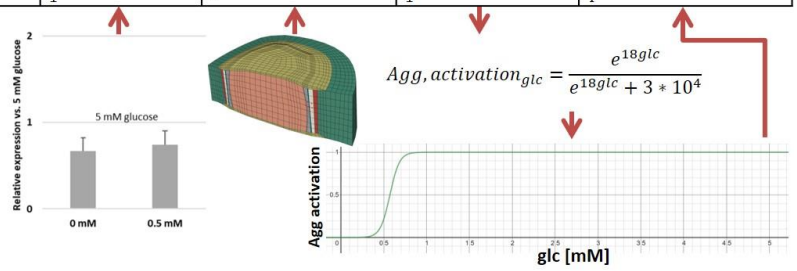

Figure 3.3: Visualization of the method to approximate continuous functions. Example of cellular activity in terms of Agg mRNA expression based on glc concentrations (Rinkler et al., 2010)

The interpolation of discrete experimental measurements suggested a sigmoidal behavior of the change of mRNA expression at critical solute concentrations. Hence, logistic functions were chosen for the interpolation of experimental points, to eventually reflect continuous changes of mRNA expressions. In many cases, experimental data suggested more than one sigmoidal shift in mRNA expression over the whole range of physiological concentrations of a stimulating solute (Gilbert et al., 2016). Therefore, a separate function was implemented for each sigmoidal shift (Figure 3.4).

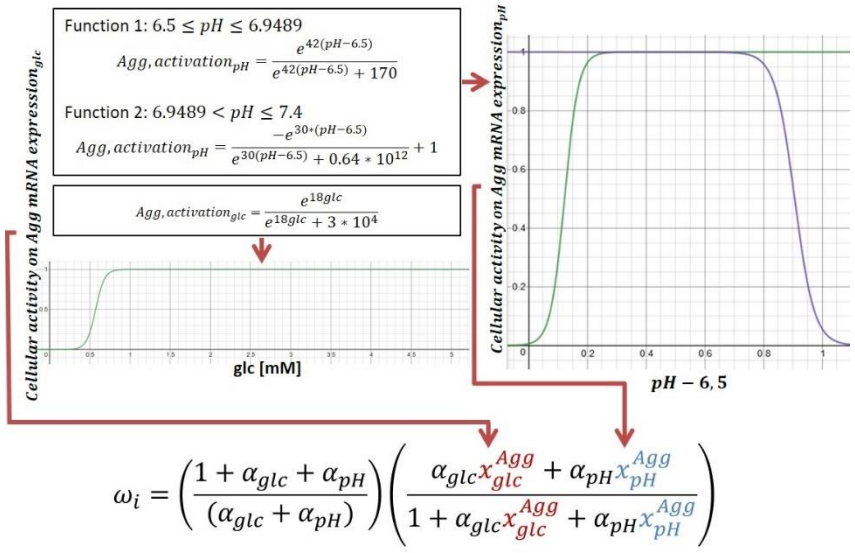

Figure 3.4: Coupling of experimental results, by using the equation from Mendoza and Xenarios, 2006. Note that pH varies from 6.5 to 7.4, thus it is represented within the function as values from 0 to 0.9

The fitting of continuous logistic functions generally required mRNA expression measurements at three different solute concentrations at least, to obtain (i) a maximum, (ii) a minimum and (iii) an intermediate mRNA expression within a given range of solute concentrations. Curve fitting was done by using the free online graphing calculator 'Desmos' (https://www.desmos.com/calculator).

To support the function fitting process, an additional datapoint derived from a mechanotransport Finite Element model was included for the glc-dependent mRNA expression curves. Since the mechanotransport simulations predicted glc values as low as ~1 mM in non-degenerated NP (Ruiz Wills et al., 2018), a datapoint at 1 mM glc was added, assuming that cell activity should not be negatively altered at such glc concentration (Figure 3.3). This point provided robustness for the determination of the start and growth rate of the sigmoid. All mRNA expression regulation functions are provided as Supplementary Material S3 (Appendix 1).

Prediction of overall mRNA expression in a multifactorial environment

To combine the respective influences of each stimulus on each mRNA expression, a network-based regulatory model proposed by Mendoza and Xenarios, 2006, was used. Briefly, the model equations regulate

continuously the nodes of the network (dx_i/dt) by analytically representing a traditional Boolean integration of the respective effects of activating (x_n^a) and inhibiting (x_m^i) nodes on a nodal input (ω_i) (Eq. (3.1)).

$$\frac{dx_i}{dt} = \frac{-e^{0.5h} + e^{-h(\omega_i - 0.5)}}{(1 - e^{0.5h})(1 + e^{-h(\omega_i - 0.5)})}$$

with (3.1)

$$\omega_i = \left(\frac{1 + \sum \alpha_n}{\sum \alpha_n}\right)\left(\frac{\sum \alpha_n x_n^a}{1 + \sum \alpha_n x_n^a}\right)\left(1 - \left(\frac{1 + \sum \beta_m}{\sum \beta_m}\right)\left(\frac{\sum \beta_m x_m^i}{1 + \sum \beta_m x_m^i}\right)\right)$$

Originally, node regulation also depended on a decay term, which was not relevant in the present work that strictly focused on comparative analyses of the normalized effects of different cell environments. The influence of each inhibiting and/or activating node can be weighted by means of activation (α_n) or inhibition (β_m) factors. Finally, the way a given nodal input affects the corresponding node is determined by a gain coefficient (*h*).

In our regulatory workflow, instead of being nodes regulated by the network, x_n^a and x_m^i were programmed as dynamical inputs determined by the current metabolic environment of the cells (Figure 3.4). Accordingly, Equation 3.1 integrates monofactorial controls of mRNA expressions depending on local glc, lac or IL-1β levels into fully coupled mRNA expressions (dx_i/dt) within a multifactorial environment.

The gain factor (*h*) was generally chosen to approximate a linear relation between the input ω_i and the overall activation, and it was set to 1. mRNA expressions based on glc and pH were also programmed to approximate a linear activating effect on ω_i, with activation factors (α) of 0.01, according to Mendoza and Xenarios, 2006. IL-1β protein was programmed to activate MMP-3 and Col-I and to inhibit Agg, Col-II and ADAMTS mRNA expressions, in non-degenerated NP cells according to Le Maitre et al., 2005. The relative activation/inhibition strengths of IL-1β on the mRNA expressions were defined based on these findings. All activation and inhibition factors are summed up in Table 3.1.

Table 3.1: Overview over estimated weights of stimuli as either activating (α) or inhibiting (β).

Solute	**Activation / inhibition factor**	**Target-mRNA**
glc	α = 0.01	Agg, Col-I, Col-II, MMP-3, ADAMTS
pH	α = 0.01	Agg, Col-I, Col-II, MMP-3, ADAMTS
IL-1β	β = 0.03	Agg
protein	β = 0.01	Col-II
	α = 0.01	Col-I
	α = 0.05	MMP-3
	β = 0.02	ADAMTS

3.3.2 Inflammation submodel

The inflammation submodel estimates the amount of immunopositive cells (cells active in terms of IL-1β mRNA expression; Figure 3.5) and a corresponding, amount of IL-1β proteins.

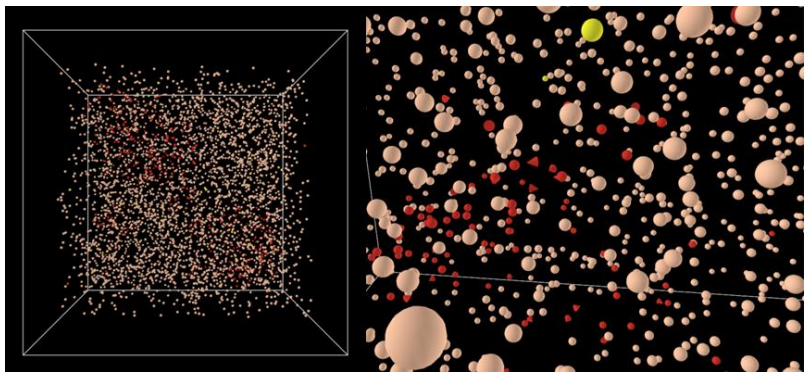

Figure 3.5: Visualization of immunopositivity within the AB model world (left) and zoom (right). Red: NP-cells immunopositive for IL-1β. Triangle shaped: dead immunopositive cells. Yellow: proliferated cells

Initial immunopositive NP cell foci were randomly placed within the AB model and surrounding cell clusters were formed and adapted according to the actual concentrations of glc, lac and IL-1β protein at each time step. To estimate the quantity of local immunopositive cells, overall IL-1β mRNA expression was determined using the approach from Mendoza and Xenarios, 2006. The normalized value of IL-1β mRNA expression was proportionally translated into an amount of

inflamed cells, assuming a maximum of 20% of inflamed cells within a non-degenerated human NP (Le Maitre et al., 2005).
Likewise, the amount of IL-1β proteins was estimated qualitatively according to the amount of IL-1β mRNA expression by assuming a linear relationship. Half-life of IL-1β proteins was taken into account by accumulating the relative amount of IL-1β over the current and the previous time step of calculation. To consider autocrine cell simulation by IL-1β protein (mentioned in e.g. Zou et al., 2017), the accumulated amount of IL-1β protein was normalized to influence the amount of immunopositive cells via feedback loop (Figure 3.6).

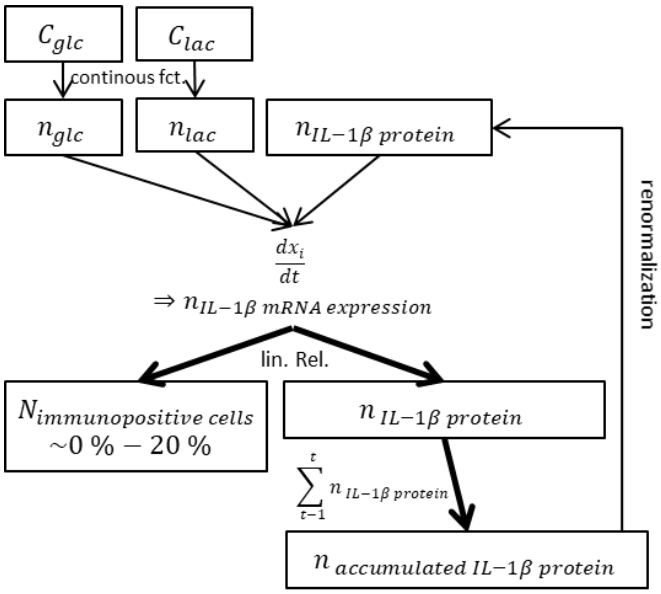

Figure 3.6: Schematic representation of the inflammation submodel. C, concentration; N, number; n, normalized

The effect of IL-1β protein on IL-1β mRNA expression was assumed to be activating with an activation factor a of 0.03, whereas the influence of glc and lac on IL-1β mRNA was set to 0.01. Given the low travelling distance of IL-1β due to the size and the short half-life of the protein, the effect of the protein on cell viability and mRNA expression was limited to immunopositive cell-foci. The inflammation submodel was initialized prior to mRNA and cell viability calculations in order to reach a steady state of IL-1β protein concentrations based on user-defined glc and lac concentrations (Figure 3.2).

3.3.3 Cell viability submodel

To estimate cell viability, continuous mathematical logistic functions and constants were established (Supplementary Material S4, Appendix 1) according to reported experimental studies (Bibby and Urban, 2004; Gilbert et al., 2016; Shen et al., 2016, Supplementary Material S5, Appendix 1, for more detailed information), reflecting an hourly percentage of decay or proliferation rates based on glc, lac and, in inflamed regions, on IL-1β protein levels. Functions considered both, experimental measurements and important elements of discussions from these studies. For example, Bibby and Urban, 2004 suggested their obtained cell viability to be affected by plenteous cellular glycogen stores due to the high-glucose preculturing media. Consequently, they assumed an adaptation of cells to adverse conditions within the first 24 h of the 48h experiment. In our model, the mathematical interpretation of this finding consisted in the calculation of an hourly rate of cell death over a time period of 24 h instead of 48 h. Influence of biochemical stimuli on cell viability was programmed to be additive. Experimentally, cell-death due to IL-1β was determined only for an IL-1β protein concentration of 10ng/ml (Shen et al., 2016). Because of the incomplete knowledge about physiological concentrations of IL-1β protein within non-degenerated NP and about the critical values of IL-1β protein causing cell death, a threshold of IL-1β protein concentrations leading to cell death was arbitrarily set to half of the maximum IL-1β protein level. Finally, to estimate the influence of cell viability on mRNA expression over time (ξ_{tot_t}), a normalized value of living NP cells (ζ : current amount, ζ_0 : initial amount) was multiplied by the instantaneous amount of mRNA expression (ξ) at each time step (t) (Eq. 3.2):

$$\xi_{tot_t} = \sum_{t=0}^{t} \left(\frac{\zeta}{\zeta_0} \cdot \xi \right) \tag{3.2}$$

3.3.4 AB model evaluation and validation

3.3.4.1 mRNA expression submodel evaluation and validation

To qualitatively validate the mRNA prediction, the experimental culture conditions used by Saggese et al., 2018 with regard to pH and glc concentrations were simulated. The Authors exposed 3D bovine NP

cell cultures to 5.5 and 0.55 mM glc at pH 7.0 for 24 h. 5 mM instead of 5.5 mM was chosen for AB model calculations because the selection for solute concentrations is limited to physiological ranges, where 5 mM reflects the highest glc concentration, according to the literature used to build the model regulatory functions.
To illustrate the effect of parameter variations of the equation presented by Mendoza and Xenarios, 2006, a three-level full factorial sensitivity analysis was performed. The tested parameters include the ones mentioned in Table 3.1, the activation of IL-1β protein on IL-1β mRNA expression and the gain coefficient, *h*. Up to five factors were considered: three factors, i.e. the gain coefficient and the activation of glc and pH affected both the immunopositive and immunonegative cells, whereas the respective effects of IL-1β protein on IL-1β mRNA expression and on the overall mRNA expression of structural proteins and proteases were additionally considered for the immunopositive cells. Hence, 27 and 243 simulations were used to analyze the sensitivity of the model to parameter variations, for immunonegative and immunopositive cells, respectively. The glc deprivation experiments of Saggese et al., 2018 were used to define the inputs of the model, i.e. cell activity for target-mRNA under 0.55 mM glc, pH 7.0 after 24 h. The most important findings are presented and discussed below, and the full sensitivity analysis with extended results and discussion was added as Supplementary Material S6 (Appendix 1).

3.3.4.2 Immunopositivity submodel evaluation

Predictions of the immunopositivity submodel were included in the validation setups for the mRNA expression submodel and the cell viability submodel.

3.3.4.3 Cell viability submodel validation

To validate cell viability, experimental setups of Horner and Urban, 2001 were simulated: during twelve days, cells were exposed to the following conditions: (i) 5 mM glc, at pH 6.0 (for the simulations, pH 6.5 was chosen, since this is the lowest value from the physiological range.); (ii) a glc-free serum, at pH 7.4.
Furthermore, the cell microenvironment imposed in the experimental setup of Saggese et al., 2018 (see above, 3.3.4, "mRNA expression submodel evaluation and validation") was simulated, to evaluate the influence of cell viability on mRNA expression over time (Supplementary Material S7, Appendix 1).

3.4 Results

3.4.1 Technical achievements

The model was computationally optimized to simulate the evolution of the system over more than four years in less than 15min of calculation, with an 'ordinary' personal computer [in this study: 16 GB RAM, Intel(R) Core™ i7-7500U CPU @ 2.70 GHz (dual core)]. During the simulations, the AB model could display the normalized IL-1β mRNA expression, the corresponding IL-1β protein concentrations, the current cell viability as well as the instantaneous and accumulated (normalized) mRNA expressions of Agg, Col-I, Col-II, MMP-3 and ADAMTS for inflamed and non-inflamed cells at each timestep (1 h).

3.4.2 mRNA expression submodel

Under glc partial deprivation, (0.55 mM) at pH 7.0, as experimentally imposed by Saggese et al., 2018, the AB model predicted a reduction of the instantaneous mRNA expression of the ECM proteins Agg and Col-II, and an increase of the instantaneous mRNA expression of Col-I, MMP-3 and ADAMTS in the immunonegative cells (Figure 3.7, a). In contrast, simulating the effect of glc partial deprivation at pH 7.0 with immunopositive cells led to increased Agg, Col-I and Col-II mRNA expressions, whereas it reduced MMP- 3 mRNA expression (Figure 3.7, b).

(a)

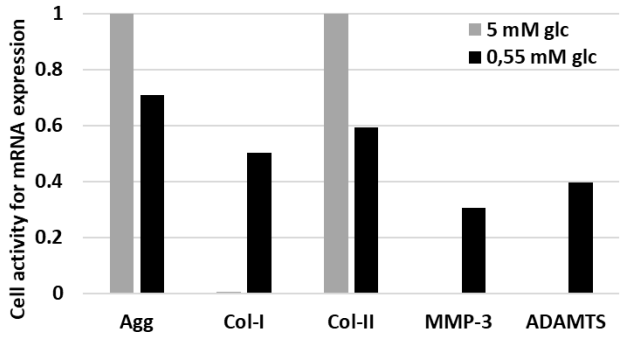

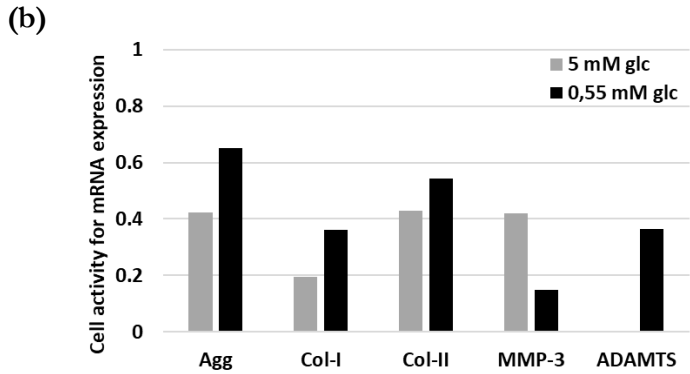

Figure 3.7: Instantaneous cellular activity in terms of mRNA expression of immunonegative (a) and immunopositive (b) NP cells under glc and pH BC imposed by Saggese et al., 2018 (pH 7.0)

The sensitivity analysis showed that due to parameter variation, values for mRNA expression were distributed over the whole normalized range, tending to accumulate around 0 and/or 1. Only values of the Agg and Col-II mRNA expressions of immunonegative cells were always higher than 0.65 and 0.25, respectively. The parameter combination effectively used within the algorithm generally led to intermediate mRNA expressions. Representative plots for Agg, Col-II and MMP-3 are presented in Figure 3.8.

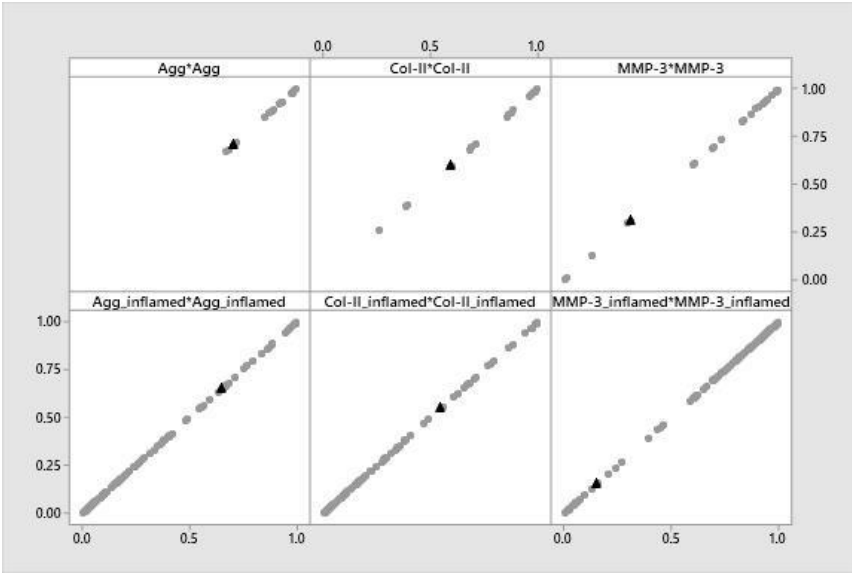

Figure 3.8: Parameter variation on Agg, Col-II and MMP-3 mRNA expression of immunonegative (upper row) and immunopositive cells (lower row)

3.4.3 Cell viability submodel

Simulations with glc and pH BC similar to those experimentally imposed by Horner and Urban, 2001 resulted in:

- 1.2 % of cell viability after 2.79 days under glc deprivation.
- cell viability decrease to around 71 % (78 % if immunopositivity is not considered) after three days, to around 41 % (50 % if immunopositivity is not considered) after 7 days and to around 11 % (14 % if immunopositivity is not considered) after 12 days, in acidic environment (pH 6.5) (Figure 3.9).

Cell decay due to relatively high IL-1β protein levels (i.e. more than half of the maximum permitted) was only activated under acidic conditions.

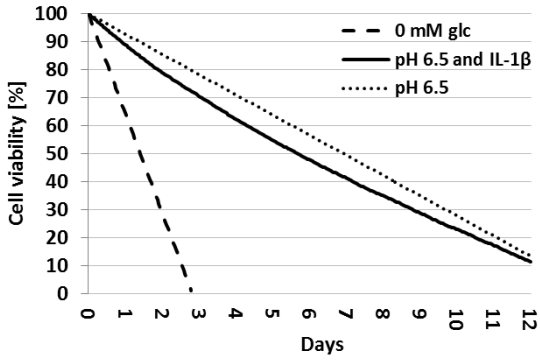

Figure 3.9: Simulation of cell viability over days in either glc-free medium or acidic environment, with and without the effect of IL-1β protein.

3.5 Discussion

To our knowledge, the presented AB model is the first *in silico* model that allows to predict the behavior of an IVD cell population within a multifactorial environment. By its ability to simulate cell behavior over long periods of time, it gathers key requirements to reveal cellular dynamics implicated in IVD failure, since disc tissue degeneration is a slow process that we hypothesize to be biologically-driven under physiological levels of cell microenvironmental cues. Importantly, our modelling approach uniquely allows the combination of existing knowledge to predict the effects of multiple interplays on cellular activity. On the one hand, experimental research providing detailed information, e.g. typical sigmoidal shifts of cell activity upon single stimulation, is crucial to enhance the model performance of such an evidence-based approach. On the other hand, an appropriate design of

the algorithm that allows straightforward modifications of individual regulatory functions according to new experimental findings is essential. In the following sections, the performance of the model is discussed in the light of independent experimental data and current knowledge.

3.5.1 mRNA expression submodel

The experimental data reported by Saggese et al., 2018 used combinations of pH and glc concentrations (7.0, 0.55 mM) that allowed evaluating the response of the AB model to combined variations of solute concentrations different from those used to build our individual regulatory functions. The predicted behaviour of non-inflamed NP cells to such glc and pH combinations (Figure 3.7a) is not surprising and supported by the widely accepted paradigm of catabolic shift in cell activity under glc deprivation, characterized by an overall decline of ECM protein mRNA expression and an increase in protease mRNA expression (Rinkler et al., 2010; Neidlinger-Wilke et al., 2012). Likewise, the predicted augmentation of Col-I expression was expected and is well supported by the literature, since replacement of Col-II with Col-I fibers (fibrosis) could be observed in degenerated NPs (Urban and Roberts, 2003; Wuertz et al., 2009). Thanks to our novel modelling approach, such shifts are now quantifiable and comparable for different user-defined conditions.

Remarkably, while the results obtained by Saggese et al., 2018 under glc deprivation support the general assumption that adverse disc cell microenvironments tend to increase Col-I and MMP-3 mRNA expression (ADAMTS is excluded from validation as those data were used as input for AB model programing), they reveal a tendency toward increased Agg and Col-II mRNA expressions, against common expectations. This was not further discussed by the Authors because significance was not reached. Interestingly, our AB model also showed higher Agg and Col-II mRNA expressions under glc deprivation, but only for the immunopositive cells (Figure 3.7b). Assumingly, this result emerged because IL-1β protein release, and the possible adverse effect thereof on cell activity, is higher at higher glc levels. Hence, less glc, less IL-1β in inflamed cells. This novel insight in cellular behavior within a complex microenvironment suggests that inflammation might shed light on the unexplained experimental findings of Saggese et al., 2018. Figure 3.7b shows that at 5mM glc, the relative mRNA expression of MMP-3 by immunopositive cells was about 0.4, while by immunonegative cells (Figure 3.7a) kept a minimum amount (i.e. 0.0) of relative MMP-3 mRNA expression. These findings agree with the

common association between inflammation and catabolic shift in NP cell activity (Le Maitre et al., 2005). Actually, the catabolic shift in cellular activity was considerable in presence of IL-1β (Figure 3.7a versus Figure 3.7b), such a result is supported by the many evidences that point out sustained inflammation as crucial factor in IVD rupture (e.g. Kepler et al., 2013). However, comparing MMP-3 mRNA expression under glc deprivation for IL-1β immunopositive and immunonegative cells (Figure 3.7a vs. Figure 3.7b), model predictions suggest a lower MMP-3 mRNA expression in inflamed cells, even though MMP-3 is programmed to be highly activated by IL-1β (Table 3.1). This apparent incoherence seems to be numerically based and suggests that the applicability of Eq. 3.1 is limited regarding the comparability between two independent networks, which must be taken into account for future model developments and interpretations.

To estimate effective inflammation, a linear relationship between IL-1β mRNA expression and the quantity of IL-1β proteins was presumed, which could be roughly observed in experimental studies (Gilbert et al., 2016). However, more detailed knowledge about the relationship between mRNA expression and the corresponding amount of synthesized IL-1β proteins, or about the half-lives of IL- 1β protein- or mRNA is required. In the present work, the half-life of IL-1β proteins has been approximated from distantly related studies (Kudo et al., 1990; Larson et al., 2006) and needs to be updated when more accurate data become available.

So far, IL-1β mRNA expression is the only factor that determines the amount of IL-1β protein. However, as well other factors are suggested to affect the levels of IL-1β protein, e.g. MMP-3 might degrade IL-1β (Ito et al., 1996). Thus, further development of the inflammation submodel should include a more sophisticated feed-back looped network for the dynamic regulation of the effective influence of IL-1β. Furthermore, regulations and effects of additional proinflammatory cytokines are deemed to be crucial in microtrauma development. In particular, the emergence and the role of the proinflammatory cytokine TNF-α, handed as a possible initiating factor in IVD degeneration (Millward-Sadler et al., 2009) should be modelled, but such necessary developments are currently hindered by limited experimental evidences in the literature.

The results of the sensitivity analysis (Figure 3.8 and Supplementary Material S6, Appendix 1) showed that a rigorous variation of the equation parameters allow to importantly influence the overall mRNA expression, unless the input parameters of a node were considerably

high (or low) such as in case for Agg and Col-II under non-inflamed conditions. Given that the equation parameters allow to reflect almost linear and Boolean behaviour and intermediate, sigmoidal steps to connect those extrema, this result was not surprising, and highlighted again the importance of a prudent choice of model parameters. In this approach, our default *h* value was chosen to approximate a linear coupling between the model outputs, x_i, and the corresponding total inputs, ω_i (Equation 3.1), which allowed to reflect the interactions of the biologically derived inputs (fitted curves) without any additional mathematical distortion. Values of the activation/inhibition factors, i.e. 0.01, were also chosen to approximate linear variations of ω_i with the respective concentrations of inhibitors and activators, and to preserve the influence of the individual experimental profiles of mRNA expression for each stimulus. Wherever additional strength should be conferred to a specific activator or inhibitor, activation/inhibition factor values can be increased to progressively induce controlled non-linearity. For future model developments, it might be welcome to develop an approach to systematically determine activation/inhibition factors of different stimuli in order to optimally adjust the model behavior to biological evidence. In the meantime, our specific default parameter values provided reasonable results, according to prior knowledge about NP cell behavior.

The presented model aimed to simulate indirect mechanotransduction phenomena. Apart from glc and pH, the role of oxygen on NP cell activity and indirect mechanotransduction is also discussed in literature. However, oxygen was not considered in the present model so far, since the implementation of oxygen effects is hindered by a lack of experimental data on cell behavior at physiological oxygen levels [1–5% (Mwale et al., 2011)] within the NP. Arguably, this is not considered as a crucial limitation, since oxygen levels were reported to have a low effect on the gene expressions hereby simulated, compared to glc and pH (Neidlinger-Wilke et al., 2012). Importantly, our specific model design permits an easy implementation of additional stimuli, allowing for future incorporation of e.g. oxygen or direct mechanotransduction effects (Baumgartner et al., 2019), for more complete simulations of the microenvironment of NP cells.

The functions that relate glc or pH to mRNA expressions of genes were built by considering both significant changes and variation tendencies of mRNA expression, among the different experimental reports used. The reason to take into account variation tendencies is, on the one hand, that the high variability in cellular behavior commonly seen in

experimental studies often hinders to reach significance. On the other hand, we hypothesize that the persistence over time of small changes measured *in vitro* can have clear effects over long time periods. Such hypothesis implies that we hereby consider the chronicity of the cell stimulators studied. Obviously, further model extensions should capture the time variations of these stimulators and the effects thereof, including any possible transient effects. At the nutrition level, such variations can be extracted from long-term Finite Element analyses (Ruiz Wills et al., 2016). Coupled to a mechanotransport Finite Element model such as the one presented by Ruiz Wills et al., 2018, this AB model is able to predict local cellular behavior according to given solute concentrations at the millimeter scale in whatever user-defined region of the NP. The model can be additionally exploited to simulate possible critical cell microenvironments worth to be experimentally explored, e.g. environments around 1mM glc concentration (Ruiz Wills et al., 2018). Furthermore, the AB model could be enriched with solute-transport and metabolic submodels that consider diffusion and metabolic cell processes to autonomically level mRNA expression in different regions of the AB model.

3.5.2 Cell viability submodel

Predicted cell viability was in good agreement with independent, experimental data of Horner and Urban, 2001, who observed a decrease in cell viability to about 65% and 50% (cells cultured without oxygen) after three and seven days exposed to low pH. In comparison, our AB model predicted 78 and 50% of viability if the influence of IL-1β is not considered, and 71 and 41% of cell viability otherwise, after three and seven days of exposure to low pH, respectively (Figure 3.9). Arguably, the minimum pH for our pH-dependent cell regulation curves depended on the lowest pH, i.e. 6.5, found within the experimental studies. In contrast, the experimental study used for independent validation was conducted at pH 6.0. Hence, whether the model might have slightly overestimated the cell viability remains to be explored.
With regard to complete glc deprivation, a cell viability of 1.2% after 2.79 days was predicted by the model (Figure 3.9), which nicely agrees with the experiments of Horner and Urban, 2001 where cells died within three days without glc.
As a limitation, it must be mentioned that the cell viability submodel currently considers cell viability based on additive contributions of biochemical factors (glc, pH and IL-1β protein). Truly, experimental observations (Bibby and Urban, 2004) suggested that coupled factor

influences exist. For further model developments, more independent data about cell death in low glc and high acidic environments would be needed to evaluate whether model predictions significantly differ from observed results. Nevertheless, a future development of the cell viability submodel may include a determination of cell viability by using network-based integrative approaches, able to weight the influence of each environmental stimulus individually. Finally, the average cell size of 10 μm might be slightly underestimated by a few micrometers, which however does not affect the interpretation of the results of the model.

3.6 Conclusion

This investigation aimed to develop and test new modelling and simulation techniques in IVD research for bottom-up virtual exploration of disc tissue regulation and of the negative perturbation thereof. Especially, the presented hybrid model exploited state-of-the-art AB and network modelling approaches. The network model was fed with experimental data to mimic the cellular behavior in a complex biochemical environment, which stands for a huge challenge, not only in IVD research, but in highly multifactorial disorders in general, where the nature and the control of the physicochemical cellular microenvironments greatly matter. Our new developed method successfully integrated discrete, experimental results into continuous cell behavior functions and exploited existing network approaches from systems biology to merge individually weighted stimuli into fully coupled mRNA expressions, which allows for the first time to quantify and compare cell activity under user-defined glc and lac concentrations. First validation tests showed that the AB model predictions agree with different types of independent experimental findings, and simulations led to novel insights in cellular behavior within a multifactorial environment. Moreover, the AB model provides rational clues to explain for the first time unexpected experimental results retrospectively. This shows the ability of *in silico* predictions to contribute to goal-orientated, systematic experimental research and tackle IVD degeneration in an interdisciplinary approach. Thus, feeding a network approach from systems biology with biological data and admitting a direct interference of local environmental conditions seems to be a promising approach for future research.

The strength of this approach is its ability to anticipate and compare new plausible scenarios where experimental quantification is still lacking. Furthermore, it enables an integration of heterogeneous,

experimental data including cells of different species, differences in cell culturing protocols and degeneration levels of IVD tissue as well as dealing with a lack of data. Importantly, the present methodology permits an easy integration of additional stimuli, and updates of the current regulatory functions as soon as new experimental results/findings become available.

Most probably, the NP represents a delicately balanced dynamical system, as local alterations in mRNA expression might lead to local alterations of protein expression. A subsequent, local change in matrix density includes local alterations of tissue porosity at the micrometer scale, which in turn affects local solute concentrations. Therefore, one of the long-term objectives of our work is to couple this AB model with a local Finite Element model. This allows to obtain continuous feedback about local changes in porosities and the effect of interactions at the microscale level on the millimeter scale tissue integrity, which allows a more holistic understanding and description of the dynamics that finally define the crucial mechanisms for microtrauma accumulation and the great diversity of phenotypes in IVD failure.

4 *Evidence-based Network Modelling to Simulate Nucleus Pulposus Multicellular Activity in different Nutritional and pro-Inflammatory Environments*

This chapter is adapted from: Baumgartner L., Sadowska A., Tío L., González Ballester M. A., Wuertz-Kozak K. and Noailly J.: *Evidence-based Network Modelling to Simulate Nucleus Pulposus Multicellular Activity in different Nutritional and pro-Inflammatory Environments* Submitted to Front. Bioeng. Biotechnol. (accepted for publication, doi: 10.3389/fbioe.2021.734258)

4.1 Abstract

Initiation of intervertebral disc degeneration is thought to be biologically-driven. This reflects a process, where biochemical and mechanical stimuli affect cell activity (CA) that compromise the tissue strength over time. Experimental research enhanced our understanding about the effect of such stimuli on different CA, such as protein synthesis or mRNA expression. However, it is still unclear how cells respond to their native environment that consists of a "cocktail" of different stimuli that might locally vary. This work presents an interdisciplinary approach of experimental and *in silico* research to approximate Nucleus Pulposus CA within multifactorial biochemical environments. Thereby, the biochemical key stimuli glucose, pH, and the proinflammatory cytokines TNF-α and IL1β were considered that were experimentally shown to critically affect CA.

To this end, a Nucleus Pulposus multicellular system was modelled. It integrated experimental findings from *in vitro* studies of human or bovine Nucleus Pulposus cells, to relate the individual effects of targeted stimuli to alterations in CA. Unknown stimulus-CA relationships were obtained through own experimental 3D cultures of bovine Nucleus Pulposus cells in alginate beads. Translation of experimental findings into suitable parameters for network modelling approaches was achieved thanks to a new numerical approach to estimate the individual sensitivity of a CA to each stimulus type. Hence, the effect of each stimulus type on a specific CA was assessed and integrated to approximate a multifactorial stimulus environment. Tackled CA were the mRNA expressions of Aggrecan, Collagen types I & II, MMP3, and ADAMTS4. CA was assessed for four different proinflammatory cell states; non-inflamed and inflamed for IL1β, TNF-α or both IL1β&TNF-α. Inflamed cell clusters were eventually predicted in a multicellular 3D agent-based model.

Experimental results showed that glucose had no significant impact on proinflammatory cytokine or ADAMTS4 mRNA expression, whereas TNF-α caused a significant catabolic shift in most explored CA. *In silico* results showed that the presented methodology to estimate the sensitivity of a CA to a stimulus type importantly improved qualitative model predictions. However, more stimuli and/or further experimental knowledge need to be integrated, especially regarding predictions about the possible progression of inflammatory environments under adverse nutritional conditions.

Tackling the multicellular level is a new and promising approach to estimate manifold responses of intervertebral disc cells. Such a top-

down high-level network modelling approach allows to obtain information about relevant stimulus environments for a specific CA and could be shown to be suitable to tackle complex biological systems, including different proinflammatory cell states. The development of this methodology required a close interaction with experimental research. Thereby, specific experimental needs were derived from systematic *in silico* approaches and obtained results were directly used to enhance model predictions, which reflects a novelty in this research field. Eventually, the presented methodology provides modelling solutions suitable for multiscale approaches to contribute to a better understanding about dynamics over multiple spatial scales. Future work should focus on an amplification of the stimulus environment by integrating more key relevant stimuli, such as mechanical loading parameters, in order to better approximate native physiological environments.

4.2 Introduction

Intervertebral disc degeneration is a major cause of low back pain, a disability that stands for one of the highest health burdens worldwide (Hoy et al., 2014). The intervertebral disc is avascular and consists of three specialized tissues: the Nucleus Pulposus (NP), a proteoglycan-rich and highly hydrated structure in the center of the disc, the Annulus Fibrosus, a juxtaposition of concentric fibrous lamellae that surrounds the NP, and the Cartilage Endplate, a thin layer of hyaline cartilage that separates the NP and the inner Annulus Fibrosus from the vertebral bodies. In each tissue, specialized cells regulate the synthesis of a finely balanced extracellular matrix (ECM) by synthesizing tissue proteins and proteases according to a "cocktail" of mechanical and biochemical stimuli sensed by the cells (reviewed in Baumgartner et al., 2021). Thanks to its specialized structure and composition, the intervertebral disc has a very high strength and classical tissue injury might happen at internal pressures higher than 10 MPa (Veres et al., 2008). Thus, organ failure is most likely a slow process, triggered by an adverse cell (micro-) environment, leading to altered cell activity (CA) that finally compromises the tissue composition and strength. These mechanisms, where compromised CA occur in response to undue biochemical and/or mechanical cues, among others, are cornerstone in injury processes. We hereby refer to these mechanisms as biologically-driven injury mechanisms.

Over the past decades, experimental studies have investigated the impact of a broad variety of stimuli on NP CA. In addition to mechanoregulatory stimuli, biochemical stimuli influence NP CA, whereby nutrition-related stimuli and proinflammatory cytokines have been investigated in most depth. The importance of nutrition-related stimuli is a consequence of the avascularity of the disc, where nutrient supply to the cells is diffusion-dependent. Consequently, gradients of pH and glucose (glc) concentration emerge between the peripheral vascular beds at the vertebral endplates and the mid-transversal plane of the NP (Urban et al., 2004). The likely consequences of these gradients in the mechanically loaded intervertebral disc were captured by quantitative *in silico* explorations (Malandrino et al., 2015a; Baumgartner et al., 2021). However, approximations of individual cell responses at the (multi-) cellular level remain poorly investigated. At the micro-/nanoscale level, cell environments are heterogenous, i.e. local cellular stimulus environments vary, e.g. due to local, proinflammatory cytokine expression. Proinflammatory cell stimulations were pointed out as possible key factors in the catabolic shift of NP CA, and might contribute to the development of different degenerative phenotypes, e.g. herniated vs. non-herniated discs (Le Maitre et al., 2007b; Risbud and Shapiro, 2014; Johnson et al., 2015b). Special focus was thereby set on the proinflammatory cytokines interleukin 1 beta (IL1β) and tumor necrosis factor alpha (TNF-α), which have the potential to alter CA by activating intracellular signaling pathways such as Notch, JNK or NF-ϰB (Baumgartner et al., 2021). In agreement with that, it could be shown that the amount of cells immunopositive for IL1β and TNF-α rises as intervertebral disc degeneration progresses (Le Maitre et al., 2005, 2007b).

In order to cope with the overwhelming complexity of the intracellular pathways and interactions thereof while enabling interpretable representations of multifactorial cell regulation, high-level physiological modelling is particularly appealing. A new modelling approach was recently proposed in intervertebral disc systems biology, focusing on the multicellular level where stimuli identified to be relevant for NP cell regulations were directly linked to CA (Baumgartner et al., 2020). Whereas the cell per-se was considered as a black box, this methodology admitted biological data as inputs to approximate the integration of the effects of individual stimuli on the effective CA in multifactorial environments. Hence, *in vitro* studies were used to provide detailed information about the relationship between different stimulus concentrations and a corresponding CA. Results were subsequently

integrated to estimate effective CA in multifactorial biochemical environments that would be closer to the reality of native tissues. However, to approach cell responses within native tissues the pre-processing of biological evidence for proper and systematic integration into systems biology models requires further investigation.

It could be experimentally shown that CA is influenced (i) by the concentration of a stimulus within the cellular (micro-) environment, and (ii) by the type of a stimulus, i.e. the effect of different stimulus concentrations affect different mRNA expression in a different way, e.g. Rinkler et al., 2010; Neidlinger-Wilke et al., 2012; Gilbert et al., 2016. In our recent work, we addressed the interpretable modelling and simulation of the combined effects of different stimulus concentrations on NP CA (Baumgartner et al., 2020). The stimuli we included were glc, pH and IL1β, and the CA studied were the mRNA expressions of Aggrecan (Agg), Collagen Types I & II (Col-I, Col-II) (the main ECM components), and MMP3 and ADAMTS4 (key proteases involved in tissue degradation). The simulated multicellular environment was represented through an agent-based (AB) model and consisted of non-inflamed and IL1β-inflamed NP cells. Normalized mRNA expressions were estimated, depending on the predicted cell states in terms of immunopositivity (non-inflamed; inflamed).

Considering that the impact of a stimulus on a CA does not only depend on the stimulus concentration, but also on the sensitivity of the CA to that stimulus type (e.g. IL1β proinflammatory cytokines might not have the same effect on MMP3 mRNA expression as TNF-α proinflammatory cytokines), we hypothesize that further modelling parameters are necessary to reflect this sensitivity and improve numerical predictions, through a better integration of experimental data. Hence, this publication is a methodological article that reports on a new enabling technology to approximate the integrative effects of multifactorial environments on disc cell stimulation within the NP. Moreover, experimental research was conducted, specifically designed based on modelling requirements, to gain additional evidences about the effect of glc and TNF-α on CA. Based on these new evidences, the modelling of the proinflammatory environment was extended.

4.3 Methods

4.3.1 Methodological approach – overview

The computational model of the system of interest included the nutrition-related stimuli glc, pH and the proinflammatory cytokines TNF-α and IL1β, as regulatory variables able to lead to four different proinflammatory cell states (CS); (i) non-inflamed cells, cells immunopositive for (ii) IL1β or (iii) TNF-α or (iv) for both IL1β&TNF-α. For each CS, targeted CA were the mRNA expressions of the key tissue proteins Agg, Col-I, Col-II and proteases MMP3, and ADAMTS4 (Figure 4.1).

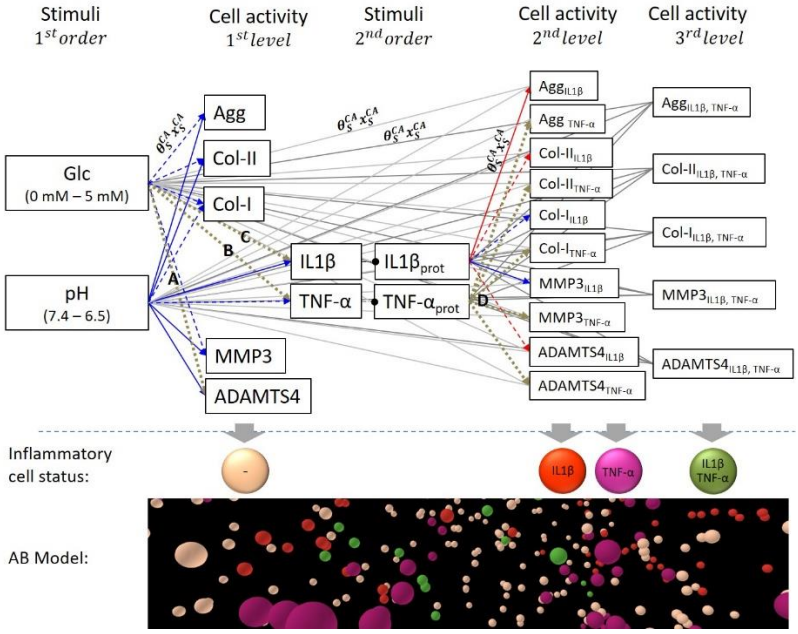

Figure 4.1: System of interest based on nutrition-related stimuli glucose (glc) and pH. Stimulus – cell activity (S-CA) relationships were either activating (blue) or inhibiting (red) according to experimental findings. Dashed blue and red arrows marked non-significant ($p > 0.05$) relationships according to experimental findings and brown dotted arrows unknown S-CA relationships. Respective connections between 1st order stimuli and 2nd/3rd level CA and 2nd order stimuli and 3rd level CA were represented as grey lines to provide a better visibility. Each S-CA relationship is determined by the sensitivity of a CA to a stimulus type (θ_S^{CA}) and by the sensitivity of a CA to a stimulus concentration (x_S^{CA}) (exemplarily illustrated within the system of interest). Resulting CA for different inflammatory cell states were calculated and displayed within a 3D Agent-based (AB) model.

Glc concentration and pH are user-defined (1st order stimuli) and regulate TNF-α and IL1β proinflammatory cytokine expressions (2nd order stimuli). Glc concentration and pH values could vary in physiologically relevant ranges of 0-5 mM glc and a pH 6.5-7.4, respectively (Rinkler et al., 2010; Gilbert et al., 2016). CA of non-inflamed cells (1st level CA) were calculated based on the nutrition-related environment, whilst CA of cells immunopositive for TNF-α and IL1β (2nd level CA) were additionally influenced by their corresponding 2nd order stimulus. Accordingly, 3rd level CA reflected cells with immunopositivity for both proinflammatory cytokines. To sum up, 1st level CA was defined by the combination of two stimuli, 2nd level CA by the combination of three stimuli and 3rd level CA by the combination of four stimuli.

Each connection between a stimulus and a CA described the individual stimulus-cell activity relationships (S-CA relationships). It was determined by the sensitivity of a CA to a stimulus type (subscript S), reflected by a weighting factor (θ_S^{CA}) and by the sensitivity of a CA to a certain stimulus concentration (x_S^{CA}) (Figure 4.1). S-CA relationships were categorized according to their activating or inhibiting nature (blue/red arrows, Figure 4.1), and to their respective biological significance (continuous vs. dashed arrows, Figure 4.1), based on experimental evidence (Le Maitre et al., 2005; Rinkler et al., 2010; Neidlinger-Wilke et al., 2012; Gilbert et al., 2016). In Figure 4.1, repeated connections with the same characteristics over different CA levels, were represented as grey lines to make the network representation visually lighter. S-CA relationships that were not found in the literature (relationships A-D, Figure 4.1) were experimentally obtained hereby through *in vitro* experimental data (Section 4.3.2).

The data-based determination of x_S^{CA} was previously detailed in Baumgartner et al., 2020. In short: to determine x_S^{CA} of nutrition-related stimuli, continuous, sigmoidal functions were built based on discrete experimental findings of x-fold changes in mRNA expressions. Thereby, each stimulus concentration within a physiologically relevant range was assigned to a normalized value (x_S^{CA}) that ranged from a minimum of 0 to a maximum of 1 (Figure 4.2).

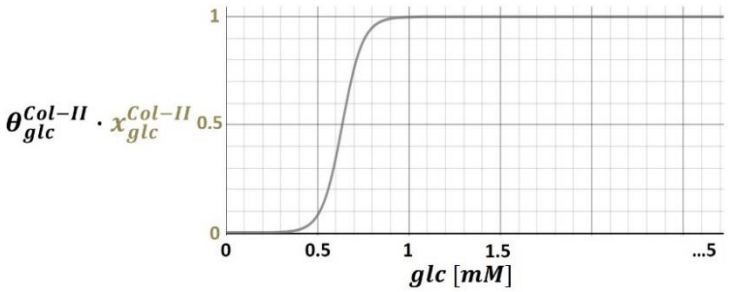

Figure 4.2: illustration of stimulus-cell activity relationships by means of the glucose (glc) – collagen type II (Col-II) relationship; continuous functions assign physiologically relevant glc concentrations (0 – 5 mM) to a normalized Col-II mRNA expression, which was multiplied by an individual weighting factor (θ_S^{CA}).

x_S^{CA} of proinflammatory cytokines was mathematically approximated by an inflammation submodel (see section 4.3.5), because of a lack of information about physiological ranges of proinflammatory cytokine concentrations. Once determined, each x_S^{CA} was multiplied by a S-CA specific weighting factor (Figure 4.2), the calculation of which is presented in Section 4.3.4.

To eventually combine the respective effects of different S-CA relationships and estimate effective CA in terms of individual mRNA expressions, a methodology was developed to semi-quantitatively predict mRNA expressions within a system of parallel networks (PN). The corresponding theoretical framework is briefly described in section 4.3.3 to ensure the comprehensibility of the predicted CA.

Eventually, the CA for each CS was computed with an AB software (NetLogo, v. 6.0.2, Wilensky, 1999) (Figure 4.1) that integrated the network calculations with the spatial dimension of a multicellular system. The 3D AB model mimicked a proinflammatory environment within a 1mm³ volume of the NP environment as previously explained (Baumgartner et al., 2020). Thereby, 4000 agents of a diameter of 10 µm were randomly distributed, representing an average cell density of NP cells (Maroudas et al., 1975). The inflammatory environment is detailed in section 4.3.5.

4.3.2 *In vitro* experiments

To determine the unknown S-CA relationships, the effect of glc on TNF-α, IL1β and ADAMTS4 mRNA expression (Figure 4.1, relationships A - C), and the effect of TNF-α on the targeted mRNA

expressions (Figure 4.1, relationships D) were assessed through *in vitro* experiments on bovine caudal NP cells.
Experimental protocols were established by considering both, previous experimental research and *in silico* findings. To determine CA under different glc concentrations, the experimental setup was inspired by Rinkler et al., 2010, whose data were previously used to determine the glc-CA relationships within the system (Figure 4.1, Baumgartner et al., 2020). Accordingly, bovine NP cells were seeded into alginate beads and exposed to glc levels of either 0 mM, 0.5 mM and 5 mM, whereby the 5 mM concentration served as control. Additional glc concentrations of 0.8 mM and 1 mM were considered to reflect hypothetical transitional nutritional conditions within the NP that might differentiate normal and early degenerated intervertebral discs, according to previous *in silico* findings (Ruiz Wills et al., 2018).
To assess the effect of TNF-α on the targeted mRNA expressions, a 5 mM glc medium was enriched with a TNF-α protein concentration of 10 ng/ml, in agreement with previous experimental research on proinflammatory cytokines (Le Maitre et al., 2005; Millward-Sadler et al., 2009; Walter et al., 2015; Likhitpanichkul et al., 2016; Yang et al., 2017). Cell cultures exposed to 5 mM glc concentration without TNF-α served as control.
In addition to the required S-CA relationships, cell viability was measured for all the conditions. The effect of glc (partial) deprivation on Agg, Col-I, Col-II and MMP3 and the effect of TNF-α on the mRNA expressions of TNF-α and IL1β was also assessed. Corresponding results are presented as supplementary material S1 and S2 (Appendix 2).

4.3.2.1 Cell isolation and culture

NP cells were isolated from bovine tails (n=5) by 0.3% Dispase II (04942078001, Roche, Basel, Switzerland) /0.2% Collagenase NB4 (17454, Serva, Heidelberg, Germany) digestions with 3% Antibiotics-Antimycotics solution in PBS as previously described (Cambria et al., 2020; Sadowska et al., 2020). Cells were then expanded in 2D conditions for around 14 days in DMEM/F-12 (Thermo Fisher/Gibco 11320033) [25 mM glc], with 10% fetal calf serum (FCS) (F7524, Sigma) and 1% Antibiotics-Antimycotics solution. Three to five days prior to the experiment, the medium was changed to DMEM (Thermo Fisher/Gibco 11965092) with 10% FCS and 1% Antibiotics-Antimycotics.

4.3.2.2 Cell stimulation

All cell stimulation experiments were conducted on passage 2 NP cells seeded into alginate beads as previously described (Krupkova et al., 2014). Briefly, NP cells were transferred to a 1.2% alginic acid sodium salt (180947, Sigma-Aldrich, St. Louis, MO, USA) at a density of $4x10^6$ cells per ml alginate (reflecting the average cell density within the NP (Maroudas et al., 1975)). A 21 G needle was used to create the alginate beads. Eventually, an average of 101 ± 8 alginate beads with a total of 8.5-9x10^6 NP cells was obtained from each donor. Beads were cultured in 5 mM glc for 24 h, to allow the cells to adapt their glycogen stores to a physiological glc environment. Subsequently, each well of a 6 well plate was exposed for 48 h to one of the aforementioned glucose concentrations or to a TNF-α enriched medium (10 ng/ml human recombinant TNF-α, (17.4kDa, PeproTech, 300-01A)) at 5mM glc, under a normoxic environment and pH 7.4. The different glc concentrations were created by mixing DMEM high glc (Thermo Fisher (Gibco) 11965092) and DMEM no glc (Thermo Fisher (Gibco) 11966025) in the respective ratios. The culture medium was changed after 24h in order to maintain the chosen glc conditions under metabolic cell activity. Imposed culture conditions were static and mRNA expression and cell viability were assessed immediately after the 48 h of exposure to the stimulus.

4.3.2.3 Cell viability measurement and mRNA expression analysis

Cell viability was assessed by exposing one bead per condition to a 10 μm Calcein AM (CaAM)/1 μM Ethidium Homodimer (EthHD) solution, for approximately 1 h. Afterwards, the bead was gently squeezed between a microscope slide and its cover glass, and cells were counted under a fluorescence microscope (Olympus IX51, Tokyo, Japan). The number of cells was analyzed within up to four different regions of the bead, and cells were counted within a predefined area, using a grid of constant size for each sample. Remaining alginate beads were dissolved during 30 min and occasional shaking in a dissolving buffer (55 mM Sodium citrate solution (71406, Sigma, in 0.9% NaCl)). Isolated cells were pelleted by centrifugation, washed 1x with PBS and subsequently lysed in the specific lysis RLT buffer (plus 1% 2-Mercaptoethanol) of the RNeasy Mini Kit 50 (QIAGEN, ID 74104). mRNA was extracted following the protocol provided by the manufacturer, and the quality and quantity of RNA was analyzed using a Nanodrop 1000 Spectrophotometer (Thermo Fisher Scientific). 1 μg

of total RNA was finally reverse transcribed into cDNA in a 30µl volume using the Taqman Reverse Transcription kit (#4374966, Applied Biosystems, USA).
cDNA was then mixed with Bovine TaqMan primers (Primer Seq. No.: ADAMTS4: Bt03224693_m1, MMP3: Bt04259497_m1, Agg: Bt03212186_m1, Col-I: Bt03214883_m1, Col-II, Bt03251861_m1) to assess changes in the gene expressions of Agg, Col-I, Col-II, ADAMTS4 and MMP3. As for TNF-α and IL1β gene expressions, cDNA was additionally amplified, as initial real-time qPCR showed a gene expression at high Cq. Amplification was performed following the manufacturer's protocol. In short, cDNA was mixed with TaqMan PreAmp Master Mix (2X) (#4391128, Thermo Fisher, Switzerland) and pooled assay mix consisting of TaqMan Primers (Thermo Fisher, Switzerland) diluted with 1X TE Buffer (AM9849, Thermo Fisher, Switzerland) to a final concentration of 0.2X. For the gene expression analysis 4.5 µL or 37.5 ng of amplified cDNA was combined with 5 µL TaqMan Fast Universal PCR Master Mix (2X) (#4352042, Thermo Fisher, Switzerland) and 0.5 µL TaqMan primers (Life Technology, Primer Seq. No: TNF-α: Bt03259156_m1, IL1β: Bt03212741_m1) to a total volume of 10 µL per well.

Gene expressions were measured by the real-time qPCR (CFX96 Touch™ Detection System, Biorad) and all conducted in duplicate. Previous testing revealed YWHAZ (TaqMan Primer Seq. No: Bt01122444_g1) as an appropriate housekeeping gene. The $-2^{\Delta\Delta Ct}$ method was used to normalize and compare the mRNA contents between treatments and the control sample (5 mM glc).

4.3.2.4 Statistics

Statistical analyses were performed using SPSS software version 23.0. Evaluations were done on the ΔCt values, i.e. on the difference of the targeted genes to the housekeeping gene, leading to statistically reliable data by obtaining a variance as well for control groups. Based on the small sample sizes, non-parametric tests were performed, consisting of a Kruskall-Wallis H test for the evaluation of the effect of different glc concentrations on mRNA expressions, and a Mann-Whitney U test to evaluate the effect of a TNF-α enriched medium. The significance level was set to $p < 0.05$.

4.3.3 Overview of the parallel networks methodology

To mathematically provide interrelated results for many parallel networks, a methodology was developed to (i) estimate the activation of each CA by integrating the effect of each corresponding S-CA relationship and (ii) to relate the activation of each CA to other concurrent CA. A network was defined as the group of S-CA relationships that converges to a specific CA. From now on, the methodology hereby defined is referred to as the parallel networks (PN)-Methodology. It required the predefinition of a system, i.e. the PN-system, of all the CA where a relative interpretation is desired. In the system of interest presented in Figure 4.1, these CA would be the 1st, 2nd and 3rd level CA.

To calculate a PN-system, an equation was developed, referred to as the PN-equation (Eq. (4.1)).

$$\omega_{CA,CS} = \left(\left(\frac{1+\sum\theta_{\alpha}}{\sum\theta_{\alpha}}\right)\left(\frac{\sum\theta_{S,\alpha}^{CA}x_{S,\alpha}^{CA}}{1+\sum\theta_{S,\alpha}^{CA}x_{S,\alpha}^{CA}}\right)\right) \cdot\left(1-\left(\left(\frac{\sum\theta_{S,\beta}^{CA}}{\sum\theta_{S,\alpha}^{CA}+\sum\theta_{S,\beta}^{CA}}\right)\left(\left(\frac{1+\sum\theta_{\beta}^{CA}}{\sum\theta_{\beta}^{CA}}\right)\left(\frac{\sum\theta_{S,\beta}^{CA}x_{S,\beta}^{CA}}{1+\sum\theta_{S,\beta}^{CA}x_{S,\beta}^{CA}}\right)\right)\right)\right) \quad (4.1)$$

The PN-equation originated from the graph-based modelling approach developed by Mendoza and Xenarios, 2006 that semi-qualitatively describes biological network dynamics at a subcellular scale, with integration of the simultaneous effects of different inputs on the effective regulation of a specific node. Accordingly, the overall activation of a CA of a certain CS, $\omega_{CA,CS}$, in Eq. (4.1), was determined by an activating (subscripts α) and an inhibiting (subscripts β) term. Thereby, θ_{α} are the weighting factors of all activating S-CA relationships within the PN-system, $\theta_{S,\alpha}^{CA}$ are the activating weighting factors of a specific network, $\theta_{S,\beta}^{CA}$ are the inhibiting weighting factors of a specific network. Finally, θ_{β}^{CA} reflects all the inhibiting connections within the same CA, independently of the CS. $\omega_{CA,CS}$ were bound between 0-1 and reflect PN-activities. PN-activities provide activation levels for the individual, interrelated CA within the PN-system. Hence, the PN-activity is a quantity that assesses the CA. Accordingly, the lower a PN-activity is, the lower the activity of a cell to express that respective mRNA.

The PN-activity is a scalar calculated with 4 decimals, determined based on pilot network calculations. The resolution was aimed to be sensitive enough to reflect small changes in CA, which were often identified within three to four decimal places (see Figure 4.10 in the results section). Such resolution makes sense with regard to the long-term cumulative effect of small persistent perturbations, as it is likely to happen in slowly developing disorders such as intervertebral disc degeneration. Accordingly, the continuous functions formerly determined (Baumgartner et al., 2020) to define the sensitivity of a CA to a stimulus concentration (briefly explained in section 4.3.1) were refined to achieve this resolution. Functions are provided as supplementary material S3 (Appendix 2).

4.3.4 Determination of weighting factors

To determine individual weighting factors, experimental information about the capacity of a stimulus to alter CA was used. This capacity is reflected in the maximal change in x-fold mRNA expression (ϵ) found within the physiologically relevant range of stimulus concentrations. Any change induced by a varying stimulus concentration led to x-fold mRNA expressions either higher ($\epsilon > 1$) or lower ($0 < \epsilon < 1$) than the control level (1). To mathematically achieve semi-bounded ranges for both increase and decrease of x-fold mRNA, reciprocal proportional relationships, $f(\epsilon) = \epsilon$ and $f(\epsilon) = \frac{1}{\epsilon}$, were implemented for $\epsilon > 1$ and for $0 < \epsilon < 1$, respectively (Figure 4.3). As such, $f(\epsilon)$, from now on called the "cellular effort", becomes infinite for both increased and decreased mRNA expressions relative to control. Note that the wording "cellular effort" does not refer to any biological intracellular activity here.

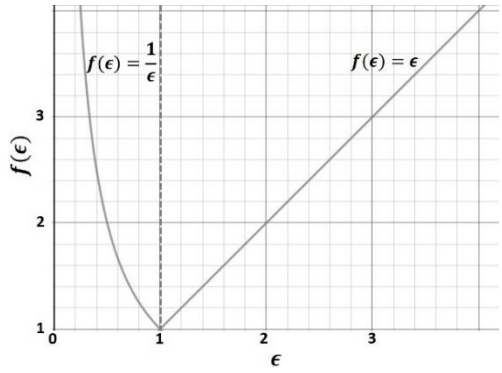

Figure 4.3: Cellular effort to compare augmentations and decreases of x-fold mRNA expressions (ϵ).

To obtain θ_S^{CA}, $f(\epsilon)$ was scaled by a constant scaling factor ($\vartheta_{\theta_{max}}$)(Eq. (4.2)) to a predefined range of $0.01 \leq \theta_S^{CA} \leq 1$. Hence $\theta_{min} = 0.01$, $\theta_{max} = 1$ and, accordingly $\vartheta_{\theta_{max}} = \vartheta_1$. Values of 0.01 (or lower) approximate a linear coupling between x_S^{CA} and $\omega_{CA,CS}$ (Mendoza and Xenarios, 2006) (Figure 4.4).

$$f(\epsilon)/\vartheta_{\theta_{max}} = \theta_S^{CA} \tag{4.2}$$

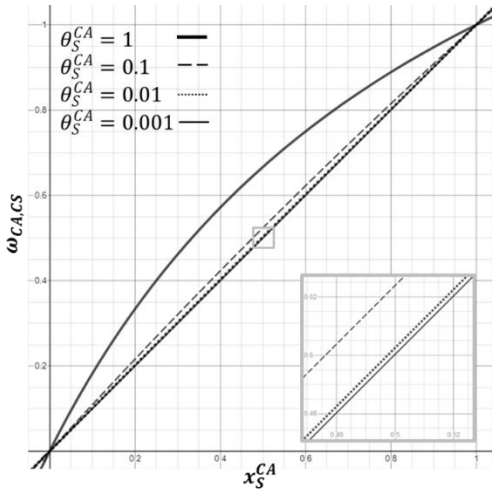

Figure 4.4: Illustration of effect of the size of a weighting factor (θ_S^{CA}) of the sensitivity of a CA to a certain stimulus concentration (x_S^{CA}) on the overall cell activity ($\omega_{CA,CS}$). Example of different values ranging from θ_S^{CA}=0.001 to θ_S^{CA}=1.

If a stimulus type did not significantly alter an x-fold mRNA expression, θ_S^{CA} was set to 0.01, approximating a linear relationship between x_S^{CA} and $\omega_{CA,CS}$. Experimental data about x-fold mRNA expressions was obtained from literature and from the actual study (see results section 4.4.1) (Table 4.1).

Table 4.1: Individual weighting factors for the tackled PN-system, i.e. 1st, 2nd and 3rd level CA (Figure 4.1), along with the scaling factors and cellular efforts. Individual weighting factors were derived from the cellular effort ($f(\epsilon)$), based on x-fold mRNA expressions (ϵ). The scaling factor $\vartheta_{\theta_{max}} = \vartheta_1 = 28.7$ was determined by the S-CA relationship pH-MMP3. NS: Not significant; act: activating; inh: inhibiting; *: estimated ϵ.

Stimulus	**mRNA**	**ϵ**	**$f(\epsilon)$**	**θ_S^{CA}** (ϑ_1=28.7)	**Source**	**Cell type**
Glc	Agg	NS, act	-	0.0100	Rinkler et al., 2010	human
	Col-I	NS, act	-	0.0100	Rinkler et al., 2010	human
	Col-II	NS, act	-	0.0100	Rinkler et al., 2010	human
	MMP3	NS, act	-	0.0100	Rinkler et al., 2010	human
	ADAMTS4	NS, act	-	0.0100	Actual study	bovine
pH	Agg	0.37	2.7027	0.0942	Gilbert et al., 2016	human
	Col-I	NS, act	-	0.0100	Gilbert et al., 2016	human bovine
	Col-II	0.63	1.5873	0.0553	Neidlinger-Wilke et al., 2012	
	MMP3	28.7	28.7000	1.0000	Gilbert et al., 2016	human
	ADAMTS4	5.7	5.7000	0.1986	Gilbert et al., 2016	human
IL1β	Agg	0.45*	2.2222	0.0774	Le Maitre et al., 2005	human
	Col-I	NS, act	-	0.0100	Le Maitre et al., 2005	human
	Col-II	NS, inh	-	0.0100	Le Maitre et al., 2005	human
	MMP3	10.8*	10.8000	0.3763	Le Maitre et al., 2005	human
	ADAMTS4	NS, inh	-	0.0100	Le Maitre et al., 2005	human
TNF-α	Agg	NS, inh	-	0.0100	Actual study	bovine

Col-I	0.31	3.2258	0.1124	Actual study	bovine
Col-II	0.06	16.6667	0.5807	Actual study	bovine
MMP3	26.85	26.8500	0.9355	Actual study	bovine
ADAMTS4	5.77	5.7700	0.2010	Actual study	bovine

To explore the impact of individualized weighting factors on a PN-activity, the respective effects of three physiologically relevant nutritional environments in terms of pH and glc concentrations were calculated: one optimal nutritional environment (i) (Nachemson, 1969; Rinkler et al., 2010), and two altered nutritional environments in the mid-transverse plane. These two mid-transverse plane environments were defined through our in-house mechanotransport finite element (FE) simulations (Ruiz Wills et al., 2018) and referred to the anterior region of the NP where the most adverse nutrient conditions arose within the mechanically loaded intervertebral disc. They respectively reflected glc concentration and pH values for (ii) non-degenerated and (iii) early degenerated cartilage endplate conditions. The nutrient concentrations around the mid-transverse plane of a non-degenerated mechanically loaded intervertebral disc (i.e. (ii)) were referred to as borderline conditions (Table 4.2).

Table 4.2: Nutrition-related stimuli, input parameters.

	Optimal conditions	**Borderline conditions**	**Early degenerated conditions**
Glucose [mM]	5	1.0293	0.8901
pH	7.1	6.9531	6.9349

A second set of calculations was run with all the weighting factors set to 0.01, in order to assess the impact of a systematic integration of stimulation strengths in the PN-system.

4.3.5 Determination of inflammation

To estimate inflammatory parameters, an inflammation submodel was developed, based on previous work reported in Baumgartner et al., 2020. Based on the user-defined nutritional environment, a global (i.e., not cell-specific) normalized CA for TNF-α ($\omega_{TNF\text{-}\alpha}$) and IL1β ($\omega_{IL1\beta}$) mRNA expressions was predicted. This global normalized CA was, moreover, used to estimate the amount of immunopositive cells and concentrations of proinflammatory cytokines (Figure 4.5).

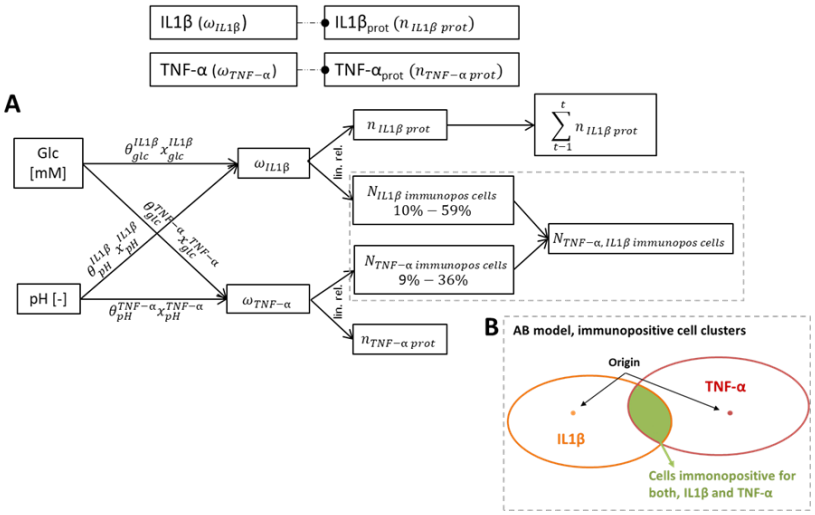

Figure 4.5: Inflammation submodel**.** A: underlying network of the schematically represented inflammation submodel in Figure 4.1 (top), to approach mRNA expressions and protein synthesis of TNF-α and IL1β. B: illustration of the determination of NP cells immunpositive for both, TNF-α and IL1β by the agent-based (AB) model. Prot: protein, immunopos: immunopositive, n: normalized, N: number, t: time, lin. rel.: linear relationship.

mRNA expressions of TNF-α and IL1β were estimated by using the regulatory network (ω_i) introduced by Mendoza and Xenarios, 2006, and they were allowed to vary within a normalized range, i.e., from 0 to 1. The proinflammatory cytokine synthesis was programmed to be proportional to the corresponding mRNA expression. The half-life of IL1β proteins was set to 2h (Baumgartner et al., 2020), whereas a half-life of 1h was imposed for TNF-α, chosen according to the distantly related data of Oliver et al., 1993. The duration of the latter corresponded to the time-step of our AB model (Baumgartner et al., 2020) and was, therefore, the shortest implementable half-life.

To estimate current amounts of inflamed cells, $\omega_{IL1\beta}$ and $\omega_{TNF\text{-}\alpha}$ were proportionally related to the percentage of inflamed human NP cells as experimentally assessed for degenerated and non-degenerated human intervertebral discs (Le Maitre et al., 2007). Those authors found that the percentage of inflamed cells ranges within approx. 10% - 59% for IL1β and approx. 9% - 36% for TNF-α (mean values ± two standard errors). For example: the percentages of IL1β inflamed cells are in a range of 17%±7% for non-degenerated NP and in a range of 52%±7% for degenerated NP. Hence, the overall range considered for IL1β inflamed cells was 10% - 59%.

To initialize the immunopositivity within the AB model, 30 out of 4000 cells were randomly selected as nucleation points for 15 IL1β and 15 TNF-α immunopositive clusters. Clusters were formed around those points according to the calculated percentage of inflamed cells consistent with current nutrient concentrations and considering the globally shortest distance from an inflamed to a non-inflamed cell. Based on the randomly chosen static position of each cell, unique forms of proinflammatory cell clusters emerged for each model setup.
The number of cells immunopositive for both IL1β&TNF-α was determined by the AB model, being the cells located in overlapping areas of IL1β and TNF-α immunopositive cell clusters (Figure 4.5, B). Eventually, proinflammatory environments were calculated for optimal, borderline and early degenerated nutritional conditions (Table 4.2). Thereby, average values were calculated out of ten AB-model simulations per modelled microenvironment with the data set of S-CA specific weighting factors. Slight differences in model predictions leading to standard deviations are likely caused by AB solver stochasticity and do not have any impact on overall interpretations (see results section 4.4.2.1). Therefore, the percentage of inflamed cells for the comparative simulations using invariant weighting factors of 0.01 is based on one single representative model simulation.
The weighting factors of the inflammation submodel, i.e., the sensitivity of IL1β and TNF-α mRNA expressions to nutrients, were obtained by using the scaling factor determined by the PN-system (ϑ_1=28.7). Note that θ_S^{CA} might become larger than 1, since $\omega_{IL1\beta}$ and $\omega_{TNF\text{-}\alpha}$ are not part of the PN-system. Required x-fold mRNA expressions to obtain the weighting factors were received out of both the literature and the *in vitro* experiments of the current study (see results section 4.4.1) (Table 4.3).

Table 4.3: Individual weighting factors for the inflammation submodel. ϵ: x-fold mRNA expression, θ_S^{CA}: cell activity and stimulus-specific weighting factor. NS: Not significant. act: activating.

Stimulus	**mRNA**	**ϵ**	**$f(\epsilon)$**	**θ_S^{CA}**	**Source**	**Cell type**
Glc	IL1β	NS, act	-	0.01	Actual study	bovine
	TNF-α	NS, act	-	0.01		
pH	IL1β	81	81.0000	2.8223	Gilbert et al., 2016	human
	TNF-α	NS, act	-	0.01		

4.4 Results

4.4.1 Experimental results and system of interest

The complete or partial deprivation of glc did not have any statistically significant effect on the mRNA expressions IL1β, TNF-α and ADAMTS4 (Figure 4.6). Yet, all measured mRNA expressions tended to decrease under complete glc deprivation. Results for IL1β and TNF-α mRNA expressions at 0.5 mM glc were based on four donors instead of five, due to experimental issues.

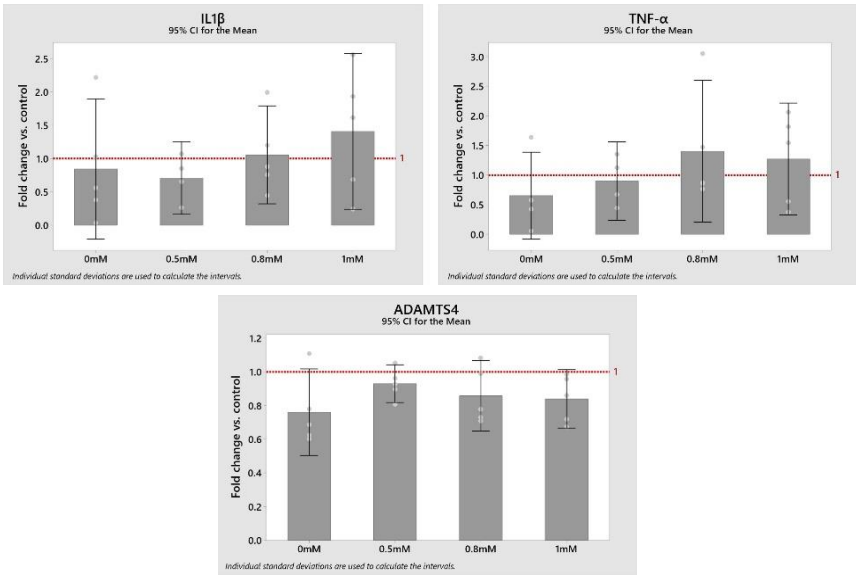

Figure 4.6: mRNA expression of the proinflammatory cytokines IL1β and TNF-α and the protease ADAMTS4 at 0 mM, 0.5 mM, 0.8 mM and 1 mM glucose concentrations compared to control (1-fold). Data is displayed as mean values with a corresponding 95% confidence interval and individual values (round dots).

In contrast, medium enrichment with 10 ng/ ml TNF-α caused a significant change in the mRNA expressions of Col-I (0.31 ± 0.09 -fold), Col-II (0.06 ± 0.02 -fold), ADAMTS4 (5.77 ± 2.50 -fold) ($p < 0.01$) and MMP3 (26.85 ± 15.43 -fold) (all $p < 0.05$), but no significant change in the mRNA expression of Agg (0.47 ± 0.22 -fold) ($p = 0.076$) (Figure 4.7).

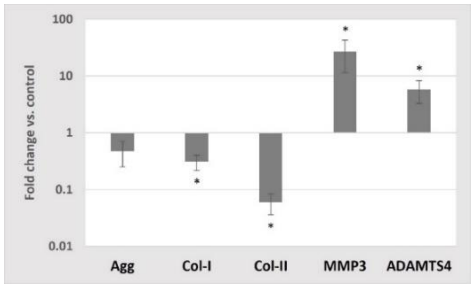

Figure 4.7: Average mRNA expressions (logarithmic scale) and standard deviations of extracellular matrix proteins and proteases after exposing cells to 10 ng/ml TNF-α, 5 mM glc and pH 7.4. *: significantly ($p < 0.05$) different from control (1-fold).

The obtained experimental measurements led to complete the PN network description of the system of interest, with all activating and inhibiting links (Figure 4.8).

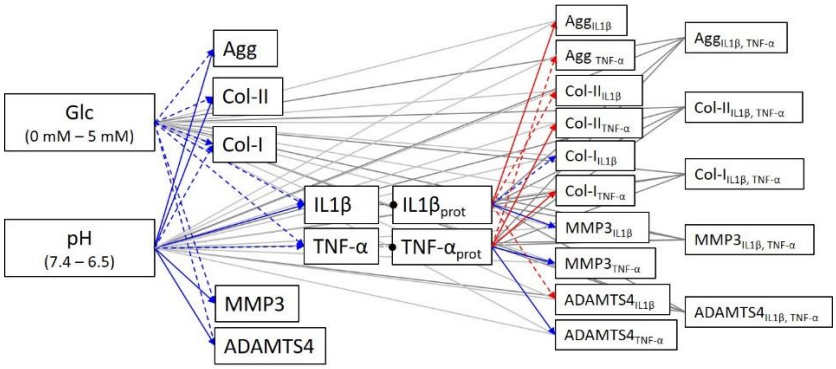

Figure 4.8: completed system of interest according to additional experimental data. Blue arrows: activating links; Red arrows: inhibiting links; Dashed arrows: statistically non-significant tendencies

4.4.2 *In silico* predictions

4.4.2.1 The proinflammatory environment

The average percentage of cells immunopositive for IL1β (i.e. the sum of cells immunopositive for only IL1β and of both, IL1β&TNF-α) was around 16%, in all three simulated microenvironments, i.e., 15.76 ± 0.11 % under optimal; 16.18 ± 0.14 % under borderline; 16.23 ± 0.16 % under early degenerated conditions. The percentage of TNF-α inflamed cells rose from around 15% under optimal to 26% under borderline up to 33% under early degenerated conditions. Model predictions for cells

immunopositive for both, IL1β&TNF-α rose from approximately 1% under physiological to around 2 % under early degenerated conditions. The numbers of inflamed cells for TNF-α only, IL1β only or for both TNF-α&IL1β are displayed in Figure 4.9 for each nutrient condition.

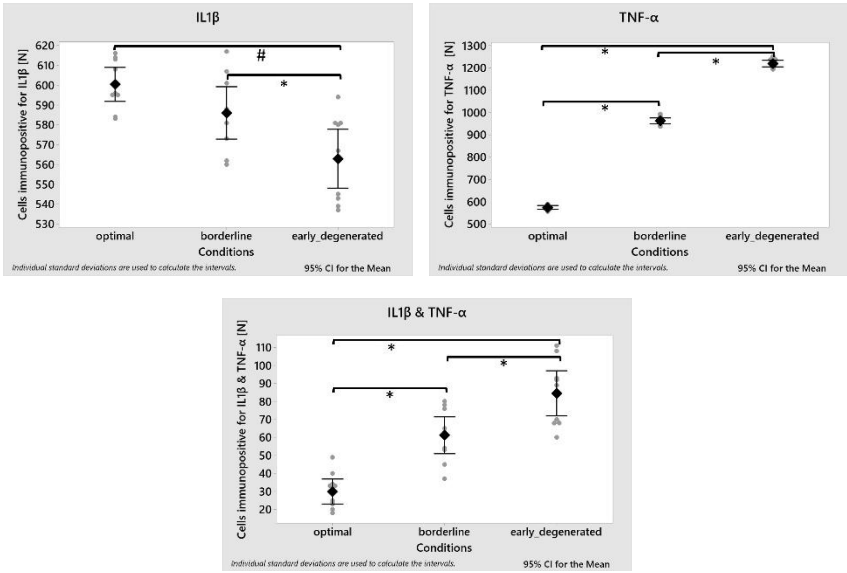

Figure 4.9: model predictions for an inflammatory environment within an optimal, borderline and early degenerated nutritional environment. Average amount of inflamed cells (square) with corresponding 95% confidence interval and individual values (grey dots) (n=10 simulations per condition). ANOVA test showed significant differences between conditions in the three groups studied (p-value < 0,001). Post-hoc analysis showed that the number of cells immunopositive for IL1β were significantly lower in the degenerated conditions compared with the optimal and borderline conditions (p-value 0,000 and 0,017, respectively). On the other hand, in the case of cells immunopositive for TNF-α and for IL1β&TNF-α, significant differences were observed between the three conditions (p-value<0,001).

The use of invariant weighting factors of 0.01 led to a cell immunopositivity for IL1β ranging from around 19% for optimal conditions to 35% for borderline and early degenerated conditions. TNF-α immunopositivity did not change, since S-CA specific weighting factors to determine TNF-α have a value of 0.01 (Table 4.3).

4.4.2.2 Cell activity

Using invariant weighting factors, predicted CA profiles of different inflammatory CS are similar under optimal nutritional conditions,

leading to a higher variation under progressively adverse nutrient environments (Figure 4.10, A, from top to bottom). The PN-activity for ADAMTS4 is generally elevated throughout all CA profiles. PN-activities of Agg and Col-II are the same or similar within a CA profile. In contrast, an application of S-CA specific weighting factors leads to distinct CA profiles for different inflammatory CS and different nutritional conditions (Figure 4.10, B). This includes a pronounced difference between the CA profiles of IL1β and TNF-α inflamed cells, standing out in particular by an elevated protease mRNA expression under the influence of TNF-α (Figure 4.10, B). The predicted PN-activity of ADAMTS4 is lower in non-inflamed and IL1β inflamed cells (Figure 4.10, B vs. A). Within individual CA profiles, Col-II is generally predicted to be lower than Agg due to an integration of S-CA specific weighting factors (Figure 4.10, B vs. A). CA profiles of cells immunopositive for both TNF-α&IL1β are similar to the ones of TNF-α inflamed cells (Figure 4.10, B).

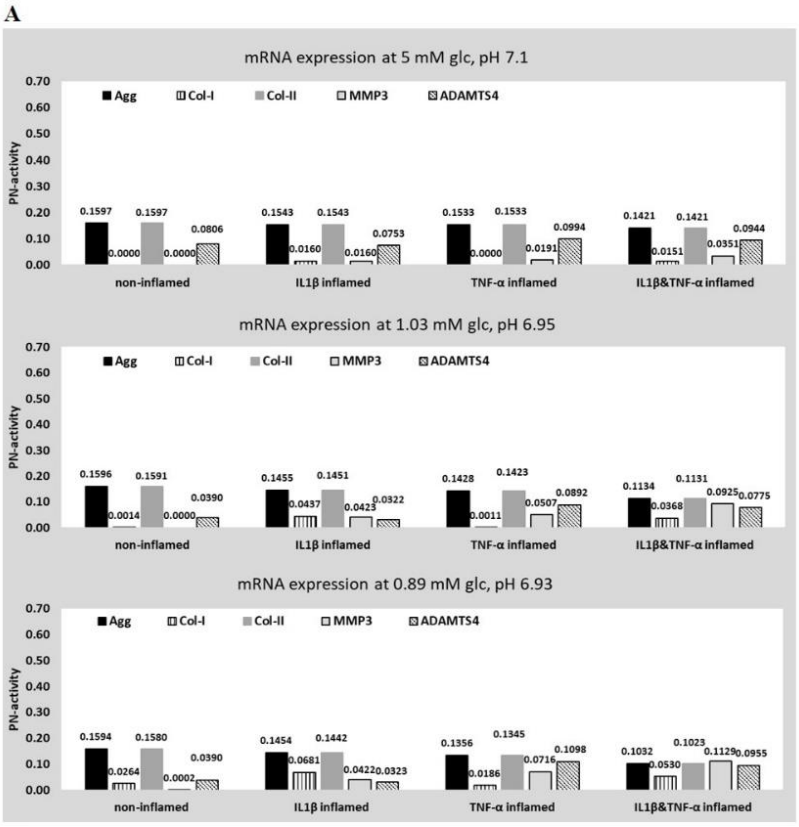

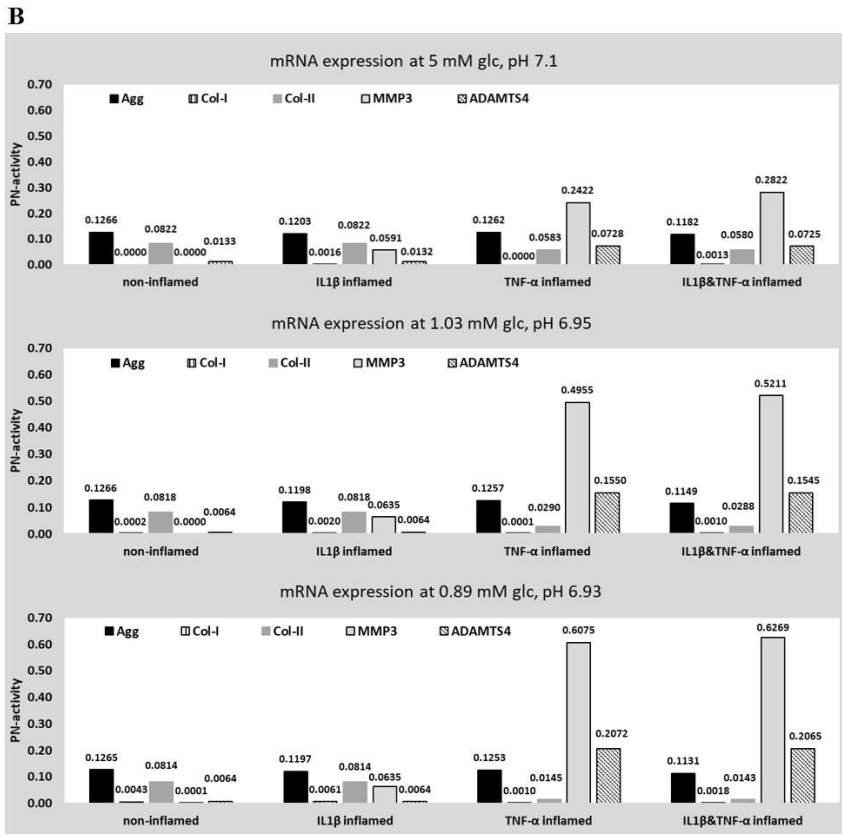

Figure 4.10: Prediction of five target mRNA expressions for four different proinflammatory states. Values were obtained for optimal, borderline and early degenerated, nutritional stimulus combinations. Data was obtained for two sets of weighting factors; an invariant weighting factor of 0.01 (A) and an individual weighting factor (B).

4.5 Discussion

4.5.1 Experimental results and system of interest

The need for experimental research was defined by specific *in silico* requirements, which reflects a novelty of this approach. As a consequence, rather unexplored relationships between nutrition-related stimuli and proinflammatory cytokine mRNA expressions were investigated. Measurements suggested non-significant effects of glc variations on the tackled proinflammatory cytokines and on ADAMTS4 (Figure 4.6). Thus, (partial) glc deprivation might not directly trigger enhanced proinflammatory conditions, even though both factors

coexist under progressive degeneration (Le Maitre et al., 2005, 2007b; Ruiz Wills et al., 2018).
Furthermore, experimental results could not confirm major differences in mRNA expressions at 0.8 mM compared to 1 mM glc concentration. This result suggests that 0.8 mM glc derived from FE predictions (Ruiz Wills et al., 2018) with early degenerated cartilage endplate, might not stand for a relevant nutritional stress for the cells. Arguably, a drop of pH (around 6.9) predicted by the aforementioned FE simulations was not imposed in the experimental setup. The reason for this was that our experiments aimed to provide information about the effect of the variation of a single stimulus at once on a CA, in order to incorporate the measured data in the parallel network model. However, we acknowledge the importance of accessing experimental data with crossed variations of the micro-environmental conditions. Furthermore, general limitations of the experimental part of this study, especially the small sample size, might have masked possible effects. However, for this modelling approach, as well non-significant data is valuable, since as well tendencies in mRNA expressions due to different stimulus concentrations were considered. The underlying reason was that the chronicity of marginal changes in cell responses might play an important role in intervertebral disc degeneration. Such marginal changes, however, might be masked in experimental research due to pronounced standard deviations and tendentially low sample sizes. Eventually, the impact of experimentally determined significances was regulated by the S-CA specific weighting factors (see section 4.3.4).
Significant catabolic shifts in CA were observed due to a TNF-α enriched culture medium. This was not surprising, as strong catabolic shifts in cell responses are generally attributed to TNF-α (Purmessur et al., 2013). Catabolic cell responses under the influence of TNF-α could be confirmed for concentrations as low as 1ng/ml (Séguin et al., 2005). In the current study, a proinflammatory cytokine concentration of 10 ng / ml was applied to facilitate comparability with data from IL1β stimulation (Le Maitre et al., 2005). Although such concentrations might be hyper physiological with physiological levels of TNF-α possibly rather being in the order of pg/ml than ng/ml (Takahashi et al., 1996; Gawri et al., 2014; Zou et al., 2017), they are commonly used *in vitro* to model a pronounced and measurable cell response, even with short stimulation periods. Hence, current predictions about the impact of inflammation on a CA might be disproportionate compared to non-inflamed cell responses. Furthermore, this study used bovine NP cells as a model for non-degenerated human NP cells. This was done before

(Rinkler et al., 2010), but, of course, it contains a certain uncertainty regarding the translation of findings between different species. Arguably, differences between cell responses of degenerated and non-degenerated intervertebral discs are known (Le Maitre et al., 2005, 2008, 2009), but these experiments aimed to provide results to inform a computational model of non-degenerated intervertebral disc cells, to numerically explore the dynamics of initial catabolic responses of those cells. Furthermore, the experiments were conducted at normoxic conditions, which does not reflect the conditions within an intervertebral disc NP. However, this bias was constantly present throughout the experimental setup, and is therefore considered to have not importantly affected the relative effects of different glc concentrations or TNF-α measured in this study.
More knowledge about the cell response to TNF-α exposure at physiological concentrations might be highly relevant for further model developments. This would allow to ideally estimate the effect of proinflammatory cytokine concentrations as continuous functions, as done for nutrition-related stimuli (Baumgartner et al., 2020, (Figure 4.2)). This includes an overall confirmation of the catabolic effect of TNF-α under physiological conditions, especially in the light of experimental research with IL1β that showed an anabolic effect on Agg mRNA expression within 0.001 - 0.1 ng/ml (Phillips et al., 2015).
Eventually, the experimental data obtained by the current experimental research completed the biological data needed to determine evidence-based S-CA relationships and allowed, therefore, to complete the system of interest (Figure 4.8).

4.5.2 *In silico* predictions

4.5.2.1 The proinflammatory environment

Expected percentages of IL1β inflamed cells for non-degenerated and degenerated intervertebral discs were provided from literature. They range around 17% ± 7% under non-degenerated and 52% ± 7% under degenerated conditions (Le Maitre et al., 2007). Thereby, the cohort included patients with severely degenerated tissues. Using S-CA specific weighting factors, the range of IL1β immunopositive cells predicted by the model ranges around 16% for all simulated conditions and hereby lies within the range estimated for non-degenerated conditions. The slight decrease of IL1β immunopositivity in simulated early degeneration (Figure 4.9) is compensated by an increased number of cells immunnopositive for both, IL1β&TNF-α. Hence the overall

amount of IL1β inflamed cells slightly rose under progressively adverse nutritional environments, from 15.76% to 16.23%. Nevertheless, the inflammation within degenerated conditions might be underestimated, given that early degeneration did not lead to a stronger catabolic shift than varying regions within the NP within a non-degenerated NP. In contrast, without considering individualized weighting factors, the values for borderline and early degenerated conditions, i.e. 35% of NP cells immunopositive for IL1β, might be overestimated, and not enough differentiated between the two conditions.

With regard to TNF-α, expected percentages of inflamed cells range around 16% ± 7% in non-degenerated and 31% ± 5% in degenerated conditions (Le Maitre et al., 2007). The model predicted ranges of proinflammatory cytokines of around 15% under optimal, around 26% under borderline and around 33% under early degenerated conditions. Hence, the percentage of TNF-α immunopositive cells under optimal conditions lied within the expected range, whilst the TNF-α immunopositivity under borderline and early degenerated conditions was considered as a clear overestimation. TNF-α is assumed to be an aggressive mediator in catabolic cell responses (Purmessur et al., 2013), and an immunopositivity for TNF-α of 26 % and 33 %, respectively, of the NP cells close to the mid transversal plane might suggest accelerated local degenerations. With this regard, it must be considered that current predictions of TNF-α rely on pH and glc that both were found to have a non-significant effect (Table 4.3). Accordingly, S-CA specific weighting factors coincide with invariant weighting factors (i.e. 0.01). Hence, *in silico* predictions of the proinflammatory environment reflect the previous findings that nutrient-environments alone are not sufficient to accurately predict inflammation (section 4.4.1). A first step to tackle such limitations is an integration of direct mechanotransduction effects into the model with a subsequent evaluation of the model performance (please check section 4.5.2.2 with this regard).

In contrast to *in silico* methodologies that consider vast network interactions including many (sub) cellular components, this approach only considers relatively few, key relevant external stimuli to estimate overall cell responses at a multicellular level. Hence, instead of using a bottom-up modelling approach to estimate current CA, experimental findings are used to directly link environmental stimulus perturbations to a final CA. Therefore, it is crucial to use external stimuli that are shown to influence the tackled CA. In contrast to tissue proteins or proteases, nutrient-related stimuli alone do not have a determinant

impact on proinflammatory cytokine regulations. As a consequence, the model responded with an inaccurate prediction of inflammatory parameters. Hence, this modelling approach seems to be able to sort out the critical characteristics of multifactorial environments to accurately capture a CA. At the same time, it allows high-level and directional modelling, which is important for proper network model interpretations in the light of available evidence.
As for the visualization of immunopositivity within the 3D AB-model environment, it was assumed that immunopositive cells were arranged in clusters (Figure 4.11).

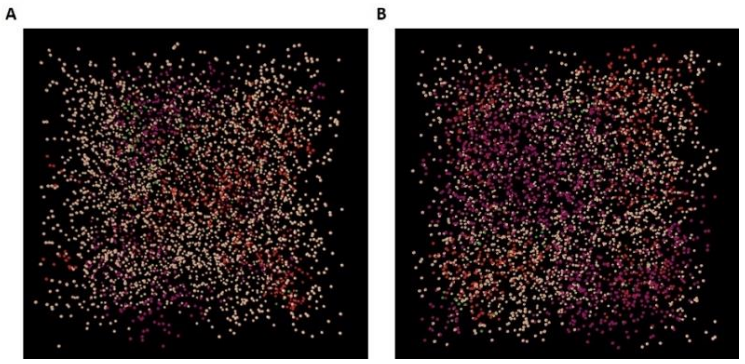

Figure 4.11: examples of a inflammatory environments within the 3D Agent-based model under optimal (A) and early degenerated (B) nutrition conditions. Cell clusters: red; cells immunopositive for IL1β, purple; cells immunopositive for TNF-α; green: cells immunopositive for both, IL1β&TNF-α.

Thereby, the location of each cluster was randomly set and the cell number forming each cluster was determined according to the proximity of the cells. Thus, the proinflammatory environment is different for every new model setup. The computational cost to setup the proinflammatory environment ranges around 8 minutes on an 'ordinary' personal computer (in this study: 16 GB RAM, Intel$^{(R)}$ Core^{TM} i7-7500U CPU @ 2.70GHz (dual core)). To our knowledge, this is the first approach that provides insights on how a proinflammatory environment might look like within the NP. The idea of immunopositive clusters arise from a combined effect of paracrine stimulation (Phillips et al., 2013, 2015), short half-life of proinflammatory cytokines and low, diffusion-dependent travel velocities. Due to a lack of data, these simulated clusters of inflammatory environments could not yet be experimentally validated. Arguably, the initial assumption of an independent seeding of IL1β and

TNF-α cell clusters might be revised in future model developments, because of the mutual stimulatory effects between TNF-α and IL1β, e.g. the effect of TNF-α on IL1β mRNA expression (supplementary material, S2, Appendix 2). Hence, the number of cells immunopositive for both IL1β&TNF-α might be underestimated. More experimental data about the inflammatory cell states of NP cells would be needed to better approximate the prediction of proinflammatory intervertebral disc environments. The decreasing costs of transcriptomic and proteomic studies may soon lead to a more comprehensive knowledge about the distribution and type of immunopositive cells within the NP. Moreover, additional information about the response of NP cells to microenvironmental cues represents relevant input data for the herein described model. While these data might help to complement /refine network models (Melas et al., 2014), their interpretation can further benefit from the current modelling approach that uniquely integrates multiple S-CA relationships.

4.5.2.2 Cell Activity

This novel methodological approach allows to tackle regional heterogeneities within the NP, which complements information from experimental research that usually obtains homogenic values for the NP as a whole. Such spatial- and CS-specific CA profiles (Figure 4.10) are defined by the (local) multifactorial environment and are the result of the interaction of three factors: the sensitivity to a stimulus concentration (x_S^{CA}), the sensitivity to a stimulus type (θ_S^{CA}) and their integration through the PN-equation. Hence, PN-activities are constant for constant nutritional boundary conditions and can be obtained within seconds with the 'ordinary' personal computer used in this study. This work focuses on the approximation and the final effect of the stimulus type, which is described with weighting factors. Hence, results are discussed focusing on the impact of weighting factors.

Without the integration of S-CA specific weighting factors, the CA profiles are largely defined by x_S^{CA}. This explains why CA profiles look similar in Figure 4.10, A. Hence, the impact of different types of inflammation can only moderately be reflected (Figure 4.10, A, first row) and the variations within CA profiles of different CS rise with a progressively adverse nutrient environment (i.e. from the first to the last row, Figure 4.10, A). On the one hand, changes due to nutrient deprivation are small, which coincides with the slow progress of intervertebral disc degeneration, i.e. the chronicity over time might be a major risk factor to eventually compromise the tissue integrity. On the

other hand, small variations between different CS would not reflect the strong effects of proinflammatory cytokines on tissue proteins and proteases as suggested by experimental findings (e.g. Figure 4.7, Le Maitre et al., 2005; Purmessur et al., 2013).
Due to an integration of S-CA specific weighting factors, more pronounced differences between CA profiles were predicted and the results show an improved, qualitative agreement with experimental findings which will subsequently be illustrated. Thereby, neither results from CA profiles with TNF-α implication of borderline nutrient environments (situated in Figure 4.10, B, middle row) nor CA profiles with either TNF-α or IL1β implication under early degenerated nutrient-conditions (situated in Figure 4.10, B, last row) will be used for argumentation as a (possible) under- and overestimation of proinflammatory cytokines (see section 4.5.2.1) affect corresponding CA-profiles (see Figure 4.5).
An implementation of an S-CA specific weighting factor predicts a highly anabolic CA profile of non-inflamed cells. Hence, the ADAMTS4 mRNA expression that was enhanced without the consideration of a weighting factor was decreased (Figure 4.10, A vs. B, first rows). A low ADAMTS4 mRNA expression coincides with low ADAMTS4 levels in the intervertebral disc NP (Molinos et al., 2015). Compared to the non-inflamed CA-profile, a moderate catabolic shift was predicted for IL1β inflamed cells, reflected by a slow downregulation of Agg and an upregulation of MMP3 and Col-I (Figure 4.10, B). A moderate catabolic shift goes along with the potential role of IL1β in the normal homeostasis of the intervertebral disc (Le Maitre et al., 2007b). Likewise, the pronounced catabolic shift due to TNF-α, reflects a previously described rather aggressive impact of TNF-α on CA (Purmessur et al., 2013). Eventually, cells inflamed with both, TNF-α&IL1β generally show a similar, but slightly more catabolic behavior than cells only inflamed with TNF-α. This prediction might be quite conservative, and possibly reflects the need for an incorporation of cross-effects among stimuli. However, few is known so far about cross-effects of different stimuli with regard to mRNA expressions. To our best knowledge, cross-effects were only particularly mentioned with regard to cell viability, where a combination of low pH and a zero glc environment was found to cause more cell death than it would be expected by a simple addition of both individual effects (Bibby and Urban, 2004). The modelling technique presented here can infer, however, on parallel effects. Should nonlinearities of these parallel effects be demonstrated experimentally, new experiment-based

functions could be incorporated in the network to eventually reflect cross effects. For example, this could be achieved by formulating the currently constant weighting factors as variables, to let them vary within a predefined range in function of the concentration of other stimuli.
Independently of the CS, an integration of S-CA specific weighting factors led to a generally lower mRNA expression of Col-II, compared to Agg within the same CA profile, whilst for invariant weighting factors same or very similar mRNA expressions of Agg and Col-II were predicted (Figure 4.10, A vs. B). For example, in case of optimal nutrient conditions of non-inflamed cells, both Agg and Col-II are maximally activated with a PN-activity of 0.1266 and 0.0822, respectively (Figure 4.10, B, first row). A prediction of a lower, maximal expression of Col-II is in agreement with the tissue composition of the NP, where Agg is more abundant (e.g. reviewed by Baumgartner et al., 2021) and has a faster turnover than Col-II in the (non-degenerated) NP (Sivan et al., 2006, 2008). This interpretation is valid if it is assumed that (i) the amount of mRNA expression is (largely) proportional to the amount of tissue proteins and (ii) that the maximum cell activity of Agg and Col-II mRNA expression is quantitatively similar.
Within this methodological approach, PN-activities are defined with four decimals. Thereby a high contrast exists between highly varying mRNA expressions between donors and consequently as well between studies from different authors and the required, mathematical accuracy within this systems biology approach. An awareness of the user to this limitation is important with regard to the detail to which the results will be interpreted. However, given that a constant weighting factor transmits a potential error throughout a given system of interest, and consequently throughout a certain set of simulations, its effect on a relative interpretation of the data might be minor.
This model approach used a determined set of biological data. Experimental findings, however, are sensitive to the experimental setup including cell types (e.g. human vs. animal), passage numbers, 2D or 3D cultures or time points, at which mRNA expressions were obtained. Given that this network modelling approach is highly evidence-based, discrepancies resulting from experimental differences would consequently be reflected within model results. With this regard, effort was made to use: (i) experimental data that is in overall consensus with widely accepted assumptions of NP cell responses (e.g. a general catabolic effect under rising acidity); (ii) studies with human cell culture data rather than animal cells, (iii) the measurement of as much required data as possible out of a same experimental study and (iv) data from 3D

cultures rather than 2D cultures. However, proper integration of possible variations in mRNA expressions at different culture times would become possible if a standardized history of mRNA read-outs is integrated to the experimental protocols for all stimuli. With this regard, focus was set to develop a model design that allows for a straightforward exchange of biological input data as soon as better suitable data is available. In the light of different sets of biological input data in future and a general presence of limitations, it would be suggested to interpret model results stochastically. Hence, by feeding the model with a variation of sets of experimental data, a final probability of the behavior of NP cells under user-defined conditions could be assessed.

Within the current model, mRNA expressions rather than protein synthesis were considered, according to available, experimental data. Unfortunately, a proportional relationship between mRNA expression and protein synthesis is not granted. Hence, the use of biological input data directly based on protein synthesis might be recommendable as soon as such experimental data is available.

The aim of this methodological approach of data integration based on *in vitro* experiments is to estimate cell responses under native conditions. Accordingly, it could also be applied to improve the interpretation of organ culture models such as presented by Ju et al., 2009; Illien-Jünger et al., 2010; Lang et al., 2018. This includes both, cell culture-based knowledge and cues transmitted to the cells through the tissues. Related to the latter, finite element models can be used to define the multiphysics boundary conditions that tissues would impose on the presented AB and network models, as done to define the nutrient environments for "borderline" and "early degenerated" conditions. The metabolic microenvironments defined for the simulated cell collection took into account the heterogeneous deformation and degeneration status of the intervertebral disc tissues, by simulating daily physical activity (Ruiz Wills et al., 2018). Hence, whereas indirect mechanotransduction phenomena are implicitly considered in the model, direct mechanotransduction phenomena are not. Yet, as the present study demonstrates, new experimental data can be aggregated to approach increasingly reasonable predictions of cell activity. In the same way the model was informed through new experiments about nutritional and pro-inflammatory cell stimulation, the parallel networks can be extended to integrate evidence about direct cell mechano-stimulation effects, which is deemed to be cornerstone (Chan et al., 2011; Neidlinger-Wilke et al., 2012; Fearing et al., 2018; Hodson et al.,

2018; Saggese et al., 2018). In this work, a proof of concept was presented that parallel networks were able to secure a reasonable description of the apparent CA due to multifactorial biochemical environments. The present study serves as a basis to tackle the complex problem of direct mechanotransduction in the future.
This network modelling approach allows to assess local CA based on given environmental conditions at sub-millimetric levels. As mentioned before, our AB input parameters, i.e. local nutrient concentrations, were obtained through the results at the element level of mechanotransport FE simulations (Ruiz Wills et al, 2018). Our predicted CA targets the differential regulation of extracellular matrix turnover that can be used to update the properties of composition-based disc tissue models (Barthelemy et al., 2016; Ruiz Wills et al., 2016), leading to incremental perturbation of local CA in a next iteration of FE-AB simulations. Hence, the present model is deemed to importantly contribute to the development of multiscale modelling approaches to explore intervertebral disc degeneration, where biologically-driven tissue injury includes dynamics over multiple spatial scales (Vergroesen et al., 2015). Likewise, our modelling approach may address the apparent limited capacity of phenomenological mechanobiology models to capture the turnover of intervertebral disc tissues along degeneration (Van Rijsbergen et al., 2018). Furthermore, the networks that control our AB model might be coupled with model developments at lower spatial scales, to integrate mechanistic molecular contributions to intervertebral disc tissue regulation (Figure 12), e.g., in terms of cell regulation pathway signalling, as proposed in osteoarthritis (Melas et al., 2014; Mukherjee et al., 2020).

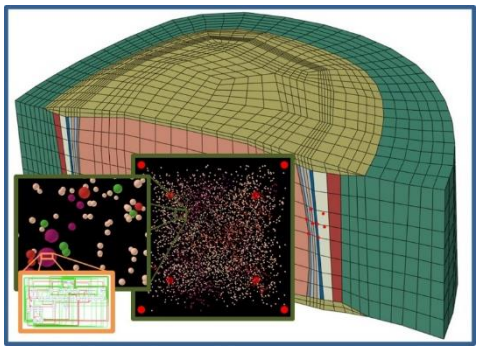

Figure 12: schematic integration of this modelling approach of the multicellular level into multiscale approaches. Organ/tissue level (blue frame), multicellular level (green frame) and subcellular level (orange frame).

4.6 Conclusion

This work reflects a multidisciplinary methodology consisting of the integration of experimental (*in vitro*), mathematical (weighting factors, network) and computational (AB) methods, to present an evidence-based enabling technology to approximate complex multifactorial, multicellular environments of the NP. Thereby, biochemical stimuli were considered, and focus was set on estimating proinflammatory environments and cell responses. To duly feed the model, current experimental evidence was completed through new *in vitro* experiments, the results of which were directly incorporated into a novel method to estimate individual CA under multifactorial environments. Remarkably, the results of such integration indicated that differential weighting of the effect of the stimulus concentration was cornerstone to improve the confidence in the simulations.

Experimental results suggest that low glc may not be a main trigger for a catabolic shift in CA. TNF-α, in turn, caused significant catabolic alterations in all mRNA expressions but Agg. The *in silico* model predicted a maximal CA generally lower for Col-II compared to Agg, according to known structural protein turnovers. Low levels of protease mRNA expression were predicted under optimal conditions and non-inflamed and IL1β inflamed cells. Interestingly, the co-existence TNF-α dramatically increases the catabolic shift of CA, with a strong overexpression of key proteases specialised in ECM degradation. Though our number of inflamed cells seemed over-predicted, model simulations indicate that further knowledge and model developments are necessary to capture additional regulators of inflammation. In particular, the incorporation of direct mechanotransduction might be key relevant.

Regarding the prediction of inflammation, the 3D AB model displayed the calculated number of inflamed cell clusters according to the proximity of cells. On the one hand, the assumption that inflammation within the NP is arranged in local cell clusters is based on experimentally known paracrine effects of proinflammatory cytokines, in combination with short half-lives and low diffusivity. On the other hand, such a modelling is a clear asset to quantitatively evaluate the capacity to predict inflammation, for direct comparisons with local biochemical measurements in intervertebral disc specimens. Such quantitative comparisons are instrumental to target specific needs both for model refinements in terms of additional stimuli, and for guided acquisition of new experimental data.

All in all, the integration of refined models and new experiments, according to our hereby presented approach (from network hypothesis to experiments and AB predictions), stand for a unique tool to generate new contrastable knowledge. Remarkably such process can be fully integrated into multiscale modelling through couplings with FE simulations, to combine both top-down and bottom-up descriptions of the dynamics involved in intervertebral disc degeneration.
At the current stage of development, this model is able to integrate key nutritional and pro-inflammatory cues in 3D multifactorial environments, e.g., enabling more detailed explorations of indirect mechanotransduction phenomena in intervertebral disc degeneration. Further developments will be facilitated by straightforward integration of new biological datasets. Moreover, as the PN mathematical framework is designed to be fully scalable, it allows to integrate any new S-CA relationship based on further experimental evidence.

5 *The PN$_t$-Methodology: a Top-Down Network Modelling Approach to Estimate Dose- and Time-Dependent Cell Responses to Complex Multifactorial Environments*

This Chapter is adapted from: Baumgartner L., González Ballester M. A. and Noailly J.: *The PN$_t$-Methodology: a Top-Down Network Modelling Approach to Estimate Dose- and Time-Dependent Cell Responses to Complex Multifactorial Environments* (Manuscript ready)

The structure of this Chapter follows the Journal's requirement: the framework of the developed methodology is considered as a result and, therefore, forms part of the Results-section. The Methods-section contains more in-depth aspects of methodological procedures and are provided at the end of the chapter. The discussion is short and focuses on the methodological aspects. Accordingly, the discussion of the actual qualitative results with biological relevance is carried out in the supplementary information (Appendix 3).

5.1 Abstract

Current methodologies to estimate cell responses usually focus on bottom-up intracellular network modeling, frequently accompanied by limitations regarding the network topology and a loss of directionality. Moreover, it is challenging to consider transient changes in cell responses due to chronic stimulus exposure or dose-dependency. Here we present a high-level top-down network modelling approach to simulate dose- and time-dependent cell responses within heterogenous multifactorial, multicellular environments. Through an interpretation of multicellular environments as time-dependent (subscript t) parallel networks (PN), fed by a systematic use of experimental findings, the PN_t-Methodology provides relative, interrelated cell responses to complex stimulus environments. Hence, the PN_t-Methodology particularly contributes to investigate dynamics within slowly developing diseases. Applied to intervertebral disc multicellular systems, the PN_t-Methodology allows for the first time to obtain qualitatively validated cell responses for daily human moving habits and tackled effects of microgravity exposure. The PN_t-Methodology is not tissue specific per-se. It is designed to be easily scalable and provides unique possibilities to approximate gradual cell responses over time.

5.2 Introduction

Highly multifactorial disorders are difficult to apprehend, since an approximation of cell responses to heterogeneous sets of stimuli is challenging. Multifactorial disorders usually evolve slowly and silently and are believed to be strongly influenced by environmental factors. Hence, a better understanding of the effect of such factors on cell responses is cornerstone to tackle slowly developing multifactorial diseases. Advances in experimental and *in silico* research importantly enhanced our understanding of intracellular regulations and cell responses to environmental cues, leading to extensive databases on signaling pathways and protein-protein interactions (Baumgartner et al., 2021) and modeling approaches to simulate complex cell dynamics. Accordingly, numerical approaches usually tackle bottom-up approaches using logic modeling such as Boolean or fuzzy-logic formalisms and ordinary differential equation (ODE) approaches (Orton et al., 2005; Mendoza and Xenarios, 2006; Yue et al., 2006; Aldridge et al., 2009; Krumsiek et al., 2010; Morris et al., 2010; Mitsos et al., 2012). However, network models can easily loose directionality, which complicates a proper integration of experimental evidence and the calculations of unequivocal results. Moreover, an integration of the

growing experimental knowledge into network models is challenging and requires often a reduction of topology and network fitting. Furthermore, graph-based models usually lead to steady-state nodal activations, often neglecting the effect of both the time and the dose of a stimulus.

To this end, we propose a new methodology to approximate complex heterogeneous dose-and time-dependent multicellular systems by introducing a top-down approach. We present this methodology as the PN_t-Methodology. Thereby, the cell per-se is considered as a "black box" and crucial cell activities (CA) are estimated by linking them to their multifactorial environment based on experimental knowledge. The different CA that are simultaneously regulated by the multifactorial environment are conceptualized as potentially time-dependent (subscript t) parallel networks (PN). The PN_t-Methodology consists of a set of methods to (i) translate biological findings into parameters suitable for systems biology approaches (cf. Chapter 3, 4), (ii) an approach to estimate the effect dose-and time dependency over long time-periods on a CA, and (iii) a core element, an ODE-based equation, to link the effect of multifactorial stimulus environments on CA of multicellular systems.

In this work, the general approach of the PN_t-Methodology, the core mathematical formulation and the method to estimate dose- and time dependencies of specific CA is presented. The PN_t-Methodology was developped to investigate the initiations of intervertebral disc (IVD) degeneration, focusing on the Nucleus Pulposus (NP)[1], which reflects a prefect, illustrative case for a multifactorial disorder. We could demonstrate that the PN_t-Methodology provides a novel, straightforward solution to estimate the CA of cells within multicellular systems exposed to multifactorial heterogenous stimulus environments, including time-dependent responses over long time periods.

5.3 Results

Determination of the system of interest. A stimulus environment usually consists of local stimuli and of stimuli coming from a distant source, introduced here as "external" stimuli. These are nutrition-

[1] The NP is the center of the IVD. It is surrounded by a juxtaposition of lamellae, the Annulus Fibrosus and separated towards the vertebral body by a cartilage endplate. The IVD is prone to degenerative changes, account for at least 40 % of the low back pain cases (Baumgartner et al., 2021) that affect up to 85% of persons during their lifes (Smith et al., 2011).

related or mechanical stimuli. It is hypothesized that alterations in CA are not spontaneous processes, but initially caused by alterations of external stimuli, which subsequently affect the cell homeostasis and local stimulus expressions.
Cell responses can be reflected as profiles of *n* crucial CA, regulated by a multifactorial environment of *m* stimuli. Thereby, a stimulus can either activate, or inhibit or dose- and/or time-dependently alter a CA. Time- and dose-dependent stimuli can be either activating or inhibiting depending on the dose and/or the duration of the stimulus. Moreover, *p* different cell states (CS) might co-exist within a representative volume of cells due to local expressions of key stimuli, e.g. locally synthesized proinflammatory cytokines (Figure 5.1, top).

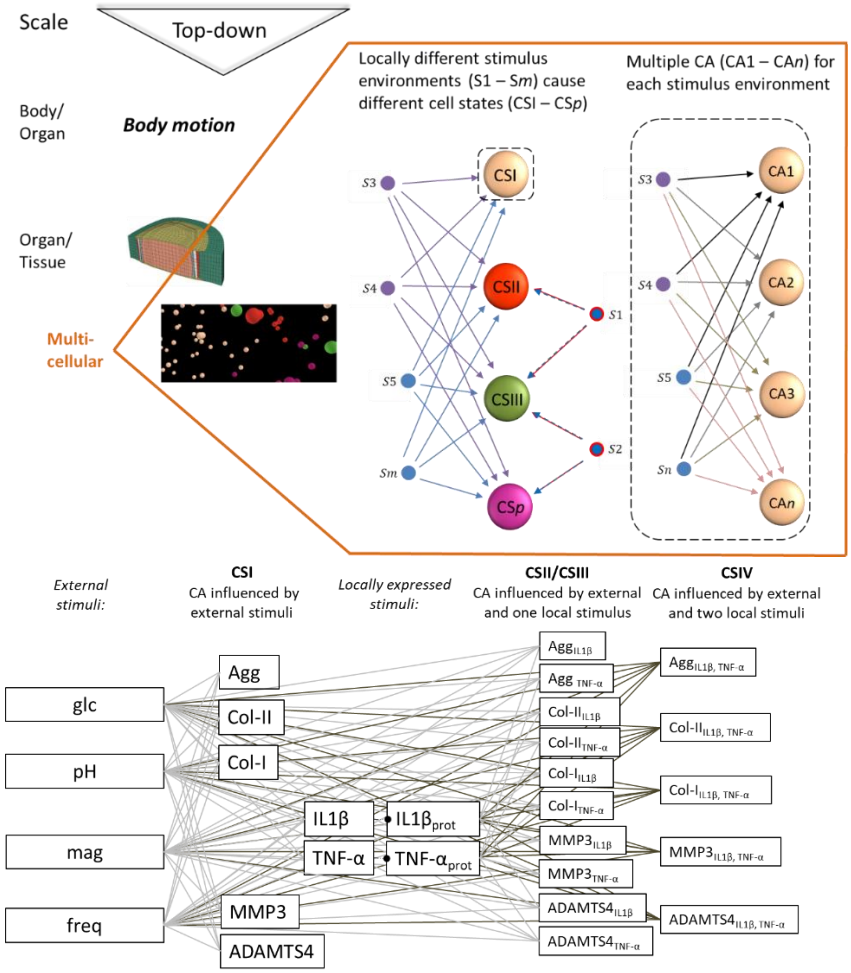

Figure 5.1: Top: the PN_t-Methodology tackles the multicellular level. Schematic visualization of a complex, multifactorial, multicellular environment, consisting of *m* stimuli, *p* cell states (CS) and *n* cell activities (CA). Individual stimulus-CA interactions (arrows) might have an activating (blue), inhibiting (red) or a time-dependent (purple) effect on a CA. Below: approach applied to approximate NP cell behavior. The system of interest consists of four external key stimuli (glc, pH, mag, freq) and the CA enclose the mRNA expressions of tissue proteins (Agg, Col-I, Col-II) and proteases (MMP3, ADAMTS4). Different cell states (CSI-IV) were induced by the presence of the locally expressed proinflammatory cytokines TNF-α and IL1β.

Based on this concept, tissue-specific systems of interest were determined (Figure 5.1, below). Key relevant stimuli in NP cell regulations were identified based on literature. External stimuli were the

nutrient-related stimuli glucose (glc) and pH and the mechanical parameters magnitude (mag) and frequency (freq) (Rinkler et al., 2010; Chan et al., 2011; Gilbert et al., 2016; Kerr et al., 2017; Saggese et al., 2018). The locally expressed key stimuli were chosen to be proinflammatory cytokines, since these were found to be critical factors in IVD degeneration (Gorth et al., 2015; Johnson et al., 2015b). Thereby, interleukin 1β (IL1β) and the tumor necrosis factor α (TNF-α) were classically related to initiations of this disorder (Johnson et al., 2015b). Considering two local stimuli, a NP cell can obtain one out of four different proinflammatory cell states (CS): non-inflamed or inflamed for either IL1β, TNF-α or for both, IL1β&TNF-α. Estimated cell responses were the mRNA expressions of the NP tissue components Aggrecan (Agg) and Collagen Types I and II (Col-I, Col-II) and proteases MMP3 and ADAMTS4 from the matrix metalloprotease (MMP) and the "a disintegrin and metalloproteinase with thrombospondin motifs" (ADAMTS) families, since those CA were deemed to be key relevant in IVD degeneration (Molinos et al., 2015; Kerr et al., 2017; Baumgartner et al., 2021).

Feeding the system of interest with evidence-based parameters and relate it to relevant PN-systems. PN-systems are subsystems of the system of interest and must be defined prior to calculations. A PN-system contains all the CA that are required to have a relative expression to each other. In the current system of interest of the NP, tissue proteins and proteases of each CS are required to be expressed relative to each other, to assess overall, relative cell responses to user-defined stimulus environments. In contrast, the prediction of local stimuli (proinflammatory cytokines) is required to determine CSII, III and IV (Figure 5.1, below) through separate PN-systems. These local stimuli were determined based on external stimulus concentrations and serve as input parameters for an inflammation submodel that semi-quantitatively estimates the concentration of the local stimulus protein concentration (cf. Chapter 4). A PN-system consists of directed parallel networks. A parallel network considers the stimuli that surround a cell and regulate a specific CA (see 5.5 Methods (Figure 5.7)). For example, the parallel network to determine Agg of non-inflamed cells (CSI, Figure 5.1) consists of the stimuli glc, pH, mag and freq and the CA Agg.

External stimulus doses cover physiologically relevant ranges for a given tissue. For the NP, this includes glc concentrations of 0 mM – 5 mM, a

pH 6.5-7.4, load mag of 0.1 MPa – 3.5 MPa and freq of 0 Hz – 40 Hz (Figure 5.2, A).
Connections between a stimulus and a CA are defined as S-CA relationships and are determined by the sensitivity of a CA to a stimulus type and the stimulus dose (cf. Chapter 4). A stimulus dose refers to biochemical stimulus concentrations or to load intensities. Parameters that estimate the effect of a stimulus type and dose on a CA are obtained from experimental findings as previously explained (Baumgartner et al., 2020, Chapter 4). In short: the sensitivity of a CA to a stimulus dose (subscript S) is reflected as x_S^{CA}. x_S^{CA} can obtain values between 0 and 1 and is optimally obtained by a continuous sigmoidal function that relates each physiologically relevant stimulus concentration to a value for x_S^{CA} (Figure 5.2, B) (Baumgartner et al., 2020, Chapter 4). Thereby, 0 reflects a minimal and 1 a maximal activity of a CA for a given stimulus concentration. The effect of the stimulus type was defined through a weighting factor (θ_S^{CA}) (Figure 5.2, B). Weighting factors can obtain values of $0.01 \leq \theta_S^{CA} \leq 1$ and are determined based on the maximal x-fold change in mRNA expression caused by differences in stimulus concentrations (cf. Chapter 4). Thereby, the lowest weighting factor of 0.01 was assigned to non-significant S-CA relationships (Figure 5.2, A, dashed lines).
For the system of interest of NP cells, specific weighting factors of the S-CA relationships of the stimuli glc, pH, TNF-α and IL1β were previously presented (Chapter 4) and newly obtained for the stimuli mag and freq (5.5 Methods).
The quality of S-CA relationships is either activating, inhibiting or dose- and/or time-dependent (blue, red or purple, respectively (Figure 5.2, A).

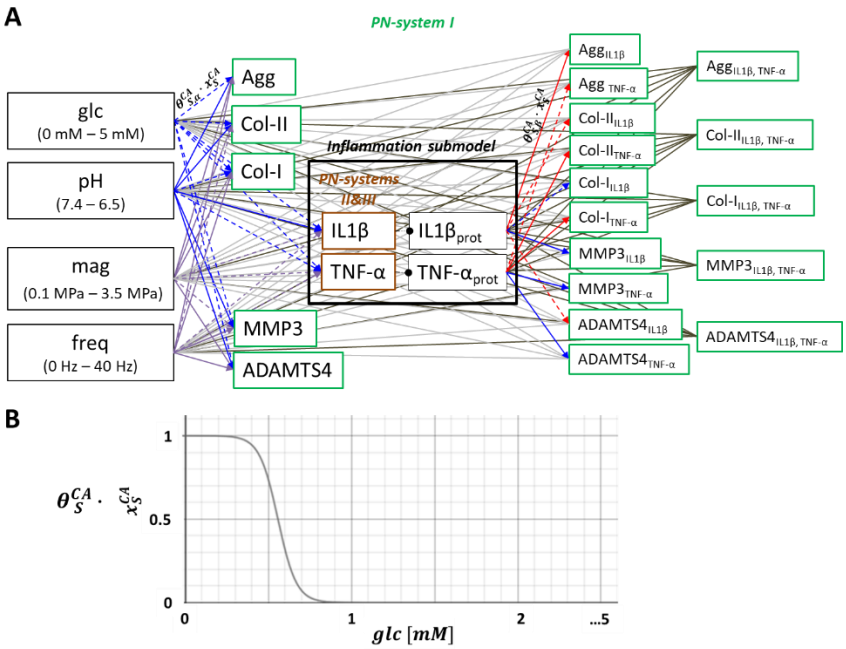

Figure 5.2: A: System of interest, subdivided into relevant PN-systems. Arrows reflect the nature of individual stimulus-cell activity (S-CA) relationships, being either activating (blue), inhibiting (red) or dose- and time-dependent (purple). Non-significant S-CA relationships are marked with dashed lines. The proinflammatory environment is estimated by an inflammation submodel (see Chapter 4) B: S-CA relationships are determined by a weighting factor (θ_S^{CA}) and a normalized sensitivity of a CA to a stimulus concentration (x_S^{CA}). Example: glucose (glc)-MMP3 relationship.

Stimuli can either be steadily present under relatively constant concentrations, or strongly fluctuating. Within the NP, nutrients were assumed to be generally present. Therefore, current nutrient concentrations were used to determine a basal level for each CA. They were considered to be always (to a smaller or bigger extent) activating (cf. Chapter 4). Proinflammatory cytokines were integrated as constantly activating or inhibiting, depending on the considered CA. Assumptions are based on experimental data from cell cultures (cf. Chapter 4) (Figure 5.2, A). In contrast, mechanical load parameters, i.e., mag and freq, depended on the physical behavior of a person. The effect of the mechanical load on a CA depended on the stimulus dose and on the exposure time (Chan et al., 2011), and it could be either anabolic or catabolic (see "Approximation of stimuli with dose-dependent anabolic or catabolic impact." (page 102)).

Calculating PN-systems with the PN-equation. The PN-equation is an ODE-based approach to resolve the PN-systems (Eq. (5.1)).

$$\frac{d\omega_{CA,CS}}{dt} = \left(\left(\frac{1+\sum\theta_{\alpha}}{\sum\theta_{\alpha}}\right)\left(\frac{\sum\theta_{S,\alpha}^{CA}x_{S,\alpha}^{CA}}{1+\sum\theta_{S,\alpha}^{CA}x_{S,\alpha}^{CA}}\right)\right) \cdot \left(1-\left(\left(\frac{\sum\theta_{S,\beta}^{CA}}{\sum\theta_{S,\alpha}^{CA}+\sum\theta_{S,\beta}^{CA}}\right)\left(\left(\frac{1+\sum\theta_{\beta}^{CA}}{\sum\theta_{\beta}^{CA}}\right)\left(\frac{\sum\theta_{S,\beta}^{CA}x_{S,\beta}^{CA}}{1+\sum\theta_{S,\beta}^{CA}x_{S,\beta}^{CA}}\right)\right)\right)\right) \quad (5.1)$$

The PN-equation was developed based on a well-established, graph-based analytical methodology to approximate single network dynamics (Mendoza and Xenarios, 2006) (5.5 Methods). It determines a time-dependent overall activation of a CA of each CS ($\frac{d\omega_{CA,CS}}{dt}$) and is built of an activating and an inhibiting part (subscript α and β, respectively). Thereby, the activating and inhibiting parts of the equation combined two and three fractional terms, respectively. The first fractional term of the activating part determines the maximal activation by considering all activating weighting factors (θ_{α}) within the PN-system. The second fraction determines the activation of the tackled CA by integrating all its activating S-CA relationships ($\theta_{S,\alpha}^{CA}x_{S,\alpha}^{CA}$). The inhibition is determined relative to the activation of a particular CA. The first fraction determines the relative weight of the inhibition, the second fraction the maximal inhibiting weight of a CA, independently of the CS (θ_{β}^{CA}) and the third fraction reflects the actual inhibition of the tackled CA ($\theta_{S,\beta}^{CA}x_{S,\beta}^{CA}$). Both, the activating and inhibiting parts are explained in detail in Methods (section 5.5).

To enable the contribution of a stimulus to either the activating or the inhibiting part depending on the exposure time, the weighting factor, θ, of this stimulus must be listed in both the activating and inhibiting parts of the PN-equation. The weighting factor within the term, where the stimulus is initially not active is called completive weighting factor (indexed with δ) and can be understood as placeholder within the PN-equation. Completive weighting factors have the same value as their counterparts. Hence, if the weighting factor that describes the impact of mag on Agg equals 0.3484 (θ_{mag}^{Agg}=0.3484) (see Table 5.4, 5.5 Methods) the corresponding, completive weighting factor, i.e. ($\theta_{\delta,mag}^{Agg}$) has the same value. An example of a complete PN-equation is shown

for the Agg mRNA expression of IL1β – inflamed cells, for an initially anabolic mag and catabolic freq (Figure 5.3).

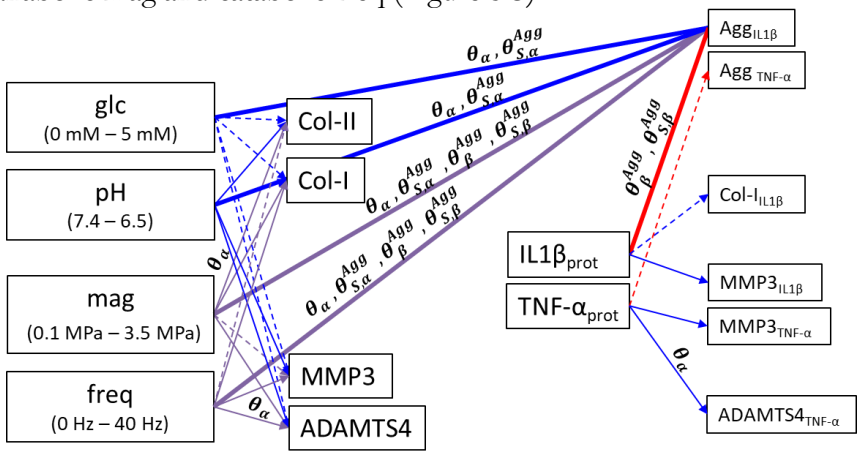

θ_α: all (potentially) activating weighting factors within the PN-System
$\theta_{S,\alpha}^{Agg}$: activating weighting factors that are directly acting on Agg of IL1β inflamed cells
θ_β^{Agg}: all (potentially) inhibiting weighting factors of Agg, independently of the CS
$\theta_{S,\beta}^{Agg}$: inhibiting weighting factors that are directly acting on Agg of IL1β inflamed cells

$$\frac{d\omega_{Agg,\,IL1\beta\,infl}}{dt} =$$

$$\left(\left(\frac{1+\sum\theta_\alpha}{\sum\theta_\alpha}\right)\left(\frac{\theta_{glc,\alpha}^{Agg}x_{glc,\alpha}^{Agg}+\theta_{pH,\alpha}^{Agg}x_{pH,\alpha}^{Agg}+\theta_{mag,\alpha}^{Agg}x_{mag,\alpha}^{Agg}}{1+\theta_{glc,\alpha}^{Agg}x_{glc,\alpha}^{Agg}+\theta_{pH,\alpha}^{Agg}x_{pH,\alpha}^{Agg}+\theta_{mag,\alpha}^{Agg}x_{mag,\alpha}^{Agg}}\right)\right)\cdot$$

$$1-\left(\left(\frac{\theta_{\delta,mag,\beta}^{Agg}+\theta_{freq,\beta}^{Agg}+\theta_{IL1\beta,\beta}^{Agg}}{(\boldsymbol{\theta_{glc,\alpha}^{Agg}+\theta_{pH,\alpha}^{Agg}})+(\boldsymbol{\theta_{\delta,mag,\beta}^{Agg}+\theta_{IL1\beta,\beta}^{Agg}+\theta_{freq,\beta}^{Agg}})}\right)\right.$$

$$\cdot\left(\frac{1+\theta_{\delta,mag,\beta}^{Agg}+\theta_{freq,\beta}^{Agg}+\theta_{IL1\beta,\beta}^{Agg}+\theta_{TNF-\alpha,\beta}^{Agg}}{\theta_{\delta,mag,\beta}^{Agg}+\theta_{freq,\beta}^{Agg}+\theta_{IL1\beta,\beta}^{Agg}+\theta_{TNF-\alpha,\beta}^{Agg}}\right)$$

$$\left.\cdot\left(\frac{\theta_{\delta,mag,\beta}^{Agg}x_{mag,\beta}^{Agg}+\theta_{freq,\beta}^{Agg}x_{freq,\beta}^{Agg}+\theta_{IL1\beta,\beta}^{Agg}x_{IL1\beta,\beta}^{Agg}}{1+\theta_{\delta,mag,\beta}^{Agg}x_{mag,\beta}^{Agg}+\theta_{freq,\beta}^{Agg}x_{freq,\beta}^{Agg}+\theta_{IL1\beta,\beta}^{Agg}x_{IL1\beta,\beta}^{Agg}}\right)\right) \qquad (5.2)$$

with

$$\sum\theta_\alpha=\theta_{glc}^{Agg}+\theta_{pH}^{Agg}+\theta_{glc}^{ColII}+\theta_{pH}^{ColII}+\theta_{glc}^{ColI}+\theta_{pH}^{ColI}+\theta_{glc}^{MMP3}+\theta_{pH}^{MMP3}+\theta_{glc}^{ADAMTS4}$$
$$+\theta_{pH}^{ADAMTS4}+\theta_{IL1\beta}^{ColI}+\theta_{IL1\beta}^{MMP3}+\theta_{TNF-\alpha}^{MMP3}+\theta_{TNF-\alpha}^{ADAMTS4}+\theta_{mag}^{Agg}+\theta_{freq}^{Agg}+\theta_{mag}^{ColII}+\theta_{freq}^{ColII}$$
$$+\theta_{mag}^{ColI}+\theta_{freq}^{ColI}+\theta_{mag}^{MMP3}+\theta_{freq}^{MMP3}+\theta_{mag}^{ADAMTS4}+\theta_{freq}^{ADAMTS4}$$

Figure 5.3: Above: PN-equation for the Agg mRNA expression of IL1β inflamed cells. Every possible contribution of the weighting factors is illustrated. θ_α is illustratively represented in the PN-system but stands for all potentially activating S-CA relationships, see $\sum\theta_\alpha$ of the equation. Below: Eq. (5.2), reflecting the Agg mRNA expression under an initially anabolic mag and catabolic freq. δ reflects completive weighting factors.

Note that time-dependent weighting factors must be mentioned only once in the denominator of the first inhibiting term (Figure 5.3, bold), to accurately reflect the relative weight of inhibition with respect to activation.

The results of the PN-equation, i.e., overall CA ($\frac{d\omega_{CA,CS}}{dt}$), are calculated as dimensionless PN-activities. The higher a PN-activity for a certain CA, the higher is the relative upregulation of that specific CA. PN-activities are real numbers and have a resolution of 4 decimals (cf. Chapter 4) that can take values between 0 and 1. The range over which an individual CA can vary is determined by the weighting factors of that CA. Hence, the more impact a CA has within the PN-system, the wider is the range of values it can obtain. As a result, PN-activities reflect relative activations of a CA with respect to other CA within the same PN-system. To obtain the maximal PN-activity for a CA, $x_{S,\alpha}^{CA}$ must be set to 1 and the inhibiting portion of the PN-equation must be 0. PN-activities continuously determine the actual CA at each user-defined timestep. To compare the CA associated with different physical activities after a given period of time, an accumulation of PN-activities (acc. PN-activity) should be calculated. This holds true also to obtain cell responses after a sequence of different physical activities (e.g. cell responses after an average day on earth, last section of Results, Figure 5.6).

The PN-systems associated with the local stimuli IL1β and TNF-α (PN-systems II & III in Figure 5.2, A) of the current system of interest are calculated independently of the targeted protein and protease mRNA expressions (PN-system I, see Figure 5.2, A). Hence, each of the PN-systems II and III stands for one parallel network. Therefore, the first fraction of the activating part of the PN-equation for the PN-systems II and III only considers the weighting factors related to the specific CA affected by these systems, as pointed out in Eq. (5.3) (example for TNF-α):

$$\frac{d\omega_{TNF-\alpha,CS}}{dt} = \left(\left(\frac{1+\theta_{glc,\alpha}^{TNF-\alpha}+\theta_{pH,\alpha}^{TNF-\alpha}+\theta_{(\delta),mag,\alpha}^{TNF-\alpha}+\theta_{(\delta),freq,\alpha}^{TNF-\alpha}}{\theta_{glc,\alpha}^{TNF-\alpha}+\theta_{pH,\alpha}^{TNF-\alpha}+\theta_{(\delta),mag,\alpha}^{TNF-\alpha}+\theta_{(\delta),freq,\alpha}^{TNF-\alpha}}\right)\left(\frac{\sum\theta_{S,\alpha}^{CA}x_{S,\alpha}^{CA}}{1+\sum\theta_{S,\alpha}^{CA}x_{S,\alpha}^{CA}}\right)\right) \cdot\left(1-\left(\left(\frac{\sum\theta_{S,\beta}^{CA}}{\sum\theta_{S,\alpha}^{CA}+\sum\theta_{S,\beta}^{CA}}\right)\left(\left(\frac{1+\sum\theta_{\beta}^{CA}}{\sum\theta_{\beta}^{CA}}\right)\left(\frac{\sum\theta_{S,\beta}^{CA}x_{S,\beta}^{CA}}{1+\sum\theta_{S,\beta}^{CA}x_{S,\beta}^{CA}}\right)\right)\right)\right) \quad (5.3)$$

Approximation of stimuli with dose-dependent anabolic or catabolic impact. To determine the anabolic and catabolic effects of a stimulus depending on its dose, logistic functions were used to determine x_S^{CA}, similar to nutrition-related stimuli (Figure 5.2, B), but the range was extended to [-1;1], so that $-1 \leq x_S^{CA} \leq 1$. Thereby, $0 < x_S^{CA} \leq 1$ reflects an activating effect of the stimulus and is integrated within the active portion of the PN-equation ($x_{S,\alpha}^{CA}$). In contrast, $0 > x_S^{CA} \geq -1$ reflects an inhibiting effect on $\omega_{CA,CS}$ and is integrated within the inhibiting portion ($x_{S,\beta}^{CA}$) of the PN-equation. Note that only the absolute values of x_S^{CA} are fed into the PN-equation, as it only accepts positive values for x_S^{CA} bound between 0 and 1 (see 5.5 Methods). Hence, the sign provided by the logistic function indicates the part of the PN-equation in which the value of x_S^{CA} should take a role. $x_S^{CA} = 0$ reflects the transition from activating to inhibiting and is determined as α-β-threshold.
Relevant, stimulus ranges and specific logistic functions for the NP were determined based on in-vivo studies (5.5 Methods) and are referred to as generic functions (X_S). Thereby, low mag and freq were assumed to be anabolic and become catabolic under rising load intensities. Consequently, in the anabolic range of the load parameter values, CA is activated for tissue proteins and inhibited for proteases, whereas in the catabolic range CA is inhibited for tissue proteins and activated for proteases. Hence, two generic functions X_S were determined for both mag and freq and were mirrored with respect to the α-β-threshold (Figure 5.4 A, B). Generic functions evolving with rising stimulus intensities, from activating to inhibiting were labelled with superscripts A;I ($X_S^{A;I}$) and those evolving from inhibiting to activating were labelled with superscripts I;A ($X_S^{I;A}$). Agg and Col-II mRNA expressions were associated to the functions $X_{mag}^{A;I}$ and $X_{freq}^{A;I}$, respectively, whilst any other mRNA expression were associated to $X_{mag}^{I;A}$ and $X_{freq}^{I;A}$. The generic function for mag was exemplarily shown in Figure 5.4, A ,B.

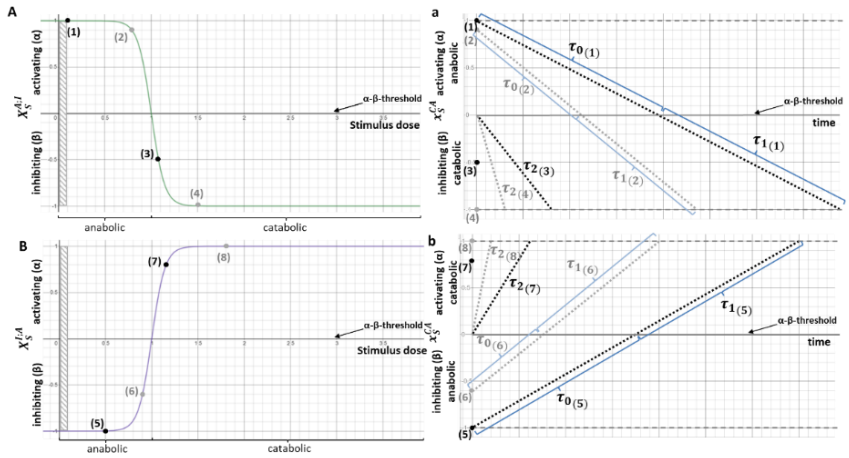

Figure 5.4: Illustration of mirrored generic functions ($X_S^{A;I}$,$X_S^{I;A}$) evolving from activating to inhibiting (A;I) (A) and from inhibiting to activating (I;A) (B) under rising stimulus intensities. a, b illustrate the time dependency (τ) that finally determines x_S^{CA}. The influence of the stimulus dose on the time-sensitivity was schematically sketched for eight randomly chosen stimulus intensities ((1)-(8)); four on each mirrored generic function (A and B). Hence, the anabolic effect of the most anabolic stimulus dose ((1), A) remains over longer time periods ((1) a) than a less anabolic stimulus (e.g. (2) A, a). Time dependencies reflect a loss of activation due to a stimulus exposure over time (τ_0) and a corresponding active inhibition after passing the α-β-threshold (τ_1). For initially catabolic stimulus intensities, a latency time before developing a maximal negative impact on a CA was considered (τ_2) (see next subsection regarding the determination and integration of time-sensitivity). Maximal x_S^{CA} are 1 and -1, respectively.

Determination and integration of time-sensitivity. Values provided by the generic functions were coupled to a time sensitivity term (τ) to eventually obtain x_S^{CA}. τ depends on three variables; the initial stimulus dose (obtained through X_S), a CA-specific time sensitivity (γ_S^{CA}) and the stimulus exposure time (t). The time effect includes i) a loss of anabolic stimulus over time, and (ii) a time delay in the development of a catabolic response to a catabolic stimulus (Table 5.1).

Table 5.1: mathematical description of the time sensitivity term (τ) and the sensitivity of CA to a stimulus dose (x_S^{CA}). Note that integration into the PN-equation requires positive values. Hence, absolute values were used for the terms known to be negative. A;I: generic functions that evolute from activating to inhibiting. I;A: generic functions that evolute from inhibiting to activating. τ are schematically plotted in Figure 5.4, a (A;I) and b (I;A), respectively.

	Range	**Time-sensitivity term (τ)**	**Time-dependent sensitivity of a CA to a stimulus dose**
A;I	anabolic	$\tau_0 = (1 - X_S^{A;I}) \cdot \gamma_{S,ana}^{CA} \cdot t$	$x_S^{CA} = X_S^{A;I} - \tau_0$
	catabolic	$\tau_1 = (1 - X_S^{A;I}) \cdot \gamma_{S,ana}^{CA} \cdot (t - t_{\tau_0})$	$x_S^{CA} = \lvert 0 - \tau_1 \rvert$
		$\tau_2 = \lvert X_S^{A;I} \rvert \cdot \gamma_{S,cata}^{CA} \cdot (t + 1)$	$x_S^{CA} = \lvert 0 - \tau_2 \rvert$
I;A	anabolic	$\tau_0 = (\lvert (-1) + \lvert X_S^{I;A} \rvert \rvert) \cdot \gamma_{S,ana}^{CA} \cdot t$	$x_S^{CA} = \lvert X_S^{I;A} + \tau_0 \rvert$
	catabolic	$\tau_1 = \left(\lvert (-1) + \lvert X_S^{I;A} \rvert \rvert\right) \cdot \gamma_{S,ana}^{CA} \cdot (t - t_{\tau_0})$	$x_S^{CA} = 0 + \tau_1$
		$\tau_2 = X_S^{I;A} \cdot \gamma_{S,cata}^{CA} \cdot (t + 1)$	$x_S^{CA} = 0 + \tau_2$

The formulation of τ varies depending on the initial stimulus dose. τ_0 defines the loss of the effect of an initially anabolic stimulus over time. After passing the individual α-β-threshold τ_1 is activated. τ_1 has the same mathematical description as τ_0, but considers as a time origin the individual time point (t_{τ_0}), when the α-β-threshold was crossed (Figure 5.4, a, b). τ_2 describes the time delay for a catabolic stimulus to reach its whole catabolic potential, which affects already the first hour of stimulus exposure. The effect of time sensitivity is applied until a maximal activating (1) or inhibiting (|-1|) impact of a stimulus is reached (Figure 5.4, a, b).

The velocity at which the anabolic effect of a stimulus decreases, or at which the catabolic effect increases depends on the stimulus dose. It was either obtained by the absolute difference between 1 and $X_S^{A;I}$ and $X_S^{I;A}$ and -1, respectively (τ_0 ,τ_1) or by the (absolute) value of X_S (τ_2) (Figure 5.5, Table 5.1).

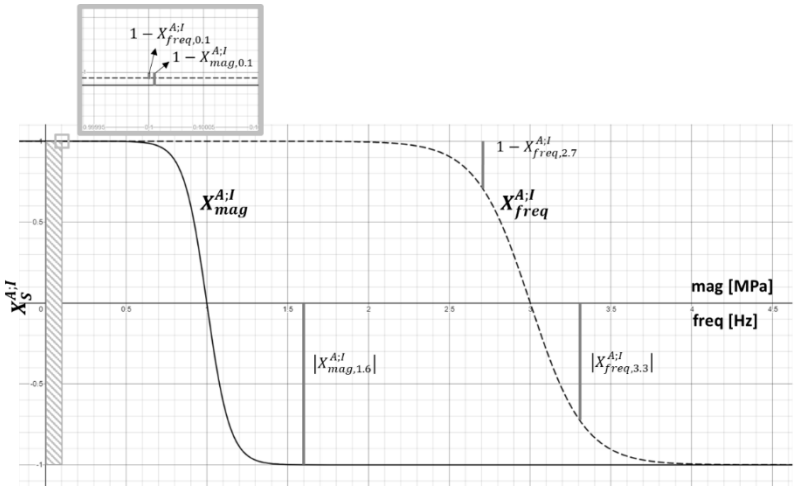

Figure 5.5: determination of the influence of a stimulus dose on the velocity (velocity is: $\frac{\partial \tau_0}{\partial t} = (1 - X^{A;I}_{freq\ 2.7}) \cdot \gamma^{CA}_{freq,ana}$ for the example of freq = 2.7 Hz within the anabolic range) at which the anabolic effect of the stimulus gets lost or at which the catabolic effect reaches its whole potential. Example for $X^{A;I}_S$ functions of mag and freq. Illustrations for the stimulus intensities at 0.1 MPa, 1.6 MPa and 0.1 Hz, 2.7 Hz and 3 Hz. Lowest values for mag reflect 0.1 MPa.

The individual time sensitivity of each CA, γ^{CA}_S, consists of the product of two parameters; an amplification factor (σ) and a CA-specific time sensitivity ($\gamma^{CA}_{S,i}$) (Eq. (5.4)).

$$\gamma^{CA}_S = \sigma \cdot \gamma^{CA}_{S,i} \tag{5.4}$$

γ^{CA}_S within the anabolic range is referred to as $\gamma^{CA}_{S,ana}$ and within the catabolic range as $\gamma^{CA}_{S,cata}$. An approximation of time sensitivities of mRNA expressions in NP cells, based on experimental findings and tissue-specific approximations of σ to amplify $\gamma^{CA}_{S,i}$ to a biologically relevant range is provided in Methods (section 5.5).

Tackling the absence of a (fluctuating) stimulus. The relevance of representing a "zero" stimulus might be highly depending on the observed system of interest. Within the current system of interest of the NP, absence of the time-dependent stimulus "freq" is a physiological condition and represents static activities. Static activities are generally deemed to be less anabolic than moderately dynamic activities (Chan et

al., 2011), which required a particular consideration to duly represent the effect of static load. Its approximation is explained in Methods (section 5.5).

Qualitative validation of the PN_t-Methodology by calculating cell responses to microgravity and to various daily human habits. CA of each CS was calculated for optimal nutritional conditions (pH 7.1, 5 mM glc) (Nachemson, 1969; Rinkler et al., 2010). Two sets of simulations were provided; a first set of results enclose predictions for microgravity exposure during six months of space flight. The duration was derived from expeditions to the International Space Station (ISS) launched by the NASA (NASA, 2011). Results were compared to those achieved through an approximation of a corresponding time spent on earth. An average day was thereby distributed in 10 h sleeping/laying down (night/day rest), two episodes of 4h sedentary work (sitting) and roughly three episodes of 2h physical activity (walking) (Table 5.2). Hence, the simulated day reflects quite an optimal human moving behavior. The period of time, during which an activity is carried out matters for calculation purposes: the day is represented by the additive effects of different activities, and the overall effect only depends on the duration of each activity. The time-step of calculation was 1h, thus, the CA was estimated after each hour of a certain physical activity. Accumulated CA after one day were then multiplied over 180 days. Simulations for four different CS (non-inflamed and inflamed for TNF-α, IL1β and both, TNF-α&IL1β) were provided.
A second set of results was obtained by simulating cell responses of non-inflamed cells for eight human moving habits. Results were generally provided as a continuous evolution over 8 h and as an accumulation over 2 h (Table 5.2). Details regarding the estimation of intradiscal pressures and freq are explained in the Methods (section 5.5).

Table 5.2: overview of the simulated movement activities, corresponding loading parameters (mag, freq) and duration (h).

	Specific activity		mag [MPa]	freq [Hz]	time [h]
Microgravity			0.25	-	4320
Average day on earth		Sleeping / laying down	0.15	-	10
		Sitting with an active back	0.55	-	2x4
		Walking	0.60	1.80	3x2
Daily moving habits					
	1	Sleeping	0.15	-	2;8
	2	Sitting, active back	0.55	-	2;8
	3	Sitting, round back	0.85	-	2;8
	4	Hiking without extra weight	0.60	1.00	2;8
	5	Hiking, 20kg extra weight	1.10	1.00	2;8
	6	Walking	0.60	1.80	2;8
	7	Jogging	0.65	2.75	2;8
	8	Sitting in/on a motor vehicle	0.55	15.00	2;8

Calculations for an approximated daily life on earth led to high CA in terms of mRNA expression of the functional structural proteins of the tissue (Agg, Col-II) and to (close to) minimal CA in terms of protease mRNA expression in non-inflamed cells. Inflammation caused an overall but modest upregulation of proteases and a slight downregulation of tissue proteins (Figure 5.6, A2). In contrast, microgravity exposure (Figure 5.6, A1, left) led to an overall reduced PN-activity of the main tissue proteins to roughly 75% and 80% for Agg and Col-II mRNA expression, respectively. MMP3 mRNA was overall similar and ADAMTS4 was enhanced, though it remained low. The rise in ADAMTS4 protease expression could be especially attributed to the end of the stay in space (Figure 5.6, A1, right). Regarding specific moving habits (Figure 5.6, B), high anabolism was found for sleeping (Figure 5.6, B1, B2), sitting with an active back (Figure 5.6, B1, B3), walking (Figure 5.6, B1, B4) and walking without extra weight (Figure 5.6, B1, B5). Catabolic shifts were predicted for any other condition after either 1h or after prolonged exposure. Especially

hiking with heavy weights (Figure 5.6, B1, B6) and exposure to vibration (Figure 5.6, B1, B9) appears to be critical, given that a catabolic shift was already expected within the first hour of stimulus exposure.

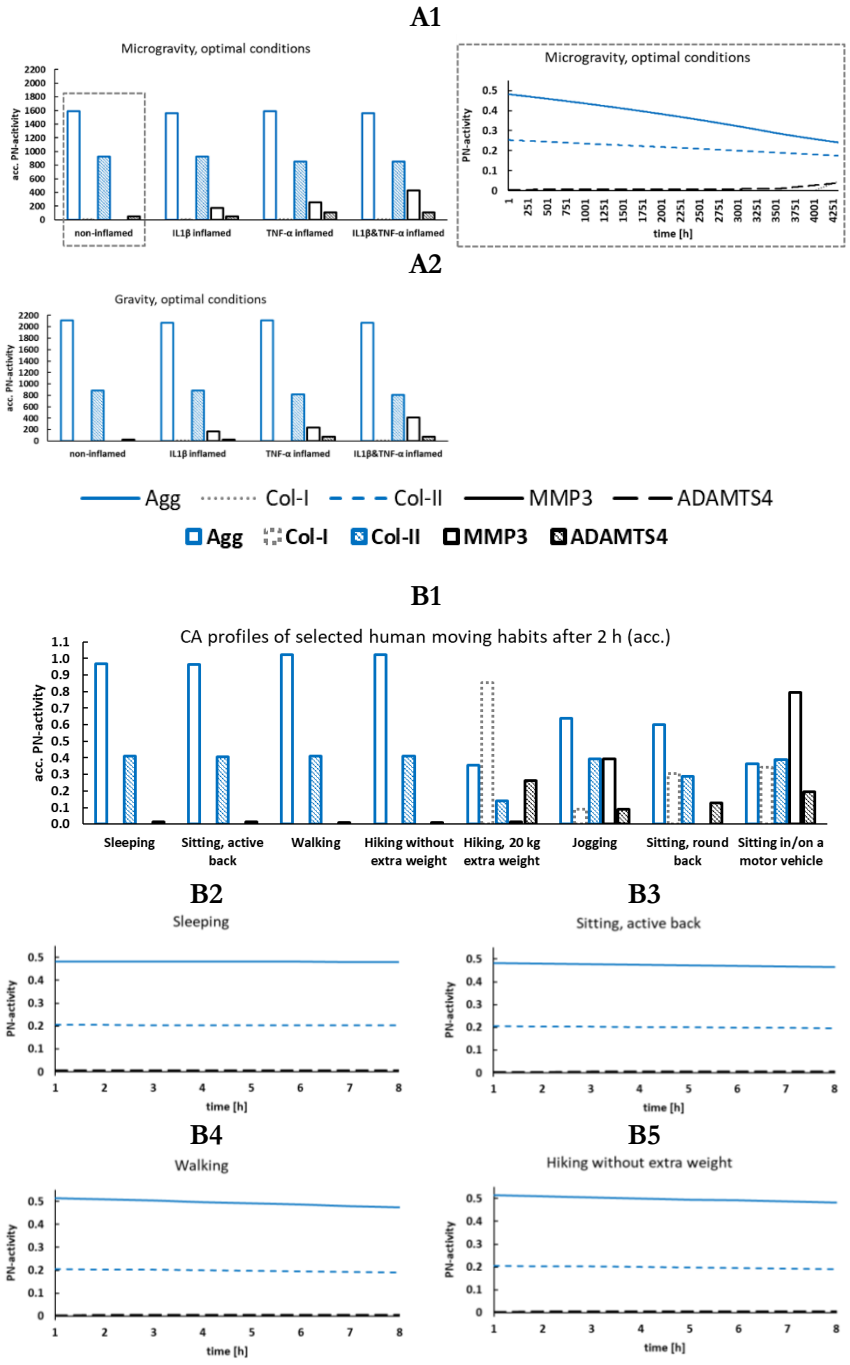

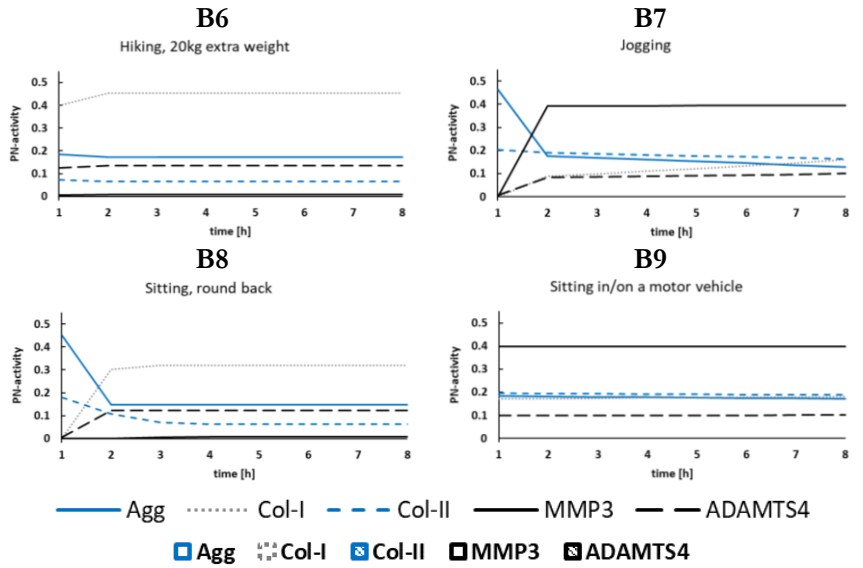

Figure 5.6: A: CA-profiles of microgravity: accumulated (acc.) PN-activity (A1, left) for four different proinflammatory cell states and the (continuous) PN-activity of non-inflamed cells (A1, right). CA-profiles of four different proinflammatory cell states (A2) for an approximated daily life on earth. Time period: six months (180 days). B: Predictions for eight selected physical activities: sleeping, walking, hiking with/without extra weight, jogging, sitting with an active/round back, exposure to vibration (as probably experienced by a motor vehicle). Accumulated (acc.) PN-activities after 2h (B1), and continuous PN-activities (B2-B9) over 8h of physical activity.

5.4 Discussion

The PN_t-Methodology reflects a high-level network modelling approach, where critical external and local stimuli were linked to relevant CA. Activations of different CA and CS were interpreted as parallel networks acting at the same time, and they were interrelated by the PN-equation. This novel top-down approach represents a strategy to evade the modeling of intracellular networks that often go along with limitations such as a loss of network directionality, difficulties in the calculation of unequivocal results or network overfitting. The PN_t-Methodology allows to approximate cellular responses to complex stimulus environments according to predictions of different experimental findings. By translating the quality of such findings into systems biology parameters, complex, dynamic multifactorial environments could be virtually approximated, including long time

effects. Thereby, the systematic design of systems of interest promotes a systematic experimental investigation of stimulus - cell responses and points out the need for standardized experimental setups, in order to enhance comparability among experimental studies.
The PN_t-Methodology was designed to allow for a straightforward replacement of experimental input data. This was deemed to be a requirement to deal with the limited reproducibility of biological results due to differences in experimental protocols, high standard deviations, and low sample sizes. Hence, optimally, multiple sets of different input data would be run to interpret the results of the PN_t-Methodology rather stochastically than absolute, always when enough experimental data is available. Moreover, the data type, i.e. mRNA expression or protein synthesis, used to feed the system of interest, strongly depends on experimental availability. Accordingly, in this work, mRNA expressions were used. Given that mRNA expressions and protein synthesis are not always proportional, additional calculations with a dataset about protein synthesis, would be instrumental to address the effect of CA on tissue remodeling in future. Such results could be used for multiscale top-down approaches, i.e. as feedback for intracellular network models.
Focus was set on a scalable design of the PN-equation that adapts to user-defined systems of interest. This is a requirement for both, a more extensive investigation of the current network and to enable the application of the PN_t-Methodology to multicellular systems of other tissues in future. Notably, compared to most other mathematical solutions, this methodology doesn't tackle the comparison to a reference value to assess activations (e.g. 1 in Boolean or fuzzy-logic approaches). This was particularly necessary to allow for the comparison of different CS. To achieve, however, a robust, relative comparability, the weight of each PN within the PN-system was assessed through weighting factors, that predefined the sensibility of each CA to the surrounding stimulus environment with respect to the sensibility of any other CA within the same PN-system.
An interesting aspect of approximating living, dynamic systems is the handling of the absence of a stimulus. In the simulated mechanosensitive multicellular system, this refers to the simulation of static condition effects. In contrast to any other external stimulus considered in this multicellular system, freq is a stimulus, the absence of which is perfectly physiological. The absence of freq was found to be less anabolic than (moderate) dynamical behavior (Chan et al., 2011). Therefore, a discontinuity of the generic function towards 0 Hz must

be assumed. Hence, the absence of freq was described as a special case, where the stimulus freq = 0 Hz was actively contributing to the response of a system (see 5.5 Methods).
From a numerical point of view, one must bear in mind that the non-linearity of the PN-equation favors the increase of PN-activities compared to decreases (Figure 5.8, section 5.5 Methods). Hence, tissue protein expressions decrease slowly, whilst the rise for proteases is more pronounced. The good qualitative findings of the current results (see supplementary information 1 & 2, Appendix 3) suggest that this tendency actually fits known biological dynamics in the NP of the IVD. Arguably, further work is required to test the performance of the PN_t-Methodology with the biology of other tissues.
Currently, the PN-equation only considers parallel effects of different stimuli, whilst possible cross-effects among different stimuli were not taken into consideration so far. Yet, the equation allows to introduce correction factors for stimulus interactions, e.g. by formulating the weighting factors as variables, in function of the surrounding stimulus environment (cf. Chapter 4), if experimental evidence points towards significant impacts of cross-effects. The quality of the model results by adding such an additional dimensionality remains to be investigated.
To integrate dose and time-sensitivities, a mathematical description was developed to interrelate time dependency and stimulus dose. This was achieved through a generic function that relates the whole range of stimulus intensities to an either activating or inhibiting effect on a CA. Generic functions are based on general assumptions about the qualitative effect of a load on a CA. Hence, moderate loading conditions, in terms of both mag and freq, were generally assumed to be anabolic, and excessive loading was generally assumed to be catabolic. Thus, in addition to the overall data-driven approach presented here, this modelling approach allows to complement missing data by an integration of knowledge-driven data. Again here, the mathematical framework was designed to allow for an easy adaptation of the generic functions in order to obtain more refined S-CA relationships as soon as corresponding information is available.
Relevant time-dependencies for the NP enclose a loss of anabolic stimulus over time and a time delay in the development of a catabolic response to a catabolic stimulus. The latter was programmed to take into consideration that short durations of high loading impacts might not promote IVD degeneration (Dudli et al., 2012), whilst sustained overload as such is considered as a risk factor for degenerative changes (Stokes and Iatridis, 2004). So far, time-dependencies were programmed

to be gradual and linear and become non-linear due to an integration into the PN-equation. Despite the overall good qualitative results (Supplementary Information 1 & 2, Appendix 3), the effect of time might be non-linear and must be adapted as soon as further insights into the time-responses of cells is available. This might be done by reconsidering the time variable as a function. Numerical incongruencies for input data close to the α-β-threshold due to the continuous formulation of the generic functions are inevitable and discussed in the supplementary information 3 (Appendix 3). Eventually, in this work time-dependencies were integrated to estimate the effect of mechanical stimuli. However, technically, they could also be programmed for biochemical stimuli.

This new methodology complements existing methodologies that cover the (sub) cellular- and tissue levels, focusing on an intermediate spatial scale. It allows to consider CA of different CS at different locations within a tissue, thanks to specific, user-defined input parameters that could be obtained by Finite Element simulations at the corresponding tissue /organ levels (as done in chapters 3, 4). Whilst this work focusses on cells of the same cell type for different CS, the PN_t-Methodology would technically allow to model heterogenous cell types within a tissue, given that this top-down approach does not rely on cell type-specific intracellular pathways.

Further work should apply this novel approach to other tissues/diseases. This might include the assessment of the capacity to add active pharmaceutical ingredients as external stimuli to the system and investigate the response of different CA to this addition. Thereby, focus must be set to carefully choose a relevant system of interest on beforehand and to have the necessary experimental data available.

To the best of our knowledge, this is the first methodology that allows a straightforward approximation of relative cell responses within heterogenous multifactorial, multicellular systems. Thanks to this novel top-down high-level network modelling approach based on experimental data and combined though an ODE, dynamic CA can be estimated over long periods of time with low computational costs (see Chapter 4), which is deemed to be an important step towards a better understanding of multifactorial disorders, such as IVD degeneration.

5.5 Methods

Determination of the weighting factors for mag and freq. To calculate the dose- and time-dependent impact of a stimulus, the corresponding weight of this stimulus (θ_S^{CA}) must be defined. Weighting factors were derived from changes in x-fold mRNA expressions, converted into a "cellular effort" as previously explained (see Chapter 4). In short: The "cellular effort" was derived from the x-fold mRNA expression (ϵ). It allows to compare increases ($1 < \epsilon < \infty$) and decreases ($0 < \epsilon < 1$) in x-fold mRNA expressions compared to a control level (1), despite of the different ranges of ϵ.

Experimental data to approximate weighting factors for mag and freq were derived from a rat study, where NP cells were exposed to a mag of 1 MPa and three different frequencies of 0.01 Hz, 0.2 Hz and 1 Hz (MacLean et al., 2004). Weighting factors of mag were estimated using data of quasi-static conditions (i.e. 0.01 Hz). Weighting factors of freq were obtained based on the maximal x-fold change in mRNA expression caused by the three aforementioned frequencies (Table 5.3).

Table 5.3: individual weighting factors for loading parameters.

Stimulus	**mRNA**	**Weighting factor ($\boldsymbol{\theta_S^{CA}}$)**	**Experimental study**
Mag	Agg	0.3484	(MacLean et al., 2004)
	Col-I	0.8711	(MacLean et al., 2004)
	Col-II	0.1394	(MacLean et al., 2004)
	MMP3	0.0100	(MacLean et al., 2004)
	ADAMTS4	0.1394	(MacLean et al., 2004)
	TNF-α	0.0100	Indications (Dudli et al., 2012; Gawri et al., 2014)
	IL1β	0.0100	Indications (Walter et al., 2012)
Freq	Agg	0.3318	(MacLean et al., 2004)
	Col-I	0.4355	(MacLean et al., 2004)
	Col-II	0.0100	(MacLean et al., 2004)
	MMP3	0.5124	(MacLean et al., 2004)
	ADAMTS4	0.1048	(MacLean et al., 2004)
	TNF-α	0.0100	No information found
	IL1β	0.0100	No information found

According to experimental observations (Dudli et al., 2012; Walter et al., 2012; Gawri et al., 2014), the effect of mag on proinflammatory cytokine expression seems to be limited. Therefore, the weighting factor of the proinflammatory cytokines TNF-α and IL1β was set to 0.01. No information was found regarding the relationship between freq and proinflammatory cytokines. Therefore, the corresponding weighting factors were also set to 0.01. A complete list of all weighting factors used in this study is provided in the supplementary information 4 (Appendix 3).

Development of the PN$_t$-Methodology. The PN$_t$-Methodology is developed based on a well-established graph based method presented by Mendoza and Xenarios in 2006 (Mendoza and Xenarios, 2006) (Eq. (5.5) & (5.6)).

$$\frac{dx_i}{dt} = \frac{-e^{0.5h} + e^{-h(\omega_i - 0.5)}}{(1 - e^{0.5h})(1 + e^{-h(\omega_i - 0.5)})} - \gamma_i x_i \tag{5.5}$$

with

$$\omega_i = \left(\frac{1 + \sum \alpha_n}{\sum \alpha_n}\right)\left(\frac{\sum \alpha_n x_n^a}{1 + \sum \alpha_n x_n^a}\right)\left(1 - \left(\frac{1 + \sum \beta_m}{\sum \beta_m}\right)\left(\frac{\sum \beta_m x_m^i}{1 + \sum \beta_m x_m^i}\right)\right) \tag{5.6}$$

In short: Eq. (5.5) determines the overall activation of a node, x_i, where the gain variable (h) allows to gradually shape the relationship between $\frac{dx_i}{dt}$ and the total nodal input, ω_i, from a linear to a step function. The overall node activation can be reduced by integrating a decay rate (γ). Eq. (5.6) expresses the total input of the node, according to the set of activators x_n^a and inhibitors x_m^i that act on the node with the respective positive strengths α_n and β_m (Figure 5.7, A). Nodal activation is always bound between 0 and 1.

A PN-network is always directional as it reflects the effect of adjacent nodes on one principal node that stands for a CA (Figure 5.7, B). Adjacent nodes represent the stimulus (micro-) environment. The impact of each adjacent node is determined by the product of a weighting factor (θ_S^{CA}) and the corresponding stimulus concentration/intensity (x_S^{CA}) (Figure 5.2, B, Results). Moreover, the integration of time- and dose dependencies within the PN-network allows a stimulus to be either activating or inhibiting, according to the user-defined stimulus dose and the time, during which the condition is maintained.

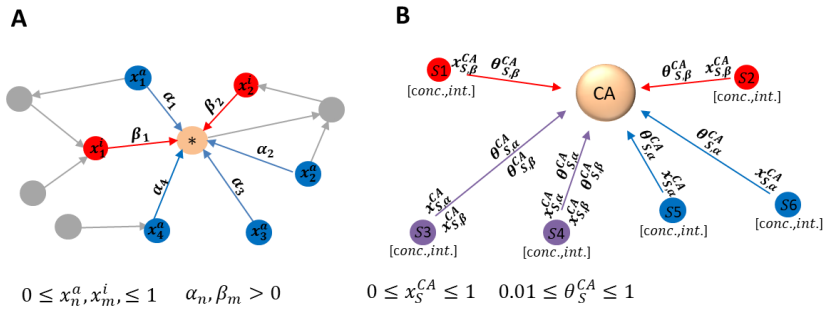

Figure 5.7: Comparison between the network presented by Mendoza and Xenarios 2006 (Mendoza and Xenarios, 2006) (A) and the concept of parallel network modelling to tackle heterogenous stimulus environments. An individual parallel network for a given stimulus environment of six stimuli is shown in figure B. The overall activity of the principal node (* vs. CA) is determined by adjacent network nodes (A), or by a local stimulus environment (B). The effect of adjacent nodes is either activating or inhibiting (A, B) or includes dose and time dependencies (B, S3, S4). Whilst network nodes are usually interconnected within each other (A), the objective of individual parallel networks (B) is to determine a final CA. α_n, β_m, θ_S^{CA}: activating/inhibiting factors. x_n^a, x_m^i, x_S^{CA}: adjacent node activation (A), normalized stimulus dose, i.e. concentration (conc.) /intensity (int.) (B).

Within the PN$_t$-Methodology, the decay term defined by Mendoza & Xenarios (Eq. (5.5)) would reflect a possible decay in mRNA expression under sustained stimulation or the half-life of a secreted protein. In the present methodology the decay terms would represent, however, an additional source of uncertainty, and they don't add further information about the regulation of the system of interest. Hence, they were not considered. Moreover, given that CA are directly obtained through the S-CA relationships that are based on experimental findings, no additional manipulation of ω_i is needed. Thus, the gain factor h in Eq. (5.5) reflects a linear relationship between $\frac{dx_i}{dt}$ and the total nodal input ω_i in the PN$_t$-Methodology. Accordingly, the overall CA was directly assessed by ω_i, leading to Eq. (5.7).

$$\frac{dx_i}{dt} = \omega_i \tag{5.7}$$

The activating portion of the PN-equation. The activating portion of the PN-equation (Eq. (5.1)) determines an overall activation of a CA relative to any other CA within the same PN-system. Hence, within the

term $\left(\frac{1+\sum\theta_\alpha}{\sum\theta_\alpha}\right)$, all activating weighting factors of the tackled PN-system were considered, which determines its size. The second fraction of the activating term defines the activation of each individual network, by $\sum\theta_{S,\alpha}^{CA}x_{S,\alpha}^{CA}$. Thus, the maximal activation of a CA is determined by $\sum\theta_{S,\alpha}^{CA}$, i.e. with $x_{S,\alpha}^{CA} = 1$.
Given the non-linearity of the approach, values of maximal activations strongly depend on the pre-established size of the PN-system. Thereby, the maximal activation of one PN-network reflects a fraction of the overall size of the PN-system, i.e. $\sum\theta_{S,\alpha}^{CA} = \lambda\sum\theta_\alpha$ with $0 < \lambda \leq 1$. Hence, λ describes the relative weight of one parallel network within the PN-system. Thus, $\lambda = 1 \rightarrow \sum\theta_{S,\alpha}^{CA} = \sum\theta_\alpha$ would reflect a reduction of the system to just one parallel network. In contrast, maximal activations of individual networks decrease with increasing PN-systems, and the results, i.e. the overall CA ($\frac{d\omega_{CA,CS}}{dt}$, Eq. (5.1)) of individual networks require a high resolution, reflected in elevated decimal places. To cope with this, the first fraction of the activating term is designed to assign higher relative weights to individual parallel networks with increasing sizes of PN-systems (Figure 5.8).

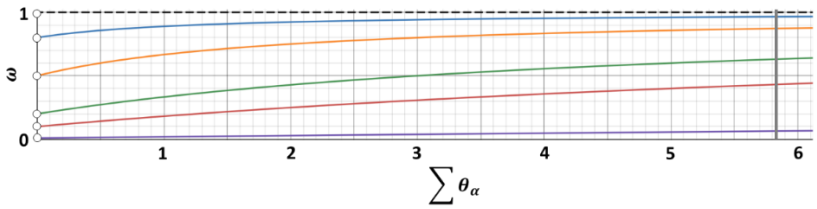

$\lambda = 1, \lambda = 0.8, \lambda = 0.5, \lambda = 0.2, \lambda = 0.1, \lambda = 0.01$

$$\omega_{max} = \frac{1 + \sum \theta_\alpha}{\sum \theta_\alpha} \cdot \frac{(\lambda \sum \theta_\alpha)}{1 + (\lambda \sum \theta_\alpha)} \; with \; 0 < \lambda \leq 1 \quad and \; \lambda \sum \theta_\alpha = \sum \theta_{S,\alpha}^{CA}$$

Example: Agg, non-inflamed cells:

$\sum \theta_{S,\alpha}^{Agg} = 0.7844, \lambda_{Agg}=0.1344^*, \omega_{max,Agg}=0.5149^*$

*rounded

Size, current PN-system: $\sum \theta_\alpha = 5.8337$

Estimation for different $x_{S,\alpha}^{CA}$:

$$\omega = \frac{1 + \sum \theta_\alpha}{\sum \theta_\alpha} \cdot \frac{((\lambda \sum \theta_\alpha) \cdot x_{S,\alpha}^{Agg})}{(1 + (\lambda \sum \theta_\alpha) \cdot x_{S,\alpha}^{Agg})}$$

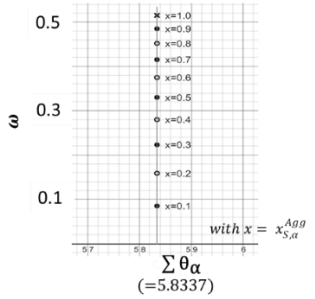

Figure 5.8: Evolution of the relative size of a parallel network with an increasing size of the PN-system. Exemplary relative sizes of individual networks are plotted (λ= 1, λ = 0.8, λ =0.2, λ =0.1, λ =0.01). Specific values for Aggrecan (Agg) of the current PN-system of the NP were exemplarily shown. The size of the PN-system is 5.8337 and marked as a grey bar within the plot. The effect of different values for $x_{S,\alpha}^{CA}$ i.e. from x=0.1 to x=1.0, was plotted for Agg. ω is not defined for $\sum \theta_\alpha = 0$.

Eventually, the PN-equation assigns an individual range to each CA, in which it varies according to its $x_{S,\alpha}^{CA}$ and its individual inhibition. The nonlinear behavior of the PN-equation due to different values of $x_{S,\alpha}^{CA}$ is schematically represented (Figure 5.8).

The inhibiting portion of the PN-equation. The inhibiting portion of the PN-equation (Eq. (5.1)) lowers the current activation of a CA and is defined relative to the activation of the CA. The first fraction determines the relative weight of the inhibition on the CA. Hence, it prevents weak inhibitors to completely erase overall cell activations. Thus, if the activation of a CA was determined on weak activators and powerful inhibitors, the impact of inhibition was strong and vice versa. The second inhibiting fraction defines the maximal inhibition of a CA by considering all the different CS of a CA. It allows for coherent inhibiting impacts of different CS. Hence, its function is equivalent to the first activating fraction of the PN-equation, but instead of

considering the whole PN-system, only different CS of the same CA were considered.
The third fraction of the inhibiting term, determines the actual weight of the inhibition, analogue to the second fraction of the activating term (Figure 5.9).

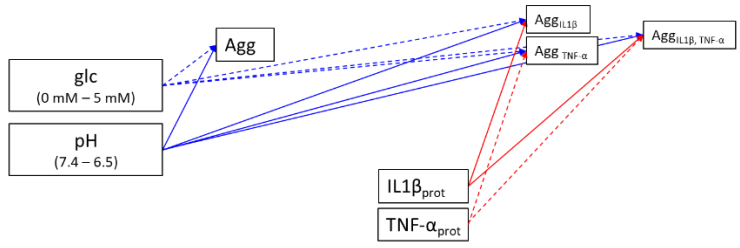

$$\frac{d\omega_{Agg,non-infl}}{dt} = \left(\left(\frac{1+\sum\theta_{\alpha}}{\sum\theta_{\alpha}}\right)\left(\frac{\sum\theta_{S,\alpha}^{Agg}x_{S,\alpha}^{Agg}}{1+\sum\theta_{S,\alpha}^{Agg}x_{S,\alpha}^{Agg}}\right)\right) = \alpha_{Agg}$$

$$\frac{d\omega_{Agg_{-IL1\beta\ infl}}}{dt} = \alpha_{Agg}\cdot\left(1-\left(\left(\frac{\theta_{IL1\beta,\beta}^{Agg}}{\theta_{glc,\alpha}^{Agg}+\theta_{pH,\alpha}^{Agg}+\theta_{IL1\beta,\beta}^{Agg}}\right)\left(\left(\frac{1+\theta_{IL1\beta,\beta}^{Agg}+\theta_{TNF-\alpha,\beta}^{Agg}}{\theta_{IL1\beta,\beta}^{Agg}+\theta_{TNF-\alpha,\beta}^{Agg}}\right)\left(\frac{\theta_{IL1\beta,\beta}^{Agg}x_{IL1\beta,\beta}^{Agg}}{1+\theta_{IL1\beta,\beta}^{Agg}x_{IL1\beta,\beta}^{CA}}\right)\right)\right)\right)$$

$$\frac{d\omega_{Agg_{-TNF-\alpha\ infl}}}{dt} = \alpha_{Agg}\cdot\left(1-\left(\left(\frac{\theta_{TNF-\alpha,\beta}^{Agg}}{\theta_{glc,\alpha}^{Agg}+\theta_{pH,\alpha}^{Agg}+\theta_{TNF-\alpha,\beta}^{Agg}}\right)\left(\left(\frac{1+\theta_{IL1\beta,\beta}^{Agg}+\theta_{TNF-\alpha,\beta}^{Agg}}{\theta_{IL1\beta,\beta}^{Agg}+\theta_{TNF-\alpha,\beta}^{Agg}}\right)\left(\frac{\theta_{TNF-\alpha,\beta}^{Agg}x_{TNF-\alpha,\beta}^{Agg}}{1+\theta_{TNF-\alpha,\beta}^{Agg}x_{TNF-\alpha,\beta}^{Agg}}\right)\right)\right)\right)$$

$$\frac{d\omega_{Agg_{-IL1\beta\&TNF-\alpha\ infl}}}{dt} = \alpha_{Agg}\cdot\left(1-\left(\left(\frac{\theta_{IL1\beta,\beta}^{Agg}+\theta_{TNF-\alpha,\beta}^{Agg}}{\theta_{glc,\alpha}^{Agg}+\theta_{pH,\alpha}^{Agg}+\theta_{IL1\beta,\beta}^{Agg}+\theta_{TNF-\alpha,\beta}^{Agg}}\right)\left(\left(\frac{1+\theta_{IL1\beta,\beta}^{Agg}+\theta_{TNF-\alpha,\beta}^{Agg}}{\theta_{IL1\beta,\beta}^{Agg}+\theta_{TNF-\alpha,\beta}^{Agg}}\right)\left(\frac{\theta_{IL1\beta,\beta}^{Agg}x_{IL1\beta}^{Agg}+\theta_{TNF-\alpha,\beta}^{Agg}x_{TNF-\alpha,\beta}^{Agg}}{1+\theta_{IL1\beta,\beta}^{Agg}x_{IL1\beta}^{CA}+\theta_{TNF-\alpha,\beta}^{Agg}x_{TNF-\alpha,\beta}^{Agg}}\right)\right)\right)\right)$$

Figure 5.9: Illustration of the determination of the inhibiting part of the PN equation. Example for the different CS of Aggrecan (Agg) exposed under the influence of glc and pH. Analogue formulations between the activating and inhibiting terms were indicated with dotted lines. Infl: inflamed

Determination of relevant stimulus ranges and specific logistic functions for mag and freq. Relevant, stimulus ranges for mag were determined based on in-vivo studies and range from 0.1 MPa to 3.5 MPa (Nachemson and Elfström, 1970; Wilke et al., 1999). Hence, in this approach, mag refers to intradiscal pressures. The range for freq was set to 0 Hz – 40 Hz, aiming to allow predictions for the effect of whole-body exposures to high-frequency in daily occasions. The minimal step size for both, mag and freq was set to 0.05. To estimate the shape of the functions, *in vivo* and *in vitro* data and knowledge were used to assign different levels of mag and freq to anabolic or catabolic cell responses (Nachemson and Elfström, 1970; Wilke et al., 1999; Walsh and Lotz, 2004; Pachi and Ji, 2005; Kasra et al., 2006; Chan et al., 2011; Vernillo et al., 2017). To fit the generic functions of mag, low and moderate pressures due to e.g. lying or walking were assumed to be highly anabolic. With rising intradiscal pressures, as obtained during jogging, anabolism gradually lowers until the stimulus becomes

catabolic. Additionally, findings from Chan, Ferguson, and Gantenbein-Ritter (Chan et al., 2011) were considered that suggest that magnitudes around 0.2 MPa and 0.8 MPa reflect a potentially beneficial range of magnitude, whereas a (static) compression loading of > 1MPa induced degenerative changes. The generic functions for freq were set assuming walking freq to be overall beneficial, with freq up to around 2.5 Hz as observed by (Pachi and Ji, 2005), whereas a freq range of 3-8 Hz, or over a threshold of 5 Hz, possibly disrupt proper cell function (Kasra et al., 2006). The functions were fitted to an accuracy of four decimals, in agreement with the fitting of the continuous functions that describe the effect of nutrition-related stimuli (Figure 5.2, B), as previously explained (Chapter 4). The mathematical formulation of the four generic functions are presented in Eq. (5.8) - (5.11).

$$X_{Mag}^{A;I} = -\frac{e^{14mag} \cdot 1.99999}{e^{14mag} + 1.2 \cdot 10^{6}} + \frac{1.99999}{2} \tag{5.8}$$

$$X_{Mag}^{I;A} = \frac{e^{14mag} \cdot 1.99999}{e^{14mag} + 1.2 \cdot 10^{6}} - \frac{1.99999}{2} \tag{5.9}$$

$$X_{Freq}^{A;I} = -\frac{e^{6freq} \cdot 1.99999}{e^{6freq} + 6.6 \cdot 10^{7}} + \frac{1.99999}{2} \tag{5.10}$$

$$X_{Freq}^{I;A} = \frac{e^{6freq} \cdot 1.99999}{e^{6freq} + 6.6 \cdot 10^{7}} - \frac{1.99999}{2} \tag{5.11}$$

Estimation of individual time sensitivities of mRNA expressions in NP cells. $\gamma_{S,i,ana}^{CA}$ was estimated based on experimental data, where the effect of 1 MPa and 1 Hz on rat NP cells was assessed after 0.5h, 2h and 4h (MacLean et al., 2005). Thereby, the ratio of a mathematically assessed "cellular effort" was used (Chapter 4) as done for the determination of the weighting factors for mag and freq. $\gamma_{S,i,cata}^{CA}$ was derived from the values assessed for $\gamma_{S,i,ana}^{CA}$. Thereby, Agg was chosen as a reference value (1) to determine the individual time delays of CA to unfold their whole catabolic potential. Time sensitivities within the catabolic range for any other CA were obtained as fractions, relative to Agg (Table 5.4).

Table 5.4: individual time sensitivities for initially anabolic (ana) and catabolic (cata) stimulus intensities. Agg was used as a reference for the determination of catabolic time sensitivities.

CA	$\gamma^{CA}_{mag,i,ana}/\gamma^{CA}_{freq,i,ana}$	$\gamma^{CA}_{mag,i,cata}/\gamma^{CA}_{freq,i,cata}$
Agg (ref)	3.1429	1
Col-II	1.7500	$\frac{1.7500}{3.1429}$=0.5568
Col-I	2.7647	$\frac{2.7647}{3.1429}$=0.8797
MMP3	2.1571	$\frac{2.1571}{3.1429}$=0.6864
ADAMTS4	3.1481	$\frac{3.1481}{3.1429}$=1.0017
TNF-α	0.3143	No catabolic time sensitivity
IL1β	0.3143	No catabolic time sensitivity

With regard to proinflammatory cytokines, no information about a possible time-sensitivity to loading conditions was found. Therefore, initially prudent time sensitivities were chosen for $\gamma^{CA}_{S,i,ana}$, being 10 times lower than the time dependency of Agg. This assumption was based on the observation that long-term exposure to microgravity does not categorically lead to IVD failure (Belavy et al., 2016), whilst excessive inflammatory conditions might provoke non recoverable catabolic shifts (Purmessur et al., 2013). Under initially catabolic loading, no time-delay was programmed, thus, values provided by the generic function were used to determine the inflammatory environment (Table 5.4).

Estimation of the amplification factor (σ) to approximate mRNA expressions in NP cells. To estimate σ, it was supposed that 8h of axial dynamic loading of 0.2 – 0.8 MPa and 0.1 – 1 Hz may not induce degeneration of the disc (Chan et al., 2011). Hence, model predictions for 0.2 MPa and 0.8 MPa at a medium freq of 0.5 Hz were calculated for rising amplification factors of σ = 1 to σ = 4 (non-inflamed cells, under optimal, nutritional conditions of 5 mM glc, pH 7.1) and results were evaluated with regard to their catabolic progression at 0.8 MPa (Figure 5.10).

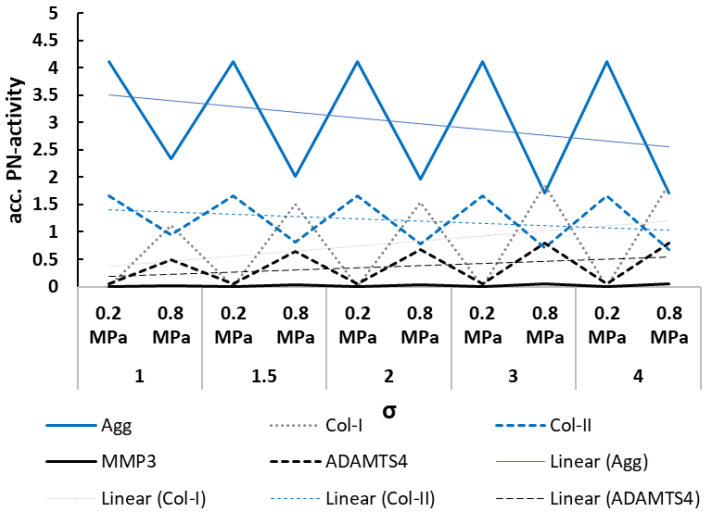

Figure 5.10: model predictions for different amplification factors (σ) and corresponding tendencies. Optimal nutritional conditions (5 mM glc, pH 7.1) and a frequency of 0.5 Hz were used.

Results showed that catabolic predictions at 0.8 MPa were already elevated for $\sigma = 2$. This is reflected by a higher acc. PN-activity for Col-I than Col-II, a considerably lower Agg mRNA expression compared to $\sigma = 1$ and a lose approximation of the CA of Col-II and ADAMTS4. Hence, as an initial approximation for an amplification factor, a medium value between $\sigma = 1$ and $\sigma = 2$, i.e. $\sigma = 1.5$ was set.

Estimation of the effect of the absence of freq. To consider static loading, the impact of "no-frequency" on a CA must be estimated. Therefore, the assumption that degeneration might not be induced during 8h dynamic axial loading with a load of 0.2 – 0.8 MPa and 0.1 – 1 Hz (Chan et al., 2011) was used. Hence, a dynamic daily human moving habit with loading parameters within the suggested range was compared to a generally anabolic, static, human behavior. As a dynamic human moving habit, comfortable walking ("hiking") was chosen. It was approximated by a mag of 0.60 MPa, reflecting a (rounded) average intradiscal pressure during walking (Wilke et al., 1999), and a freq of 1.00 Hz. The static control was chosen to be "sleeping", reflected by an intradiscal pressure of 0.15 MPa, being the (rounded) average intradiscal pressure during night, over a period of 7h (Wilke et al., 1999). Agg was chosen as the reference protein for the fitting (Figure 5.11).

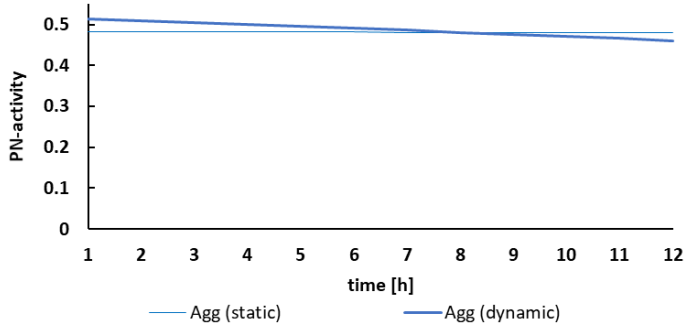

Figure 5.11: Illustration of the model prediction with $X_{freq,0} = 0.75$ for Agg (ref).

Results showed that, a loss of anabolism due to dynamic loading compared to a static control after 8h was approximated with $X_{freq,0} = 0.75$. An example for Agg: within the first hour of an anabolic static condition, e.g. sitting, the x_{freq}^{Agg} contributes to the overall activation with a value of 0.75, which then continuously decreased due to time dependency. The time-dependency for static loading was defined using the generic function of freq at 0 Hz as explained in Results (section 5.3).

Estimation of intradiscal pressures and freq for the results (listed in Table 5.2). Intradiscal pressures were obtained from in-vivo measurements (Wilke et al., 1999) and rounded to the minimal step size of loading parameters (i.e. 0.05). Whenever intradiscal pressures were provided as ranges, average values were used for the simulation (e.g. walking: 0.53 MPa – 0.65 MPa (Wilke et al., 1999) was approximated as 0.60 MPa). For microgravity calculations, the intradiscal pressure reflected the (rounded) value after 7h of rest (Wilke et al., 1999). Freq for hiking was reasonably estimated to be around 1 Hz, whilst values for walking and jogging were within the range as found in observational studies (Pachi and Ji, 2005; Vernillo et al., 2017). The vibration freq for "sitting in/on a motor vehicle" was estimated within the range of maximal, catabolic predictions.

6 *Conclusion and Future Work*

This work focused on the development of a new methodology to estimate cell responses to complex, multifactorial environments, with the overall aim to tackle biologically-driven injury mechanisms. The approach was developed by analyzing multicellular systems within the IVD, a tissue that is prone to degenerative changes. To the best of our knowledge, this is the first *in silico* approach that tackles IVD degeneration at the cellular level.

The presented PN_t-Methodology reflects a methodological approach, where the cell is considered as a "black box" and CA were directly linked to the multifactorial stimulus environment. Hence, each CA was interpreted as a cell response to its current multifactorial environment. Consequently, many CA reflect many responses to a stimulus environment at the same time. Each CA was approximated as the result of a regulatory network and, thus, the whole cellular response was interpreted as many parallel ongoing networks.

Key external stimuli and their effect on CA were identified based on experimental findings. This includes a consideration of dose-dependent time sensitivities of individual CA to tackle chronic stimulus exposure, which is deemed to be key relevant in slowly developing diseases.

Eventually, a set of integrative methods was developed to translate experimental findings into suitable parameters for systems biology approaches. Parameters emerging from those methods were then fed in an ODE-based core element of the PN_t-Methodology, the PN-equation, which allowed to estimate and interrelate different CA. As a result, a relative expression of different CA as a response to heterogenous multifactorial environments was obtained, reflected as PN-activities.

The PN_t-Methodology is a generic approach and might, therefore, be translated to approximate multicellular systems of other tissues. Due to its scalable design, it allows to individually adapt to user-defined systems of interest, whilst computational costs remain very low.

In this work, the PN_t-Methodology was embedded within a 3D AB model that simulated the multicellular environment. Its volume of $1mm^3$ was chosen as reasonable size to approximate multicellular environments, whilst it lies within the range of the size of FE model elements of our in-house FE model. Hence, the developed model is designed to be suitable for multiscale approaches which are deemed to be key relevant to unravel critical dynamics in IVD degeneration.

6.1 Research summary

The research summary wraps up the PN_t-Methodology (section 6.1.1) and highlights the evaluation of the methodology and the tissue-relevant findings as part of the evolution of this work (section 6.1.2).

6.1.1 The PN_t-Methodology

The PN_t-Methodology initially requires an establishment of a system of interest, consisting of stimuli and CA. The system of interest is then split into PN-systems, where the user defines all the CA that need to be interpreted relatively to each other. PN-systems (usually) consist of a set of individual networks. Each network determines the effect of a multifactorial stimulus environment on a specific CA.

PN-systems were fed with data derived from experimental studies. Thereby, two principal qualities on how a stimulus affect a CA were considered: (i) the sensitivity of the CA to a stimulus dose and (ii) the sensitivity of a CA to a stimulus type. Sensitivities were biologically reflected by a change in CA under different stimulus doses (i) and by a maximal change in CA within a (physiological) stimulus range (ii). Accordingly, two methods were developed to translate experimental information into suitable parameters for network modelling approaches. A further, integrative method eventually allowed to tackle time-dependent effects in CA due to chronic stimulus exposure.

The CA might reflect mRNA expressions or protein synthesis, depending on the availability of experimental data and the research objective.

To calculate the PN-systems an equation (PN-equation) was developed that allows to estimate and interrelate all the parallel networks within a PN-system. Results of the PN-equation are provided as PN-activities. PN-activities reflect a qualitative estimation of different CA and CS relative to each other. The overall response of a cell in terms of different CA was provided as CA profiles.

6.1.2 Biologically-driven injury mechanisms within the Nucleus Pulposus of the intervertebral disc

In **Chapter 3**, the 3D Agent-based model was introduced and submodels to estimate cell viability, inflammation and mRNA expression were presented (Figure 6.1).

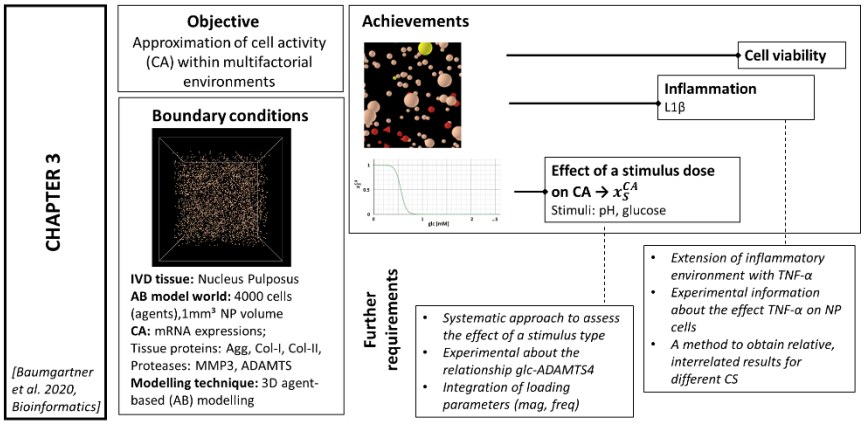

Figure 6.1: overview of the objective and achievements of Chapter 3, including future requirements that reflect the motivation and the direction of this research.

The proinflammatory environment considered non-inflamed and IL1β inflamed cells. Cell viability was estimated based on the effects of glc, lac and IL1β. To approximate the mRNA expression, a method to estimate the effect of a stimulus dose on a CA (x_S^{CA}) was presented. Data integration was done through the ODE-based approach of Mendoza and Xenarios (Mendoza and Xenarios, 2006).

Predictions of cell viability were in good agreement with independent experimental data. Likewise, the method to estimate mRNA expressions of inflamed and non-inflamed cells provided good results that were, moreover, able to retrospectively provide possible explanations for unexpected experimental findings. This was, to our knowledge, the first publication that provided insights into possible cell responses to complex multifactorial environments within the NP according to user-defined stimulus environments. With this, we could show that feeding a network with biological data seemed to be a promising approach for future research.

Further research enclosed a systematic assessment of the effect of a stimulus type. Furthermore, a lack of experimental data did not allow to specify a protease within the ADAMTS family and impeded the integration of TNF-α as a potentially key relevant inflammatory mediator. Finally, technical limitations met by comparing the CA of two different CS needed to be tackled and the stimulus environment should be extended to include key relevant effects of direct mechanotransduction.

In **Chapter 4**, focus was set on improving the estimation of mRNA expressions and extending the proinflammatory environment. Therefore, specific experimental knowledge regarding the effect of glc and TNF-α on CA was required that was not found in literature. Hence, Chapter 4 presented an interdisciplinary work. It enclosed experimental research, a modelling approach to simulate different CS within complex, multicellular environments and a numerical approach to estimate the effect of a stimulus type on a CA (θ_S^{CA}) (Figure 6.2).

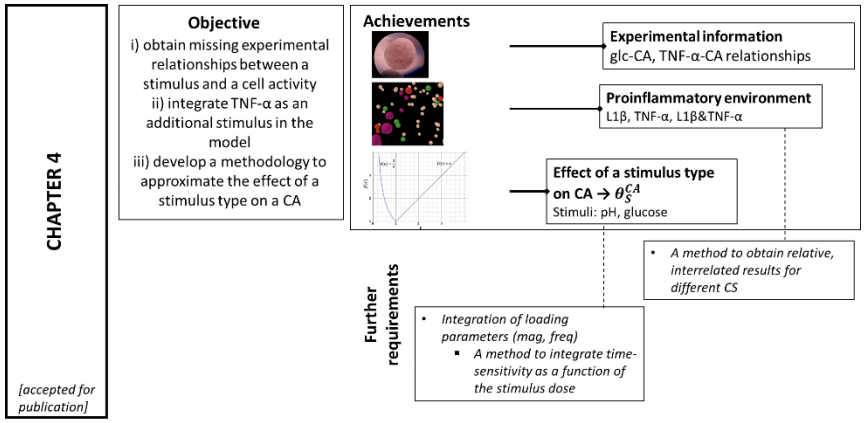

Figure 6.2: overview of the objective and achievements of Chapter 4, including future requirements that reflect the motivation and the direction of this research.

Experimental findings showed that TNF-α caused significant catabolic shifts in NP cells, whilst the effect of (partial) glc deprivation affected the cells much less. *In silico* findings revealed that mRNA predictions were importantly improved by an integration of systematic weighting factors (that estimate the impact of the stimulus type on a CA). This included distinct CA profiles for different proinflammatory CS and a generally lower PN-activity of Col-II compared to Agg, both in good agreement with literature.

CA profiles could now be obtained for non-inflamed cells and cells immunopositive for IL1β, TNF-α and both, IL1β&TNF-α and results could be specified for the protease ADAMTS4 of the protease family ADAMTS.

So far, however, the estimation of the proinflammatory environment under adverse nutrient condition was limited, which we related to the lack of the integration of direct mechanotransduction effects into the model. To integrate direct mechanotransduction, a method was required that tackled the effect of dose-dependent chronic stimulus

exposures on CA. Furthermore, a method was needed that allowed to integrate the developed parameters, i.e. the effect of the stimulus dose and stimulus type, to estimate and interrelate the different CA within each other.

Eventually, in **Chapter 5**, the development of an ODE-based equation was presented that reflects the core of the PN_t-Methodology. Furthermore, a method was introduced to tackle direct mechanotransduction effects, which was coupled with a dose-dependent time sensitivity approach (Figure 6.3). Finally, this work allowed to estimate cell responses of NP cells under the influence of six most relevant stimuli in IVD degeneration: the nutrition parameter glc and lac (through pH), the proinflammatory cytokines IL1β and TNF-α and the loading parameters mag and freq.

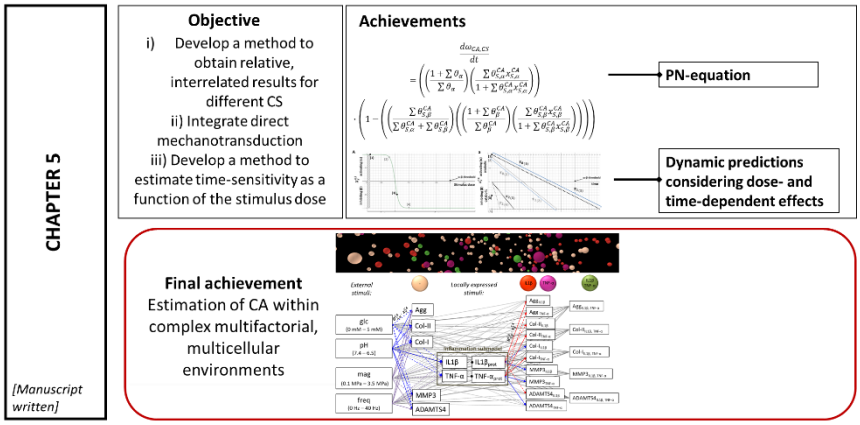

Figure 6.3: overview of the objective and achievements of Chapter 5, which include the final achievement of this research.

Final model results (presented in both, Chapter 5 and corresponding annex) uniquely allowed to approximate continuous changes in CA due to constant stimulus exposure and allowed to compare CA-profiles of cells exposed to heterogenous stimulus environments. A consideration of the four key relevant external stimuli glc, pH, mag and freq led to reasonable predictions of proinflammatory cytokines, also under adverse nutrient conditions. The overall conservative predictions of proinflammatory environments, together with pronounced PN-activities for protease mRNA expressions support the hypothesis of ECM breakdown products as an endogenous trigger of inflammation (Medzhitov, 2008). In particular, this effect was observed under the influence of TNF-α, which goes along with its role as a strong catabolic

mediator. Qualitative model predictions of the effect of direct mechanotransduction were in good agreement with findings in literature and were able to tackle long-term conditions such as prolonged microgravity exposure or bedrest. Moreover, CA of a daily life with different activities could be approximated. Simulations of different physical activities showed that the biological response to a mechanical stimulus environment is highly depending on the stimulus combinations and, hence, the biologically-driven injury mechanism does most probably not follow a systematic pattern. This goes along with highly diverse phenotypes of IVD degeneration at the tissue/organ level. Furthermore, important alterations of CA suggest that the presence of subcellular regulations are important mediating responses to such alterations, especially because visible adaptions at the tissue level progress slowly. Hence, maintained, adverse conditions, i.e. chronicity, is suggested as a possible key factor in degenerative processes, indicating that frequent changes in moving habits might be beneficial to maintain IVD integrity.

6.2 Future work

This work invites for a wide range of different upcoming research, from further developments of the current NP model, over new mathematical expressions to refine the PN_t-Methodology up to application possibilities PN_t-Methodology for other tissues.

Further work with the NP model should focus on an *integration of this model within multiscale approaches*. This includes bottom-up approaches to better understand dynamics of biologically-driven injury mechanisms over multiple scales, and top-down approaches to contribute to a better understanding of regulatory mechanisms from mRNA to protein synthesis. Regarding the latter, the current model might be fed with experimental data for protein synthesis which allow for a comparative evaluation of model predictions.
A decoupling of the model from general user-defined nutritional environments by *simulating nutrient diffusion* within the AB model would allow to investigate effects of nutrient gradients beyond the limitation of FE mesh sizes. This would allow to consider as well the impact of inhomogeneities of the NP tissue at a nanoscale level. Hence, an integration of diffusion would autonomically regulate CA according to the anatomical location of the cell and the local tissue density. Within a first approach, the AB model world was subdivided in five layers

according to the anatomical location of the cell with regard to their distance to the model boundaries (Figure 6.4).

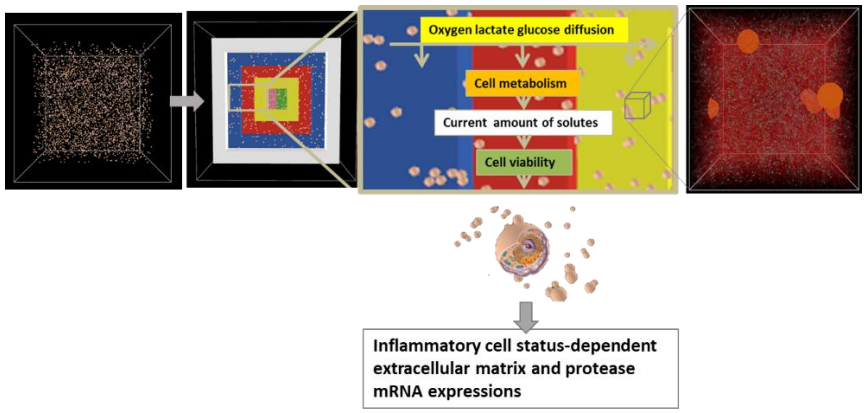

Figure 6.4: schematic description of the integration of an autonomous diffusion as a possible further development of the current AB model (left). Thereby, cells are grouped according to their location within the AB model (highlighted in white, blue, red, yellow, pink/green) with respect to the model boundary. To investigate molecular dynamics at the nanoscale level, a separate 3D nanoscale AB model was built (right). It reflects cells (orange), nutrient molecules (small green, gray and blue dots) and tissue fibers (red, translucent). Image of the nanoscale model obtained from Anton Kaniewski, Master Student, in charge of the model development. The cell anatomy was obtained from: https://www.thinglink.com/user/611122 694879969280, accessed the 18.04.2018.

Additionally, a 3D nanoscale AB model of the NP tissue was built, which included Agg and Collagen structures, NP cells and the nutrients glc, lac and oxygen (Figure 6.4, right) and allowed to simulate different dynamics depending on e.g. the metabolic cell activity or the tissue density. Future work will further exploit those preliminary approaches. Improvements regarding an *integration of additional stimuli*, such as oxygen, load amplitude, the impact of osmolarity or additional locally expressed stimuli are furthermore key relevant to better approximate native tissue environments.

A further improvement of the current model would enclose the update of the *cell viability* submodel. A coupling of the currently obtained mRNA expressions of tissue proteins and proteases with (local) cell viability would directly allow to estimate the impact of cell viability within IVD degeneration. Thereby, an update of the current approach would be needed to avoid a direct addition of the effect of each

individual stimulus and include cross-effects between stimuli that were found to influence cell viability (Bibby and Urban, 2004).
Eventually, *coupled with advances of experimental knowledge*, the actual NP model should be fed with additional experimental datasets in order to allow for more robust predictions thanks to a stochastic interpretation of the model results. With this regard, more detailed information regarding the effect of load and time on CA are deemed to be key relevant to confirm or adapt current model predictions. Further refinements might include the modelling of inflammation, where linear S-CA relationships might be replaced with more detailed nonlinear functions, as done for nutrient environments. Therefore, an advanced understanding about the range of physiological concentrations of proinflammatory cytokines and their effect on CA would be required. Moreover, a better understanding of location and appearance of cell immunopositivity within the NP would allow to update the current simulation of inflammation within multicellular environments.
Finally, currently used datasets allow to simulate dynamics within the transition of non-degenerative to early degenerative conditions. This model could, however, also be used to simulate later stages of degeneration by exchanging the biological input datasets with data of degenerated NP cells.

Future developments of the PN_t-Methodology should dig into mathematical formulations to integrate possible cross-effects between stimuli. A possible approach reflects a formulation of weighting factors as functions of surrounding stimulus concentrations. However, more experimental knowledge about cross-effects between stimulus concentrations and mRNA expressions would be needed.
To date, no endogenous triggers were considered to predict proinflammatory environments and corresponding effects on CA. Their consideration would contribute to a less conservative prediction of proinflammatory environments.
Currently, time is directly implemented as a variable to approximate time-dependent changes in PN-activities, which leads to a linear effect of time on a given CA. However, time effects are most probably non-linear. Hence, updating the time variable with a nonlinear function would most probably enhance time-dependent predictions. However, therefore more experimental knowledge is needed to estimate the evolution of mRNA expressions exposed to chronic stimulus environments over time.

Future applications of the PN_t-Methodology include both, the simulation of CEP or AF cells to holistically tackle IVD degeneration, and its application on other biologically-driven diseases. Within the long-term and after adequate validation processes, the PN_t-Methodology might also be provided as a software package, where third parties such as hospitals, universities, human movement specialists, pharmaceutical companies or space agencies can estimate the effect of crucial conditions or their new therapeutical methods on cell responses of a specific tissue.

Appendix 1 – Supplementary Material Chapter 3

Supplement 1:

Table S1: Overview of model parameters. Values marked with an asterisk (*): numerically simulated. S: Supplement. Norm: normalized. Target mRNA: Aggrecan, Collagen types I & II, MMP-3, ADAMTS

	Model world para-meters	**Input para-meters**	**Equation para-meters**	**Output range**	**Other**
Programmed world size [patches]	12x12x12				
Real world size [patches]	10x10x10				
Real world size [mm]	1x1x1				
Agents: NP cells (initially seeded)	4000				
Cell size [µm]	10				
Immunopositive cell foci (random amount)	11				
Immunopositive cells [%]	0 – 20				
Glucose [mM] *		0 – 5			
Lactate [mM] *		0 – 10			
≈ pH [-]		7.4 – 6.5			
Gain coefficient (h)			1		
Nodal input, activating (x_n^a)			Table S3, Appendix 1		
Nodal input, inhibiting (x_m^i)			Table S3, Appendix 1		
Cell viability submodel					
Estimation of cell viability			Table S4, Appendix 1		
Threshold of cell-death due to IL-1β protein concentration (conc.) (1/2 of max value)					1

Inflammation submodel			
Glc – IL-1β mRNA : Activation factor (α) [-]		0.01	
Lac – IL-1β mRNA : Activation factor (α) [-]		0.01	
IL-1β protein – IL-1β mRNA : Activation factor (α) [-]		0.03	
IL-1β mRNA (norm) *			0 – 1
IL-1β protein (norm) *			0 – 1
IL-1β protein, accumulated (norm) *			0 – 2
mRNA expression submodel			
Target mRNA: Activation factor (α) [-]		Table 3.1, Chapter 3	
Target mRNA: Inhibition factor (β) [-]		Table 3.1, Chapter 3	
Immunonegative cells, target mRNA (norm) *			0 – 1
Immunopositive cells, target mRNA (norm) *			0 – 1

Supplement 2

Table S2: Overview of the experimental studies used to estimate mRNA expression based on the solutes glc, lac and the proinflammatory cytokine IL-1β. Deg: degenerated. Non-deg: non-degenerated. Expr: expression

Study	Cell type	Culture system	Data used for the AB model	
			Varying micro-environment	mRNA expressions/ protein concentrations*
(Rinkler et al., 2010)	Human, NP, deg and presumably non-deg	Alginate Beads	glc	Agg, Col-I, Col-II, MMP-3
(Saggese et al., 2018)	Bovine, NP	Alginate Beads	glc	ADAMTS
(Moroney et al., 2002)	Porcine, NP	not specified	glc	IL-1β*
(Gilbert et al., 2016)	Human, NP, deg and non-deg	not specified	pH	IL-1β, Agg, Col-I, MMP-3, ADAMTS
(Neidlinger-Wilke et al., 2012)	Bovine, NP	Alginate Beads	pH	Col-II

Supplement 3

Table S3: Continuous functions that assign a physiological range of pH and glc, respectively, to a cellular activity in mRNA expression.

Cellular activity in … mRNA expression	Glc	pH
Agg	$\frac{e^{18*glc}}{e^{18*glc}+3*10^4}$	Function 1: $6.5 \leq pH \leq 6.9489$ $\frac{e^{42(pH-6.5)}}{e^{42(pH-6.5)}+170}$ Function 2: $6.9489 < pH \leq 7.4$ $\frac{-e^{30(pH-6.5)}}{e^{30(pH-6.5)}+0.64*10^{12}}+1$

Col-I	Function 1: $0 \leq glc \leq 0.5$: $\frac{e^{12*glc}}{e^{12*glc}+1.525}+0.0037$ Function 2: $0.5 < glc \leq 5$: $\frac{-e^{14*glc}}{e^{14*glc}+1.11*10^5}+1.0097$	Function 1: $6.5 \leq pH < 7.1$ $\frac{-e^{30(pH-6.5)}}{e^{30(pH-6.5)}+1.55*10^4}+1$ Function 2: $7.1 \leq pH \leq 7.4$ $\frac{e^{45(pH-6.5)}}{(e^{45(pH-6.5)}+6*10^{14})*3.89}$
Col-II	$\frac{e^{18*glc}}{e^{18*glc}+9.4*10^4}$	$\frac{e^{28(\mathrm{pH}-6.5)}}{e^{28(\mathrm{pH}-6.5)}+4.7*10^3}$
MMP-3	$\frac{-e^{13*glc}}{e^{13*glc}+2*10^3}+1$	Function 1: $6.5 \leq pH \leq 6.9605$ $\frac{-e^{40(pH-6.5)}}{e^{40(pH-6.5)}+2*10^3}+1$ Function 2: $6.9605 < pH \leq 7.4$ $\frac{e^{15(pH-6.5)}}{e^{15(pH-6.5)}+5*10^7}$
ADAMTS	$\frac{-e^{19*glc}}{e^{19*glc}+1.26*10^5}+1$	$\frac{-e^{44(pH-6.5)}}{e^{44(pH-6.5)}+1*10^3}+1$
IL1-β	$\frac{1}{5}*glc$	Function 1: $6.5 \leq pH \leq 6.7969$: $\left(-\frac{e^{50(pH-6.5)}}{(e^{50(pH-6.5)}+7*10^3}+1.05\right)*\frac{1}{1.05}$ Function 2: $6.7969 < pH \leq 7$: $\left(-\frac{e^{25(pH-6.5)}}{(e^{25(pH-6.5)}+3.5*10^7}+1\right)*\frac{1}{20}$

Supplement 4

Table S4: Continuous functions that determine the percentage of hourly cell-death or cell-proliferation depending on glc and pH levels, and death rate of cells immunopositive for IL-1β after the treshold of IL-1β protein levels has been overcome.

	Glc	**pH**	**IL-1β [%]**
Cell death	$2.1*\frac{e^{16*glc}}{e^{16*glc}+922}-2.1$	Function 1: $6.5 \leq pH \leq 6.9$ $\left(\frac{1.12*e^{40(pH-6,5)}}{e^{40(pH-6,5)}+80}-1.12\right)*\frac{1}{3.57}$	1.05

Cell proliferation	-	Function 2: $6.9 < pH \leq 7.4$ $\left(\frac{1.12 * e^{42(pH-6,5)}}{e^{42(pH-6,5)} + 5.7 * 10^{10}}\right) * \frac{1}{1.775}$	-

Supplement 5:

Table S5: Overview over experimental studies and their conditions used to estimate cell viability based on the solutes glc, lac and the proinflammatory cytokine IL-1β. AB: Alginate beads. Deg: degenerated. Non-deg: non-degenerated.

Author	Cell type	Cell culturing	Microenvironment
(Bibby and Urban, 2004)	Bovine NP	AB	glc
(Gilbert et al., 2016)	Human NP, deg and non-deg	not specified	pH
(Shen et al., 2016)	Human NP, non-deg	AB	IL-1β

Supplement 6: Sensitivity analysis evaluating the effect of parameter variation of the parameters of Mendoza and Xenarios, 2006.

To evaluate the effect of the parameters of the equation of Mendoza and Xenarios, 2006, a full factorial sensitivity analysis was performed over five factors and three levels. Therefore, the Minitab 19 Statistical Software (www.minitab.com) was used. As input parameters, the values of the experimental design for glc deprivation of Saggese et al. 2018 were chosen, i.e. cell activity for target-mRNA under 0.55 mM glc, pH 7.0 after 24 h. Table S6 provides an overview of the parameter variations.

Table S6: Parameters and parameter values chosen to perform the sensitivity analysis. Parameter variation 1: pronounced sigmoid (h) and bulging (activation / inhibition). Parameter variation 2: gentle sigmoid (h) and bulging (activation / inhibition).

Parameters		**Original Parameters**	**Parameter variation 1**	**Parameter variation 2**
Gain coefficient (h)		1	10	2
Activation glc		0.01	9	2
Activation pH		0.01	9	2
Activation IL-1β protein – IL-1β mRNA		0.03	9	2
IL-1β protein – Target mRNA	Activation IL-1β – Col-I	0.01	9	2
	Activation IL-1β – MMP-3	0.05		
	Inhibition IL-1β – Col-II	0.01		
	Inhibition IL-1β - ADAMTS	0.02		
	Inhibition IL-1β – Agg	0.03		

Gain, activation glc and activation pH influenced both, immunopositive as well as immunonegative cells, whereas the activation of IL-1β protein on IL-1β mRNA expression and the effect of IL-1β on target mRNA expression only accounted for immunopositive cells. Hence, a three-level full factorial analysis led to 27 combinations for target mRNA expression of immunonegative cells and 243 combinations for target mRNA expression of immunopositive cells (Figure S1). Note that an error in mRNA calculation was found for six calculations, all of them only affecting mRNA prediction of inflamed cells, containing a parameter combination of a gain of 10, an activation factor of 0.01 for both, glc and pH and an IL-1β protein – IL-1β mRNA expression of either 2 or 9. The reason was that this specific parameter combination led to a drop of inflamed cells to zero.

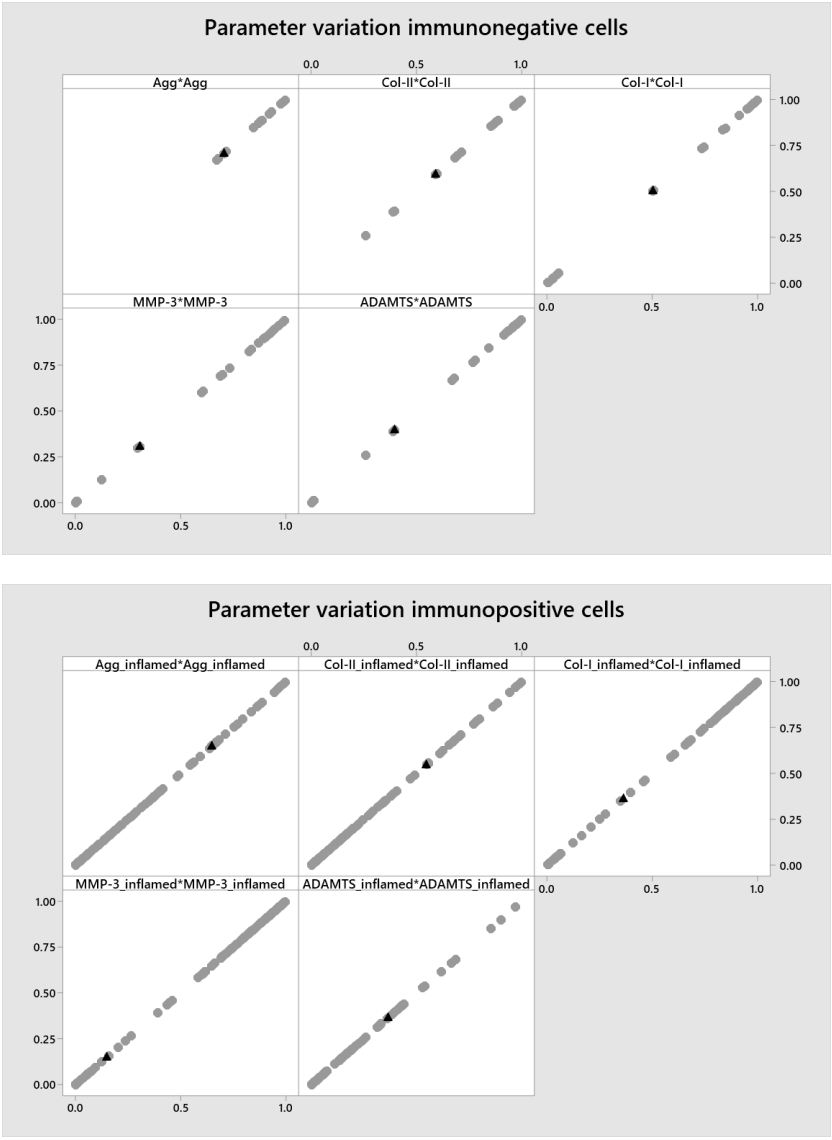

Figure S1: Outcome of parameter variations for both immunonegative and immunopositive cells, over the 27 and 243 simulations, respectively. Results of parameter combination as effectively used within the algorithm are represented with a black triangle.

Supplement 7: Illustration of the influence of cell viability on mRNA expression over time for Agg mRNA expression (Figure S2).

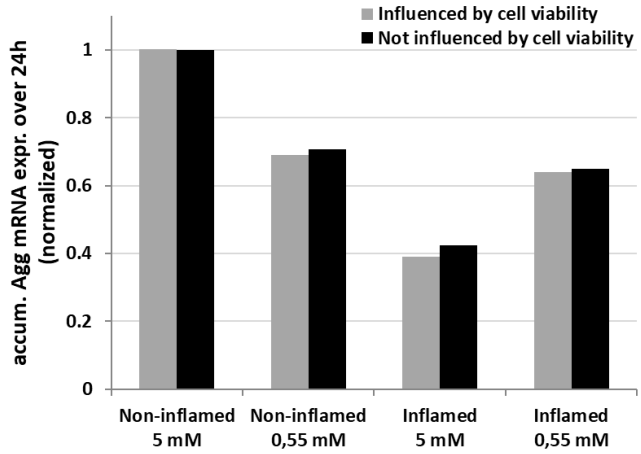

Figure S2: Influence of cell viability on normalized, accumulated (accum.) Agg mRNA expression (expr.). BC as used in Saggese et al. 2018.

Results: Agg mRNA expression slightly increased for non-inflamed cells at 5 mM glc, whereas it decreased in any other condition.
Discussion: According to the predicted influence of cell viability on the overall mRNA expression over time (24h), this model allows decoupled quantification of mRNA expression and cell viability to estimate the individual influence of cell death and adverse mRNA expression on the possible subsequent changes in tissue integrity. This is interesting, since cell viability and mRNA expression appear to be decoupled mechanisms (e.g. high glc levels lead to anabolic cell behavior but apparently not to cell proliferation (Bibby and Urban, 2004)). Hence, this model might provide future insight in possibly different pathways of tissue breakdown on different phenotypes of IVD degeneration.

Appendix 2 – Supplementary Material Chapter 4

S1 Cell viability

A tendency of lower cell viability is observed as nutritional stress increases, although this change is not significant, whereas an enhanced TNF-α level within the culture serum did not reveal any cytotoxic effect (Supplementary Figure 1)

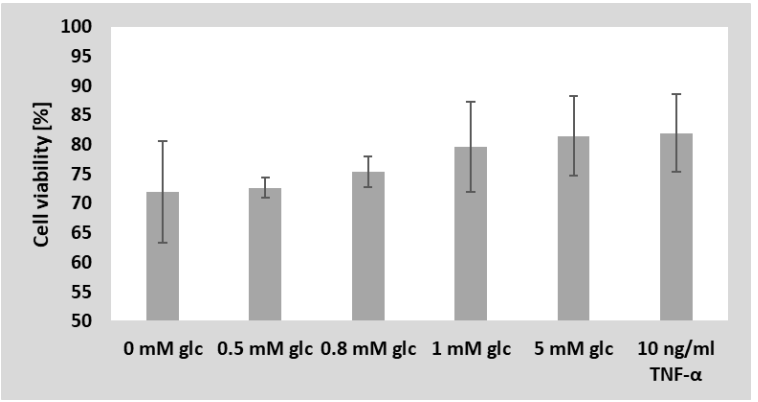

Supplementary Figure 1: Cell viability at different glucose (glc) levels and at exposure to 10 ng/ml TNF-α. Therefore, one alginate bead of each condition was exposed to a 10 µm Calcein AM (CaAM)/1 µM Ethidium Homodimer (EthHD) solution and gently squeezed for analysis under a fluorescence microscope. Each bead was analyzed within up to four different regions of the bead, and cells were counted within a predefined area. Evaluation was based on all five donors for each culture condition.

Our findings were consistent with findings in literature. Rinkler et al., 2010 stated a decrease in cell viability on (partial) glucose deprivation, whereas enhanced TNF-α levels within the culture serum did not affect NP cell viability (Li et al., 2017b).

S2 mRNA expressions of Nucleus Pulposus cells under reduced glucose conditions or TNF-α supply

Significant gene expression modifications are observed under nutritional stress (p=0,039). However, univariate analysis does not show

any single mRNA level expression responsible for this difference suggesting a synergistic effect of all of them (Supplementary Figure 2 A). In contrast, the effect of TNF-α (10 ng/ml) on both, TNF-α and IL1β mRNA expression was found to be significant ($p<0.05$) (Supplementary Figure 2, B).

A

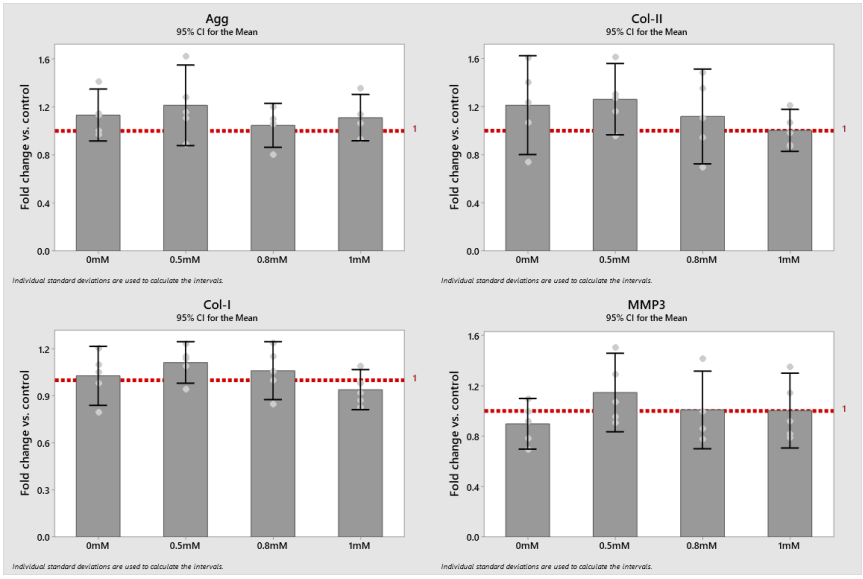

B

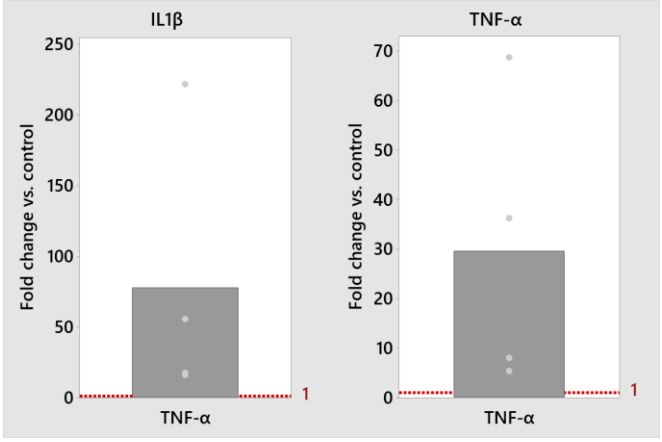

Supplementary Figure 2: A: mRNA expressions of Aggrecan (Agg), Collagen types I and II (Col-I, Col-II) and MMP3 at glucose (glc) concentrations of 0 mM, 0.5 mM, 0.8 mM, 1 mM and 5 mM (control; 1-fold mRNA expression) (n=5). B: IL1β and TNF-α mRNA expressions due to an exposure to 10 ng/ml TNF-α compared to control (5mM glc; 1-fold mRNA expression) (n=4).

Non-significant effects of reduced glucose supply on MMP3 mRNA expressions of bovine NP cells was as well found by Rinkler et al., 2010. However, our study could not confirm significant downregulations of Agg, Col-I and Col-II mRNA expressions of bovine NP cells due to decreases in glc concentrations found by those authors, despite the similar experimental protocol. Previously known stimulatory effects of TNF-α on proinflammatory cytokines (Millward-Sadler et al., 2009; Purmessur et al., 2013) could be confirmed by this study.

S3 Sensitivity of a Cell Activity to a Stimulus Dose

Supplementary Table 1: Functions to relate physiological ranges of stimulus concentrations to a normalized sensitivity of a cell activity to a stimulus dose. Tackled cell activities: mRNA expressions of proinflammatory cytokines, tissue proteins and proteases.

mRNA expression	Glc	pH
Agg	$x_{glc}^{Agg} = \frac{e^{18glc}}{e^{18glc} + 3 * 10^4}$	$6.5 \leq pH \leq 6.892$ $x_{pH}^{Agg} = \frac{e^{68(\mathrm{pH}-6.5)}}{e^{68(\mathrm{pH}-6.5)} + 2 * 10^4}$ $6.892 < pH \leq 7.4$ $x_{pH}^{Agg} = \frac{-e^{32(\mathrm{pH}-6.5)}}{e^{32(\mathrm{pH}-6.5)} + 5.035 * 10^{12}} + 1$
Col-I	$0 \leq glc \leq 0.5043$ $x_{glc}^{Col-I} = \frac{e^{20glc}}{e^{20glc} + 1.083}$ $0.5043 < glc \leq 5$ $x_{glc}^{Col-I} = \frac{-e^{28glc}}{e^{28glc} + 3 * 10^{10}} + 1$	$6.5 \leq pH < 7.1207$ $x_{pH}^{Col-I} = \frac{-e^{35(\mathrm{pH}-6.5)}}{e^{35(\mathrm{pH}-6.5)} + 6.002 * 10^4} + 1$ $7.1207 \leq pH \leq 7.4$ $x_{pH}^{Col-I} = \frac{e^{35(\mathrm{pH}-6.5)}}{e^{35(\mathrm{pH}-6.5)} + 1.2376 * 10^{14}}$
Col-II	$x_{glc}^{Col-II} = \frac{e^{18*glc}}{e^{18*glc} + 9.4 * 10^4}$	$x_{pH}^{Col-II} = \frac{e^{34(\mathrm{pH}-6.5)}}{e^{34(\mathrm{pH}-6.5)} + 2.845 * 10^4}$
MMP3	$x_{glc}^{MMP3} = \frac{-e^{18glc}}{e^{18glc} + 2.283 * 10^4} + 1$	$6.5 \leq pH \leq 6.974$ $x_{pH}^{MMP3} = \frac{-e^{48(\mathrm{pH}-6.5)}}{e^{48(\mathrm{pH}-6.5)} + 2.18 * 10^4} + 1$

		$6.974 < pH \leq 7.4$ $x_{pH}^{MMP3} = \frac{e^{20(\mathrm{pH}-6.5)}}{e^{20(\mathrm{pH}-6.5)} + 4.62 * 10^{9}}$
ADAMTS4	$0 \leq glc \leq 1.197$ $x_{glc}^{ADAMTS4} = \frac{e^{38glc} * 0.4817}{e^{38glc} + 1 * 10^{4}}$ $1.197 < glc \leq 5$ $x_{glc}^{ADAMTS4} = \frac{e^{6glc} * 0.520}{e^{6glc} + 4 * 10^{5}} + 0.48$	$x_{pH}^{ADAMTS4} = \frac{-e^{44(\mathrm{pH}-6.5)}}{e^{44(\mathrm{pH}-6.5)} + 1 * 10^{3}} + 1$
IL1β	$0 \leq glc \leq 1.4578$ $x_{glc}^{IL1\beta} = \frac{e^{55glc}}{e^{55glc} + 1.62507 * 10^{19}}$ $1.4578 < glc \leq 5$ $x_{glc}^{IL1\beta} = -\frac{e^{4glc} * 0.648}{e^{4glc} + 1.314 * 10^{6}} + 1.000168$	$6.5 \leq pH \leq 7.0372$ $x_{pH}^{IL1\beta} = \left(\frac{-e^{55(\mathrm{pH}-6.5)}}{(e^{55(\mathrm{pH}-6.5)} + (1.94 * 10^{4})} + 1.036\right) * \frac{1}{1.036}$ $7.0372 < pH \leq 7.4$ $x_{pH}^{IL1\beta} = \left(\frac{-e^{35(\mathrm{pH}-6.5)}}{(e^{35(\mathrm{pH}-6.5)} + (5.4 * 10^{10})} + 1\right) * \frac{1}{28.7}$
TNF-α	$0 \leq glc \leq 0.8134$ $x_{glc}^{TNF-\alpha} = \frac{e^{36glc}}{e^{36glc} + 0.135196 * 10^{9}}$ $0.8134 < glc \leq 5$ $x_{glc}^{TNF-\alpha} = \frac{-e^{24glc} * 0.5389}{e^{24glc} + 0.53304 * 10^{11}} + 1.003$	$6.5 \leq pH < 6.8042$ $x_{pH}^{TNF-\alpha} = \frac{e^{32(\mathrm{pH}-6.5)}}{e^{32(\mathrm{pH}-6.5)} + 0.6474}$ $6.8042 \leq pH \leq 7.1115$ $x_{pH}^{TNF-\alpha} = \frac{-e^{68(\mathrm{pH}-6.5)}}{e^{68(\mathrm{pH}-6.5)} + 2.5 * 10^{13}} + 1$ $7.1115 \leq pH \leq 7.4$ $x_{pH}^{TNF-\alpha} = \frac{e^{42(\mathrm{pH}-6.5)}}{e^{42(\mathrm{pH}-6.5)} + 6.5 * 10^{15}}$

Appendix 3 – Supplementary Material Chapter 5

Supplementary information 1: Results and discussion of the relevance of the obtained results for the NP

This approach aims to contribute to a better understanding of the activity of intervertebral disc (IVD) nucleus pulposus (NP) cells by modeling dose- and time-dependent cell regulatory processes that are extremely difficult to measure directly either *in vitro* or *in vivo*. It uniquely combines experimental data and knowledge with mathematical, approaches to estimate cell responses to multifactorial stimulations in micro-environments that include cell nutrition, biochemical and mechanical cues, as it happens *in vivo*. In particular, this is the first *in silico* approach, to our knowledge, that allows to approximate combined effects of mag and freq in intricate dose- and time dependent loading conditions in CA. Results presented in the paper are subsequently presented again and analyzed in context of the NP (Figure S1 and Figure S2, respectively).

Predictions of daily moving habits. Fluctuating mechanical stimuli affect the CA in terms of both tissue proteins and protease mRNA expression. Thereby, the cell response to different stimulus concentrations does not seem to follow a systematic pattern, especially for the motions expected to involve catabolic cell activity. For example, while two-hours sitting with a round back and hiking with extra weight was predicted to particularly upregulate the mRNA expressions of Col-I, followed by ADAMTS4, jogging and vibration might rather trigger MMP3 mRNA expressions (Figure S1, A1).

A1

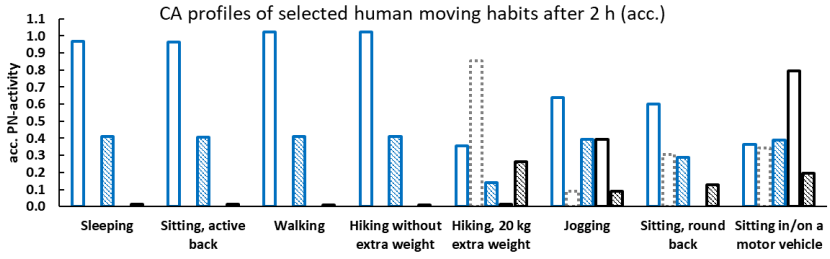

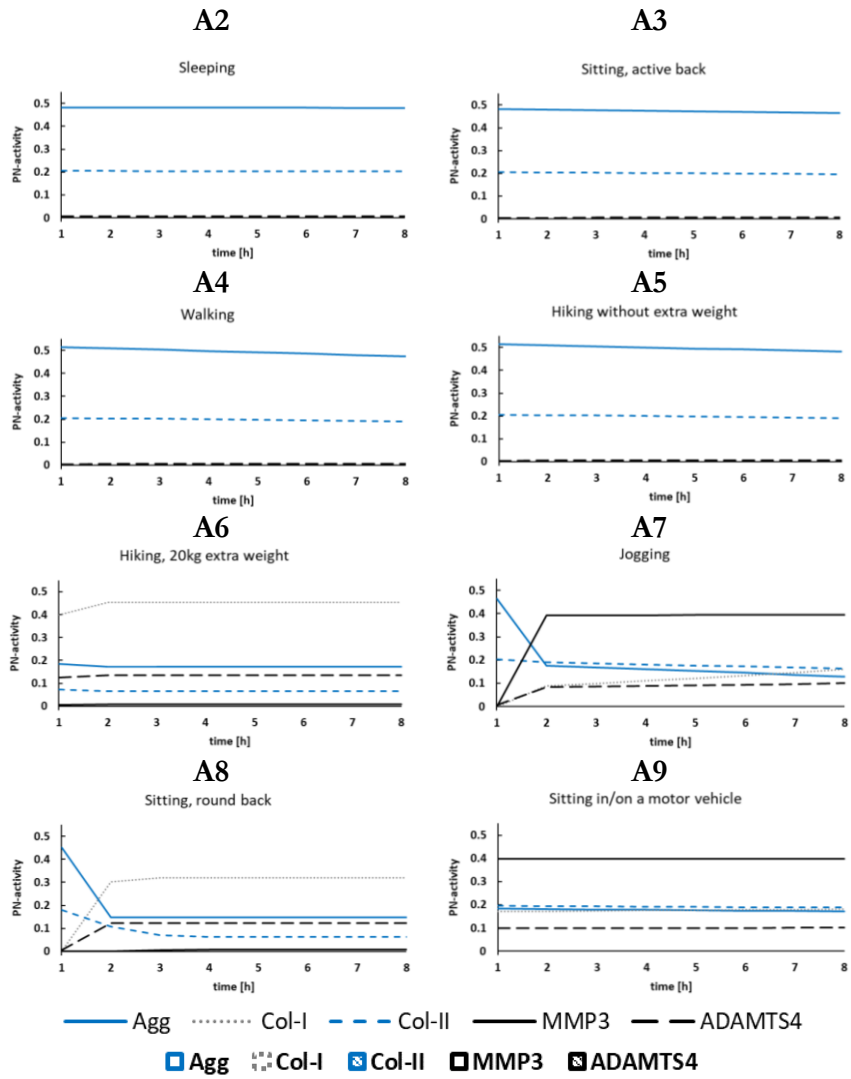

Figure S1: Predictions for eight selected physical activities: sleeping, walking, hiking with/without extra weight, jogging, sitting with an active/round back, exposure to vibration (as probably experienced by a motor vehicle). Accumulated (acc.) PN-activities after 2h (A1), and continuous PN-activities (A2-A9) over 8h of physical activity.

Moving habits that were generally less related with IVD degeneration were sitting (office workers) (Luoma et al., 2000) and walking (Belavý et al., 2017; Takatalo et al., 2017). In contrast, moving habits classically related to IVD degeneration or to catabolic changes in NP cell responses were weight lifting (Videman et al., 1995), heavy work (carpenters) (Luoma et al., 2000) or whole body vibration exposure

(machine drivers) (Luoma et al., 2000). Model simulations are supported by these findings, as they predict walking and hiking without extra weight to be highly anabolic, followed by sleeping and sitting with active back (Figure S1, A1, A2-A5). Accordingly, walking with extra weight or vibrations were predicted by the model to cause a quite catabolic cell response (Figure S1, A1, A6 & A9). However, hiking does not seem to be specifically linked to IVD degeneration, which could be explained with the use of supporting hip belts for (heavy) backpacks. Hence, hikers most probably carry heavy weights rather on their hips than on their shoulders and CA profiles of hikers generally rather resemble the predictions seen for "hiking without extra weight" (Figure S1, A1, A5). Interestingly, sitting with a round back was also catabolic in contrast to sitting with an active back (Figure S1, A3 vs. A8), which nicely corresponds to current ergonomic paradigms.

A possible limitation related with the modelling of the effect of mag and freq is that rodent experimental data had to be used to estimate the weighting factors and time dependencies of different CA. Moreover, there is also a lack of further individualization of time-sensitivities and amplification factors between mag and freq, due to the limited availability of experimental data for quantification. Likewise, more experimental evidence about the relationship between proinflammatory cytokines and (physiological) loading parameters would contribute to confirm or adapt current modelling assumptions. Eventually, to determine weighting factors, ideally, the maximal effect of a stimulus within a physiological range on a CA should be addressed in experimental studies to be fully exploited in the model. For example, the available data about the mechanostimulation were measured at 1 MPa and 0.01 Hz, 0.2 Hz and 1 Hz, respectively (MacLean et al., 2004). *In vivo* measurements in humans clearly indicate that the physiological range is much broader (Nachemson and Elfström, 1970; Wilke et al., 1999). Consequently, our weighting factor for mag and freq might have been underestimated compared to the effect of nutrient environments, for which measurements over the whole range were available.

Whilst IVD aging appears to be a physiological adaptation of the tissue, accelerated IVD degeneration is not affecting everyone, despite the catabolic shifts possibly caused by moving habits that many people experience more or less frequently (e.g. carrying heavy weights on the shoulders, exposure to vibration). Assuming that acute physiological moving habits are well regulated by the human organism, stimulus chronicity and, therefore, the factor time seems to be important in IVD degeneration. Furthermore, the high diversity of cellular responses due

to different combinations of stimuli suggests that the mechanisms finally leading to (micro-) injuries are manifold, without following one general systematic pattern, which would go along with the high variability of phenotypes in IVD degeneration.
The impact of chronicity is particularly interesting in the model predictions for jogging. The anabolism of jogging has a strongly time dependent component. Whilst its accumulated PN-activity was predicted to be considerably lower than e.g. walking (Figure S1, A1), insights into the evolution over time (Figure S1, A7) suggest that the catabolic impact is pronounced after the second hour of the activity, whilst the first hour is still largely anabolic. Accordingly, findings in literature regarding the effect of jogging are controversial: whereas a study of young adults found a relationship between frequent jogging and degenerative changes in lumbar IVD (Takatalo et al., 2017), other findings did not reveal a significant effect (Hangai et al., 2009) or jogging was found to be even beneficial compared to a non-physiologically active control group (Belavý et al., 2017; Mitchell et al., 2020). Assuming that the chronicity of cell stressors is crucial in the dynamics in IVD degeneration, as suggested by the model predictions, a frequent switch among different moving habits can contribute to reduce the risk of IVD degeneration and/or decelerate its development.

Predictions of the effect of microgravity and daily life under gravity and for different proinflammatory CS. Simulations of a daily life on earth show low to minimal Col-I and protease mRNA expressions and elevated Agg and Col-II mRNA expressions. Due to the presence of proinflammatory cytokines, protease mRNA expressions rise, whilst the mRNA expressions of tissue proteins show an overall slight decrease. Microgravity exposure over six months led to a general downregulation of the expression of tissue proteins by predicting a roughly 25% and 20% lower PN-activity of Agg and Col-II mRNA expression, respectively, independently of the CS (Figure S2, B vs. C, left). MMP3 mRNA expression was not particularly affected by simulations of microgravity exposure. In contrast, ADAMTS4 mRNA expression was predicted to slightly rise, which could be generally attributed to the end of the stay ins space (Figure S2, C, right). Independently of the simulated condition, Col-II mRNA expression is lower, relative to Agg mRNA expression (Figure S2).
Model predictions simulating daily life under gravity (Figure S2, B) were in agreement with general expectations: minimal or close to minimal CA for MMP3 and ADAMTS4 mRNA expressions go along with low

MMP3 and ADAMTS4 protease levels found within the tissue (Molinos et al., 2015). Elevated CA for Agg and Col-II mRNA expressions reflect the cellular function to maintain the tissue. Generally, lower CA for Col-II than for Agg along with a both, a lower tissue turnover of collagen compared to Agg (Sivan et al., 2006, 2008) and a lower fraction of Col-II tissue compared to Agg (Baumgartner et al., 2021). The predicted catabolic shift in TNF-α inflamed cells goes along with experimental findings that identify TNF-α as a strong catabolic mediator (Purmessur et al., 2013). IL1β, on the other side, was predicted to be less catabolic than TNF-α, which goes along with its possible role in normal cell homeostasis (Le Maitre et al., 2007b).

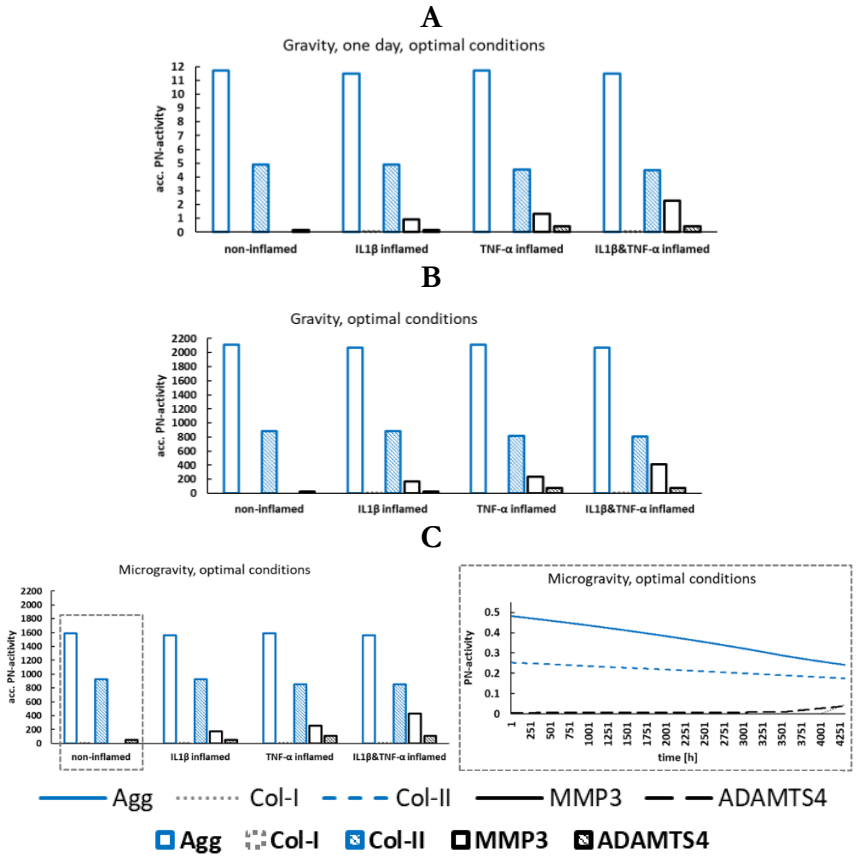

Figure S2: estimated CA profiles for an average daily moving habit (A) its accumulation over six months (B) and after six months microgravity exposure (C). Microgravity exposure is presented as accumulated PN-activity for each proinflammatory cell state (C, left) and as a continuous development over time exemplarily shown for non-inflamed cells (C, right). Non-degenerated nutritional conditions were used (5 mM glc, pH 7.1).

Compared to gravity, simulated microgravity exposure usually caused a downregulation of glycosaminoglycan contents (Figure S2, B vs. C), which is supported by various animal models (Belavy et al., 2016). Agg is the major proteoglycan in cartilaginous tissues and is a complex macromolecule with numerous chondroitin sulfate glycosaminoglycan chains. Because these chains are negatively charged, Agg are responsible to attract water through Donnan osmosis effects. A reduced Agg content goes along with a reduced fixed charge density, which in turn could be related to a lower hydration of the IVD (Baumgartner et al., 2021). Although such findings at first glance would explain disc desiccations found after long-term space flights (Garcia et al., 2018), the slow turnover of tissue proteins with half-lives of around 12 (Agg) and 95 (collagen) years (Sivan et al., 2006, 2008), questions whether the effect of microgravity exposure should become visible *in vivo* at the tissue level, after only six months.

The model predicts ADAMTS4 to substantially rise within the last weeks of the research stay, i.e. after around 3500 h (Figure S2, C, right). The value of the amplification factor is deterministic for the velocity of the continuous evolution of CA profiles over time. Given that the amplification factor could not be specified yet between mag and freq, and that rather the range, than its effective size was determined (see Chapter 5, 5.5 Methods) requires a generally prudent interpretation of the specific timepoints observed in continuous CA-profiles.

Remarkably, though, the continuous evolution of a CA over time (Figure S2, C, right) shows a general trend of a constant low level of proteases within the first months of simulated microgravity exposure. Such expressions were similar to the simulated day under gravity (Figure S2, A). However, the daily moving habit was chosen to be quite "optimal", whilst "suboptimal" moving under gravity (i.e. carrying heavy weights or exposure to vibration) upregulated protease activity (Figure S1, A1, A6-A9). The absence of such "suboptimal" stimuli in space maintain simulations of protease mRNA expression constantly low, which might contribute to an increased swelling behavior of the IVD. Swelling behavior of the IVD was particularly observed head-down-tilt bedrest (Koy et al., 2014), the most common analogue to investigate effects of microgravity. Yet, the existence of IVD swelling during spaceflight is debated, since pre-to post-flight differences in disc water content after six months microgravity exposure were non-significant (Bailey et al., 2018), and signs for disc desiccation were observed already during microgravity exposure in ultrasound images (Garcia et al., 2018).

Hence, the model predicts indications for both, disc desiccation on the one hand, due to a downregulation of tissue protein mRNA expression, whilst, on the other hand, constantly low levels of protease mRNA expression might contribute to findings of disc swelling. Both is actually observed under similar mechanical conditions, i.e. under microgravity exposure and bed rest studies. A better understanding of a final consolidation at the tissue level might be obtained by a quantification of actual mRNA expressions coupled to a CA. Moreover, besides the mechanical loading conditions, peculiarities of microgravitational conditions, e.g. lumbar flattening and possible, corresponding changes in intradiscal nutrient supply should be considered in future work to confirm or adapt current predictions under microgravity.

Conclusions of the tissue-specific findings

This work is the first contribution that allows for comparable cell responses within complex, heterogenous stimulus environments. The aim was to approximate the cell responses to a native stimulus environment by considering crucial external and local stimuli. Thanks to the integration of dose-and time-dependent effects, this work allowed to estimate continuous approximations of the time-dependent effects of maintained mechanical loads due to combined, user-defined loading conditions.

Novel insights of biological responses to different human moving habits and the effect of microgravity exposure were in good agreement with findings in literature and coincide with changes found at the tissue level. Simulations using the PN_t-Methodology capture the fact that IVD NP degeneration is most probably not the result of one, principal biological response, but highly depending on the (micro-) environmental stimulus combinations. It further points out that chronicity might be key relevant in IVD NP degeneration. Hence, a frequent change of moving habits, e.g. sitting positions or breaks with walking periods, might be beneficial to maintain IVD integrity.

Future work should further tackle the injury mechanisms due to microgravity exposure and it should focus on a more sensitive integration of loading conditions. Moreover, light might be shed on the extent and timescale at which cellular changes manifest at the tissue level. Eventually, a coupling of this model to models to higher and lower spatial scales is deemed to be key relevant to holistically tackle injury dynamics within the IVD.

Supplementary information 2: Additional simulations to model early degenerated nutritional conditions and predictions of the PN_t-Methodology coupled to a 3D agent-based model, simulating a multicellular environment

Supplementary Methods: To simulate most critical impacts of early degenerated nutritional conditions, the region was chosen where the most adverse nutrient environment was found. Its location was identified by our in-house mechanotransport finite element (FE) model (Ruiz Wills et al., 2018). Therefore, the cartilage endplate permeability was adapted as expected at early stages of IVD degeneration and nutrient concentrations were estimated throughout the IVD. Most critical nutrient concentrations were found within the anterior NP around the mid-transverse plane, with a prediction of an average glc concentration of 0.8901 mM and pH 6.9349.
The PN_t-Methodology was embedded in a 3D Agent-based model (Netlogo (Wilensky, 1999)) that simulated a NP environment consisting of 4000 agents (diameter 10μm) and a volume of $1mm^3$(cf. Chapter 3). Agents represent NP cells at an average density (Maroudas et al., 1975). Agents were randomly placed into the volume and immobile throughout simulations. Each NP cell obtains one out of four cell states; immunonegative or immunopositive for IL1β, for TNF-α or for both IL1β&TNF-α. The setup of the multicellular environment is explained in detail in our previous publication (see Chapter 4). In short: the model predicts a global, normalized amount of IL1β and TNF-α mRNA expression (according to external stimulus concentrations), based on which the percentage of immunopositive cells for IL1β and TNF-α was determined. Corresponding numbers of inflamed cells were distributed in randomly placed cell clusters. Within regions where IL1β and TNF-α immunopositive cell clusters overlap, cells were considered to be immunopositive for both, IL1β&TNF-α. The minimal calculation time step was set to 1h.

Results: Early degenerated conditions led to similar CA profiles for non-inflamed and IL1β inflamed cells as found for non-degenerated conditions, but caused a worse catabolic shift under TNF-α presence, under both, gravity and microgravity exposure. Thereby, the catabolic shift consists of a downregulation of Col-II and an upregulation of MMP3 and ADAMTS4. In contrast, Agg mRNA expression is similar for non-degenerated and early degenerated conditions under both, gravity and microgravity exposure (Figure S2, B, C (left) vs. Figure S3).

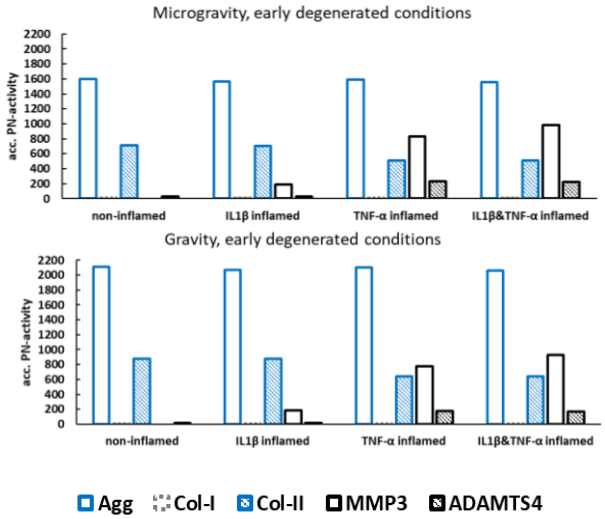

Figure S3: estimated CA profiles for an average daily moving habit over six months compared to microgravity exposure for the same period of time. Simulation of an early degenerated nutrient environment.

The proinflammatory environment in case of IL1β is maintained around 15-16% for every simulated condition, whilst TNF-α proinflammatory environments rise from around 10-11% for non-degenerated to 15-16% under early degenerated conditions (Table S1).

Table S1: predicted, proinflammatory environments for non-degenerated and early degenerated conditions at gravity and microgravity exposure. Cells inflamed for both, IL1β&TNF-α were added to the respective percentages of TNF-α and IL1β inflamed cells. Detailed information was previously presented (Chapter 4). Percentages of inflamed cells are rounded and based on three model runs for each condition.

		IL1β	**TNF-α**
Non-degenerated	Gravity	~15.5%	~10.5%
	Microgravity	~15.5%	~10.5%
Early degenerated	Gravity	~16%	~15.5%
	Microgravity	~16%	~16%

Discussion: the effect of early degeneration on tissue proteins is small, which is in agreement of the generally slow development of this disease. Hence, during a period of time of six months, no major changes were found. In contrast, the change in nutrient conditions caused an elevated TNF-α presence, leading to a catabolic shift of CA of cells exposed to TNF-α and to a higher number of cells inflamed with TNF-α (Table

S1). Hence catabolic shifts might be locally enhanced within the NP under early degenerated conditions.
Overall, predicted proinflammatory environments lie within plausible ranges, albeit they still lie within ranges as expected in non-degenerated NP, i.e. 17% ± 7%, for IL1β and 16% ± 7%, respectively, for TNF-α (Le Maitre et al., 2007b). Hence, the currently estimated percentage of inflamed cells might be conservative and, consequently, as well the catabolic shifts of the CA profiles of inflamed cells are conservative estimations.
Current results might suggest TNF-α inflammation to play a role under early degenerated conditions. However, the prediction of inflammation underlies various uncertainties, given that experimental studies about the effect of loading on proinflammatory cytokine expression are largely unknown. Moreover, critical factors such as effects between proinflammatory cytokines (see Chapter 4) or possible endogenous triggers of inflammation such as ECM breakdown products (Medzhitov, 2008) (i.e. damage-associated molecular patterns) were not considered, which coincides with an overall conservative prediction of inflammation. However, model simulations predict enhanced protease activity due to the presence of proinflammatory cytokines, which might (locally) lead to an accumulation of ECM breakdown products. Hence, model results support the hypothesis that an upregulation of a proinflammatory environment is initiated by altered protease activities, as locally generated ECM breakdown products can secondarily activate the inflammatory response of NP cells.

Supplementary information 3: additional analysis of the performance of the PN_t-Methodolog around the α-β-threshold

Methods: To investigate the model performance around the α-β-threshold, one loading parameter at a time was varied. Hence, one parameter was set to respective minimal values, i.e. either 0.1 MPa or 0 Hz, whilst the other parameter was variated, covering the range around the α-β-threshold of the generic functions. Hence, i) a static condition (0 Hz) was simulated under varying loading conditions of 0.90 MPa, 0.95 MPa, 1.00 MPa, 1.05 MPa and 1.10 MPa and ii) dynamic conditions were simulated under a constant load of 0.10 MPa at 2.90 Hz, 2.95 Hz, 3.00 Hz, 3.05 Hz and 3.10 Hz (note that the minimal step increase of loading parameters was 0.05). Thereby, the loading conditions 0.90 MPa, 0.95 MPa and 2.90 Hz, 2.95 Hz, 3.00 Hz,

respectively, were initally anabolic, whilst higher loading conditions caused catabolic responses (Figure S4). Optimal nutrient conditions (5 mM glc, pH 7.1) were simulated and the response of non-inflamed cells was plotted.

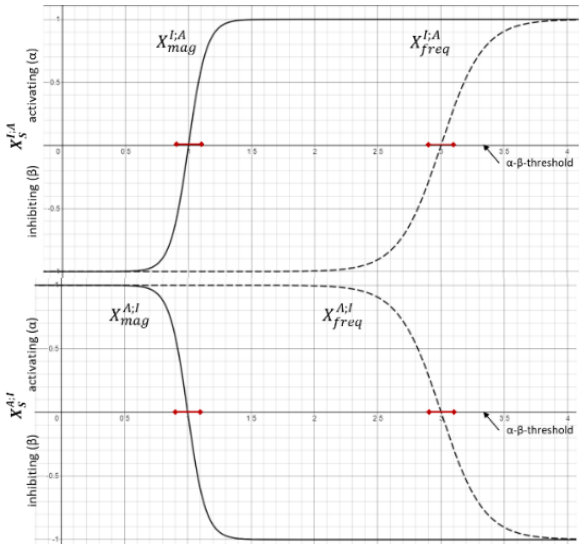

Figure S4: generic functions reflecting I;A (top) and A;I (below) evolutions, with critical ranges around the α-β-threshold marked as red bars.

Results: Model predictions were influenced by the steepness of the sigmoidal slope and the impact of the respective stimulus on a specific CA. Hence, the steeper the slope, the shorter the time range of incoherent predictions. The less important the stimulus for a CA, the smaller the incoherent predictions. Predictions based on the A;I generic function, i.e. tissue protein expressions, quickly converged to the same PN-activity, independently of the initial value of the stimulus. In contrast, predictions for I;A generic functions (Col-I and protease expressions) converged much slower. Hence, the PN-activity of Col-I and protease converge to two different PN-activities over the first hours of simulation. Thereby, initially anabolic stimulus ranges converge to another PN-activity than initially catabolic stimulus ranges. Predictions at 1.00 MPa led to systematically erroneous results (Figure S5, left column).

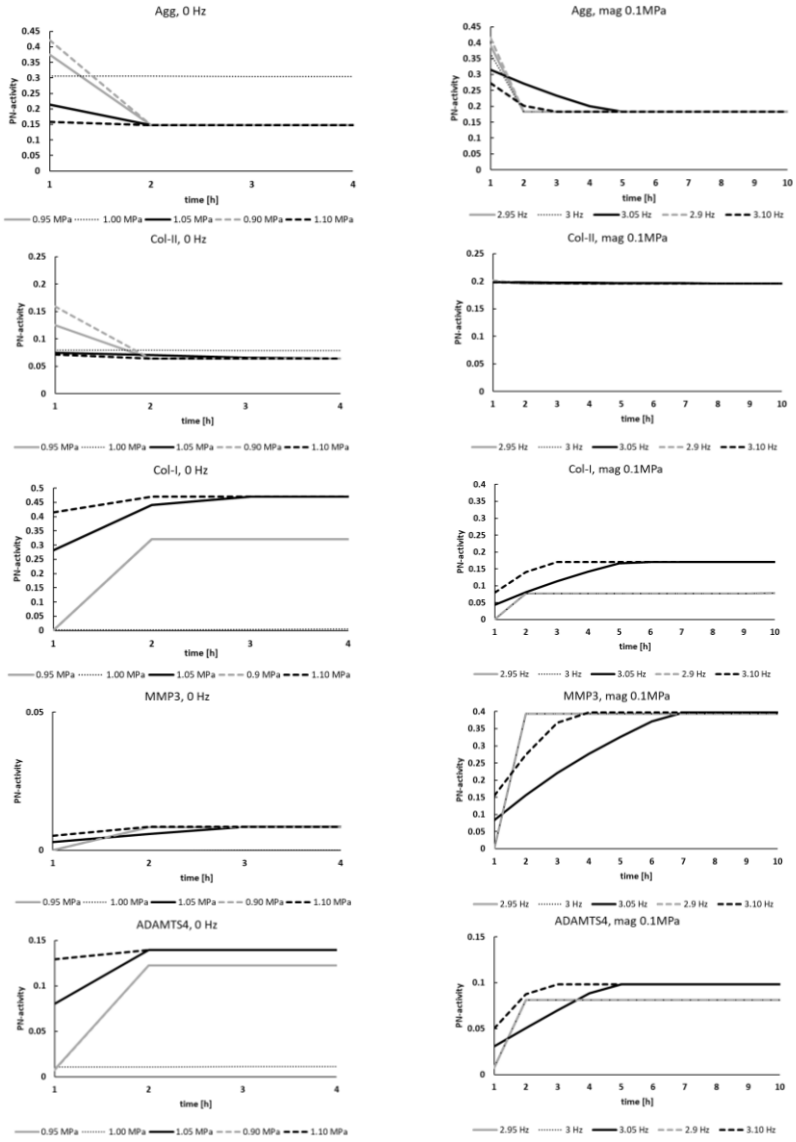

Figure S5: predictions around the α-β-threshold of the generic functions of mag (left) and freq (right). Note that predictions at 0.9 and 0.95 MPa are identical for Col-I and MMP3 mRNA expressions at 0 Hz and almost identical for ADAMTS4 mRNA expression at 0 Hz. Likewise, predictions at 2.90 Hz, 2.95 Hz and 3.00 Hz have the same values for Col-I and MMP3 mRNA expressions at 0 Hz and almost identical values in case of ADAMTS4 mRNA expressions at 0 Hz.

Discussion: an influence of the steepness of the sigmoidal shape is not surprising, given that the time sensitivity is based on the generic

functions. Hence, a less steep slope includes a smaller effect of time at each time step, which leads to a slower evolution of the CA due to the variable "time". Likewise, the effect of a stimulus on a CA is closely coupled to the size of the respective weighting factor. Thus, if the impact of a stimulus is not-significant for the evolution of a CA, e.g. in case of the mag-MMP3 and the freq-Col-II relationships (Table S2), a variation of the PN-activity over time is small. In contrast, if weighting factors are elevated, e.g. in case of the effect of loading conditions on Col-I mRNA expression (Table S2), the changes in PN-activity are pronounced (Figure S5).

Stimulus doses closest to the α-β-threshold are 1.00 MPa and 3.00 Hz, respectively (Figure S4). Whilst the prediction of 1.00 MPa generally led to incoherent predictions (Figures S5, left column), predictions around 3.00 Hz did not show any peculiar behavior (Figure S5, right column). The reason is that 3.00 Hz is still considered as an anabolic stimulus by the algorithm, whilst 1.00 MPa is already slightly catabolic. Hence, according to the setup of time sensitivity, anabolic stimuli closely to the α-β-threshold rapidly lose their anabolism, whilst the programming of the latency time assumes that weak catabolic stimulus doses are longer tolerated than strong catabolic stimulus doses. Given that 1.00 MPa is that close to the α-β-threshold, this assumption led to incoherent results.

To overcome limitations leading to incoherent results around the α-β-threshold, it is generally recommended to rather approximate the PN-activity by an extrapolation of results calculated at higher and lower stimulus doses.

Whilst the effect of time on CA based on A;I generic functions, i.e. Agg and Col-II mRNA expressions, converge to same PN-activities within a short period of time (with exception of the previously addressed predictions at 1.00 MPa), mRNA expression based on I;A generic functions converge to two different levels of PN-activities, depending on the anabolic or catabolic character of the initial stimulus dose. Thereby, initially anabolic loading led to a generally lower catabolic response than initially catabolic loads (Figure S5). The source of this difference comes from the formulation of the inhibiting part of the PN-equation, more precisely, from the first fraction of the inhibiting part. The weight that this fraction provides to the inhibiting part is different of the weight within the activating portion of the PN-equation. This is considered to be a limitation of the PN-equation. However, qualitatively the results are coherent. Hence, initially anabolic values are also more anabolic over time.

The relative difference between the two different PN-activities depends on the size of the weighting factor. Hence, if the anabolically maintained stimulus had a pronounced effect on the CA, the relative difference between the PN-activities of initially anabolic and catabolic stimuli is elevated. Within the calculation in Figure S5, freq was the anabolically maintained stimulus where mag was varied (Figure S5, left column). Accordingly, mag was the anabolically maintained stimulus where freq was varied (Figure S5, right column). For example, mag and freq have a significant effect on Col-I mRNA expression, and therefore elevated weighting factors (Table S2). As a consequence, the difference within the two PN-activities for Col-I mRNA expression is pronounced (Figure S5, Col-I, 0 Hz and Col-I 0.1 MPa). In contrast, non-significant weighting factors lead to small differences between the two PN-activities. For example, the prediction of MMP3 was programmed to have a non-significant relationship to mag. Hence, the effect of different mag on the PN-activity are small (Figure S5, MMP3, 0 Hz), and, consequently, the (absolute) effect of an anabolic mag is small too (Figure S5, MMP3, 0.1 MPa).
Bottomline: whilst the time dependency of the anabolically maintained stimulus affects protein mRNA expressions (based on A;I generic functions) equally, independently of the initial (anabolic or catabolic) stimulus dose, the evolution over time of protease and Col-I mRNA expressions (based on I;A generic functions) converge at two different PN-activities within the first hours of stimulus exposure.
This effect vanishes as soon as the inhibiting part of the PN-equation becomes 0. This is subsequently demonstrated by plotting the evolution of Col-I and Agg mRNA expressions over time (Figure S6). Note that the freq was elevated from 0 Hz to 2 Hz, to accelerate the decrease of the inhibiting part of the PN-equation to zero.

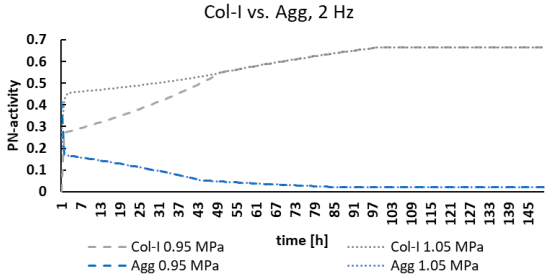

Figure S6: evolution of initially anabolic (0.95 MPa) and catabolic (1.05 MPa) mag doses over time on the example of Col-I and Agg. The same PN-activity for Col-I is obtained after 50h of stimulus exposure. In contrast, the PN-activity of Agg exposed to different mag are already reached after 4h stimulus exposure.

Supplementary information 4: Overview of weighting factors considered in the system of interest of the NP

The subsequent Table S2 contains an overview of the weighting factors used to calculate the current results. The information for indirect mechanotransduction was previously presented, together with the mathematical derivation of weighting factors (Chapter 4).

Table S2: Complete overview of weighting factors for the tackled system of interest of the NP. Individual weighting factors were derived from the cellular effort ($f(\epsilon)$), based on x-fold mRNA expressions (ϵ). The scaling factor $\vartheta_{\theta_{max}}=\vartheta_1=28.7$ was determined by the S-CA relationship pH-MMP3. NS: Not significant; act: activating; inh: inhibiting; *: estimated ϵ.

Stimulus	mRNA	ϵ	$f(\epsilon)$	θ_S^{CA} (ϑ_1= 28.7)	Source	Cell type
Glc	Agg	NS, act	-	0.0100	Rinkler et al., 2010	human
	Col-I	NS, act	-	0.0100	Rinkler et al., 2010	human
	Col-II	NS, act	-	0.0100	Rinkler et al., 2010	human
	MMP3	NS, act	-	0.0100	Rinkler et al., 2010	human
	ADAMTS4	NS, act	-	0.0100	Chapter 4	bovine
	IL1β	NS, act	-	0.0100	Chapter 4	bovine
	TNF-α	NS, act	-	0.0100	Chapter 4	bovine
pH	Agg	0.37	2.7027	0.0942	Gilbert et al., 2016	human
	Col-I	NS, act	-	0.0100	Gilbert et al., 2016	human
	Col-II	0.63	1.5873	0.0553	Neidlinger-Wilke et al., 2012	bovine
	MMP3	28.7	28.7000	1.0000	Gilbert et al., 2016	human
	ADAMTS4	5.7	5.7000	0.1986	Gilbert et al., 2016	human
	IL1β	81	81.0000	2.8223	Gilbert et al., 2016	human
	TNF-α	NS, act	-	0.0100	Gilbert et al., 2016	human
IL1β	Agg	0.45*	2.2222	0.0774	Le Maitre et al., 2005	human
	Col-I	NS, act	-	0.0100	Le Maitre et al., 2005	human
	Col-II	NS, inh	-	0.0100	Le Maitre et al., 2005	human
	MMP3	10.8*	10.8000	0.3763	Le Maitre et al., 2005	human
	ADAMTS4	NS, inh	-	0.0100	Le Maitre et al., 2005	human

TNF-α	Agg	NS, inh	-	0.0100	Chapter 4	bovine
	Col-I	0.31	3.2258	0.1124	Chapter 4	bovine
	Col-II	0.06	16.6667	0.5807	Chapter 4	bovine
	MMP3	26.85	26.8500	0.9355	Chapter 4	bovine
	ADAMTS4	5.77	5.7700	0.2010	Chapter 4	bovine
Mag	Agg	10	10	0.3484	(MacLean et al., 2004)	rat
	Col-I	25	25	0.8711	(MacLean et al., 2004)	rat
	Col-II	4	4	0.1394	(MacLean et al., 2004)	rat
	MMP3	NS	-	0.0100	(MacLean et al., 2004)	rat
	ADAMTS4	4	4	0.1394	(MacLean et al., 2004)	rat
	TNF-α	NS	-	0.0100	Indications (Dudli et al., 2012; Gawri et al., 2014)	
	IL1β	NS	-	0.0100	Indications (Walter et al., 2012)	
Freq	Agg	10 1.05*	$\frac{10}{1.05}$ (=9.5238)	0.3318	(MacLean et al., 2004)	rat
	Col-I	25 0.50*	$\frac{25}{2}$ (=12.5000)	0.4355	(MacLean et al., 2004)	rat
	Col-II	NS	-	0.0100	(MacLean et al., 2004)	rat
	MMP3	15 1.02*	$\frac{15}{1.02}$ (=14.7059)	0.5124	(MacLean et al., 2004)	rat
	ADAMTS4	8 2.66	$\frac{8}{2.66}$ (=3.0075)	0.1048	(MacLean et al., 2004)	rat
	TNF-α	NS	-	0.0100	No information found	
	IL1β	NS	-	0.0100	No information found	

Bibliography

Accadbled, F., Laffosse, J. M., Ambard, D., Gomez-Brouchet, A., De Gauzy, J. S., and Swider, P. (2008). Influence of Location, Fluid Flow Direction, and Tissue Maturity on the Macroscopic Permeability of Vertebral End Plates. *Spine (Phila. Pa. 1976).* 33, pp 612-619.

Adams, M. A., and Dolan, P. (2012). Intervertebral disc degeneration: Evidence for two distinct phenotypes. *J. Anat.* 221, 497–506. doi:10.1111/j.1469-7580.2012.01551.x.

Adams, M. A., and Roughley, P. J. (2006). What is intervertebral disc degeneration, and what causes it? *Spine (Phila. Pa. 1976).* 31, 2151–2161. doi:10.1097/01.brs.0000231761.73859.2c.

Aldridge, B. B., Saez-Rodriguez, J., Muhlich, J. L., Sorger, P. K., and Lauffenburger, D. A. (2009). Fuzzy Logic Analysis of Kinase Pathway Crosstalk in TNF/EGF/Insulin-Induced Signaling. *PLoS Comput. Biol.* 5, e1000340. doi:10.1371/journal.pcbi.1000340.

Alexopoulos, L. G., Saez-Rodriguez, J., and Espelin, C. W. (2008). "High-Throughput Protein-Based Technologies and Computational Models for Drug Development, Efficacy, and Toxicity," in *Drug Efficacy, Safety, and Biologics Discovery* (Hoboken, NJ, USA: John Wiley & Sons, Inc.), 29–52. doi:10.1002/9780470431818.ch2.

Antoniou, J., Steffen, T., Nelson, F., Winterbottom, N., Hollander, A. P., Poole, R. A., et al. (1996). The human lumbar intervertebral disc: Evidence for changes in the biosynthesis and denaturation of the extracellular matrix with growth, maturation, ageing, and degeneration. *J. Clin. Invest.* 98, 996–1003. doi:10.1172/JCI118884.

Bailey, J. F., Miller, S. L., Khieu, K., O´Neill, C. W., Healey, R. M., Coughlin, D. G., et al. (2018). From the international space station to the clinic: how prolonged unloading may disrupt lumbar spine stability. *Spine J* 18, 7–14. doi:10.1016/j.spinee.2017.08.261.

Barthelemy, V. M. P., van Rijsbergen, M. M., Wilson, W., Huyghe, J. M., van Rietbergen, B., and Ito, K. (2016). A computational spinal motion segment model incorporating a matrix composition-based model of the intervertebral disc. *J. Mech. Behav. Biomed. Mater.* 54, 194–204.

doi:10.1016/j.jmbbm.2015.09.028.

Battié, M. C., Videman, T., Kaprio, J., Gibbons, L. E., Gill, K., Manninen, H., et al. (2009). The Twin Spine Study: Contributions to a changing view of disc degeneration†. *Spine J.* 9, 47–59. doi:10.1016/j.spinee.2008.11.011.

Baumgartner, L., González Ballester, M. Á., and Noailly, J. (2019). Simulation of the Multifactorial Cellular Environment within the Intervertebral disc to better understand Microtrauma Emergence. in *IRC-19-67*, 484–485.

Baumgartner, L., Reagh, J. J., González Ballester, M. A., and Noailly, J. (2020). Simulating intervertebral disc cell behaviour within 3D multifactorial environments. *Bioinformatics*, 1–8. doi:10.1093/bioinformatics/btaa939.

Baumgartner, L., Wuertz-Kozak, K., Le Maitre, C. L., Wignall, F., Richardson, S. M., Hoyland, J., et al. (2021). Multiscale regulation of the intervertebral disc: Achievements in experimental, in silico, and regenerative research. *Int. J. Mol. Sci.* 22, 703. doi:10.3390/ijms22020703.

Belavy, D. L., Adams, M., Brisby, H., Cagnie, B., Danneels, L., Fairbank, J., et al. (2016). Disc herniations in astronauts: What causes them, and what does it tell us about herniation on earth? *Eur. Spine J.* 25, 144–154. doi:10.1007/s00586-015-3917-y.

Belavý, D. L., Quittner, M. J., Ridgers, N., Ling, Y., Connell, D., and Rantalainen, T. (2017). Running exercise strengthens the intervertebral disc. *Sci. Rep.* 7, 1–8. doi:10.1038/srep45975.

Benneker, L. M., Heini, P. F., Alini, M., Anderson, S. E., and Ito, K. (2005a). 2004 Young Investigator Award Winner: Vertebral Endplate Marrow Contact Channel Occlusions and Intervertebral Disc Degeneration. *Spine (Phila. Pa. 1976).* 30, 167–173. doi:10.1097/01.brs.0000150833.93248.09.

Benneker, L. M., Heini, P. F., and Anderson, S. E. (2005b). Correlation of radiographic and MRI parameters to morphological and biochemical assessment of intervertebral disc degeneration. *Eur Spine j* 14, 27–35. doi:10.1007/s00586-004-0759-4.

Bibby, S. R. S., Jones, D. a, Ripley, R. M., and Urban, J. P. G. (2005). Metabolism of the intervertebral disc: effects of low levels of oxygen, glucose, and pH on rates of energy metabolism of bovine nucleus pulposus cells. *Spine (Phila. Pa. 1976).* 30, 487–96. doi:10.1097/01.brs.0000154619.38122.47.

Bibby, S. R. S., and Urban, J. P. G. (2004). Effect of nutrient

deprivation on the viability of intervertebral disc cells. *Eur. Spine J.* 13, 695–701. doi:10.1007/s00586-003-0616-x.

Binch, A. L. A., Cole, A. A., Breakwell, L. M., Michael, A. L. R., Chiverton, N., Creemers, L. B., et al. (2015a). Class 3 semaphorins expression and association with innervation and angiogenesis within the degenerate human intervertebral disc. *Oncotarget* 6. doi:10.18632/oncotarget.4274.

Binch, A. L. A., Cole, A. A., Breakwell, L. M., Michael, A. L. R., Chiverton, N., Creemers, L. B., et al. (2015b). Nerves are more abundant than blood vessels in the degenerate human intervertebral disc. *Arthritis Res. Ther.* 17, 370. doi:10.1186/s13075-015-0889-6.

Binch, A. L. A., Shapiro, I. M., and Risbud, M. V. (2016). Syndecan-4 in intervertebral disc and cartilage: Saint or synner? *Matrix Biol.* 52–54, 355–362. doi:10.1016/j.matbio.2016.01.005.

Biot, M. A. (1941). General theory of three-dimensional consolidation. *J. Appl. Phys.* 12, 155–164. doi:10.1063/1.1712886.

Bonnevie, E. D., Gullbrand, S. E., Ashinsky, B. G., Tsinman, T. K., Elliott, D. M., Chao, P. G., et al. (2019). Aberrant mechanosensing in injured intervertebral discs as a result of boundary-constraint disruption and residual-strain loss. *Nat. Biomed. Eng.* 3, 998–1008. doi:10.1038/s41551-019-0458-4.

Boopathy, G. T. K., and Hong, W. (2019). Role of Hippo Pathway-YAP/TAZ Signaling in Angiogenesis. *Front. Cell Dev. Biol.* 7, 49. doi:10.3389/fcell.2019.00049.

Bradshaw, R. A., and Dennis, E. A. (2003). *Handbook of Cell Signaling, Three-Volume Set*.

Bray, S. J. (2016). Notch signalling in context. *Nat. Rev. Mol. Cell Biol.* 17, 722–735. doi:10.1038/nrm.2016.94.

Brickley-Parsons, D., and Glimcher, M. J. (1984). Is the chemistry of Collagen in Intervertebral Discs an Expression of Wolff's Law? A Study of the Human Lumbar Spine. *Spine (Phila. Pa. 1976).* 9, 148–163.

Bruehlmann, S. B., Rattner, J. B., Matyas, J. R., and Duncan, N. A. (2002). Regional variations in the cellular matrix of the annulus fibrosus of the intervertebral disc. *J. Anat.* 201, pp 159-171. doi:10.1046/j.1469-7580.2002.00080.x.

Buckwalter, J. A. (1995). Spine Update Aging and Degeneration of the Human Intervertebral Disc. *Spine (Phila. Pa. 1976).* 11, 1307–1214.

Cambria, E., Arlt, M. J. E., Wandel, S., Krupkova, O., Hitzl, W.,

Passini, F. S., et al. (2020). TRPV4 Inhibition and CRISPR-Cas9 Knockout Reduce Inflammation Induced by Hyperphysiological Stretching in Human Annulus Fibrosus Cells. *Cells* 9, 1736. doi:10.3390/cells9071736.

Carroll, V. A., and Ashcroft, M. (2005). Targeting the molecular basis for tumour hypoxia. *Expert Rev. Mol. Med.* 7, 1–16. doi:10.1017/S1462399405009117.

Cerami, E. G., Gross, B. E., Demir, E., Rodchenkov, I., Babur, O., Anwar, N., et al. (2011). Pathway Commons, a web resource for biological pathway data. *Nucleic Acids Res.* 39, D685–D690. doi:10.1093/nar/gkq1039.

Ceresa, M., Olivares, A. L., Noailly, J., and Ballester, M. A. G. (2018). Coupled immunological and biomechanical model of emphysema progression. *Front. Physiol.* 9, 1–16. doi:10.3389/fphys.2018.00388.

Chan, S. C. W., Ferguson, S. J., and Gantenbein-Ritter, B. (2011). The effects of dynamic loading on the intervertebral disc. *Eur. Spine J.* 20, 1796–1812. doi:10.1007/s00586-011-1827-1.

Chan, S. C. W., Walser, J., Käppeli, P., Shamsollahi, M. J., Ferguson, S. J., and Gantenbein-Ritter, B. (2013). Region Specific Response of Intervertebral Disc Cells to Complex Dynamic Loading: An Organ Culture Study Using a Dynamic Torsion-Compression Bioreactor. *PLoS One* 8, e72489. doi:10.1371/journal.pone.0072489.

Chan, W. C. W., Au, T. Y. K., Tam, V., Cheah, K. S. E., and Chan, D. (2014). Coming together is a beginning: The making of an intervertebral disc. *Birth Defects Res. Part C Embryo Today Rev.* 102, 83–100. doi:10.1002/bdrc.21061.

Chen, J.-W., Li, B., Yang, Y.-H., Jiang, S.-D., and Jiang, L.-S. (2014a). Significance of Hypoxia in the Physiological Function of Intervertebral Disc Cells. *Crit. Rev. Eukaryot. Gene Expr.* 24, 193–204. doi:10.1615/CritRevEukaryotGeneExpr.2014010485.

Chen, J.-W., Ni, B.-B., Li, B., Yang, Y.-H., Jiang, S.-D., and Jiang, L.-S. (2014b). The Responses of Autophagy and Apoptosis to Oxidative Stress in Nucleus Pulposus Cells: Implications for Disc Degeneration. *Cell. Physiol. Biochem.* 34, 1175–1189. doi:10.1159/000366330.

Chen, J.-W., Ni, B.-B., Zheng, X.-F., Li, B., Jiang, S.-D., and Jiang, L.-S. (2015). Hypoxia facilitates the survival of nucleus pulposus cells in serum deprivation by down-regulating excessive autophagy through restricting ROS generation. *Int. J. Biochem. Cell*

Biol. 59, 1–10. doi:10.1016/j.biocel.2014.11.009.
Chen, J., Jing, L., Gilchrist, C. L., Richardson, W. J., Fitch, R. D., and Setton, L. A. (2009). Expression of laminin isoforms, receptors, and binding proteins unique to nucleus pulposus cells of immature intervertebral disc. *Connect. Tissue Res.* 50, 294–306. doi:10.3109/03008200802714925.
Choi, K.-S., and Harfe, B. D. (2011). Hedgehog signaling is required for formation of the notochord sheath and patterning of nuclei pulposi within the intervertebral discs. *Proc. Natl. Acad. Sci. U. S. A.* 108, 9484–9489. doi:10.1073/pnas.1007566108.
Clarke, D. C., Morris, M. K., and Lauffenburger, D. A. (2013). Normalization and Statistical Analysis of Multiplexed Bead-based Immunoassay Data Using Mixed-effects Modeling. *Mol. Cell. Proteomics* 12, 245–262. doi:10.1074/mcp.M112.018655.
Clerc, O., Deniaud, M., Vallet, S. D., Naba, A., Rivet, A., Perez, S., et al. (2019). MatrixDB: integration of new data with a focus on glycosaminoglycan interactions. *Nucleic Acids Res.* 47, D376–D381. doi:10.1093/nar/gky1035.
Crean, J. K. G., Roberts, S., Jaffray, D. C., Eisenstein, S. M., and Duance, V. C. (1997). Matrix Metalloproteinases in the Human Intervertebral Disc: Role in Disc Degeneration and Scoliosis. *Spine (Phila. Pa. 1976).* 22, 2877–2884. doi:10.1097/00007632-199712150-00010.
DeLucca, J. F., Cortes, D. H., Jacobs, N. T., Vresilovic, E. J., Duncan, R. L., and Elliott, D. M. (2016). Human cartilage endplate permeability varies with degeneration and intervertebral disc site. *J. Biomech.* 49, 550–557. doi:10.1016/j.jbiomech.2016.01.007.
Ding, F., Shao, Z. W., and Xiong, L. M. (2013). Cell death in intervertebral disc degeneration. *Apoptosis* 18, 777–785. doi:10.1007/s10495-013-0839-1.
Disc4All – Training Network to advance integrated computational simulations in translational medicine, applied to intervertebral disc degeneration (2020). *H2020-MSCA-ITN-ETN-2020 GA 955735*. Available at: https://www.upf.edu/web/disc4all.
Dong, Z.-H., Wang, D., Liu, T.-T., Li, F., Liu, R., Wei, J., et al. (2014). The Roles of MAPKs in Rabbit Nucleus Pulposus Cell Apoptosis Induced by High Osmolality. *Glob. Spine J.* 18, 2835–45. doi:10.1055/s-0034-1376584.
Duance, V. C., Crean, J. K. G., Sims, T. J., Avery, N., Smith, S., Menage, J., et al. (1998). Changes in Collagen Cross-Linking in Degenerative Disc Disease and Scoliosis. *Spine (Phila. Pa. 1976).*

23, 2545–2551. doi:10.1097/00007632-199812010-00009.
Dudli, S., Fields, A. J., Samartzis, D., Karppinen, J., and Lotz, J. C. (2016). Pathobiology of Modic changes. *Eur. Spine J.* 25, 3723–3734. doi:10.1007/s00586-016-4459-7.
Dudli, S., Haschtmann, D., and Ferguson, S. J. (2012). Fracture of the vertebral endplates, but not equienergetic impact load, promotes disc degeneration in vitro. *J. Orthop. Res.* 30, 809–816. doi:10.1002/jor.21573.
Dudli, S., Liebenberg, E., Magnitsky, S., Lu, B., Lauricella, M., and Lotz, J. C. (2018). Modic type 1 change is an autoimmune response that requires a proinflammatory milieu provided by the "Modic disc." *Spine J.* 18, 831–844. doi:10.1016/j.spinee.2017.12.004.
Duncan, N. A. (2006). Cell Deformation and Micromechanical Environment in the Intervertebral Disc. *J. Bone Jt. Surg.* 88, 47–51. doi:10.2106/JBJS.F.00035.
Dupont, S., Morsut, L., Aragona, M., Enzo, E., Giulitti, S., Cordenonsi, M., et al. (2011). Role of YAP/TAZ in mechanotransduction. *Nature* 474, 179–183. doi:10.1038/nature10137.
Encyclopaedia of Occupational Health and Safety 4th Edition *ILO Encycl. Occup. Heal. Saf.* Available at: http://www.ilocis.org/en/contilo1.html.
Fabregat, A., Sidiropoulos, K., Garapati, P., Gillespie, M., Hausmann, K., Haw, R., et al. (2016). The Reactome pathway Knowledgebase. *Nucleic Acids Res.* 44, D481–D487. doi:10.1093/nar/gkv1351.
Fang, W., Zhou, X., Wang, J., Xu, L., Zhou, L., Yu, W., et al. (2018). Wogonin mitigates intervertebral disc degeneration through the Nrf2/ARE and MAPK signaling pathways. *Int. Immunopharmacol.* 65, 539–549. doi:10.1016/j.intimp.2018.10.024.
Fardon, D. F., Williams, A. L., Dohring, E. J., Murtagh, F. R., Rothman, S. L. G., and Sze, G. K. (2014). Lumbar Disc Nomenclature: Version 2.0: Recommendations of the Combined Task Forces of the North American Spine Society, the American Society of Spine Radiology, and the American Society of Neuroradiology. *Spine (Phila. Pa. 1976).* 39, pp E1448-E1465. doi:10.1097/BRS.0b013e3182a8866d.
Fearing, B. V., Hernandez, P. A., Setton, L. A., and Chahine, N. O. (2018). Mechanotransduction and cell biomechanics of the intervertebral disc. *JOR Spine* 1.

doi:10.1002/cncr.27633.Percutaneous.
Fearing, B. V., Jing, L., Barcellona, M. N., Witte, S. E., Buchowski, J. M., Zebala, L. P., et al. (2019). Mechanosensitive transcriptional coactivators MRTF-A and YAP/TAZ regulate nucleus pulposus cell phenotype through cell shape. *FASEB J.* 33, 14022–14035. doi:10.1096/fj.201802725RRR.
Feng, C., Liu, H., Yang, M., Zhang, Y., Huang, B., and Zhou, Y. (2016). Disc cell senescence in intervertebral disc degeneration: Causes and molecular pathways. *Cell Cycle* 15, 1674–84. doi:10.1080/15384101.2016.1152433.
Fernandes, R. J., Schmid, T. M., and Eyre, D. R. (2003). Assembly of collagen types II, IX and XI into nascent hetero-fibrils by a rat chondrocyte cell line. *Eur. J. Biochem.* 270, 3243–3250. doi:10.1046/j.1432-1033.2003.03711.x.
Fields, A. J., Rodriguez, D., Gary, K. N., Liebenberg, E. C., and Lotz, J. C. (2014). Influence of biochemical composition on endplate cartilage tensile properties in the human lumbar spine. *J. Orthop. Res.* 32, 245–252. doi:10.1002/jor.22516.
Freemont, A. J., Watkins, A., Le Maitre, C., Baird, P., Jeziorska, M., Knight, M. T. N., et al. (2002). Nerve growth factor expression and innervation of the painful intervertebral disc. *J. Pathol.* 197, 286–92. doi:10.1002/path.1108.
Freemont, A., Peacock, T., Goupille, P., Hoyland, J., O'Brien, J., and Jayson, M. (1997). Nerve ingrowth into diseased intervertebral disc in chronic back pain. *Lancet* 350, 178–181. doi:10.1016/S0140-6736(97)02135-1.
Gajghate, S., Hiyama, A., Shah, M., Sakai, D., Anderson, D. G., Shapiro, I. M., et al. (2009). Osmolarity and Intracellular Calcium Regulate Aquaporin2 Expression Through TonEBP in Nucleus Pulposus Cells of the Intervertebral Disc. *J. Bone Miner. Res.* 24, 992–1001. doi:10.1359/jbmr.090103.
Galbusera, F., van Rijsbergen, M., Ito, K., Huyghe, J. M., Brayda-Bruno, M., and Wilke, H.-J. (2014). Ageing and degenerative changes of the intervertebral disc and their impact on spinal flexibility. *Eur. Spine J.* 23, Suppl 3. doi:10.1007/s00586-014-3203-4.
Garcia-Alonso, L., Holland, C. H., Ibrahim, M. M., Turei, D., and Saez-Rodriguez, J. (2019). Benchmark and integration of resources for the estimation of human transcription factor activities. *Genome Res.* 29, 1363–1375. doi:10.1101/gr.240663.118.
García-Cosamalón, J., Del Valle, M. E., Calavia, M. G., García-Suárez,

O., López-Muñiz, A., Otero, J., et al. (2010). Intervertebral disc, sensory nerves and neurotrophins: who is who in discogenic pain? *J. Anat.* 217, 1–15. doi:10.1111/j.1469-7580.2010.01227.x.

Garcia, K. M., Harrison, M. F., Sargsyan, A. E., Ebert, D., and Dulchavsky, S. A. (2018). Real-time Ultrasound Assessment of Astronaut Spinal Anatomy and Disorders on the International Space Station. *J. Ultrasound Med.* 37, 987–999. doi:10.1002/jum.14438.

Gawri, R., Rosenzweig, D. H., Krock, E., Ouellet, J. A., Stone, L. S., Quinn, T. M., et al. (2014). High mechanical strain of primary intervertebral disc cells promotes secretion of inflammatory factors associated with disc degeneration and pain. *Arthritis Res. Ther.* 16, R21. doi:10.1186/ar4449.

Gennarelli, T. (2019). Back to the Basics: Revisiting the future, a retrospective of reminiscences. in *IRC-19-01*.

Gilbert, H. T. J., Hodson, N., Baird, P., Richardson, S. M., and Hoyland, J. A. (2016). Acidic pH promotes intervertebral disc degeneration: Acid-sensing ion channel -3 as a potential therapeutic target. *Sci. Rep.* 6, 1–12. doi:10.1038/srep37360.

Gilbert, H. T. J., Hoyland, J. A., and Millward-Sadler, S. J. (2010). The response of human anulus fibrosus cells to cyclic tensile strain is frequency-dependent and altered with disc degeneration. *Arthritis Rheum.* 62, 3385–3394. doi:10.1002/art.27643.

Gilbert, H. T. J., Nagra, N. S., Freemont, A. J., Millward-Sadler, S. J., and Hoyland, J. A. (2013). Integrin – Dependent Mechanotransduction in Mechanically Stimulated Human Annulus Fibrosus Cells: Evidence for an Alternative Mechanotransduction Pathway Operating with Degeneration. *PLoS One* 8, e72994. doi:10.1371/journal.pone.0072994.

Glick, D., Barth, S., and Macleod, K. F. (2010). Autophagy: cellular and molecular mechanisms. *J. Pathol.* 221, 3–12. doi:10.1002/path.2697.

Gorth, D. J., Shapiro, I. M., and Risbud, M. V (2015). Disc-overy of the Drivers of Inflammation Induced Chronic Low Back Pain: From Bacteria to Diabetes. *Discov Med.* 20, 177–184. doi:10.1016/j.physbeh.2017.03.040.

Gruber, H. E., and Hanley, E. N. (1998). Analysis of aging and degeneration of the human intervertebral disc: Comparison of surgical specimens with normal controls. *Spine (Phila. Pa. 1976).* 23, 751–757. doi:10.1097/00007632-199804010-00001.

Gruber, H. E., and Hanley, E. N. (2002). Observations on

morphologic changes in the aging and degenerating human disc: secondary collagen alterations. *BMC Musculoskelet. Disord.* 3, 9. doi:10.1186/1471-2474-3-9.

Gruber, H. E., Ingram, J. A., Norton, H. J., and Hanley, E. N. (2007). Senescence in Cells of the Aging and Degenerating Intervertebral Disc: Immunolocalization of Senescence-Associated Beta-Galactosidase in Human and Sand Rat Discs. *Spine (Phila. Pa. 1976).* 32, 321–327. doi:10.1097/01.brs.0000253960.57051.de.

Gruber, H. E., Jones, B., Marrero, E., and Hanley, E. N. (2017). Proinflammatory Cytokines IL-1β and TNF-α Influence Human Annulus Cell Signaling Cues for Neurite Growth: In Vitro Coculture Studies. *Spine (Phila. Pa. 1976).* 42, 1529–1537. doi:10.1097/BRS.0000000000002155.

Gruber, H., Hoelscher, G., Bethea, S., and Hanley, E. (2012). Interleukin 1-beta upregulates brain-derived neurotrophic factor, neurotrophin 3 and neuropilin 2 gene expression and NGF production in annulus cells. *Biotech. Histochem.* 87, 506–511. doi:10.3109/10520295.2012.703692.

Gu, W. Y., Mao, X. G., Foster, R. J., Weidenbaum, M., Mow, V. C., and Rawlins, B. A. (1999). The anisotropic hydraulic permeability of human lumbar anulus fibrosus: Influence of age, degeneration, direction, and water content. *Spine (Phila. Pa. 1976).* 24, 2449–2455. doi:10.1097/00007632-199912010-00005.

Gu, W., Zhu, Q., Gao, X., and Brown, M. D. (2014). Simulation of the Progression of Interverteral Disc Degeneration due to Decreased Nutrition Supply. *Spine (Phila Pa 1976)* 39, E1411–E1417. doi:10.1097/BRS.0000000000000560.

Guo, Y., Meng, Y., Liu, H., Wang, B., Ding, C., Rong, X., et al. (2019). Acid-sensing ion channels mediate the degeneration of intervertebral disc via various pathways—A systematic review. *Channels* 13, 367–373. doi:10.1080/19336950.2019.1664038.

Halterman, J. A., Kwon, H. M., and Wamhoff, B. R. (2012). Tonicity-independent regulation of the osmosensitive transcription factor TonEBP (NFAT5). *Am. J. Physiol. Physiol.* 302, C1–C8. doi:10.1152/ajpcell.00327.2011.

Han, S., Xu, W., Wang, Z., Qi, X., Wang, Y., Ni, Y., et al. (2016). Crosstalk between the HIF-1 and Toll-like receptor/nuclear factor-κB pathways in the oral squamous cell carcinoma microenvironment. *Oncotarget* 7, 37773–37789. doi:10.18632/oncotarget.9329.

Hangai, M., Kaneoka, K., Hinotsu, S., Shimizu, K., Okubo, Y.,

Miyakawa, S., et al. (2009). Lumbar intervertebral disk degeneration in athletes. *Am. J. Sports Med.* 37, 149–155. doi:10.1177/0363546508323252.

Hayes, A., Shu, C., Lord, M., Little, C., Whitelock, J., and Melrose, J. (2016). Pericellular colocalisation and interactive properties of type VI collagen and perlecan in the intervertebral disc. *Eur. Cells Mater.* 32, 40–57. doi:10.22203/eCM.v032a03.

Heathfield, S., Le Maitre, C., and Hoyland, J. (2008). Caveolin-1 expression and stress-induced premature senescence in human intervertebral disc degeneration. *Arthritis Res. Ther.* 10, R87. doi:10.1186/ar2468.

Hebert, D. N., and Molinari, M. (2007). In and Out of the ER: Protein Folding, Quality Control, Degradation, and Related Human Diseases. *Physiol. Rev.* 87, 1377–1408. doi:10.1152/physrev.00050.2006.

Hiyama, A., Gajghate, S., Sakai, D., Mochida, J., Shapiro, I. M., and Risbud, M. V. (2009). Activation of TonEBP by Calcium Controls β1,3-Glucuronosyltransferase-I Expression, a Key Regulator of Glycosaminoglycan Synthesis in Cells of the Intervertebral Disc. *J. Biol. Chem.* 284, 9824–9834. doi:10.1074/jbc.M807081200.

Hiyama, A., Sakai, D., and Mochida, J. (2013). Cell Signaling Pathways Related to Pain Receptors in the Degenerated Disk. *Glob. Spine J.* 3, 165–174. doi:10.1055/s-0033-1345036.

Hiyama, A., Sakai, D., Risbud, M. V, Tanaka, M., Arai, F., Abe, K., et al. (2010). Enhancement of intervertebral disc cell senescence by WNT/β-catenin signaling-induced matrix metalloproteinase expression. *Arthritis Rheum.* 62, 3036–47. doi:10.1002/art.27599.

Hiyama, A., Skubutyte, R., Markova, D., Anderson, D. G., Yadla, S., Sakai, D., et al. (2011). Hypoxia activates the notch signaling pathway in cells of the intervertebral disc: Implications in degenerative disc disease. *Arthritis Rheum.* 63, 1355–1364. doi:10.1002/art.30246.

Hodson, N. W., Patel, S., Richardson, S. M., Hoyland, J. A., and Gilbert, H. T. J. (2018). Degenerate intervertebral disc-like pH induces a catabolic mechanoresponse in human nucleus pulposus cells. *JOR Spine* 1, e1004. doi:10.1002/jsp2.1004.

Holcombe, M., Adra, S., Bicak, M., Chin, S., Coakley, S., Graham, A. I., et al. (2012). Modelling complex biological systems using an agent-based approach. *Integr. Biol.* 4, 53–64. doi:10.1039/c1ib00042j.

Holm, S., Maroudas, A., Urban, J. P. G., Selstam, G., and Nachemson, A. (1981). Nutrition of the Intervertebral Disc: Solute Transport and Metabolism. *Connect. Tissue Res. (Connect Tissue Res)* 8, 101–119. doi:10.3109/03008208109152130.

Hori, K., Sen, A., and Artavanis-Tsakonas, S. (2013). Notch signaling at a glance. *J. Cell Sci.* 126, 2135–2140. doi:10.1242/jcs.127308.

Horner, H. A., and Urban, J. P. G. (2001). 2001 Volvo Award Winner in Basic Science Studies : Effect of Nutrient Supply on the Viability of Cells From the Nucleus Pulposus of the Intervertebral Disc. *Spine (Phila. Pa. 1976).* 26, 2543–2549.

Hoy, D., March, L., Brooks, P., Blyth, F., Woolf, A., Bain, C., et al. (2014). The global burden of low back pain: Estimates from the Global Burden of Disease 2010 study. *Ann. Rheum. Dis.* 73, 968–974. doi:10.1136/annrheumdis-2013-204428.

Hoyland, J. A., Le maitre, C., and Freemont, A. J. (2008). Investigation of the role of IL-1 and TNF in matrix degradation in the intervertebral disc. *Rheumatology* 47, 809–814. doi:10.1093/rheumatology/ken056.

Huang, C.-Y., and Gu, W. Y. (2008). Effects of Mechanical Compression on Metabolism and Distribution of Oxygen and Lactate in Intervertebral Disc. *J Biomech* 41, 1184–1196. doi:10.1016/j.jbiomech.2008.02.002.

Huang, Y. C., Urban, J. P. G., and Luk, K. D. K. (2014). Intervertebral disc regeneration: Do nutrients lead the way? *Nat. Rev. Rheumatol.* 10, 561–566. doi:10.1038/nrrheum.2014.91.

Hughes, S. P. F., Freemont, A. J., Hukins, D. W. L., McGregor, A. H., and Roberts, S. (2012). The pathogenesis of degeneration of the intervertebral disc and emerging therapies in the management of back pain. *J. Bone Jt. Surg. - J Bone Jt. Surg Br* 94 B, 1298–1304. doi:10.1302/0301-620X.94B10.28986.

Huyghe, J. M., Houben, G. B., Drost, M. R., and van Donkelaar, C. C. (2003). An ionised/non-ionised dual porosity model of intervertebral disc tissue. *Biomech. Model. Mechanobiol.* 2, 3–19. doi:10.1007/s10237-002-0023-y.

Iatridis, J. C., MacLean, J. J., O'Brien, M., and Stokes, I. A. . F. (2007). Measurements of Proteoglycan and Water Content Distribution in Human Lumbar Intervertebral Discs. *Spine (Phila Pa 1976)* 32, 1493–1497. doi:10.1097/BRS.0b013e318067dd3f.

Iatridis, J. C., MacLean, J. J., Roughley, P. J., and Alini, M. (2006). Effects of Mechanical Loading on intervertebral Disc Metabolism In Vivo. *J. Bone Jt. Surg. (J Bone Jt. Surg Am)* 88, 41–

46. doi:10.2106/JBJS.E.01407.
Illien-Jünger, S., Gantenbein-Ritter, B., Grad, S., Lezuo, P., Ferguson, S. J., Alini, M., et al. (2010). The combined effects of limited nutrition and high-frequency loading on intervertebral discs with endplates. *Spine (Phila. Pa. 1976).* 35, 1744–1752. doi:10.1097/BRS.0b013e3181c48019.
Ishihara, H., Warensjo, K., Roberts, S., and Urban, J. P. (1997). Proteoglycan synthesis in the intervertebral disk nucleus: the role of extracellular osmolality. *Am. J. Physiol. Physiol.* 272, C1499–C1506. doi:10.1152/ajpcell.1997.272.5.C1499.
Ito, A., Mukaiyama, A., Nagase, H., Thøgersen, I. B., Jan, J., Sasaguri, Y., et al. (1996). Communications : Degradation of Interleukin 1 β by Matrix Metalloproteinases Degradation of Interleukin 1 □ by Matrix Metalloproteinases *. *J. Biol. Chem.* 271, 14657–14661. doi:10.1074/jbc.271.25.14657.
Ito, M., Yurube, T., Kakutani, K., Maeno, K., Takada, T., Terashima, Y., et al. (2017). Selective interference of mTORC1/RAPTOR protects against human disc cellular apoptosis, senescence, and extracellular matrix catabolism with Akt and autophagy induction. *Osteoarthr. Cartil.* 25, 2134–2146. doi:10.1016/j.joca.2017.08.019.
Jackson, A. R., Eismont, A., Yu, L., Li, N., Gu, W., Eismont, F., et al. (2018). Diffusion of antibiotics in intervertebral disc. *J. Biomech.* 76, 259–262. doi:10.1016/j.jbiomech.2018.06.008.
Jiang, L., Zhang, X., Zheng, X., Ru, A., Ni, X., Wu, Y., et al. (2013). Apoptosis, senescence, and autophagy in rat nucleus pulposus cells: Implications for diabetic intervertebral disc degeneration. *J. Orthop. Res.* 31, 692–702. doi:10.1002/jor.22289.
Jiang, W., Zhang, X., Hao, J., Shen, J., Fang, J., Dong, W., et al. (2014). SIRT1 protects against apoptosis by promoting autophagy in degenerative human disc nucleus pulposus cells. *Sci. Rep.* 4, 7456. doi:10.1038/srep07456.
Johnson, W. E. B., Sivan, S., Wright, K. T., Eisenstein, S. M., Maroudas, A., and Roberts, S. (2006). Human Intervertebral Disc Cells Promote Nerve Growth Over Substrata of Human Intervertebral Disc Aggrecan. *Spine (Phila. Pa. 1976).* 31, 1187–1193. doi:10.1097/01.brs.0000217669.04903.61.
Johnson, Z. I., Doolittle, A. C., Snuggs, J. W., Shapiro, I. M., Le Maitre, C. L., and Risbud, M. V. (2017). TNF-α promotes nuclear enrichment of the transcription factor TonEBP/NFAT5 to selectively control inflammatory but not osmoregulatory

responses in nucleus pulposus cells. *J. Biol. Chem.* 292, 17561–17575. doi:10.1074/jbc.M117.790378.

Johnson, Z. I., Gogate, S. S., Day, R., Binch, A., Markova, D. Z., Chiverton, N., et al. (2015a). Aquaporin 1 and 5 expression decreases during human intervertebral disc degeneration: novel HIF-1-mediated regulation of aquaporins in NP cells. *Oncotarget* 6. doi:10.18632/oncotarget.3631.

Johnson, Z. I., Schoepflin, Z. R., Choi, H., Shapiro, I. M., and Risbud, M. V. (2015b). Disc in flames: Roles of TNF-α and IL-1β in intervertebral disc degeneration. *Eur. Cells Mater.* 30, 104–117. doi:10.22203/eCM.v030a08.

Johnson, Z. I., Shapiro, I. M., and Risbud, M. V. (2014). Extracellular osmolarity regulates matrix homeostasis in the intervertebral disc and articular cartilage: Evolving role of TonEBP. *Matrix Biol.* 40, 10–16. doi:10.1016/j.matbio.2014.08.014.

Joyce, K., Isa, I. L. M., Fahey, R., Creemers, L., Devitt, A., and Pandit, A. (2018). The Glycomic Profile of the Intervertebral Disc in Health and Degeneration for Biomaterial Functionalization. *Orthop. Proc.* 100–B.

Ju, S., Gantenbein-ritter, B., Lezuo, P., Alini, M., Ferguson, S. J., and Ito, K. (2009). Effect of Limited Nutrition on In Situ Intervertebral Disc Cells Under Simulated-Physiological Loading. 34, 1264–1271.

Jung, W.-W., Kim, H.-S., Shon, J.-R., Lee, M., Lee, S.-H., Sul, D., et al. (2011). Intervertebral Disc Degeneration-induced Expression of Pain-related Molecules: Glial Cell-derived Neurotropic Factor as a Key Factor. *J. Neurosurg. Anesthesiol.* 23, 329–334. doi:10.1097/ANA.0b013e318220f033.

Kakiuchi, Y., Yurube, T., Kakutani, K., Takada, T., Ito, M., Takeoka, Y., et al. (2019). Pharmacological inhibition of mTORC1 but not mTORC2 protects against human disc cellular apoptosis, senescence, and extracellular matrix catabolism through Akt and autophagy induction. *Osteoarthr. Cartil.* 27, 965–976. doi:10.1016/j.joca.2019.01.009.

Kanehisa, M., and Goto, S. (2000). KEGG: Kyoto Encyclopedia of Genes and Genomes. *Nucleic Acids Res.* 28, 27–30. doi:10.1093/nar/28.1.27.

Kao, T.-H., Peng, Y.-J., Tsou, H.-K., Salter, D. M., and Lee, H.-S. (2014). Nerve growth factor promotes expression of novel genes in intervertebral disc cells that regulate tissue degradation. *J. Neurosurg. Spine* 21, 653–661. doi:10.3171/2014.6.SPINE13756.

Kasra, M., Merryman, W. D., Loveless, K. N., Goel, V. K., Martin, J. D., and Buckwalter, J. A. (2006). Frequency Response of Pig Intervertebral Disc Cells Subjected to Dynamic Hydrostatic Pressure. 1967–1973. doi:10.1002/jor.

Kepler, C. K., Ponnappan, R. K., Tannoury, C. A., Risbud, M. V., and Anderson, D. G. (2013). The molecular basis of intervertebral disc degeneration. *Spine J.* 13, 318–330. doi:10.1016/j.spinee.2012.12.003.

Kerkhofs, J., Leijten, J., Bolander, J., Luyten, F. P., Post, J. N., and Geris, L. (2016). A qualitative model of the differentiation network in chondrocyte maturation: A holistic view of chondrocyte hypertrophy. *PLoS One* 11, 1–27. doi:10.1371/journal.pone.0162052.

Kerr, G. J., Veras, M. A., Kim, M. K. M., and S?guin, C. A. (2017). Decoding the intervertebral disc: Unravelling the complexities of cell phenotypes and pathways associated with degeneration and mechanotransduction. *Semin. Cell Dev. Biol.* 62, 94–103. doi:10.1016/j.semcdb.2016.05.008.

Kerttula, L., Luoma, K., Vehmas, T., Grönblad, M., and Kääpa, E. (2012). Modic type i change may predict rapid progressive, deforming disc degeneration: A prospective 1-year follow-up study. *Eur. Spine J.* 21, 1135–1142. doi:10.1007/s00586-012-2147-9.

Khan, A. N., Jacobsen, H. E., Khan, J., Filippi, C. G., Levine, M., Lehman, R. A., et al. (2017). Inflammatory biomarkers of low back pain and disc degeneration: a review. *Ann. N. Y. Acad. Sci.* 1410, 68–84. doi:10.1111/nyas.13551.

Klamt, S., Saez-Rodriguez, J., Lindquist, J. A., Simeoni, L., and Gilles, E. D. (2006). A methodology for the structural and functional analysis of signaling and regulatory networks. *BMC Bioinformatics* 7, 56. doi:10.1186/1471-2105-7-56.

Kong, C. G., Park, J. B., Kim, M. S., and Park, E. Y. (2014). High glucose accelerates autophagy in adult rat intervertebral disc cells. *Asian Spine J.* 8, 543–548. doi:10.4184/asj.2014.8.5.543.

Koy, T., Zange, J., Rittweger, J., Pohle-Fröhlich, R., Hackenbroch, M., Eysel, P., et al. (2014). Assessment of lumbar intervertebral disc glycosaminoglycan content by gadolinium-enhanced MRI before and after 21-days of head-down-tilt bedrest. *PLoS One* 9. doi:10.1371/journal.pone.0112104.

Kraemer, J., Kolditz, D., and Gowin, R. (1985). Water and Electrolyte Content of Human Intervertebral Discs Under Variable Load.

Spine (Phila. Pa. 1976). 10, 69–71. doi:10.1097/00007632-198501000-00011.

Krock, E., Currie, J. B., Weber, M. H., Ouellet, J. A., Stone, L. S., Rosenzweig, D. H., et al. (2016). Nerve growth factor is regulated by toll-like receptor 2 in human intervertebral discs. *J. Biol. Chem.* 291, 3541–3551. doi:10.1074/jbc.M115.675900.

Krock, E., Rosenzweig, D. H., Chabot-Doré, A.-J., Jarzem, P., Weber, M. H., Ouellet, J. A., et al. (2014). Painful, degenerating intervertebral discs up-regulate neurite sprouting and CGRP through nociceptive factors. *J. Cell. Mol. Med.* 18, 1213–1225. doi:10.1111/jcmm.12268.

Krumsiek, J., Pölsterl, S., Wittmann, D. M., and Theis, F. J. (2010). Odefy - From discrete to continuous models. *BMC Bioinformatics* 11, 233. doi:10.1186/1471-2105-11-233.

Krupkova, O., Sekiguchi, M., Klasen, J., Hausmann, O., Konno, S., Ferguson, S. J., et al. (2014). Epigallocatechin 3-gallate suppresses interleukin-1β-induced inflammatory responses in intervertebral disc cells in vitro and reduces radiculopathic pain in rats. *Eur. Cell. Mater.* 28, 372–386. doi:10.22203/eCM.v028a26.

Krupkova, O., Zvick, J., and Wuertz-Kozak, K. (2017). The role of transient receptor potential channels in joint diseases. *Eur. Cells Mater.* 34, 180–201. doi:10.22203/eCM.v034a12.

Kudo, S., Mizuno, K., Hirai, Y., and Shimizu, T. (1990). Clearance and Tissue distribution of Recombinant Human Interleukin 1b in Rats. *Cancer Res. (Cancer Res)* 50, 5751–5755. doi:10.1158/0008-5472.CAN-17-0628.

LA Binch, A., Cole, A. A., Breakwell, L. M., Michael, A. L., Chiverton, N., Cross, A. K., et al. (2014). Expression and regulation of neurotrophic and angiogenic factors during human intervertebral disc degeneration. *Arthritis Res. Ther.* 16, 416. doi:10.1186/s13075-014-0416-1.

Lama, P., Claireaux, H., Flower, L., Harding, I. J., Dolan, T., Le Maitre, C. L., et al. (2019). Physical disruption of intervertebral disc promotes cell clustering and a degenerative phenotype. *Cell Death Discov.* 5, 154. doi:10.1038/s41420-019-0233-z.

Lama, P., Le Maitre, C. L., Dolan, P., Tarlton, J. F., Harding, I. J., and Adams, M. A. (2013). Do intervertebral discs degenerate before they herniate , or after ? *Bone Jt. J.* 95–B, 1127–1133. doi:10.1302/0301-620X.95B8.31660.

Lama, P., Le Maitre, C. L., Harding, I. J., Dolan, P., and Adams, M. A. (2018). Nerves and blood vessels in degenerated intervertebral

discs are confined to physically disrupted tissue. *J. Anat.* 233, 86–97. doi:10.1111/joa.12817.

Lang, G., Liu, Y., Geries, J., Zhou, Z., Kubosch, D., Südkamp, N., et al. (2018). An intervertebral disc whole organ culture system to investigate proinflammatory and degenerative disc disease condition. *J. Tissue Eng. Regen. Med.*, 1–11. doi:10.1002/term.2636.

Larson, J. W., Levicoff, E. A., Gilbertson, L. G., and Kang, J. D. (2006). Biologic modification of animal models of intervertebral disc degeneration. *J. Bone Jt. Surg. - Ser. A* 88, 83–87. doi:10.2106/00004623-200604002-00017.

Latridis, J. C., Godburn, K., Wuertz, K., Alini, M., and Roughley, P. J. (2011). Region-dependent aggrecan degradation patterns in the rat intervertebral disc are affected by mechanical loading in vivo. *Spine (Phila. Pa. 1976).* 36, 203–209. doi:10.1097/BRS.0b013e3181cec247.

Le Maitre, C. L., Frain, J., Fotheringham, A. P., Freemont, A. J., and Hoyland, J. A. (2008). Human cells derived from degenerate intervertebral discs respond differently to those derived from non-degenerate intervertebral discs following application of dynamic hydrostatic pressure. *Biorheology* 45, 563–575. doi:10.3233/BIR-2008-0498.

Le Maitre, C. L., Frain, J., Millward-Sadler, J., Fotheringham, A. P., Freemont, A. J., and Hoyland, J. A. (2009). Altered integrin mechanotransduction in human nucleus pulposus cells derived from degenerated discs. *Arthritis Rheum.* 60, 460–469. doi:10.1002/art.24248.

Le Maitre, C. L., Freemont, A. J., and Hoyland, J. A. (2004). Localization of degradative enzymes and their inhibitors in the degenerate human intervertebral disc. *J. Pathol.* 204, 47–54. doi:10.1002/path.1608.

Le Maitre, C. L., Freemont, A. J., and Hoyland, J. A. (2005). The role of interleukin-1 in the pathogenesis of human intervertebral disc degeneration. *Arthritis Res. Ther.* 7, R732–R745. doi:10.1186/ar1732.

Le Maitre, C. L., Freemont, A. J., and Hoyland, J. A. (2007a). Accelerated cellular senescence in degenerate intervertebral discs: A possible role in the pathogenesis of intervertebral disc degeneration. *Arthritis Res. Ther.* 9, R45. doi:10.1186/ar2198.

Le Maitre, C. L., Hoyland, J. A., and Freemont, A. J. (2007b). Catabolic cytokine expression in degenerate and herniated human intervertebral discs: IL-1beta and TNFalpha expression profile.

Arthritis Res. Ther. 9, R77. doi:10.1186/ar2275.
Le Maitre, C. L., Pockert, A., Buttle, D. J., Freemont, A. J., and Hoyland, J. A. (2007c). Matrix synthesis and degradation in human intervertebral disc degeneration. *Biochem. Soc. Trans.* 35, 652–655. doi:10.1042/BST0350652.
Lee, H.-W., and Kwon, Y.-M. (2013). Traumatic Intradural Lumbar Disc Herniation without Bone Injury. *Korean J. Spine* 10, 181–184. doi:10.14245/kjs.2013.10.3.181.
Lee, J. M., Song, J. Y., Baek, M., Jung, H.-Y., Kang, H., Han, I. B., et al. (2011a). Interleukin-1β induces angiogenesis and innervation in human intervertebral disc degeneration. *J. Orthop. Res.* 29, 265–269. doi:10.1002/jor.21210.
Lee, S. Do, Choi, S. Y., Lim, S. W., Lamitina, S. T., Ho, S. N., Go, W. Y., et al. (2011b). TonEBP stimulates multiple cellular pathways for adaptation to hypertonic stress: organic osmolyte-dependent and -independent pathways. *Am. J. Physiol. Physiol.* 300, F707–F715. doi:10.1152/ajprenal.00227.2010.
Li, H., Liang, C. Z., and Chen, Q. X. (2013). Regulatory Role of Hypoxia Inducible Factor in the Biological Behavior of Nucleus Pulposus Cells. *Yonsei Med. J.* 54, 807–812. doi:10.3349/ymj.2013.54.4.807.
Li, J., Yuan, W., Jiang, S., Ye, W., Yang, H., Shapiro, I. M., et al. (2015). Prolyl-4-hydroxylase Domain Protein 2 Controls NF-*κ*B/p65 Transactivation and Enhances the Catabolic Effects of Inflammatory Cytokines on Cells of the Nucleus Pulposus. *J. Biol. Chem.* 290, 7195–7207. doi:10.1074/jbc.M114.611483.
Li, P., Gan, Y., Wang, H., Xu, Y., Li, S., Song, L., et al. (2017a). Role of the ERK1/2 pathway in osmolarity effects on nucleus pulposus cell apoptosis in a disc perfusion culture. *J. Orthop. Res.* 35, 86–92. doi:10.1002/jor.23249.
Li, P., Gan, Y., Xu, Y., Song, L., Wang, L., Ouyang, B., et al. (2017b). The inflammatory cytokine TNF-α promotes the premature senescence of rat nucleus pulposus cells via the PI3K/Akt signaling pathway. *Sci. Rep.* 7, 1–12. doi:10.1038/srep42938.
Li, Y., Li, K., Han, X., Mao, C., Zhang, K., Zhao, T., et al. (2016). The imbalance between TIMP3 and matrix-degrading enzymes plays an important role in intervertebral disc degeneration. *Biochem. Biophys. Res. Commun.* 469, 507–514. doi:10.1016/j.bbrc.2015.12.020.
Liang, C., Li, H., Tao, Y., Shen, C., Li, F., Shi, Z., et al. (2013). New hypothesis of chronic back pain: low pH promotes nerve

ingrowth into damaged intervertebral disks. *Acta Anaesthesiol. Scand.* 57, 271–277. doi:10.1111/j.1399-6576.2012.02670.x.

Liang, H., Yang, X., Liu, C., Sun, Z., and Wang, X. (2018). Effect of nf-kb signaling pathway on the expression of mif, tnf-α, il-6 in the regulation of intervertebral disc degeneration. *J. Musculoskelet. Neuronal Interact.* 18, 551–556.

Liebscher, T., Haefeli, M., Wuertz, K., Nerlich, A. G., and Boos, N. (2011). Age-Related Variation in Cell Density of Human Lumbar Intervertebral Disc. *Spine (Phila. Pa. 1976).* 36, 153–159. doi:10.1097/BRS.0b013e3181cd588c.

Likhitpanichkul, M., Torre, O. M., Gruen, J., Walter, B. A., Hecht, A. C., and Iatridis, J. C. (2016). Do mechanical strain and TNF-α interact to amplify pro-inflammatory cytokine production in human annulus fibrosus cells? *J. Biomech.* 49, 1214–1220. doi:10.1016/j.jbiomech.2016.02.029.

Livshits, G., Popham, M., Malkin, I., Sambrook, P. N., MacGregor, A. J., Spector, T., et al. (2011). Lumbar disc degeneration and genetic factors are the main risk factors for low back pain in women: The UK Twin Spine Study. *Ann. Rheum. Dis.* 70, 1740–1745. doi:10.1136/ard.2010.137836.

Long, J., Wang, X., Du, X., Pan, H., Wang, J., Li, Z., et al. (2019). JAG2/Notch2 inhibits intervertebral disc degeneration by modulating cell proliferation, apoptosis, and extracellular matrix. *Arthritis Res. Ther.* 21, 213. doi:10.1186/s13075-019-1990-z.

López-Rodríguez, C., Aramburu, J., Jin, L., Rakeman, A. S., Michino, M., and Rao, A. (2001). Bridging the NFAT and NF-κB Families: NFAT5 dimerization regulates cytokine gene transcription in response to osmotic stress. *Immunity* 15, 47–58. doi:10.1016/S1074-7613(01)00165-0.

Lopiccolo, J., Blumenthal, G., Bernstein, W., and Dennis, P. (2008). Targeting the PI3K/Akt/mTOR pathway: Effective combinations and clinical considerations. *Drug Resist. Updat.* 11, 32–50. doi:10.1016/j.drup.2007.11.003.

Luoma, K., Riihimäki, H., Luukkonen, R., Raininko, R., Viikari-Juntura, E., and Lamminen, A. (2000). Low Back Pain in Relation to Lumbar Disc Degeneration. *Spine (Phila Pa 1976)* 25, 487–492. doi:10.1002/ca.22404.

Ma, K.-G., Shao, Z.-W., Yang, S.-H., Wang, J., Wang, B.-C., Xiong, L.-M., et al. (2013). Autophagy is activated in compression-induced cell degeneration and is mediated by reactive oxygen species in nucleus pulposus cells exposed to compression.

Osteoarthr. Cartil. 21, 2030–2038. doi:10.1016/j.joca.2013.10.002.
Määttä, J. H., Kraatari, M., Wolber, L., Niinimäki, J., Wadge, S., Karppinen, J., et al. (2014). Vertebral endplate change as a feature of intervertebral disc degeneration: a heritability study. *Eur. Spine J.* 23, 1856–1862. doi:10.1007/s00586-014-3333-8.
Määttä, J. H., Rade, M., Freidin, M. B., Airaksinen, O., Karppinen, J., and Williams, F. M. K. (2018). Strong association between vertebral endplate defect and Modic change in the general population. *Sci. Rep.* 8, 16630. doi:10.1038/s41598-018-34933-3.
MacGregor, A. J., Andrew, T., Sambrook, P. N., and Spector, T. D. (2004). Structural, psychological, and genetic influences on low back and neck pain: A study of adult female twins. *Arthritis Care Res. (Hoboken).* 51, 160–167. doi:10.1002/art.20236.
Machado, D., Costa, R. S., Rocha, M., Ferreira, E. C., Tidor, B., and Rocha, I. (2011). Modeling formalisms in systems biology. *AMB Express* 1, 45. doi:10.1186/2191-0855-1-45.
MacLean, J. J., Lee, C. R., Alini, M., and Iatridis, J. C. (2004). Anabolic and catabolic mRNA levels of the intervertebral disc vary ... *J. Orthop. Res.* 22, 1193–1200. doi:10.1016/.j.orthres.2004.04.004.
MacLean, J. J., Lee, C. R., Alini, M., and Iatridis, J. C. (2005). The effects of short-term load duration on anabolic and catabolic gene expression in the rat tail intervertebral disc. *J. Orthop. Res.* 23, 1120–1127. doi:10.1016/j.orthres.2005.01.020.
Magnier, C., Boiron, O., Wendling-Mansuy, S., Chabrand, P., and Deplano, V. (2009). Nutrient distribution and metabolism in the intervertebral disc in the unloaded state: A parametric study. *J. Biomech.* 42, 100–108. doi:10.1016/j.jbiomech.2008.10.034.
Malandrino, A., Jackson, A. R., Huyghe, J. M., and Noailly, J. (2015a). Poroelastic modeling of the intervertebral disc: A path toward integrated studies of tissue biophysics and organ degeneration. *MRS Bull.* 40, 324–332. doi:10.1557/mrs.2015.68.
Malandrino, A., Lacroix, D., Hellmich, C., Ito, K., Ferguson, S. J., and Noailly, J. (2014). The role of endplate poromechanical properties on the nutrient availability in the intervertebral disc. *Osteoarthr. Cartil.* 22, 1053–1060. doi:10.1016/j.joca.2014.05.005.
Malandrino, A., Noailly, J., and Lacroix, D. (2011). The effect of sustained compression on oxygen metabolic transport in the intervertebral disc decreases with degenerative changes. *PLoS Comput. Biol.* 7. doi:10.1371/journal.pcbi.1002112.
Malandrino, A., Pozo, J. M., Castro-Mateos, I., Frangi, A. F., van Rijsbergen, M. M., Ito, K., et al. (2015b). On the Relative

Relevance of Subject-Specific Geometries and Degeneration-Specific Mechanical Properties for the Study of Cell Death in Human Intervertebral Disk Models. *Front. Bioeng. Biotechnol.* 3, 1–15. doi:10.3389/fbioe.2015.00005.

Maroudas, A., Stockwell, R. A., Nachemson, A., and Urban, J. (1975). Factors involved in the nutrition of the human lumbar intervertebral disc: cellularity and diffusion of glucose in vitro. *J. Anat. (J. Anat.)* 120, 113–130. Available at: http://eutils.ncbi.nlm.nih.gov/entrez/eutils/elink.fcgi?dbfrom=pubmed&id=1184452&retmode=ref&cmd=prlinks.

Martirosyan, N. L., Patel, A. A., Carotenuto, A., Kalani, M. Y. S., Belykh, E., Walker, C. T., et al. (2016). Genetic Alterations in Intervertebral Disc Disease. *Front. Surg.* 3, 59. doi:10.3389/fsurg.2016.00059.

McCann, M. R., Tamplin, O. J., Rossant, J., and Seguin, C. A. (2012). Tracing notochord-derived cells using a Noto-cre mouse: implications for intervertebral disc development. *Dis. Model. Mech.* 5, 73–82. doi:10.1242/dmm.008128.

Meaney, D. F., Morrison, B., and Bass, C. D. (2014). The mechanics of traumatic brain injury: A review of what we know and what we need to know for reducing its societal burden. *J. Biomech. Eng.* 136. doi:10.1115/1.4026364.

Medzhitov, R. (2008). Origin and physiological roles of inflammation. *Nature* 454, 428–435. doi:10.1038/nature07201.

Melas, I. N., Chairakaki, A. D., Chatzopoulou, E. I., Messinis, D. E., Katopodi, T., Pliaka, V., et al. (2014). Modeling of signaling pathways in chondrocytes based on phosphoproteomic and cytokine release data. *Osteoarthr. Cartil.* 22, 509–518. doi:10.1016/j.joca.2014.01.001.

Mendoza, L., and Xenarios, I. (2006). A method for the generation of standardized qualitative dynamical systems of regulatory networks. *Theor. Biol. Med. Model. (Theor Biol Med Model.* 3, 13. doi:10.1186/1742-4682-3-13.

Meng, X., Zhuang, L., Wang, J., Liu, Z., Wang, Y., Xiao, D., et al. (2018). Hypoxia-inducible factor (HIF)-1alpha knockout accelerates intervertebral disc degeneration in mice. *Int. J. Clin. Exp. Pathol.* 11, 548–557. Available at: http://www.ncbi.nlm.nih.gov/pubmed/31938140.

Millward-Sadler, S. J., Costello, P. W., Freemont, A. J., and Hoyland, J. A. (2009). Regulation of catabolic gene expression in normal and degenerate human intervertebral disc cells: implications for the

pathogenesis of intervertebral disc degeneration. *Arthritis Res. Ther.* 11, R65. doi:10.1186/ar2693.

Mitchell, U. H., Bowden, J. A., Larson, R. E., Belavy, D. L., and Owen, P. J. (2020). Long-term running in middle-aged men and intervertebral disc health , a cross-sectional pilot study. *PLoS One* 15, e0229457. doi:10.1371/journal.pone.0229457.

Mitsos, A., Melas, I. N., Morris, M. K., Saez-Rodriguez, J., Lauffenburger, D. A., and Alexopoulos, L. G. (2012). Non Linear Programming (NLP) Formulation for Quantitative Modeling of Protein Signal Transduction Pathways. *PLoS One* 7. doi:10.1371/journal.pone.0050085.

Mitsos, A., Melas, I. N., Siminelakis, P., Chairakaki, A. D., Saez-Rodriguez, J., and Alexopoulos, L. G. (2009). Identifying Drug Effects via Pathway Alterations using an Integer Linear Programming Optimization Formulation on Phosphoproteomic Data. *PLoS Comput. Biol.* 5. doi:10.1371/journal.pcbi.1000591.

Mokhbi Soukane, D., Shirazi-Adl, A., and Urban, J. P. G. (2009). Investigation of solute concentrations in a 3D model of intervertebral disc. *Eur. Spine J.* 18, 254–262. doi:10.1007/s00586-008-0822-7.

Molinos, M., Almeida, C. R., Caldeira, J., Cunha, C., Goncalves, R. M., and Barbosa, M. A. (2015). Inflammation in intervertebral disc degeneration and regeneration. *J R Soc Interface* 12, 20141191. doi:10.1098/rsif.2014.1191.

Moroney, P. J., Watson, R. W. G., Burke, J. G., O'Byrne, J., and Fitzpatrick, J. M. (2002). PH and anti-inflammatory agents modulate nucleus pulposus cytokine secretion. in *Proceedings of the NASS 17th Annual Meeting / The Spine Journal*, 49S–50S.

Morris, M. K., Saez-Rodriguez, J., Sorger, P. K., and Lauffenburger, D. A. (2010). Logic-Based Models for the Analysis of Cell Signaling Networks. *Biochemistry* 49, 3216–3224. doi:10.1021/bi902202q.

Mow, V. C., Kuei, S. C., Lai, W. M., and Armstrong, C. G. (1980). Biphasic creep and stress relaxation of articular cartilage in compression: Theory and experiments. *J. Biomech. Eng.* 102, 73–84. doi:10.1115/1.3138202.

Mukherjee, S., Nazemi, M., Jonkers, I., and Geris, L. (2020). Use of Computational Modeling to Study Joint Degeneration: A Review. *Front. Bioeng. Biotechnol.* 8, 1–12. doi:10.3389/fbioe.2020.00093.

Munir, S., Freidin, M. B., Rade, M., Määttä, J., Livshits, G., and Williams, F. M. K. (2018a). Endplate defect is heritable,

associated with low back pain and triggers intervertebral disc degeneration: A longitudinal study from Twinsuk. *Spine (Phila. Pa. 1976)*. 43, 1496–1501. doi:10.1097/BRS.0000000000002721.

Munir, S., Rade, M., Määttä, J. H., Freidin, M. B., and Williams, F. M. K. (2018b). Intervertebral Disc Biology: Genetic Basis of Disc Degeneration. *Curr. Mol. Biol. Reports*, 1–8. doi:10.1007/s40610-018-0101-2.

Mwale, F., Ciobanu, I., Giannitsios, D., Roughley, P., Steffen, T., and Antoniou, J. (2011). Effect of oxygen levels on proteoglycan synthesis by intervertebral disc cells. *Spine (Phila. Pa. 1976)*. 36, 131–138. doi:10.1097/BRS.0b013e3181d52b9e.

Mwale, F., Roughley, P., and Antoniou, J. (2004). Distinction between the extracellular matrix of the nucleus pulposus and hyaline cartilage: a requisite for tissue engineering of intervertebral disc. *Eur. Cells Mater.* 8, 58–64. doi:10.22203/eCM.v008a06.

Nachemson, A. (1969). Intradiscal measurements of ph in patients with lumbar rhizopathies. *Acta Orthop. Scand.* 40, 23–42. doi:10.3109/17453676908989482.

Nachemson, A., and Elfström, G. (1970). Intravital dynamic pressure measurements in lumbar discs. *Scand. J. Rehabil. Medicat.* 2, 1–40.

NASA (2011). Astronauts answer student questions. 5. Available at: https://www.nasa.gov/centers/johnson/pdf/569954main_astronaut _FAQ.pdf.

Navone, S. E., Marfia, G., Canzi, L., Ciusani, E., Canazza, A., Visintini, S., et al. (2012). Expression of neural and neurotrophic markers in nucleus pulposus cells isolated from degenerated intervertebral disc. *J. Orthop. Res.* 30, 1470–1477. doi:10.1002/jor.22098.

Neidlinger-Wilke, C., Galbusera, F., Pratsinis, H., Mavrogonatou, E., Mietsch, A., Kletsas, D., et al. (2014). Mechanical loading of the intervertebral disc: From the macroscopic to the cellular level. *Eur. Spine J.* 23. doi:10.1007/s00586-013-2855-9.

Neidlinger-Wilke, C., Mietsch, A., Rinkler, C., Wilke, H. J., Ignatius, A., and Urban, J. (2012). Interactions of environmental conditions and mechanical loads have influence on matrix turnover by nucleus pulposus cells. *J. Orthop. Res. (J Orthop Res)* 30, 112–121. doi:10.1002/jor.21481.

Neidlinger-Wilke, C., Würtz, K., Liedert, A., Schmidt, C., Börm, W., Ignatius, A., et al. (2005). A three-dimensional collagen matrix as a suitable culture system for the comparison of cyclic strain and hydrostatic pressure effects on intervertebral disc cells. *J.*

Neurosurg. Spine 2, 457–465. doi:10.3171/spi.2005.2.4.0457.
Nerlich, A. G., Boos, N., Wiest, I., and Aebi, M. (1998). Immunolocalization of major interstitial collagen types in human lumbar intervertebral discs of various ages. *Virchows Arch.* 432, 67–76. doi:10.1007/s004280050136.
Ngo, K., Yurube, T., Pohl, P., Qing, D., Miller, R., Roughley, P., et al. (2014). Effects Of The Anti-aging Agent Rapamycin On Disc Matrix Homeostasis. in *ORS 2014 Annual Meeting*, Poster No:1647.
Ohtori, S., Miyagi, M., and Inoue, G. (2018). Sensory nerve ingrowth, cytokines, and instability of discogenic low back pain: A review. *Spine Surg. Relat. Res.* 2, 11–17. doi:10.22603/ssrr.2016-0018.
Olivares, A. L., González Ballester, M. A., and Noailly, J. (2016). Virtual exploration of early stage atherosclerosis. *Bioinformatics* 32, 3798–3806. doi:10.1093/bioinformatics/btw551.
Oliver, J. C., Bland, L. A., Oettinger, C. W., Arduino, M. J., McAllister, S. K., Aguero, S. M., et al. (1993). Cytokine kinetics in an in vitro whole blood model following an endotoxin challenge. *Lymphokine Cytokine Res.* 12, 115–20. Available at: http://www.ncbi.nlm.nih.gov/pubmed/8324076.
Orton, R. J., Sturm, O. E., Vyshemirsky, V., Calder, M., Gilbert, D. R., and Kolch, W. (2005). Computational modelling of the receptor-tyrosine-kinase-activated MAPK pathway. *Biochem. J.* 392, 249–261. doi:10.1042/BJ20050908.
Osti, O. L., Vernon-Roberts, B., Moore, R., and Fraser, R. D. (1992). Annular tears and disc degeneration in the lumbar spine - A post-mortem study of 135 discs. *J Bone Jt. Surg Br* 74–B, 678–682.
Pachi, A., and Ji, T. (2005). Frequency and velocity of people walking. *Struct. Eng.*, 36–40.
Pandit, A., and Mohd Isa, L. (2020). United States, Patent Application Publication. Available at: https://patentimages.storage.googleapis.com/09/c9/56/0d323ff869c6ee/US20200038551A1.pdf.
Patil, P., Falabella, M., Saeed, A., Lee, D., Kaufman, B., Shiva, S., et al. (2019). Oxidative stress-induced senescence markedly increases disc cell bioenergetics. *Mech. Ageing Dev.* 180, 97–106. doi:10.1016/j.mad.2019.04.006.
Patil, P., Niedernhofer, L. J., Robbins, P. D., Lee, J., Sowa, G., and Vo, N. (2018). Cellular Senescence in Intervertebral Disc Aging and Degeneration. *Curr. Mol. Biol. Reports* 4, 180–190. doi:10.1007/s40610-018-0108-8.

Pfirrmann, C. W. A., Metzdorf, A., Zanetti, M., Hodler, J., and Boos, N. (2001). Magnetic resonance classification of lumbar intervertebral disc degeneration. *Spine (Phila. Pa. 1976).* 26, 1873–1878. doi:10.1097/00007632-200109010-00011.

Phillips, K. L. E., Chiverton, N., Michael, A. L., Cole, A. A., Breakwell, L. M., Haddock, G., et al. (2013). The cytokine and chemokine expression profile of nucleus pulposus cells: implications for degeneration and regeneration of the intervertebral disc. *Arthritis Res. Ther.* 15, R213. doi:10.1186/ar4408.

Phillips, K. L. E., Cullen, K., Chiverton, N., Michael, A. L. R., Cole, A. A., Breakwell, L. M., et al. (2015). Potential roles of cytokines and chemokines in human intervertebral disc degeneration: Interleukin-1 is a master regulator of catabolic processes. *Osteoarthr. Cartil.* 23, 1165–1177. doi:10.1016/j.joca.2015.02.017.

Piccolo, S., Dupont, S., and Cordenonsi, M. (2014). The Biology of YAP/TAZ: Hippo Signaling and Beyond. *Physiol. Rev.* 94, 1287–1312. doi:10.1152/physrev.00005.2014.

Pocaterra, A., Romani, P., and Dupont, S. (2020). YAP/TAZ functions and their regulation at a glance. *J. Cell Sci.* 133. doi:10.1242/jcs.230425.

Pockert, A. J., Richardson, S. M., Le Maitre, C. L., Lyon, M., Deakin, J. A., Buttle, D. J., et al. (2009). Modified expression of the ADAMTS enzymes and tissue inhibitor of metalloproteinases 3 during human intervertebral disc degeneration. *Arthritis Rheum.* 60, 482–491. doi:10.1002/art.24291.

Poillot, P., O'Donnell, J., O'Connor, D. T., Ul Haq, E., Silien, C., Tofail, S. A. M., et al. (2020). Piezoelectricity in the Intervertebral disc. *J. Biomech.* 102, 109622. doi:10.1016/j.jbiomech.2020.109622.

Pokharna, H. K., and Phillips, F. M. (1998). Collagen Crosslinks in Human Lumbar Intervertebral Disc Aging. *Spine (Phila. Pa. 1976).* 23, 1645–1648. doi:10.1097/00007632-199808010-00005.

Purmessur, D., Freemont, A. J., and Hoyland, J. A. (2008). Expression and regulation of neurotrophins in the nondegenerate and degenerate human intervertebral disc. *Arthritis Res. Ther.* 10, R99. doi:10.1186/ar2487.

Purmessur, D., Walter, B. a, Roughley, P. J., Laudier, D. M., Hecht, a C., and Iatridis, J. (2013). A role for TNFα in intervertebral disc degeneration: a non-recoverable catabolic shift. *Biochem. Biophys. Res. Commun.* 433, 151–6. doi:10.1016/j.bbrc.2013.02.034.

Quero, L., Klawitter, M., Schmaus, A., Rothley, M., Sleeman, J., Tiaden, A. N., et al. (2013). Hyaluronic acid fragments enhance the inflammatory and catabolic response in human intervertebral disc cells through modulation of toll-like receptor 2 signalling pathways. *Arthritis Res. Ther.* 15, R94. doi:10.1186/ar4274.

Raj, P. P. (2008). Intervertebral disc: Anatomy-physiology-pathophysiology-treatment. *Pain Pract.* 8, 18–44. doi:10.1111/j.1533-2500.2007.00171.x.

Rajasekaran, S., Babu, J. N., Arun, R., Armstrong, B. R. W., Shetty, A. P., and Murugan, S. (2004). ISSLS prize winner: A study of diffusion in human lumbar discs: A serial magnetic resonance imaging study documenting the influence of the endplate on diffusion in normal and degenerate discs. *Spine (Phila. Pa. 1976).* 29, pp 2654-2667.

Rajasekaran, S., Kanna, R. M., Senthil, N., Raveendran, M., Cheung, K. M. C., Chan, D., et al. (2013). Phenotype variations affect genetic association studies of degenerative disc disease: Conclusions of analysis of genetic association of 58 single nucleotide polymorphisms with highly specific phenotypes for disc degeneration in 332 subjects. *Spine J.* 13, 1309–1320. doi:10.1016/j.spinee.2013.05.019.

Richardson, S. M., Knowles, R., Marples, D., Hoyland, J. A., and Mobasheri, A. (2008a). Aquaporin expression in the human intervertebral disc. *J. Mol. Histol.* 39, 303–309. doi:10.1007/s10735-008-9166-1.

Richardson, S. M., Knowles, R., Tyler, J., Mobasheri, A., and Hoyland, J. A. (2008b). Expression of glucose transporters GLUT-1, GLUT-3, GLUT-9 and HIF-1α in normal and degenerate human intervertebral disc. *Histochem. Cell Biol.* 129, 503–511. doi:10.1007/s00418-007-0372-9.

Richardson, S. M., Purmessur, D., Baird, P., Probyn, B., Freemont, A. J., and Hoyland, J. A. (2012). Degenerate Human Nucleus Pulposus Cells Promote Neurite Outgrowth in Neural Cells. *PLoS One* 7, e47735. doi:10.1371/journal.pone.0047735.

Rinkler, C., Heuer, F., Pedro, M. T., Mauer, U. M., Ignatius, A., and Neidlinger-Wilke, C. (2010). Influence of low glucose supply on the regulation of gene expression by nucleus pulposus cells and their responsiveness to mechanical loading. *J. Neurosurg. Spine J Neurosurg Spine* 13, 535–542. doi:10.3171/2010.4.SPINE09713.

Risbud, M. V., Schipani, E., and Shapiro, I. M. (2010). Hypoxic regulation of nucleus pulposus cell survival: From niche to notch.

Am. J. Pathol. 176, 1577–1583. doi:10.2353/ajpath.2010.090734.

Risbud, M. V., Schoepflin, Z. R., Mwale, F., Kandel, R. A., Grad, S., Iatridis, J. C., et al. (2015). Defining the phenotype of young healthy nucleus pulposus cells: Recommendations of the Spine Research Interest Group at the 2014 annual ORS meeting. *J. Orthop. Res.* 33, 283–293. doi:10.1002/jor.22789.

Risbud, M. V., and Shapiro, I. M. (2011). Notochordal Cells in the Adult Intervertebral Disc: New Perspective on an Old Question. *Crit. Rev. Eukaryot. Gene Expr.* 21, 29–41. doi:10.1615/CritRevEukarGeneExpr.v21.i1.30.

Risbud, M. V, and Shapiro, I. M. (2014). Role of Cytokines in Intervertebral Disc Degeneration: Pain and Disc-content. *Nat. Rev. Rheumatol.* 10, 44–56. doi:10.1038/nrrheum.2013.160.

Roberts, N., Hogg, D., Whitehouse, G. H., and Dangerfield, P. (1998). Quantitative analysis of diurnal variation in volume and water content of lumbar intervertebral discs. *Clin. Anat.* 11, 1–8. doi:10.1002/(SICI)1098-2353(1998)11:1<1::AID-CA1>3.0.CO;2-Z.

Roberts, S., Caterson, B., Menage, J., Evans, E. H., Jaffray, D. C., and Eisenstein, S. M. (2000). Matrix metalloproteinases and aggrecanase: their role in disorders of the human intervertebral disc. *Spine (Phila. Pa. 1976).* 25, 3005–13. doi:10.1097/00007632-200012010-00007.

Roberts, S., Evans, E. H., Kletsas, D., Jaffray, D. C., and Eisenstein, S. M. (2006). Senescence in human intervertebral discs. *Eur. Spine J.* 15, 312–316. doi:10.1007/s00586-006-0126-8.

Roberts, S., Urban, J. P., Evans, H., and Eisenstein, S. M. (1996). Transport properties of the human cartilage endplate in relation to its composition and calcification. *Spine (Phila. Pa. 1976)* 21, 415–420. doi:10.1097/00007632-199602150-00003.

Roberts, S., and Urban, J. P. G. (2011). "Intervertebral discs," in *Encyclopaedia of Occupational health and Safety* (Geneva).

Rodriguez, A. G., Slichter, C. K., Acosta, F. L., Rodriguez-Soto, A. E., Burghardt, A. J., Majumdar, S., et al. (2011). Human disc nucleus properties and vertebral endplate permeability. *Spine (Phila Pa 1976)* 36, 512–520. doi:10.1097/BRS.0b013e3181f72b94.

Roos, R. W., Petterson, R., and Huyghe, J. M. (2013). Confined compression and torsion experiments on a pHEMA gel in various bath concentrations. *Biomech. Model. Mechanobiol.* 12, 617–626. doi:10.1007/s10237-012-0429-0.

Roth, I., Leroy, V., Kwon, H. M., Martin, P.-Y., Féraille, E., and

Hasler, U. (2010). Osmoprotective Transcription Factor NFAT5/TonEBP Modulates Nuclear Factor-κB Activity. *Mol. Biol. Cell* 21, 3459–3474. doi:10.1091/mbc.e10-02-0133.

Roughley, P. J., Melching, L. I., Heathfield, T. F., Pearce, R. H., and Mort, J. S. (2006). The structure and degradation of aggrecan in human intervertebral disc. *Eur. Spine J. (Eur Spine J)* 15, S326–S332. doi:10.1007/s00586-006-0127-7.

Ruiz-Fernández, C., Francisco, V., Pino, J., Mera, A., González-Gay, M. A., Gómez, R., et al. (2019). Molecular Relationships among Obesity, Inflammation and Intervertebral Disc Degeneration: Are Adipokines the Common Link? *Int. J. Mol. Sci.* 20, E2030. doi:10.3390/ijms20082030.

Ruiz Wills, C. (2015). A computational study of intervertebral disc degeneration in relation to changes in regional tissue composition and disc nutrition.

Ruiz Wills, C., Foata, B., González Ballester, M. Á., Karppinen, J., and Noailly, J. (2018). Theoretical Explorations Generate New Hypotheses About the Role of the Cartilage Endplate in Early Intervertebral Disk Degeneration. *Front. Physiol.* 9, 1–12. doi:10.3389/fphys.2018.01210.

Ruiz Wills, C., Malandrino, A., Van Rijsbergen, M., Lacroix, D., Ito, K., and Noailly, J. (2016). Simulating the sensitivity of cell nutritive environment to composition changes within the intervertebral disc. *J. Mech. Phys. Solids* 90, 108–123. doi:10.1016/j.jmps.2016.02.003.

Sabatini, D. M. (2017). Twenty-five years of mTOR: Uncovering the link from nutrients to growth. *Proc. Natl. Acad. Sci.* 114, 11818–11825. doi:10.1073/pnas.1716173114.

Sadowska, A., Altinay, B., Hitzl, W., Ferguson, S. J., and Wuertz-Kozak, K. (2020). Hypo-Osmotic Loading Induces Expression of IL-6 in Nucleus Pulposus Cells of the Intervertebral Disc Independent of TRPV4 and TRPM7. *Front. Pharmacol.* 11, 1–16. doi:10.3389/fphar.2020.00952.

Sadowska, A., Kameda, T., Krupkova, O., and Wuertz-Kozak (2018). Osmosensing, osmosignalling and inflammation: how intervertebral disc cells respond to altered osmolarity. *Eur. Cells Mater.* 36, 231–250. doi:10.22203/eCM.v036a17.

Saez-Rodriguez, J., Alexopoulos, L. G., Epperlein, J., Samaga, R., Lauffenburger, D. A., Klamt, S., et al. (2009). Discrete logic modelling as a means to link protein signalling networks with functional analysis of mammalian signal transduction. *Mol. Syst.*

Biol. 5, 331. doi:10.1038/msb.2009.87.

Saggese, T., Thambyah, A., Wade, K., and McGlashan, S. R. (2018). Differential Response of Bovine Mature Nucleus Pulposus and Notochordal Cells to Hydrostatic Pressure and Glucose Restriction. *Cartilage* 0, 1–13. doi:10.1177/1947603518775795.

Sambrook, P. N., MacGregor, A. J., and Spector, T. D. (1999). Genetic influences on cervical and lumbar disc degeneration: A magnetic resonance imaging study in twins. *Arthritis Rheum.* 42, 366–372. doi:10.1002/1529-0131(199902)42:2<366::AID-ANR20>3.0.CO;2-6.

Schmitt, K.-U., Niederer, P. F., Cronin, D. S., Morrison III, B., Muser, M. H., and Walz, F. (2019). *Trauma Biomechanics*. doi:10.1007/978-3-030-11659-0.

Schroeder, Y., Huyghe, J. M., Van Donkelaar, C. C., and Ito, K. (2010). A biochemical/biophysical 3D FE intervertebral disc model. *Biomech. Model. Mechanobiol.* 9, 641–650. doi:10.1007/s10237-010-0203-0.

Schroeder, Y., Sivan, S., Wilson, W., Merkher, Y., Huyghe, J. M., Maroudas, A., et al. (2007). Are Disc Pressure, Stress, and Osmolarity Affected by Intra- and Extrafibrillar Fluid Exchange? *J. Orthop. Res.* 25, 1317–1324. doi:10.1002/jor.

Schroeder, Y., Wilson, W., Huyghe, J. M., and Baaijens, F. P. T. (2006). Osmoviscoelastic finite element model of the intervertebral disc. *Eur. Spine J.* 15, 361–371. doi:10.1007/s00586-006-0110-3.

Séguin, C. A., Pilliar, R. M., Madri, J. A., and Kandel, R. A. (2008). TNF-α Induces MMP2 Gelatinase Activity and MT1-MMP Expression in an In Vitro Model of Nucleus Pulposus Tissue Degeneration. *Spine (Phila. Pa. 1976).* 33, 356–365. doi:10.1097/BRS.0b013e3181642a5e.

Séguin, C. A., Pilliar, R. M., Roughley, P. J., and Kandel, R. A. (2005). Tumor necrosis factorα modulates matrix production and catabolism in nucleus pulposus tissue. *Spine (Phila. Pa. 1976).* 30, 1940–1948. doi:10.1097/01.brs.0000176188.40263.f9.

Sélard, É., Shirazi-Adl, A., and Urban, J. P. G. (2003). Finite Element Study of Nutrient Diffusion in the Human Intervertebral Disc. *Spine (Phila. Pa. 1976).* 28, 1945–1953. doi:10.1097/01.BRS.0000087210.93541.23.

Setton, L. A., and Chen, J. (2004). Cell mechanics and mechanobiology in the intervertebral disc. *Spine (Phila. Pa. 1976).* 29, 2710–2723. doi:10.1097/01.brs.0000146050.57722.2a.

Setton, L. A., and Chen, J. (2006). Mechanobiology of the Intervertebral Disc and Relevance to Disc Degeneration. *J. Bone Jt. Surg.* 88, 52–7. doi:10.2106/JBJS.F.00001.

Shapiro, I. M., and Risbud, M. V. (2016). *The Intervertebral Disc - Molecular and Structural Studies of the disc in Health and Disease*. Springer, Vienna doi:https://doi.org/10.1007/978-3-7091-1535-0.

Sharma, A., Pilgram, T., and Wippold, F. J. (2009). Association between annular tears and disk degeneration: A longitudinal study. *Am. J. Neuroradiol.* 30, 500–506. doi:10.3174/ajnr.A1411.

Shen, C., Yan, J., Jiang, L.-S., and Dai, L.-Y. (2011). Autophagy in rat annulus fibrosus cells: evidence and possible implications. *Arthritis Res. Ther.* 13, R132. doi:10.1186/ar3443.

Shen, J., Fang, J., Hao, J., Zhong, X., Wang, D., Ren, H., et al. (2016). SIRT1 Inhibits the Catabolic Effect of IL-1 beta Through TLR2/SIRT1/NF-kappa B Pathway in Human Degenerative Nucleus Pulposus Cells. *Pain Physician* 19, E215–E226.

Shen, L., Xiao, Y., Wu, Q., Liu, L., Zhang, C., and Pan, X. (2019). TLR4/NF-κB axis signaling pathway-dependent up-regulation of miR-625-5p contributes to human intervertebral disc degeneration by targeting COL1A1. *Am. J. Transl. Res.* 11, 1374–1388. Available at: http://www.ncbi.nlm.nih.gov/pubmed/30972168.

Silagi, E. S., Novais, E. J., Bisetto, S., Telonis, A. G., Snuggs, J., Le Maitre, C. L., et al. (2020). Lactate Efflux From Intervertebral Disc Cells Is Required for Maintenance of Spine Health. *J. Bone Miner. Res.* 35, 550–570. doi:10.1002/jbmr.3908.

Silagi, E. S., Schoepflin, Z. R., Seifert, E. L., Merceron, C., Schipani, E., Shapiro, I. M., et al. (2018). Bicarbonate Recycling by HIF-1-Dependent Carbonic Anhydrase Isoforms 9 and 12 Is Critical in Maintaining Intracellular pH and Viability of Nucleus Pulposus Cells. *J. Bone Miner. Res.* 33, 338–355. doi:10.1002/jbmr.3293.

Silver, F. H., Horvath, I., and Foran, D. J. (2002). Mechanical implications of the domain structure of fiber-forming collagens: Comparison of the molecular and fibrillar flexibilities of the α1-chains found in types I-III collagen. *J. Theor. Biol.* 216, 243–254. doi:10.1006/jtbi.2002.2542.

Singh, K., Masuda, K., Thonar, E. J.-M. ., An, H. S., and Cs-Szabo, G. (2009). Age-related changes in the Extracellular Matrix of Nucleus Pulposus and Anulus Fibrosus of Human Intervertebral Disc. *Spine (Phila Pa 1976)* 34, 10–16.

doi:10.1097/BRS.0b013e31818e5ddd.

Sivan, S. S., Hayes, A. J., Wachtel, E., Caterson, B., Merkher, Y., Maroudas, A., et al. (2014). Biochemical composition and turnover of the extracellular matrix of the normal and degenerate intervertebral disc. *Eur. Spine J.* 23, 344–353. doi:10.1007/s00586-013-2767-8.

Sivan, S. S., Tsitron, E., Wachtel, E., Roughley, P. J., Sakkee, N., Van Der Ham, F., et al. (2006). Aggrecan turnover in human intervertebral disc as determined by the racemization of aspartic acid. *J. Biol. Chem.* 281, 13009–13014. doi:10.1074/jbc.M600296200.

Sivan, S. S., Wachtel, E., Tsitron, E., Sakkee, N., Van Der Ham, F., DeGroot, J., et al. (2008). Collagen turnover in normal and degenerate human intervertebral discs as determined by the racemization of aspartic acid. *J. Biol. Chem.* 283, 8796–8801. doi:10.1074/jbc.M709885200.

Slenter, D. N., Kutmon, M., Hanspers, K., Riutta, A., Windsor, J., Nunes, N., et al. (2018). WikiPathways: a multifaceted pathway database bridging metabolomics to other omics research. *Nucleic Acids Res.* 46, D661–D667. doi:10.1093/nar/gkx1064.

Smith, L. J., Nerurkar, N. L., Choi, K.-S., Harfe, B. D., and Elliott, D. M. (2011). Degeneration and regeneration of the intervertebral disc: lessons from development. *Dis. Model. Mech.* 4, 31–41. doi:10.1242/dmm.006403.

Snuggs, J. W., Day, R. E., Bach, F. C., Conner, M. T., Bunning, R. A. D., Tryfonidou, M. A., et al. (2019). Aquaporin expression in the human and canine intervertebral disc during maturation and degeneration. *JOR SPINE* 2, e1049. doi:10.1002/jsp2.1049.

Soukane, D. M., Shirazi-Adl, A., and Urban, J. P. (2005). Analysis of Nonlinear Coupled Diffusion of Oxygen and Lactic Acid in Intervertebral Discs. *J. Biomech. Eng.* 127, 1121–6. doi:10.1115/1.2073674.

Soukane, M. D., Shirazi-Adl, A., and Urban, J. P. G. (2007). Computation of coupled diffusion of oxygen, glucose and lactic acid in an intervertebral disc. *J. Biomech.* 40, 2645–2654. doi:10.1016/j.jbiomech.2007.01.003.

Stefanakis, M., Al-Abbasi, M., Harding, I., Pollintine, P., Dolan, P., Tarlton, J., et al. (2012). Annulus Fissures Are Mechanically and Chemically Conducive to the Ingrowth of Nerves and Blood Vessels. *Spine (Phila. Pa. 1976).* 37, 1883–1891. doi:10.1097/BRS.0b013e318263ba59.

Stokes, I. A. F., and Iatridis, J. C. (2004). Mechanical conditions that accelerate intervertebral disc degeneration: Overload versus immobilization. *Spine (Phila. Pa. 1976).* 29, 2724–2732. doi:10.1097/01.brs.0000146049.52152.da.

Szklarczyk, D., Gable, A. L., Lyon, D., Junge, A., Wyder, S., Huerta-Cepas, J., et al. (2019). STRING v11: protein-protein association networks with increased coverage, supporting functional discovery in genome-wide experimental datasets. *Nucleic Acids Res.* 47, D607–D613. doi:10.1093/nar/gky1131.

Sztrolovics, R., Alini, M., Roughley, P. J., and Mort, J. S. (1997). Aggrecan degradation in human intervertebral disc and articular cartilage. *Biochem. J.* 326, 235–241. doi:10.1042/bj3260235.

Takahashi, H., Suguro, T., Okazima, Y., Motegi, M., Okada, Y., and Kakiuchi, T. (1996). Inflammatory Cytokines in the Herniated Disc of the Lumbar Spine. *Spine (Phila. Pa. 1976).* 21, pp 218-224.

Takatalo, J., Karppinen, J., Näyhä, S., Taimela, S., Niinimäki, J., Blanco Sequeiros, R., et al. (2017). Association between adolescent sport activities and lumbar disk degeneration among young adults. *Scand. J. Med. Sci. Sport.* 27, 1993–2001. doi:10.1111/sms.12840.

Tavakoli, J., Elliott, D. M., and Costi, J. J. (2016). Structure and mechanical function of the inter-lamellar matrix of the annulus fibrosus in the disc. *J. Orthop. Res. (J Orthop Res)* 34, 1307–1315. doi:10.1002/jor.23306.

Teichtahl, A. J., Urquhart, D. M., Wang, Y., Wluka, A. E., O'Sullivan, R., Jones, G., et al. (2016). Lumbar disc degeneration is associated with modic change and high paraspinal fat content – a 3.0T magnetic resonance imaging study. *BMC Musculoskelet. Disord.* 17, 439. doi:10.1186/s12891-016-1297-z.

Terfve, C., Cokelaer, T., Henriques, D., MacNamara, A., Goncalves, E., Morris, M. K., et al. (2012). CellNOptR: a flexible toolkit to train protein signaling networks to data using multiple logic formalisms. *BMC Syst. Biol.* 6, 133. doi:10.1186/1752-0509-6-133.

Tessier, S., Tran, V. A., Ottone, O. K., Novais, E. J., Doolittle, A., DiMuzio, M. J., et al. (2020). TonEBP-deficiency accelerates intervertebral disc degeneration underscored by matrix remodeling, cytoskeletal rearrangements, and changes in proinflammatory gene expression. *Matrix Biol.* 87, 94–111. doi:10.1016/j.matbio.2019.10.007.

Thorpe, A. A., Bach, F. C., Tryfonidou, M. A., Le Maitre, C. L., Mwale, F., Diwan, A. D., et al. (2018). Leaping the hurdles in developing regenerative treatments for the intervertebral disc

from preclinical to clinical. *JOR Spine* 1, e1027. doi:10.1002/jsp2.1027.

Thorpe, A. A., Binch, A. L. A., Creemers, L. B., Sammon, C., and Le Maitre, C. L. (2016). Nucleus pulposus phenotypic markers to determine stem cell differentiation: fact or fiction? *Oncotarget* 7, 2189–200. doi:10.18632/oncotarget.6782.

Tolofari, S. K., Richardson, S. M., Freemont, A. J., and Hoyland, J. A. (2010). Expression of semaphorin 3A and its receptors in the human intervertebral disc: potential role in regulating neural ingrowth in the degenerate intervertebral disc. *Arthritis Res. Ther.* 12, R1. doi:10.1186/ar2898.

Tomaszewski, K. A., A. Walocha, J., Mizia, E., Gładysz, T., Głowacki, R., and Tomaszewska, R. (2015). Age- and degeneration-related variations in cell density and glycosaminoglycan content in the human cervical intervertebral disc and its endplates. *Polish J. Pathol.* 66, 296–309. doi:10.5114/pjp.2015.54964.

Tsai, T.-T., Danielson, K. G., Guttapalli, A., Oguz, E., Albert, T. J., Shapiro, I. M., et al. (2006). TonEBP/OREBP Is a Regulator of Nucleus Pulposus Cell Function and Survival in the Intervertebral Disc. *J. Biol. Chem.* 281, 25416–25424. doi:10.1074/jbc.M601969200.

Tsai, T.-T., Guttapalli, A., Agrawal, A., Albert, T. J., Shapiro, I. M., and Risbud, M. V (2007). MEK/ERK Signaling Controls Osmoregulation of Nucleus Pulposus Cells of the Intervertebral Disc by Transactivation of TonEBP/OREBP. *J. Bone Miner. Res.* 22, 965–974. doi:10.1359/jbmr.070322.

Tsai, T. T., Cheng, C. M., Chen, C. F., and Lai, P. L. (2014). Mechanotransduction in intervertebral discs. *J. Cell. Mol. Med.* 18, 2351–2360. doi:10.1111/jcmm.12377.

Türei, D., Korcsmáros, T., and Saez-Rodriguez, J. (2016). OmniPath: guidelines and gateway for literature-curated signaling pathway resources. *Nat. Methods* 13, 966–967. doi:10.1038/nmeth.4077.

Urban, J. P. G. (1994). The Chondrocyte: a Cell under Pressure. *Rheumatology* 33, 901–908. doi:10.1093/rheumatology/33.10.901.

Urban, J. P. G., and Roberts, S. (2003). Degeneration of the intervertebral disc. *Arthritis Res. Ther. (Arthritis Res Ther)* 5, 120–130. doi:10.1186/ar629.

Urban, J. P. G., Smith, S. Dp., and Fairbank, J. C. T. (2004). Nutrition of the Intervertebral Disc. *Spine (Phila. Pa. 1976).* 29, 2700–2709.

Urban, J. P., Holm, S., Maroudas, A., and Nachemson, A. (1977). Nutrition of the intervertebral disk. An in vitro study of solute

transport. *Clin Orthop Relat Res* 129, 101–14.
van der Werf, M., Lezuo, P., Maissen, O., van Donkelaar, C. C., and Ito, K. (2007). Inhibition of vertebral endplate perfusion results in decreased intervertebral disc intranuclear diffusive transport. *J. Anat.* 211, 769–774. doi:10.1111/j.1469-7580.2007.00816.x.
van Dijk, B., Potier, E., and Ito, K. (2011). Culturing Bovine Nucleus Pulposus Explants by Balancing Medium Osmolarity. *Tissue Eng. Part C Methods* 17, 1089–1096. doi:10.1089/ten.tec.2011.0215.
van Rijsbergen, M. M., Barthelemy, V. M. P., Vrancken, A. C. T., Crijns, S. P. M., Wilke, H. J., Wilson, W., et al. (2017). Moderately degenerated lumbar motion segments: Are they truly unstable? *Biomech. Model. Mechanobiol.* 16, 537–547. doi:10.1007/s10237-016-0835-9.
Van Rijsbergen, M., Van Rietbergen, B., Barthelemy, V., Eltes, P., Lazáry, Á., Lacroix, D., et al. (2018). Comparison of patient-specific computational models vs. clinical follow-up, for adjacent segment disc degeneration and bone remodelling after spinal fusion. *PLoS One* 13, 1–24. doi:10.1371/journal.pone.0200899.
Vázquez-Portalatín, N., Kilmer, C. E., Panitch, A., and Liu, J. C. (2016). Characterization of Collagen Type I and II Blended Hydrogels for Articular Cartilage Tissue Engineering. *Biomacromolecules* 17, 3145–3152. doi:10.1021/acs.biomac.6b00684.
Veres, S. P., Robertson, P. a, and Broom, N. D. (2008). ISSLS Prize Winner: Microstructure and Mechanical Disruption of the Lumbar Disc Annulus - Part II: How the Annulus Fails Under Hydrostatic Pressure. *Spine (Phila. Pa. 1976).* 33, 2711–2720. doi:10.1097/BRS.0b013e31817bb906.
Vergroesen, P. P. A., Kingma, I., Emanuel, K. S., Hoogendoorn, R. J. W., Welting, T. J., van Royen, B. J., et al. (2015). Mechanics and biology in intervertebral disc degeneration: A vicious circle. *Osteoarthr. Cartil.* 23, 1057–1070. doi:10.1016/j.joca.2015.03.028.
Vernillo, G., Giandolini, M., Edwards, W. B., Morin, J. B., Samozino, P., Horvais, N., et al. (2017). Biomechanics and Physiology of Uphill and Downhill Running. *Sport. Med.* 47, 615–629. doi:10.1007/s40279-016-0605-y.
Videman, T., Sarna, S., Battié, M. C., Koskinen, S., Gill, K., Paananen, H., et al. (1995). The Long-Term Effects of Physical Loading and Exercise Lifestyles on Back-Related Symptoms, Disability, and Spinal Pathology Among Men. *Spine (Phila. Pa. 1976).* 20, 699–709. doi:10.1097/00007632-199503150-00011.

Vo, N. V., Hartman, R. A., Patil, P. R., Risbud, M. V., Kletsas, D., Iatridis, J. C., et al. (2016). Molecular mechanisms of biological aging in intervertebral discs. *J. Orthop. Res.* 34, 1289–1306. doi:10.1002/jor.23195.

Vo, N. V., Hartman, R. A., Yurube, T., Jacobs, L. J., Sowa, G. A., Kang, J. D., et al. (2013). Expression and regulation of metalloproteinases and their inhibitors in interertebral disc aging and degeneration. *Spine J* 13, 331–341. doi:10.1016/j.spinee.2012.02.027.

von Kamp, A., Thiele, S., Hädicke, O., and Klamt, S. (2017). Use of CellNetAnalyzer in biotechnology and metabolic engineering. *J. Biotechnol.* 261, 221–228. doi:10.1016/j.jbiotec.2017.05.001.

Wade, K. R., Schollum, M. L., Robertson, P. A., Thambyah, A., and Broom, N. D. (2016). ISSLS Prize Winner: Vibration Really Disrupt the Disc: A Microanatomical Investigation. *Spine (Phila. Pa. 1976).* 41, 1185–98. doi:10.1097/BRS.0000000000001594.

Walsh, A. J. L., and Lotz, J. C. (2004). Biological response of the intervertebral disc to dynamic loading. *J. Biomech.* 37, 329–337. doi:10.1016/S0021-9290(03)00290-2.

Walter, B. A., Purmessur, D., Likhitpanichkul, M., Weinberg, A., Cho, S. K., Qureshi, S. A., et al. (2015). Inflammatory kinetics and efficacy of anti-inflammatory treatments on human nucleus pulposus cells. *Spine (Phila. Pa. 1976).* 40, 955–963. doi:10.1097/BRS.0000000000000932.

Walter, B., Korecki, C., Purmessur, D., Roughley, P., Michalek, A., and Iatridis, J. (2012). Complex Loading Affects Intervertebral Disc Mechanics and Biology. *Osteoarthr. Cartil.* 19, 1011–1018. doi:10.1016/j.joca.2011.04.005.

Walter, P., and Ron, D. (2011). The Unfolded Protein Response: From Stress Pathway to Homeostatic Regulation. *Science (80-.).* 334, 1081–1086. doi:10.1126/science.1209038.

Wang, D., Zhu, H., Cheng, W., Lin, S., Shao, R., and Pan, H. (2019). Effects of hypoxia and ASIC3 on nucleus pulposus cells: From cell behavior to molecular mechanism. *Biomed. Pharmacother.* 117, 109061. doi:10.1016/j.biopha.2019.109061.

Wang, H., Tian, Y., Wang, J., Phillips, K. L. E., Binch, A. L. a, Dunn, S., et al. (2013). Inflammatory cytokines induce NOTCH signaling in nucleus pulposus cells: implications in intervertebral disc degeneration. *J. Biol. Chem.* 288, 16761–74. doi:10.1074/jbc.M112.446633.

Wang, J., Markova, D., Anderson, D. G., Zheng, Z., Shapiro, I. M.,

and Risbud, M. V. (2011). TNF-a and IL-1b promote a disintegrin-like and metalloprotease with thrombospondin type I motif-5-mediated aggrecan degradation through syndecan-4 in intervertebral disc. *J. Biol. Chem. (J Biol Chem)* 286, 39738–39749. doi:10.1074/jbc.M111.264549.

Weiler, C., Nerlich, A. G., Zipperer, J., Bachmeier, B. E., and Boos, N. (2002). SSE Award Competition in Basic Science: expression of major matrix metalloproteinases is associated with intervertebral disc degradation and resorption. *Eur Spine J* 11, 308–20. doi:10.1007/s00586-002-0472-0.

Wilensky, U. (1999). NetLogo. NetLogo. http://ccl.northwestern.edu/netlogo/.

Wilke, H. J., Neef, P., Caimi, M., Hoogland, T., and Claes, L. E. (1999). New in vivo measurements of pressures in the intervertebral disc in daily life. *Spine (Phila. Pa. 1976).* 24, 755–62. doi:10.1097/00007632-199904150-00005.

Wilson, W., Van Donkelaar, C. C., Van Rietbergen, B., and Huiskes, R. (2005). A fibril-reinforced poroviscoelastic swelling model for articular cartilage. *J. Biomech.* 38, 1195–1204. doi:10.1016/j.jbiomech.2004.07.003.

Wilusz, R. E., Sanchez-Adams, J., and Guilak, F. (2014). The structure and function of the pericellular matrix of articular cartilage. *Matrix Biol.* 39, 25–32. doi:10.1016/j.matbio.2014.08.009.

Wognum, S., Huyghe, J. M., and Baaijens, F. P. T. (2006). Influence of osmotic pressure changes on the opening of existing cracks in 2 intervertebral disc models. *Spine (Phila. Pa. 1976).* 31, 1783–1788. doi:10.1097/01.brs.0000227267.42924.bb.

Wu, B., Yang, L., and Peng, B. (2019). Ingrowth of Nociceptive Receptors into Diseased Cervical Intervertebral Disc Is Associated with Discogenic Neck Pain. *Pain Med.* 20, 1072–1077. doi:10.1093/pm/pnz013.

Wuertz, K., Godburn, K., MacLean, J. J., Barbir, A., Donnelly, J. S., Roughley, P. J., et al. (2009). In vivo remodeling of intervertebral discs in response to short- and long-term dynamic compression. *J. Orthop. Res. (J Orthop Res)* 27, 1235–1242. doi:10.1002/jor.20867.

Wuertz, K., and Haglund, L. (2013). Inflammatory mediators in intervertebral disk degeneration and discogenic pain. *Glob. spine J.* 3, 175–84. doi:10.1055/s-0033-1347299.

Xu, J., Li, H., Yang, K., Guo, S., Wang, J., Feng, C., et al. (2019). Hyper-osmolarity environment-induced oxidative stress injury

promotes nucleus pulposus cell senescence in vitro. *Biosci. Rep.* 39. doi:10.1042/BSR20191711.

Yang, W., Yu, X.-H., Wang, C., He, W.-S., Zhang, S.-J., Yan, Y.-G., et al. (2015). Interleukin-1β in intervertebral disk degeneration. *Clin. Chim. Acta* 450, 262–272. doi:10.1016/j.cca.2015.08.029.

Yang, X., Wang, L., Yuan, Z., Zhou, P., Chu, G., Li, B., et al. (2017). Interleukin-1β induces metabolic and reactive oxygen species changes and apoptosis in annulus fibrosus cells. *Int. J. Clin. Exp. Med.* 10, 16144–16153.

Yang, Y., Wang, X., Liu, Z., Xiao, X., Hu, W., and Sun, Z. (2018). Osteogenic protein-1 attenuates nucleus pulposus cell apoptosis through activating the PI3K/Akt/mTOR pathway in a hyperosmotic culture. *Biosci. Rep.* 38, BSR20181708. doi:10.1042/BSR20181708.

Ye, W., Zhu, W., Xu, K., Liang, A., Peng, Y., Huang, D., et al. (2013). Increased macroautophagy in the pathological process of intervertebral disc degeneration in rats. *Connect. Tissue Res.* 54, 22–8. doi:10.3109/03008207.2012.715702.

Yue, H., Brown, M., Knowles, J., Wang, H., Broomhead, D. S., and Kell, D. B. (2006). Insights into the behaviour of systems biology models from dynamic sensitivity and identifiability analysis: a case study of an NF-κB signalling pathway. *Mol. BioSyst.* 2, 640–649. doi:10.1039/B609442B.

Yurube, T., Ito, M., Kakiuchi, Y., Kuroda, R., and Kakutani, K. (2020). Autophagy and mTOR signaling during intervertebral disc aging and degeneration. *JOR Spine* 3, e1082. doi:10.1002/jsp2.1082.

Zhang, C., Wang, F., Xie, Z., Chen, L., Sinkemani, A., Yu, H., et al. (2018a). AMOT130 linking F-actin to YAP is involved in intervertebral disc degeneration. *Cell Prolif.* 51, e12492. doi:10.1111/cpr.12492.

Zhang, C., Wang, F., Xie, Z., Chen, L., Sinkemani, A., Yu, H., et al. (2018b). Dysregulation of YAP by the Hippo pathway is involved in intervertebral disc degeneration, cell contact inhibition, and cell senescence. *Oncotarget* 9, 2175–2192. doi:10.18632/oncotarget.23299.

Zhang, F., Zhao, X., Shen, H., and Zhang, C. (2016a). Molecular mechanisms of cell death in intervertebral disc degeneration (Review). *Int. J. Mol. Med.* 37, 1439–1448. doi:10.3892/ijmm.2016.2573.

Zhang, S.-J., Yang, W., Wang, C., He, W.-S., Deng, H.-Y., Yan, Y.-G.,

et al. (2016b). Autophagy: A double-edged sword in intervertebral disk degeneration. *Clin. Chim. Acta.* 457, 27–35. doi:10.1016/j.cca.2016.03.016.

Zhang, W., Chien, J., Yong, J., and Kuang, R. (2017). Network-based machine learning and graph theory algorithms for precision oncology. *npj Precis. Oncol.* 1, 25. doi:10.1038/s41698-017-0029-7.

Zhao, C.-Q., Jiang, L.-S., and Dai, L.-Y. (2006). Programmed cell death in intervertebral disc degeneration. *Apoptosis* 11, 2079–88. doi:10.1007/s10495-006-0290-7.

Zhao, C.-Q., Liu, D., Li, H., Jiang, L.-S., and Dai, L.-Y. (2007). Interleukin-1beta enhances the effect of serum deprivation on rat annular cell apoptosis. *Apoptosis* 12, 2155–61. doi:10.1007/s10495-007-0137-x.

Zhu, Q., Gao, X., Brown, M. D., Eismont, F., and Gu, W. (2019). Effects of diurnal loading on the transport of charged antibiotics into intervertebral discs. *J. Biomech.* 87, 177–182. doi:10.1016/j.jbiomech.2019.03.013.

Zou, J., Chen, Y., Qian, J., and Yang, H. (2017). Effect of a low-frequency pulsed electromagnetic field on expression and secretion of IL-1β and TNF-α in nucleus pulposus cells. *J. Int. Med. Res.* 45, 462–470. doi:10.1177/0300060516683077.

Curriculum Vitae

I graduated from the Swiss Federal Institute of Technology (ETH) in Zurich, Switzerland with a Bachelor in Human Movement Sciences and a Master in Biomechanics. Focusing on a career in injury biomechanics, I wrote my Master thesis about consequences of blunt head impacts, where I investigated the risk of bridging vein ruptures (and consequent intracranial hemorrhages) caused by hits against the face and subsequent falls on the back of the head. Out of this, I published my first paper together with Prof. Dr. Kai-Uwe Schmitt, entitled: "Computer Simulations to Investigate the Consequence of Blunt Head Impact" published in the Journal of Forensic Sciences (Vol. 59, No: 5) in 2014 (DOI: 10.1111/1556-4029.12458).

My first research experience in the field of Trauma Biomechanics followed, as I got a temporary job at AXA Winterthur in Winterthur, Switzerland. In the "Accident Research & Prevention" team, led by Bettina Zahnd, I was able to gather – amongst others – valuable insights in preparing and conducting automotive crash tests (Crashtests Wildhaus). Subsequently, I worked for the working group on accident mechanics (AGU) in Zurich, Switzerland, led by Dr. Markus Muser, where I was in charge of analyzing road traffic and sports accidents and writing corresponding expert opinions. Additionally, I participated in national and international projects related to road traffic safety. This work confirmed my deep interest and dedication to the field of Trauma Biomechanics and it rose my curiosity in amplifying my knowledge from "macro" Trauma Biomechanics to "micro" Trauma Biomechanics, as the expert opinions I was writing for accident victims often underlie an individual "borderland", which required more information about the processes of trauma developments from a lower (i.e. tissue/cellular) scale.

This curiosity and my interest in gathering research experience in a non-German speaking country assured my decision to move to Barcelona, Spain, where I applied as a PhD candidate in the Biomechanics and Mechanobiology (BMMB) research group led by Dr. Jérôme Noailly. BMMB is one of eight research areas of BCN MedTech of the Universitat Pompeu Fabra. I was glad to be accepted as a PhD candidate in the late 2016, out of which this work emerged.

Publications and recognitions

This work is related to various scientific contributions and recognitions by scientific societies

Journal papers

1. **Baumgartner L**, Kaniewski A, González Ballester M A, Noailly J.: *diffusion dynamics within the intervertebral disc nucleus pulposus at the nanoscale level* [in preparation]
2. **Baumgartner L**, González Ballester M A, Noailly J. (2021): *The PN_t-Methodology: a Top-Down Network Modelling Approach to Estimate Dose- and Time-Dependent Cell Responses to Complex Multifactorial Environments* [manuscript ready]
3. **Baumgartner L**, Sadowska A, Tío L, González Ballester M A, Wuertz-Kozak K and Noailly J (2021): *Evidence-Based Network Modelling to Simulate Nucleus Pulposus Multicellular Activity in different Nutritional and pro-Inflammatory Environments, Front. bioeng. biotechnol* [accepted for publication, doi: 10.3389/fbioe.2021.734258]
4. **Baumgartner L**, Wuertz-Kozak K, Le Maitre C L, Wignall F, Richardson S M, Hoyland J, Ruiz Wills C, González Ballester M A, Neidlin M, Alexopoulos L G, Noailly J (2021): *Multiscale regulation of the intervertebral disc: achievements in experimental, in silico and regenerative research*, Int. J. Mol. Sci. 22:703, doi: 10.3390/ijms22020703
5. **Baumgartner L**, Reagh J J, González Ballester M A, Noailly J (2020): *Simulating intervertebral disc cell behaviour within 3D multifactorial Environments*, Bioinformatics, online ahead of print, doi: 10.1093/bioinformatics/btaa939

Short communications (indexed)

1. **Baumgartner L**, González Ballester M A, Noailly J (2020): *Revealing Interactions of Load Magnitude, Frequency and Exposure Time in Intervertebral Disc Microtrauma Accumulation*, (conference cancelled due to covid) Proc. Ircobi, Conf., Paper no. IRC-20-91
2. **Baumgartner L**, González Ballester M A, Noailly J (2019): *Simulation of the Multifactorial Cellular Environment within the Intervertebral Disc to better understand Microtrauma Emergence,* accepted as oral presentation at the International IRCOBI

Conference on the Biomechanics of Injury, Sep. 11th – 13th, 2019, Florence, Italy, Proc. Ircobi, Conf., Paper no. IRC-19-67

3. **Baumgartner L**, González Ballester M A, Noailly J (2018): *The Role of Indirect Mechanotransduction Phenomena in Microtrauma Development within Intervertebral Discs – A Computational Biophysical Analysis*, accepted as oral presentation at the International IRCOBI Conference on the Biomechanics of Injury, Sep. 12th – 14th, 2018, Athens, Greece, Proc. Ircobi, Conf., Paper no. IRC-18-97

Conference Abstracts

1. **Baumgartner L**, González Ballester M A, Noailly J (2020): *Integration of experimental data to simulate intervertebral disc cell activity*, accepted as oral presentation at the 14th World Congress in Computational Mechanics (WCCM), ECCOMAS Congress 2020, July 19th-24th, Paris, France, cancelled due to covid
2. **Baumgartner L**, González Ballester M A, Noailly J (2020): *Agent-based simulations of intervertebral disc cell activity under static and dynamic loading conditions,* accepted as poster presentation at the virtual physiological human conference (VPH), August 24th – 28th, Paris, France (online)
3. **Baumgartner L**, González Ballester M A, Noailly J (2019): *investigating microtrauma emergence within intervertebral discs by predicting local cellular behavior,* accepted as oral presentation at the IX Reunión del Capítulo Español de la Sociedad Europea de Biomecánica (ESB), October 24th – 25th, 2019, Las Palmas, Gran Canaria
4. **Baumgartner L**, González Ballester M A, Noailly J (2019): *Combining Multiple Micro-environmental Factors in the Prediction of Intervertebral Disc Cell Behavior Through Agent-based Modelling",* accepted as poster presentation at the 18th conference of European Conference on Computational Biology / 27th conference on Intelligent Systems for Molecular Biology, July 21th – 25th, 2019, Basel, Switzerland
5. **Baumgartner L**, González Ballester M A, Noailly J (2019): *A 3D ABM simulates Indirect Mechanotransduction Effects on Intervertebral Disc Nucleus Pulposus Cells,* accepted as oral presentation at the 25th Congress of the European Society of Biomechanics, July 7th – 10th, 2019, Vienna, Austria
6. **Baumgartner L**, González Ballester M A, Noailly J (2018): *3D Agent Based Modelling of Intervertebral Disc Nucleus Pulposus cells to simulate the effects of disc tissue property alterations*, accepted as oral

presentation at the virtual physiological human conference (VPH), Sep. 5th – 7th, 2018, Zaragoza, Spain

7. **Baumgartner L**, Ruiz Wills C, González Ballester M A, Noailly J (2018): *Simulating Cell-Matrix Biophysical Interactions in the Intervertebral Disc for the Exploration of Disc Degeneration,* accepted as poster presentation at the 8th World Congress of Biomechanics, July 8th – 12th, 2018, Dublin, Ireland
8. **Baumgartner L**, Reagh J J, Ruiz Wills C, González Ballester M A, Noailly J (2017): *Altered Cell Activity in the Intervertebral disc Transition Zone due to early Cartilage Endplate Degeneration,* accepted as oral presentation at the ECCOMAS Thematic Conference on Multiscale Problems in Biomechanics and Mechanobiology (MultiBioMe), Sep. 11th – 13th, 2017, Vienna, Austria
9. **Baumgartner L**, Reagh J J, Ruiz Wills C, González Ballester M A, Noailly J (2017): *Altered Cell Activity in the Intervertebral Disc Transition Zone due to early Cartilage Endplate Degeneration,* accepted as oral presentation at the 23rd Congress of the European Society of Biomechanics, June 2th – 5th, 2017, Seville, Spain

Recognitions

2019	IRCOBI travel grant: € 320 and conference fees to attend the IRCOBI conference in Florence, 2019
2019	Special recognition Award 2019 (for outstanding research) for the VPHi best poster award competition
2018	IRCOBI travel grant: € 380 and conference fees to attend the IRCOBI conference in Athens, 2018
2018	ESB Mobility Award: € 4000 to realize an internship at ETH Zürich
2018	VPHi Best Poster Award: € 1000 to attend conferences from September 2018 to December 2019
2018	3rd VPH Summer School, 18.06.2018 – 22.06.2018, Barcelona, Spain – best hands-on sessions in multiscale modelling – responsible for the (sub-)cellular scale, agent-based modelling